School of
Civil Engineering and Geosciences
University of Newcastle upon Tyne

Behaviour of Finned Piles in Sand under Lateral Loading

By

Jing-Rui Peng

Supervisors

Prof B. G. Clarke & Dr M. Rouainia

A thesis submitted to the University of Newcastle upon Tyne in partial fulfilment of the requirement for the degree of Doctor of Philosophy

Declaration

This is to certify that I am responsible for the work submitted in this thesis, that the original work is my own except as specified in acknowledgements or within the text, and that neither the thesis nor the original work contained therein has been submitted to this or any other institution for a higher degree.

Signed: .....Peng Jing Ke

Date: .....21.01.06....

Acknowledgement

First of all, I would like to thank almighty God – our heavenly Father for His gracious love and mercy towards me. Every day of my life has been and will be in His caring hands.

I would also like to express my most sincere gratitude towards my 5* supervisor Professor B. G. Clarke for his constant support, guidance, enthusiasm and inspiration over the past years. Then I would like to give my thanks to my second supervisor Dr M. Rouainia for his guidance, encouragement and great help. Much appreciation must also be shown towards all other lecturers including Dr. C. Dave, Mr R. Forth, Dr S. Glendinning, Dr P. Gosling and Dr S. Wilkinson in Geotechnical and Structural groups.

A special thank goes to the School of Civil Engineering in Newcastle University, which has provided excellent learning and research facilities for the completion of my postgraduate research. I must express deep appreciation towards my technical and leisure team including Mr F. Beadle, Mr W. Cragie, Mr P. Dawber, Mr D. Dick, Mr C. Hunt, Mr R. Hunter, Mr D. Innes, Mr S. Patterson and Mr E. Thompson. I acknowledge their technical support and pints of beer.

My colleagues Addy, Ali, Denis, Edmond, Jean, Jeff, Lei, May and especially Paul have been most encouraging and helpful. I am truly grateful to them.

I would like to give thanks to Dr P. Allan and Mr J. Irvine from SEtech Ltd. who have given much useful advice and information which have been of great help to this study.

I also appreciate support and prayers from my home group members in Jesmond Parish Church. Their continual encouragement has inspired me throughout my PhD journey.

Very special thanks to my parents and family for their constant love and care during the past 30 years. Without them I would not be what I am today. I am also very grateful towards Prof. Der-Wen Chang, my supervisor during my undergraduate course, who has been a great inspiration to me in my academic career.

Last but not least, many thanks to my wife Siaw Yein for her support and patience.

Abstract

Reviewing the development of offshore wind farms, large-diameter monopiles have been widely used as foundations for offshore wind structures. Unlike onshore foundations which are mainly used to transmit vertical load into the ground, offshore foundations are usually subjected to large environmental loads from wind, wave and current which could exceed 30% of their gravity load. In order to improve the lateral resistance of monopiles, a finned pile has been proposed.

Empirical and Numerical methods were used to simulate pile head lateral load and displacement (P-Y) curves, and the efficiency of fins under static loading has been estimated. Pile soil response along the pile was predicted based on the distribution of deflection, bending moment, shear force and soil resistance. Three-dimensional charts from FEM analysis represent pile and soil responses especially the soil reaction around the fins. To compare the lateral resistances of a monopile and of finned piles with various fin dimensions, 1G model tests were carried out. Tests were conducted in a 1 cubic metre steel tank filled with dry dense sand. Based on the results of ultimate lateral loads, fin efficiency under static and repeated loadings was determined. A modified relationship of load deflection behaviour has been suggested. Small-scale lateral cyclic load tests were performed in order to determine the effect of fin length on the lateral displacement of laterally loaded piles. Ten thousand cycles were used in each test to represent twenty years of environmental loading on offshore structures. Variables included the magnitude, frequency and direction of the load, the pile tip condition and the fin length. The efficiency of fins was evaluated by measuring the reduction of displacement of the pile head. The relationship between maximum load and displacement established from lateral load-displacement curves demonstrates that fins have significant impact on vertical and horizontal displacements. Piles subjected to combined loads were tested, and the failure envelopes of normalised combined loads represent the lateral resistance increase resulted from the use of finned piles. Under combined cyclic loading with various load features, a finned pile showed better performance in lateral resistance than a monopile.

In order to achieve the optimum fin efficiency, the ideal fin width should be equal to half of the pile diameter and the fin length should be equal to half of the pile length. Outcomes from this research provide concepts for laterally loaded piles and useful parameters for the design of finned piles. The device of cyclic loading system and the use of 3D finite element method (FEM) can be applied in the future study of finned piles.

Key-words: laterally loaded pile, finned pile, cyclic loading, combined loading, lateral resistance, numerical modelling

Contents

List of figures

List of tables

Notation

A	=	cyclic loading factor
a	=	rotation point from ground level (Equation 2.6)
	=	factor derived from regression analysis (Equation 2.12)
	=	degradation parameter from the results of cyclic pressuremeter tests (Equation 2.15)
	=	factor (Equation 7.3)
$\underline{a}$	=	displacement of the nodal
$\underline{\underline{B}}$	=	the strain-displacement matrix
b	=	the power function
C_1	=	coefficient of functions of ϕ'
C_2	=	coefficient of functions of ϕ'
C_3	=	coefficient of functions of ϕ'
c	=	Cohesion
D	=	pile outer diameter or pile width
$\underline{\underline{D^e}}$	=	elastic material stiffness matrix
$\underline{\underline{D}}$	=	material stiffness matrix
D_{60}	=	diameter corresponding to percents finer than 60%
D_{30}	=	diameter corresponding to percents finer than 30%
D_{10}	=	diameter corresponding to percents finer than 10%
d	=	pile width
	=	the distance between the measuring point and the pile centriod which is the inner diameter of the pile (Equation. 4.2)
E_p	=	modulus of elasticity for pile (including fins)
Es	=	modulus of elasticity for soil (Young's modulus)
e	=	eccentricity of horizontal loading
$\underline{\varepsilon^e}$	=	elastic strain
$\underline{\varepsilon^p}$	=	plastic strain
F	=	fin width
$\underline{F}$	=	concentrated loads
f	=	body force
$\underline{f}$	=	body force matrix
G_s	=	shear stress modulus of soil
	=	secant shear modulus taken from the secant slope of the unloading parts of a cycle section (Fig. 4.21)
I_P	=	moment of inertia for pile
I_x	=	moment of inertia with respect to the x axis
I_{x1}	=	moment of inertia with respect to all angles of rotation
I_y	=	moment of inertia with respect to the y axis
I_{xy}	=	product of inertia with respect to the x and y axes
J_2	=	second stress deviator
K_b	=	coefficient of net passive earth pressure
K_0	=	earth pressure at rest
K_p	=	Rankin's passive earth pressure
K_a	=	Rankin's active earth pressure

K_q = Hansen earth pressure coefficient
$\underline{K}$ = structure stiffness matrix
k = coefficient of subgrade reaction
= elastic stiffness (Section 3.3.2)
k_h = coefficient of soil subgrade reaction modulus
k_{hN} = subgrade soil reaction after N cycles
k_{hl} = subgrade soil reaction at static loading
L = embedded length of the pile
L_p = pile length
L_f = fin length
L_h = length of pile above ground surface
M = moment at the pile head
M_u = ultimate moment at the pile head
M_i = bending moment at i section
M_0 = Pure lateral moment at the pile head (when P =0)
N = number of cycles
$\underline{N}$ = displacement interpolation
N_q = bearing capacity factor
$\underline{N_S}$ = interpolation functions for the surface of the elements
n = number of elements in the analysis
n_h = constant of horizontal subgrade reaction
n_{hn} = constant of horizontal subgrade reaction after N cycles
n_{hl} = constant of horizontal subgrade reaction at static loading
P = lateral load at the pile head
P_u = ultimate lateral load at the pile head
Px = axial pile load per unit section
P_0 = pure lateral load at the pile head (when M = 0)
= initial resistance (Equation 7.3)
P_1 = 1st reading of the pressure (see Fig. 4.19)
P_2 = 2nd reading of the pressure (see Fig. 4.19)
ΔP = difference of load (see Fig.6.8)
p = soil resistance unit of force per pile length
p_u = ultimate resistance of the soil unit of force per pile length
p(z) = soil resistance along the pile shaft at z position
p_{max} = maximum ultimate normal resistance
$P_{u(FPS)}$ = ultimate lateral load of finned piles
$P_{u(MPS)}$ = ultimate lateral load of monopile
Q = vertical load at the pile head
Q_U = ultimate vertical load at the pile head
R_n = cyclic modulus ratio
Rs = reduction of strain ratio
$\underline{R}$ = structure force vector including body loads, surface tractions, concentrated loads as well as initial stresses and strains
R_1 = Reduction ratio of displacement (see Equation 6.1)
R_2 = Reduction ratio of displacement (see Equation 6.3)
R_3 = Reduction ratio of displacement (see Equation 6.4)
R_4 = Reduction ratio of displacement (see Equation 6.5)
S(z) = reaction force at z position

$Slope_{(i)}$ = slope of load/displacement taken at point I
$Slope_{(i+1)}$ = slope of load/displacement taken at point i+1
T = characteristic length ($=(E_pI_p/n_h)^{0.2}$)
T_p = wall thickness of pile
T_f = wall thickness of fin
t = relative effect of cyclic loading on the deterioration of n_h (Equation. 2.16)
= relative effect of cyclic loading (degradation factor) (Equation 2.17)
= surface forces (Equation 3.5)
$\underline{t}$ = surface force matrix
V_1 = volume reading at P_1 (see Fig. 4.19)
V_2 = volume reading at P_2 (see Fig. 4.19)
V_{ini} = initial volume reading (see Fig. 4.19)
$W_{(FPS)}$ = weight of finned piles
$W_{(MPS)}$ = weight of monopole
Y = pile head lateral displacement
Y* = increase in displacement (see Fig. 6.8)
Y** = initial point of the first loop at each load level (see Fig. 6.8)
ΔY = difference of displacement (see Fig. 6.8)
y = lateral pile deflection at depth z
y_c = lateral displacement when $p = 0.5\ p_u$
z = embedded depth of pile
γ' = effective unit weight of soil
γ_p = unit weight of pile
γ_s = unit weight of soil
γ_{dry} = dry unit weight of soil
σ'_v = effective vertical overburden pressure
σ_b = lateral pressure at base level
σ'_h = horizontal stress measured at the start of unloading (see Fig. 4.21)
σ_n = normal stress
$\underline{\sigma}$ = stress of the element
ϕ' = angle of internal friction (effective stress)
$\theta(z)$ = tilt at z position
η = pile shape factor
$\underline{\mu}$ = displacement of the element
ε = calculated strain
ε_1 = laterally loaded strain in static loading
ε_N = aterally loaded strain after N cycles
ε_i = strain at i section
$\underline{\varepsilon}$ = strain of the element
ε^* = difference of volumetric strain between the start point and the measured point on the unload curve at each load level (see Fig. 4.21)
τ = shear stress
τ_{max} = maximum shear resistance

θ = load angle in Mohr-Coulomb yield function
ν_p = Poisson ratio of pile
ν_s = Poisson ratio of soil

1 Introduction

1.1. Introduction

This thesis investigates the potential for the use of *finned piles* as foundations for offshore wind farms in order to improve lateral capacity of monopile foundations. A rocket or a finned pile was described as a pile that has four plates welded to the top of a traditional monopile at 90° to each other (Lee and Gilbert, 1980). The focus of the research concentrates on measuring and calculating the lateral capacity of finned piles subjected to various types of loading and then analysing that behaviour to determine the efficiency of fins to resist lateral load.

This research has been motivated by economic concerns over the large diameter and length of traditional monopile foundations with the associated costs. Monopile foundations have been widely used in offshore wind systems worldwide including two current wind farms in UK due to their merits include ease of manufacturing, and simple installation. Offshore pile foundations transmit large vertical loads from the superstructure through weaker subsoil into the underlying bearing strata, they are also subjected to very significant lateral loads from wind, wave, current and tide. Lateral loads acting on the pile can exceed one third of the gravity load. The increase in pile flexural stiffness EI due to the fins over the upper part of pile can increase the lateral capacity, thus reducing the pile diameter or length.

In recent years, behaviour of piles subjected to both static and cyclic loading in different ground conditions has been assessed. Numerous empirical equations have been proposed to predict the ultimate lateral load of the pile head and pile soil response along the pile. The practical design guidelines for offshore pile foundations are provided by American Petroleum Institute (API, 1993) and Det Norske Veritas (DNV, 2004). If the finned piles are to be used then their behaviour has to be validated against the design codes or a new design method has to be developed as a result of experimental and numerical analysis.

1.2. Aims and objectives

Previous studies of finned piles are very limited, and the current empirical methods may not be appropriate for the analysis of finned pile behaviour. Although it

has been proposed that the lateral resistance of a pile can be improved by the use of fins, the efficiency and pile soil response of finned piles are still unknown. This research aims to assess the behaviour of finned piles under both static and cyclic lateral loadings so that efficiency of the fins to the increase the lateral resistance can be assessed.

In order to achieve these aims a series of small scale tests and numerical analyses have been completed. The specific objectives are:

Lateral capacity of finned pile

- Determine the appropriate empirical equations, numerical methods and testing equipment to investigate finned piles under lateral loading.
- Establish pile head lateral load-displacement (P-Y) curves of finned piles with different fin dimensions by 1G model tests and numerical modelling.
- Assess the influence of fin positions and load direction for a finned pile under static loading.
- Establish the relationship between lateral displacements and number of cycles of finned piles with different fin lengths by cyclic loading tests.
- Assess the influence of load magnitude, load frequencies, and manner of cyclic loading on the lateral resistance of finned piles.
- Assess the effect of combined load on the lateral resistance of finned piles under both static and cyclic loadings.
- Investigate the pile soil response along the finned piles under different loading conditions.
- Assess the stress distribution on the fins and the soil reaction around the fins.

Fin efficiency

- Propose a modified equation to simulate the ultimate lateral resistance of finned piles.
- Evaluate the increase in lateral resistance by increasing fin dimensions; determine the optimum fin dimensions.
- Compare the increase in lateral resistance with the reduction in material.
- Determine the increase in lateral resistance by increasing the fin length.
- Establish the failure envelope to show how the lateral resistance increases by using finned piles.

1.3. Overview of project

A review of the development of offshore wind farms and previous study of lateral loaded piles is presented in Chapter 2. Important features of UK offshore sites and the typical foundation types for offshore wind structures were established. The study of piles subjected to lateral loading was based on analysis and testing. Analysis includes empirical, finite difference and finite element methods; testing includes full scale and small-scale piles subjected to both static and cyclic lateral loads.

Numerical analyses for finned piles under lateral loading are presented in Chapter 3. Current empirical methods were used to calculate the ultimate lateral load of the pile head. A finite difference analysis using LPILE and a finite element analysis using LUSAS were used to predict pile head load displacement (P-Y) curves and the pile soil response of finned piles.

Chapter 4 presents the equipment developed for small scale finned pile testing. Detailed descriptions of model finned piles, soil, static and lateral loading devices and measurements are given. This covers the design of the testing equipment including the means of applying load, measuring the pile response and determining the properties of the soils.

Results of static and cyclic loading tests are presented in Chapter 5 and 6, respectively. In static loading tests, the lateral resistance of finned piles was assessed for different fin dimensions, fin positions and loading directions. In cyclic loading tests, reduction of lateral displacement by using finned piles was verified from tests with different loading sequence, frequencies, magnitudes and pile tip conditions. Finned piles subjected to combined loading are also presented in these chapters.

In Chapter 7, the results of the experimental and numerical analyses are discussed leading to guidelines on the efficiency of the fins. Chapter 8 presents the conclusion to this study and recommendations for future work.

2 Literature review

2.1. Development of offshore wind foundations

2.1.1. Offshore wind farms in UK

The current interest in renewable energy for electricity generation can be traced back to the oil crisis in 1970's. Most interest has been in wind energy because of its resources and energy costs compared to other kinds of renewable energies. The global wind energy market (Fig. 2.1) could rise from £ 50m in 2005 to £ 800m by 2025 (SeaScape Energy, 2001). In the UK, however, renewable energy is only 3% of total electricity energy. In order to reduce global warming and to explore new sources of energy, the UK Government has a target that 10% of energy must come from renewable resources by 2010 (DTI, 2003). In addition, the new Cabinet Office Performance and Innovation Unit (PIU) report recommends this rises to 20% by 2020 (see Fig. 2.2).

In order to achieve the energy target, the government has decided to commission more offshore wind farms around the UK. Offshore wind energy has the potential to deliver substantial quantities of energy cheaper than many other forms of renewable energy. Offshore wind has many advantages over onshore wind such as higher quality of wind sources and less environmental constraints. Noise produced by operation of the wind turbine is not considered in offshore wind farms, but noise pollution is an issue for residents living near onshore wind farms. For a similar wind energy system in the same area, the wind speed over water is typically 20% higher than that measured onshore; and according to the relationship between wind velocity and power, an offshore wind turbine can generate 50% more energy than an onshore wind turbine (Reeves, 2003). The costs of offshore wind farms must be driven down through the use of mature technology and volume production so they can become commercially competitive. The variation in the price of offshore and onshore wind systems can expect to be greatly reduced after 2005 (Fig 2.3).

The UK's first offshore wind farm containing two 2MW wind turbines has been operating in Blyth since 2000: it is a landmark of UK offshore wind industry. The second offshore wind farm was constructed at North Hoyle in 2004; the wind farm comprises thirty 2MW wind turbines and is the UK's first commercial offshore

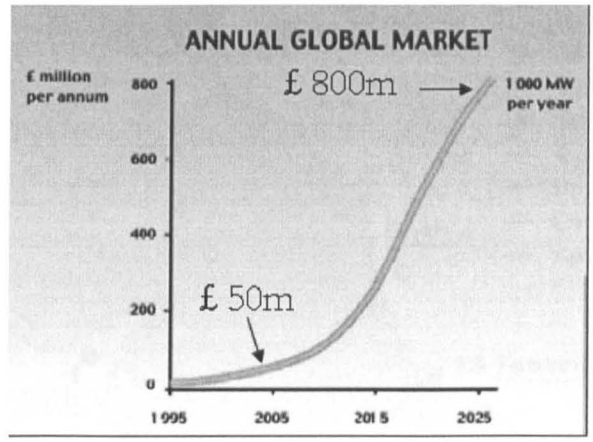

Fig. 2.1 Global renewable energy market (SeaScape Energy, 2001)

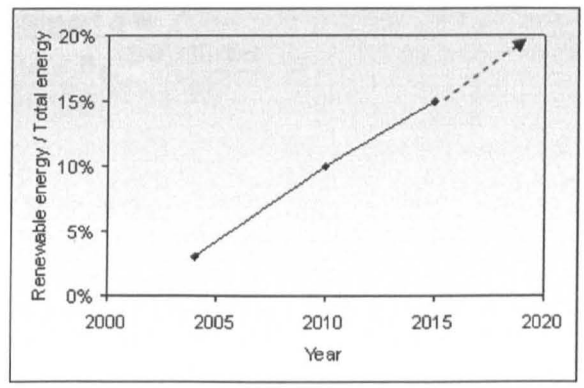

Fig. 2.2 UK renewable energy target

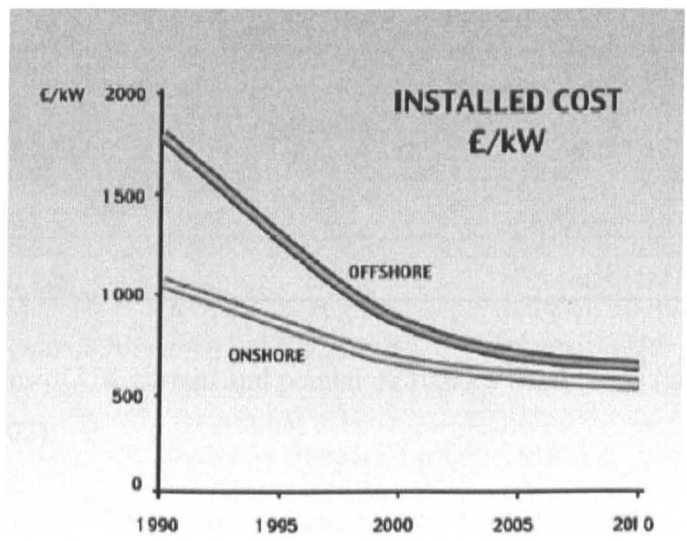

Fig. 2.3 Comparison of prices in onshore and offshore wind energy price (Source: SeaScape Energy, 2001)

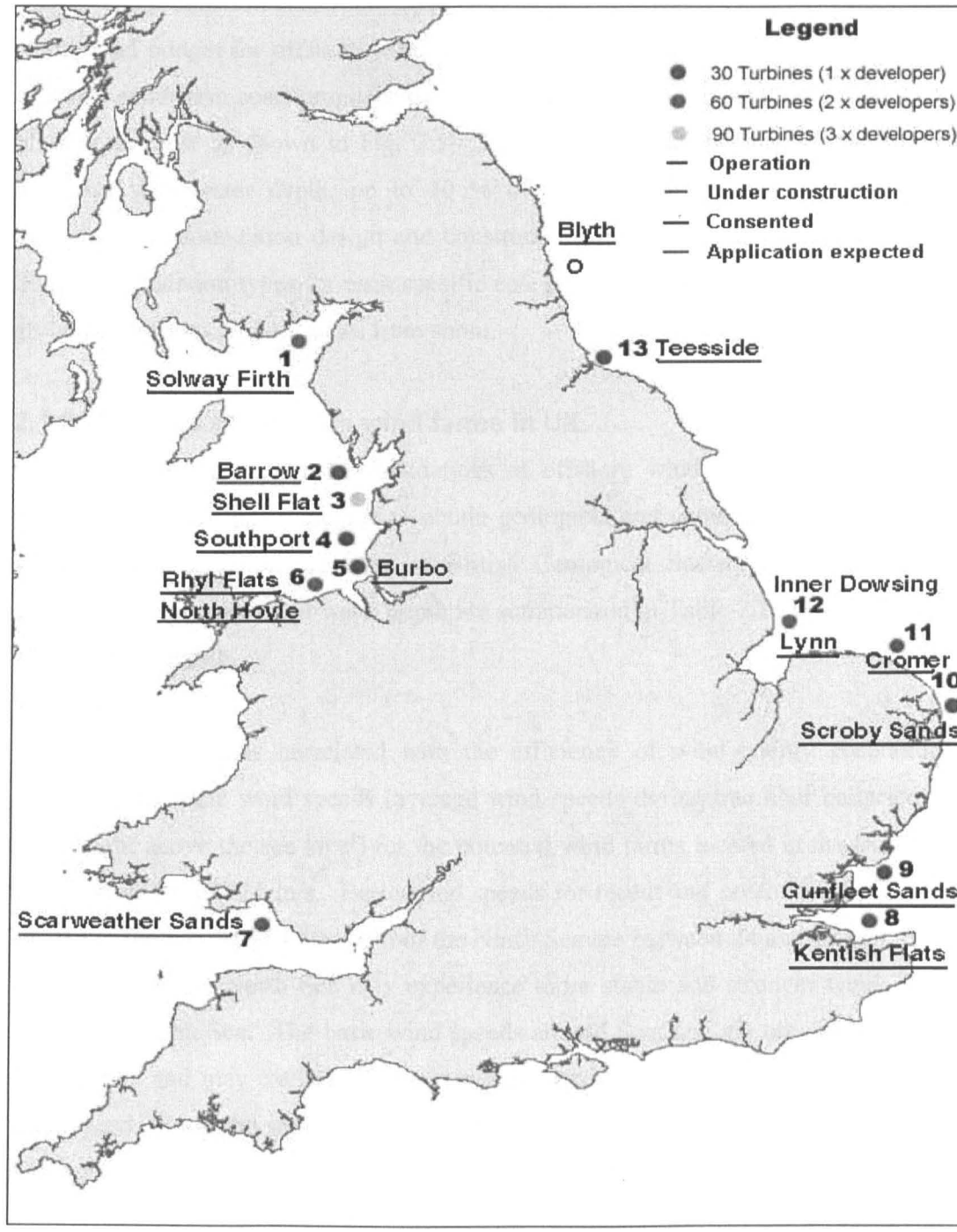

Fig. 2.4 Locations of UK current and potential offshore wind farms (after. Powergen Renewables, 2002)

wind farm project. There are a further twelve offshore wind projects being considered. Locations of these potential and current offshore wind farms around the UK are shown in Fig. 2.4.

The foundation construction cost for offshore renewable energy is a large part of the total budget for offshore wind farm construction. According to the European offshore wind farm costs proposed by the OWE in 2001, the foundation cost is 25 % of the total cost as shown in Fig. 2.5. The need for more expensive foundations increases with water depth, up to 30 % of the total cost. This highlights the importance of foundation design and construction for offshore renewable energies. Suitable foundation types for each specific energy system are based on water depths, ground conditions and distances from shore.

2.1.2. Features of offshore wind farms in UK

In order to design the foundations of offshore wind energy systems, it is necessary to characterise the site to obtain geological and geotechnical information. Wind farm information provided by British Geological Society including seabed conditions, wind speed and water depth are summarized in Table 2.1 to help offshore wind farm selection.

Wind speed

Wind speed is correlated with the efficiency of wind energy generation. Basically, the basic wind speeds (average wind speeds during one hour collected at 10m height above the sea level) for the potential wind farms located in the Irish Sea are between 22 and 24 m/s. Basic wind speeds for recent and potential wind farms located in the middle and the south of the North Sea are between 24 and 25 m/s. The wind farms in the North Sea may experience more stable and stronger winds than those in the Irish Sea. The basic wind speeds around Scotland are obviously higher than 25 m/s and may exceed 27 m/s in the northwest area. On the other hand, the wind speeds along the south coast of England coastlines are only 22 m/s, which are relatively low compared to other coastlines in the UK.

Generally, the basic wind speeds in the offshore areas around the UK are of good quality for offshore wind development because the nominal wind speed (operational wind speed for wind turbine) to drive large offshore wind turbines may be as low as 20 m/s. Indeed, the nominal wind speed for the Blyth offshore wind turbines (two megawatt) is only 17 m/s.

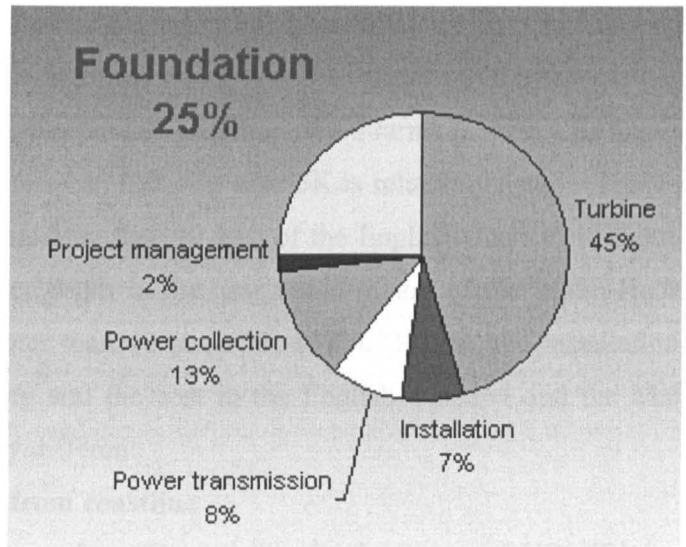

Fig. 2.5 Breakdown of initial capital cost (OWE, 2001)

Table 2.1 Features of UK current and potential wind farms

Map ref	Project Site	D (km)	W.D/M.W.H	B.W.S/C.S	Site Geology	Seabed Sediment
Current	Blyth	1	8/20	25/0.6	Sandstone	Sand, Muddy Sand
1	Solway Firth	8.5	20/14.5	24/1.5	Mudstone	Muddy Sand
2	Barrow	10	20/16	24/1.0	Mudstone	Gravel, Gravelly Sand
3	Shell Flat	7	20/16.5	23.5/1.0	Mudstone	Muddy Gravel
4	Southport	10	20/16.5	23/1.0	Mudstone	Sand
5	Burbo	5.2	18/17	22.7/1.0	Mudstone	Sand, Muddy Sand
6	North Hoyle	6	18/17	22.7/0.9	Sandstone	Sandy Gravel, Gravelly Sand
7	Scarweather Sand	9.5	20/15	22/1.5	Mudstone	Sandy Gravel, Gravelly Sand
8	Kentish Flats	8	10/8	24.5/0.9	Limestone	Sand, Gravelly Sand
9	Gunfleet Sands	7	10/8	24/1.25	Silstone	Muddy Sand
10	Scroby Sands	3	8/18	25/1.3	Mudstone	Sand, Gravelly Sand
11	Cromer	6.5	15/20	25/1.5	Chalk	Sandy Gravel
12	Lynn and Inner Dowsing	5.2	10/20	24.5/1.1	Chalk	Sand
13	Teesside	1.5	20/20	25/0.65	Mudstone	Sand, Muddy Sand

D: Distance away from coastline (km) B.W.S: Basic wind speed (m/s)
M.W.H: Maximum wave height (m) C.S: Current speed (m/s)
W.D: Water depth (m)

Water depth

For existing and former offshore wind farm projects such as Blyth and Scroby Sands, wind systems are only planned to be installed in shallow water areas where shallow is defined as less than 20 m. The water depth for later projects will exceed 20 m in some cases. Currently few existing offshore wind farms in the world are

installed in such water depth, but many potential projects in Europe will be designed for deep water (over 20 m).

Compared to potential offshore wind farms in west UK, the water depth of the potential offshore wind farms in east UK is relatively small. The water depth in the near shore region (less than 10 km) of the English Channel is about 20-40 m (BGS, 1992). The water depth in the near shore region of the Malin-Hebrides sea area in Scotland is greater than 40 m (BGS, 1993). Hence, the installation techniques, the hydraulic loading and the cost in the English Channel and the Malin-Hebrides sea sites will be very different.

Distance away from coastline

The distance from the coastline for the proposed UK offshore wind farms has increased dramatically. In existing and recent projects, the distance is normally less than 3 km away from the coastline. On the contrary, a distance of 5 km to 10 km is to be selected for later projects.

Maximum wave height

It is expected that the offshore wind systems in east UK will encounter relatively high waves (say 20 m), and it should be borne in mind that high waves will increase the dynamic wave impact especially in shallow water conditions. Hence, the selection of a shallow water site should be avoided in a high wave area.

Current speed

Based on the data in Table 1, the farms east of England have higher current speed than those west of England. The water depth may be limited for the wind farms east of England, which normally have high current speed (1.1-1.5m/s). The current force acting on the wind structure is in proportion to the water depth and the current speed. Sites with high current speed should be avoided if possible. The development of tidal stream energy farms should be considered in these locations.

Site sediment

The sediments in current and potential sites are mostly sand, gravelly sand or muddy sand, which can be described as cohesionless siliceous soils. The soil strength at a site will depend on the property of the site sediment. Generally, the end bearing capacity varies from 2 MPa for very loose sand or muddy sand to 12 MPa for very dense sand or gravel; the skin friction value varies from 48 kPa for very loose sand or muddy sand to 115 kPa for very dense sand or gravel (API, 1993).

Sands may be loose on sites with sand waves such as Kentish Flats, Gunfleet Sands and Scroby Sands. So the friction angle of the sand sediment will decrease with an increase in its void ratio. In addition, the liquefaction of soil may occur due to the rapid reduction of effective stress during installation. Hence, gravity foundations may be unsuitable for these sites. Taking the Scroby Sands wind farm project as an example, steel monopiles are to be used and they are designed to pass through the 5-10 m sand layer to reach the clay layer underneath. On sites with muddy sand, which contain a portion of silt and clay sediments, the soil capacity could be reduced and consolidation may occur. The seabed sediments in the English Channel are gravel and sand; gravelly sand as well as sandy gravel, so this area may be stable for gravity and pile foundations (BGS, 1992). The near shore seabed sediments in the Malin-Hebrides sea area in Scotland mainly consist of muddy sand and sandy mud which contain a high portion of silt and clay. Pile foundations or gravity caissons may be used (BGS, 1993).

Seabed condition

Generally the underlying rocks at the planned and current sites are mostly composed of mudstone, but some sites such as Blyth and North Hoyle are composed of sandstone. A few sites such as Cromer and Lynn and Inner Dowsing are composed of chalk. Drilling with water in mudstone and chalk should be avoided to prevent softening. In addition, faults across or close to the site should be avoided especially for the sites in the Irish Sea region.

The geological profile in the English Channel may contain Lower Greensand, Upper Chalk, London Clay, sandstone and mudstone along the east-west coastline (BGS, 1992). The geological condition in the Malin-Hebrides sea area is complex due to the inclusion of some metamorphic rocks. From the north to the south of the coastline the seabed may mainly include Proterozoic Torridonian rocks (contain unmetamorphosed predominantly arkosic sandstones, siltstones and mudstones), Moine rock (sequence predominantly composed of merasediments) and Dalradian rock (late Precambrian metamorphosed marine sediments) (BGS, 1993). If the site is on the rock, the capacity is normally sufficient for gravity or pile foundations. If drill piles are to be used, seabed strength may decide the selection of drilling machines and grouting materials.

2.1.3. Current offshore wind farm types

The configuration of foundations for offshore wind turbines can be categorized into four basic types: gravity foundations, monopile foundations, tripod foundations and floating structures. Key properties are provided by DNV (2004) and include water depth, installation and structure geometry which are summarized in Table 2.2 for offshore structure selection.

Table 2.2 Features of offshore foundations

Features	Monopile	Gravity	Tripod	Floating
Main structure	A cylinder steel tube with a large diameter	A ballast pumped-in sand, concrete, rock or iron	Three cylinder tubes and a three-leg structure	Tensile piles or anchors with steel cables
Structure property	Simple fabrication easy installation	Lots of ballast material needed to providing sufficient dead loads	Structure complexity	A fully commissioned condition from the fabrication and out-fitting yard
Sea bed preparation	No	Need	No	No
Suitable water depth (m)	0 – 25 Max. 50 m	0 – 10 Shallow water	20 – 50	50 – 500 Deep water
Unsuitable ground	Dense soil above soft soil (punctual shear and tensile force)	Soft soil (differential settlement, scour)	Dense soil above soft soil (punching shear and tensile force); soft soil (scour); large boulder	Soft soil (scour)
Installation	A floating crane vessel may needed for pile driven or flat top barges mounted with a land based crawler crane for drilling jack-up	Placing in the position	A floating crane vessel may needed for pile driving or flat top barges mounted with a land based crawler crane for drilling jack-up	Under water pile driven or drilled method
Transportation	Lift or float into position	Draft during sea transport	Lift or float	Float
Design concern	Overall deflection and vibration	Scour protection and shear between sea bad and base	Sufficient depth to against scour; deflection	Sufficient depth to against scour

Gravity foundations

Generally, gravity base structures or gravity foundations (see Fig. 2.6) have been used in medium water (about 12m) in the Norwegian sector of the North Sea and in the UK sector.

According to many publications on offshore wind energy, gravity foundations represent the traditional solution. The extremely heavy weight of the gravity base is used to maintain the whole structure in an upright position while the wind turbine and the support structure carry the wind and wave loading, respectively. It should be borne in mind that lateral resistance of this structure is based on the gravity load and the friction between the foundation and the seabed. Thus the weight of gravity foundations needs to be enlarged with respect to the increase in water depth, because of additional lateral loading from waves and currents. The wave height is scaled up

with the water depth, causing greater drag force. Soker et al. in 2000 mentioned that the gravity foundation is commercially unfavorable in water depths in excess of 10 m while its physical characteristics limit its use in areas of more than 20 m.

When carrying out the stable gravity foundation design, the bearing capacity, overturning stability, resistance to sliding as well as allowable settlement should be considered. The analysis of bearing capacity is based on the equations for shallow foundation capacity proposed by CEN Eurocode 7 Part 1 (2004). According to API RP 2A-LRFD (1993), the factor of safety for shallow foundation capacity is recommended to be 1.5. The ultimate bearing capacity of shallow foundations on sand can be obtained from standard penetration tests, SPT, and cone penetration tests, CPT. Empirical formulae are suggested by Tomlinson, 2001.

The risk of overturning still exists at the toe of the foundation and has to be considered. The resistance of overturning is mainly produced by the weight of the structure to overcome the overturning moment caused by lateral force applied at the pile head. The resistance to sliding of a wind tower foundation may depend on the friction resistance caused by gravity loads to resist the maximum horizontal forces acting on the structure. According to API RP-2A LRFD (1993) and DNV (2004), the factor of safety for sliding is recommended to be 1.25.

Foundation settlement can be roughly divided into three types: immediate settlement, and primary and secondary consolidation settlements. Immediate settlement takes place during or immediately after the construction. Primary consolidation settlement takes place with time after construction due to the

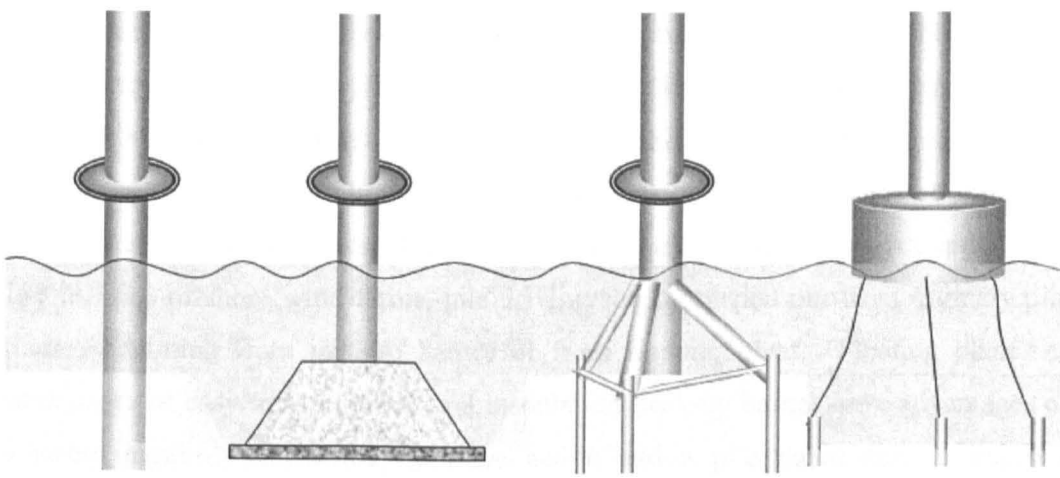

Fig. 2.6 Foundation types for offshore wind farm

dissipation of pore pressure inside the soil. Secondary consolidation (creep) settlement takes place after the primary consolidation because of the adjustment of the soil fabric.

Pile foundations

Pile foundations have been used to support offshore oil and gas platforms, and many recommended practices and guidelines for offshore pile designs have been published. For instance, the American Petroleum Institute issued its own recommended practices for fixed offshore platforms. Monopile foundations (see Fig. 2.6) have been developed in conventional offshore industries and been used for wind farms. Compared with oil and gas platforms, which are normally supported by 3 or 4 big legs, a wind platform is only supported by a monopile. The application of monopile foundations seems more conservative, because the maximum water depth for a monopile structure is identified to be 20m, which is proposed by Soker et al. in 2000. Compared with gravity foundations, which require the seabed to be flattened and covered with a layer of shingle, monopiles do not need special seabed preparation. Monopiles used for offshore wind energy foundations may be subjected to a larger proportion of live load compared to dead load (Fig. 2.9). So the foundations may have to endure large shear forces, bending moments as well as a relatively small proportion of axial compressive loads. Cyclic loading of top soils and the potential of soil erosion near the surface should be considered.

Monopiles used for offshore wind farms are usually installed by pile driving techniques which are preferred for loose water-bearing sands and gravels. Pile driving can be carried out by different types of hammers: drop hammer, compressed-air hammer, double-acting pile hammer, diesel pile hammer as well as hydraulically operated hammer. Amongst all these hammers, the hydraulically operated type is widely used in offshore piling because it produces less noise and vibration, and it does not emit exhaust fumes. Importantly, it can be operated in water depths up to 100 m. For offshore wind farms, pile driving can be carried out from ordinary pile frames operating from jack-up barges or from floating plant. Floating plant has advantages of easy transportation and installation; jack-up barges have advantages of a stable platform unaffected by wave action and a pile guide unit to improve installation accuracy. A monopile is usually an open-end tubular steel tube with a large diameter. The circular section offers less resistance to waves and currents than the rectangular section. The open-end at the pile tip provides sufficient penetration to

resist lateral and uplift loading. When driving to a deep penetration into very stiff clays, dense granular soils, or rocks, a pile tip should be protected by a steel ring or a cast-steel shoe. In addition, a drill-and-drive technique may be adopted in difficult ground conditions; a rotary cutter can be used for drilling out the soil plug from within the tube pile after the pile is driven down to the maximum depth where the driving stresses exceeding tolerable limits. When the installation is completed, a rigid plate can be placed at the pile tip in order to provide sufficient pile-end bearing capacity.

When carrying out the pile foundation design, the bearing capacity, horizontal load and bending moment on a pile and allowable settlements should be considered. Based on the load transformation on the pile, the ultimate bearing capacity of a pile can be estimated by calculating the load-carrying capacity of the pile point and frictional resistance on soil-pile interface. According to API RP 2A-LRFD (1993) and DNV (2004), the factor of safety for pile foundations under extreme environmental conditions is recommended to be 1.25. For pile point capacity, calculations may refer to CEN Eurocode 7 Part 1 (2004). For frictional resistance in sand, calculations may refer to Bhusan (1982).

Horizontal loads and bending moments acting on the superstructure can be transformed into a horizontal component of load and a component of moment acting on the pile head respectively. The magnitude of moment on the pile head can be presented by equivalent lateral load times a distance between the ground level and loading position. In the same way, the lateral load on the pile head can also be described as equivalent bending moment acting on the pile at the ground level. There are two types of pile head; one with a pile cap is defined as a fixed head pile whereas the other without a pile cap is defined as a free head pile. For this reason, a monopile foundation connected under a steel wind tower can be classified as a free head pile. The analysis of a free head pile is given by Tomlinson (2001).

The total settlement of a pile, S, is composed of the settlement of pile shaft, S_1; the settlement of pile caused by the load at the pile point, S_2; and the compression of pile caused by the load transmitted along the pile shaft, S_3. Details are given by Vesic (1977) and Das (1995), for example.

Tripod foundations

Tripods were originally used for oil and gas offshore foundations, and this type of foundation was adopted for offshore wind energy system in 1990 in Blekinge,

Sweden with 6 m water depth (OWE, 2001). A normal tripod foundation is composed of three sections: a centre column, a steel space frame and three driven piles (see Fig. 2.6). The centre column supports the superstructure, and the load on the column is transmitted through the steel space frame to the three driven piles at the three corners. The seabed does not need preparation, but the gap between piles and pile sleeves on the steel space frame should be fixed with grout. The penetration depth and bearing capacity for each tripod driven pile are similar to monopile designs. A tripod structure is treated as a lightweight structure when compared to a monopile but with smaller allowance for aerodynamic damping. The bending moment caused by wave loading for a tripod foundation is only 10 – 25 % that of a monopile when the water depth is less than 11 m. Although greater water depths cause higher wave loading, the aerodynamic force is still the main contribution to the bending moment acting on the tripod. Hence, this kind of structure is suitable for greater water depths. The three driven piles may be replaced by three drilled and grouted piles when the ground is very stiff soil or rock (Soker et al., 2000).

Floating foundations

Floating offshore wind farms have been developed since the 1990's, but this kind of wind farm has not been used until now. To overcome the limitation of water depth (more than 100 m) for other types of offshore wind foundations, floating structures are going to be used with a maximum water depth of 500 m (Tong, 1998). Floating wind farms are suitable for use in the northern North Sea, parts of the Irish Sea, the Baltic and most of the Mediterranean Sea due to deep and steep seabeds (UCL, 2001).

Floating structures can be divided into the buoy type where the main structure floats at sea level and the submersible type where the main structure submerges (see Fig. 2.6). The buoy type is composed of a floater system (includes the tower, the floater hull and a rotor), a hull, and a mooring system (includes mooring lines and piled anchors). Piled anchors are used to resist the tensile force transmitted through moorings. The semi-submersible type is composed of a submerged pontoon with some turbine towers and a permanent mooring system. Piled anchors may be used as well. The amount of force distributed on each anchor will depend on the buoyant force from the floating structure and the number of moorings. The length of the anchors must provide enough friction capacity to resist the tensile forces. In addition,

seabed erosion at the anchors caused by cyclic loading should be investigated, and the cable near the seabed surface needs to be protected by grouting.

Tension (anchoring) pile foundations are used for floating platform systems. The tensile force is transmitted from the floating structure through the steel cable into the anchored pile foundation. There are various types of anchoring piles, but the theory for pile design is similar. Details of calculation of pullout resistance for a monopile are given by Das (1995), for example.

2.1.4. Offshore monopile foundations

An overview of the features of offshore foundations presented in Section 2.1.3, shows that monopiles have more advantages than other types of foundations (see Table 2.2). The water depths of UK's current and potential wind farms are between 8 and 20 m which are suitable for pile foundations. These foundations can also be used when water depth exceeds 30 m which not be appropriate for gravity foundations. Floating foundations may be used only when the wind farm is in deep water (more than 50m). Monopiles may be more suitable than tripod foundations because of the reduction of effect of scour in soft soils. Again, the techniques of transportation and installation also show many advantages for monopiles. Recent wind farm construction vessels are able to store 10 sets of wind turbine assemblies and their foundations (Note: each monopile can be 300t in mass, 60 m long and 6 m in diameter); wind structures can be transported to anywhere with maximum operating water depth of 36m. The jacking speed is between 1.5-2 m per minute depending on pay loads, and the vessels can stay at sea for 30 days.

A 50 m long steel tube with a diameter of 4 m was used for the monopile foundation at the wind farm of North Hoyle (see Fig. 2.7). Installation was carried out by using jack-up barge "Excalibur". The piles were hammer driven to a depth of 10-15m below seabed (see Fig. 2.8). The average installation rate was 1 pile every 132 hours (about 5 days). The successful project in North Hoyle suggests that monopile is the best choice for UK offshore 2MW wind turbines.

Loading conditions for onshore and offshore wind farms are very different as indicated in Fig. 2.9. Onshore pile foundations are usually used to transmit large vertical loads from the superstructure through weaker subsoil into the underlying bearing strata. Horizontal loads acting on pile foundations are often ignored as they are much smaller than the vertical loads. Foundations for offshore structures,

however, withstand significant environmental loads from waves, currents and wind giving rise to lateral loads that could be up to one third of the vertical loads (Soker et al., 2000). The structure of a 2MW offshore wind turbine in 10m of water could be

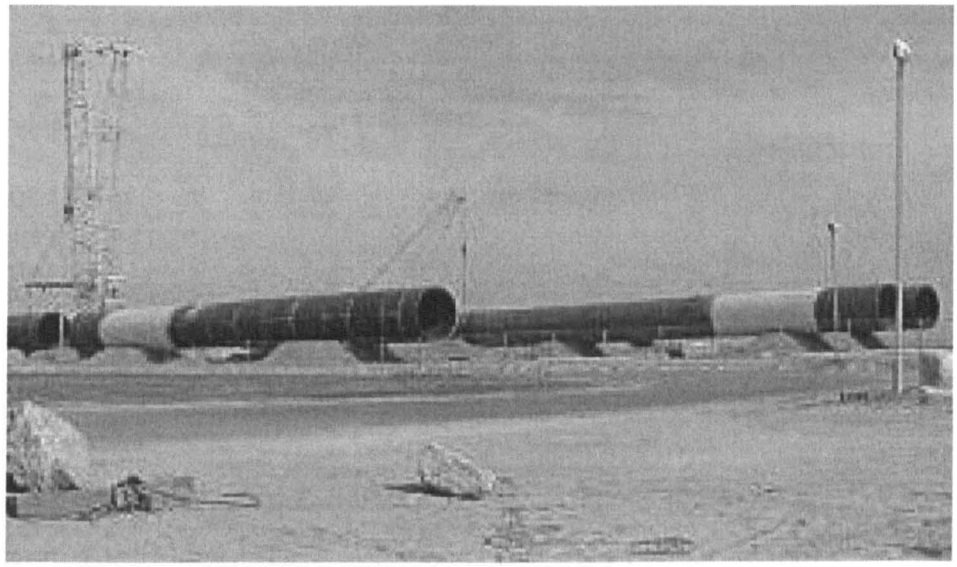

Fig. 2.7 Monopile foundations for offshore wind used in North Hoyle (source: www.natwindpower.co.uk, 2003)

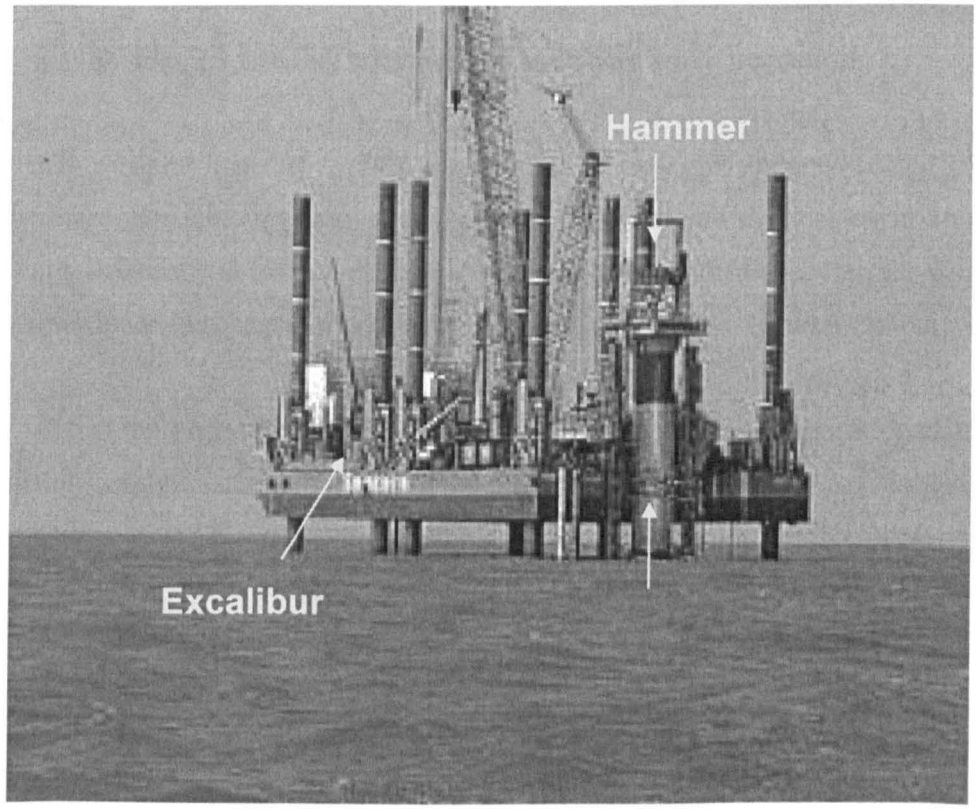

Fig. 2.8 Installation of pile foundations in North Hoyle (source: www.natwindpower.co.uk, 2003)

	Onshore	Offshore
Self weight	√	√
Wind load	√	√
Wave load	X	√
Current load	X	√
Scour	X	√

Lateral load acting on **onshore** wind structure only **10%** of the total vertical load < Lateral load acting on **offshore** wind structure may up to **30%** of the total vertical load

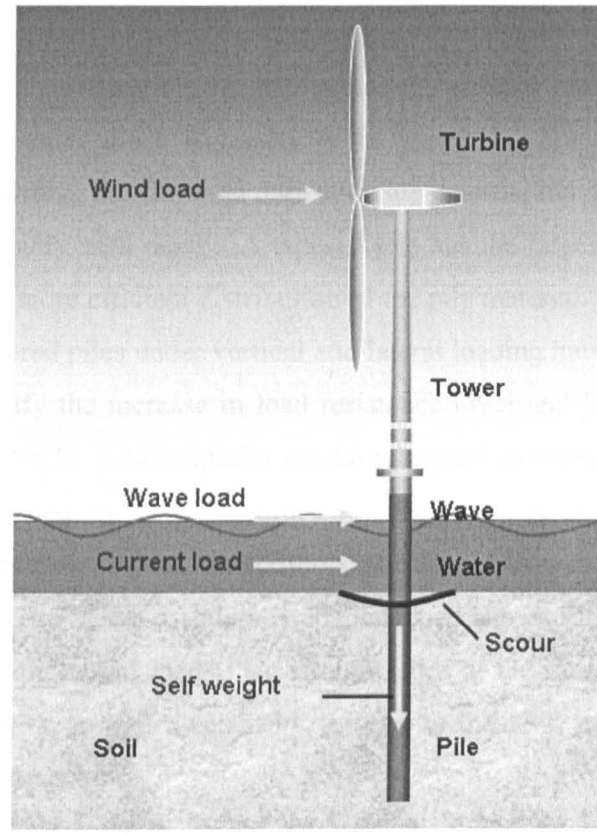

Fig. 2.9 Loading conditions of a offshore wind foundation

subjected to lateral loads of 1.2 MN compared to its total gravitational load of 3 MN. Furthermore, the structure might be subjected to significant cyclical environmental loads at a frequency of around 0.1 Hz. At critical levels and frequencies, the cyclical horizontal loads can cause a reduction in lateral resistance (Ramakrishna and Rao, 1999).

Thus the costs of foundations are more significant for offshore foundations. Reductions of the pile length and the pile diameter are two important cost factors due to the cost of material, transportation and installation. Sufficient bearing capacity and lateral resistance are to be maintained when trying to reduce the pile size. Alternative methods to increase pile vertical and lateral capacities should be considered. For example, the close-end tip can increase the pile end bearing capacity but it does increase the installation cost. In order to improve pile lateral resistance, many innovative piles such as taper, tripod and finned pile foundations have been proposed.

2.2. Innovative pile foundations

2.2.1. Taper pile

In order to improve the lateral resistance of pile foundations, tapered piles have been proposed by many researchers since Robinsky et al. in 1964. For a laterally loaded pile, the maximum bending moment and deflection are near the top of the pile, and both values decrease rapidly with depth. A tapered pile has the largest cross section at the top representing a more efficient distribution of the pile material.

A series of model tests on tapered piles under vertical and lateral loading have been carried out, respectively, to verify the increase in load resistance (Wei and El Naggar., 1998; El Naggar and Wei, 1999). Load capacity on the pile head increases with an increase in the taper angle. Capacity increases with an increase in the taper angle especially when the confining pressure is low. In addition, pile tip pressure can be reduced by using tapered piles. The study of laterally loaded piles shows that tapered piles can resist up to 75% more lateral loads than straight piles at the same displacement. Again, the increase in taper angles can help to increase the ultimate lateral load and reduce the lateral displacement.

A tapered pile could replace a monopile for an offshore wind foundation because of the improved lateral load resistance. The efficient use of material is an important merit for tapered piles. However, the pile end resistance could be lost due to the reduction of the tapered pile bottom cross section. The cost of manufacturing tapered piles is likely exceed that of tubular piles. Further study should be carried out to verify reliability of tapered piles. The installation method of tapered piles may be the same as that for monopiles.

2.2.2. Tripod pile

Tripods have been used in offshore oil and gas structures because of smaller installation equipment needed compared to monopiles. Tripods have been used in offshore wind farms in Sweden and Denmark where water depths are 6 m and 50 m, respectively (OWE, 2001). The three piles on a tripod structure can be replaced by suction bucket anchors in order to eliminate the need for pile driving.

1G model tests of tripod foundations (one vertical tripod and three inclined tripods with various tilt angles) have been carried out; both lateral static and cyclic loading were included. The lateral load increases with an increase in tilt, and the

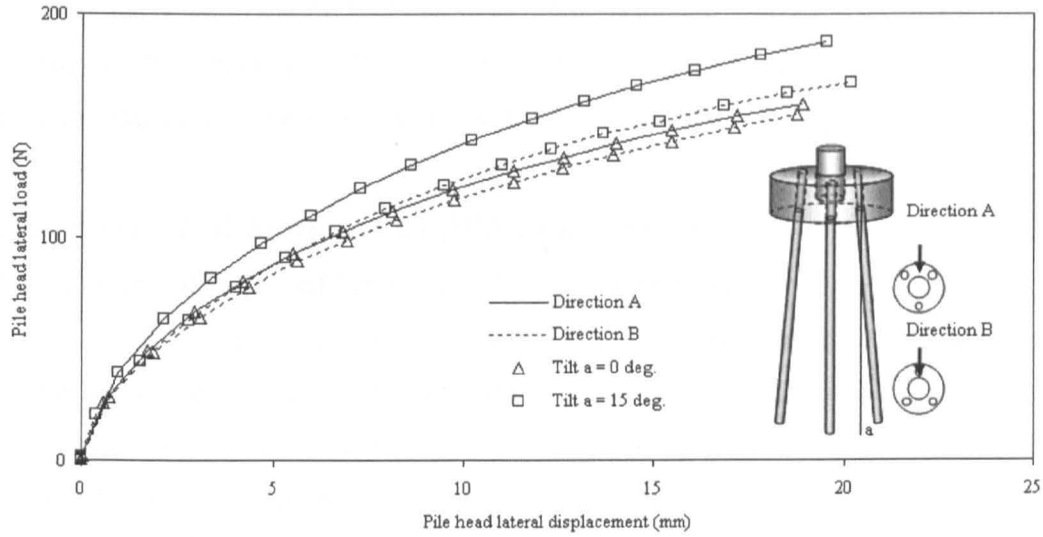

Fig. 2.10 P-Y curves of tripods subjected a static lateral load (source: Ozsu, 2005)

group efficiencies are from 60% up to 80%. The load direction affects the lateral resistance with the difference being 10% (Fig.2.10).

Zaaijer (2002) compared monopile and tripod foundations under the same loading capability. The cost of a tripod is slightly more expensive than that of a monopile due to the increased complexity and workspace requirements.

2.2.3. Finned (Rocket) pile

Lee and Gilbert (1980) and Irvine et al. (2003) described a rocket or a finned pile as a pile that has four plates welded to the top of a traditional monopile at 90° to each other. Many observations show that the maximum bending moment and lateral deflection of a lateral loaded pile are usually in the upper part of the pile. By using fins, the lateral resistance may improve because of the increase in flexural rigidity, EI, of the pile and of the cross section area.

Finned pile tests in soft clay under static and repeated loading were carried out by Lee and Gilbert (1980). The finned pile (Fig. 2.11(a)) was subjected to a lateral force through a cable provided by a loading crane shown in Fig. 2.11(b).

Movements of the finned pile subjected to various loading conditions are shown in Fig. 2.11(c). The deformations enlarge with an increase in load value; deformations in cyclic loading are higher than in static loading. The measured and calculated results of bending moments along the pile are presented in Fig. 2.11(d). Although there was a general agreement between measured and calculated results, the

bending moments in the fin sections were not presented to verify the influence of fins on the bending moment. The improvement of lateral resistance of a finned pile compared to a monopile pile was not included in the study.

2.3. Review of analysis of pile foundation

2.3.1. Determination of limit state for lateral loaded pile

A limit state is a condition when a structure can no longer satisfy the design requirement; and a load at the limit state is called an allowable load. The ultimate limit state (ULS) corresponds to the maximum load carrying resistance; the serviceability limit state (SLS) corresponds to tolerance criteria applicable to normal use. For laterally loaded piles, the ultimate lateral load represents the maximum load in ULS design; and allowable lateral displacement and tilt represent the tolerance criteria in SLS design. In addition, the fatigue limit state (FLS) corresponds to failure due to the effect of cyclic loading. For piles under cyclic lateral loading, the reduction of pile-soil stiffness due to the number of cycles should be related to a factor of safety.

DNV (2004) proposed the FLS should be considered within the SLS; and SLS is the main consideration due to the displacement and tilt of offshore pile foundations. In the design of laterally loaded piles, two requirements should be fulfilled: the total lateral pile resistance should not be less than the lateral load; the lateral displacement at the pile head should not exceed some specified limit, typically 10% of the pile diameter.

Empirical methods

In order to predict the ultimate lateral load, many simplified empirical methods have been proposed. Laterally loaded piles in these studies are divided into two types, rigid and flexible piles. The characteristic length, T, is defined to be $(E_pI_p/n_h)^{0.2}$ where E_pI_p is the pile flexibility and n_h is the constant of horizontal subgrade reaction. When the pile length $L \geq 5T$, the pile is considered to be a long pile. When the pile length $L \leq 2T$, the pile is considered to be a rigid pile. The piles can also be divided into two types, free and fixed head piles, depending on their pile head conditions. When there is no restraint of rotation on the pile head, the pile is considered to be a free head pile, otherwise the pile is considered to be a fixed head

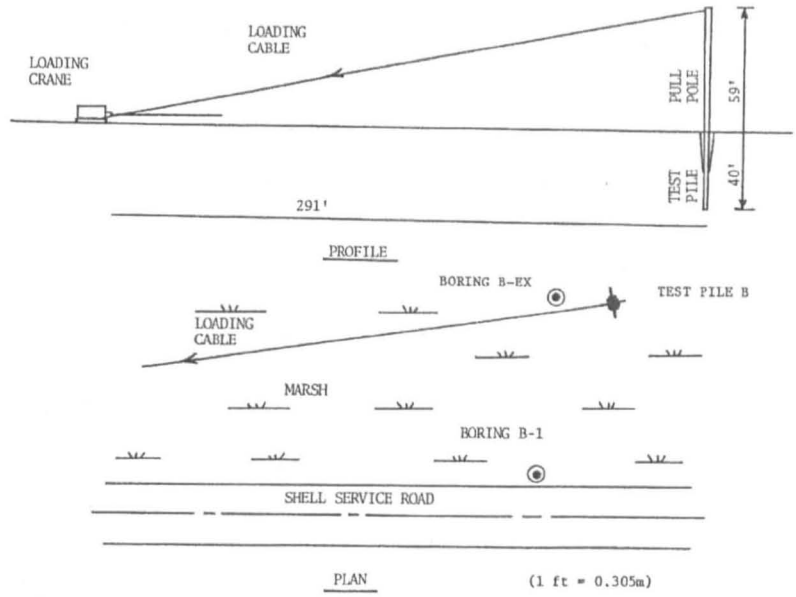

Fig. 2.11(a) Arrangement of a lateral loading test of a finned pile (source: Lee and Gilbert, 1980)

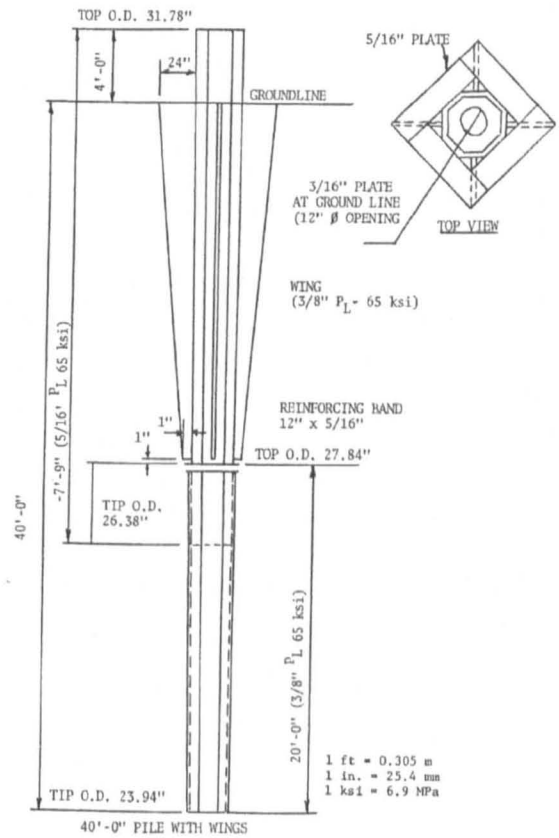

Fig. 2.11(b) Schematic diagram of a finned pile (source: Lee and Gilbert, 1980)

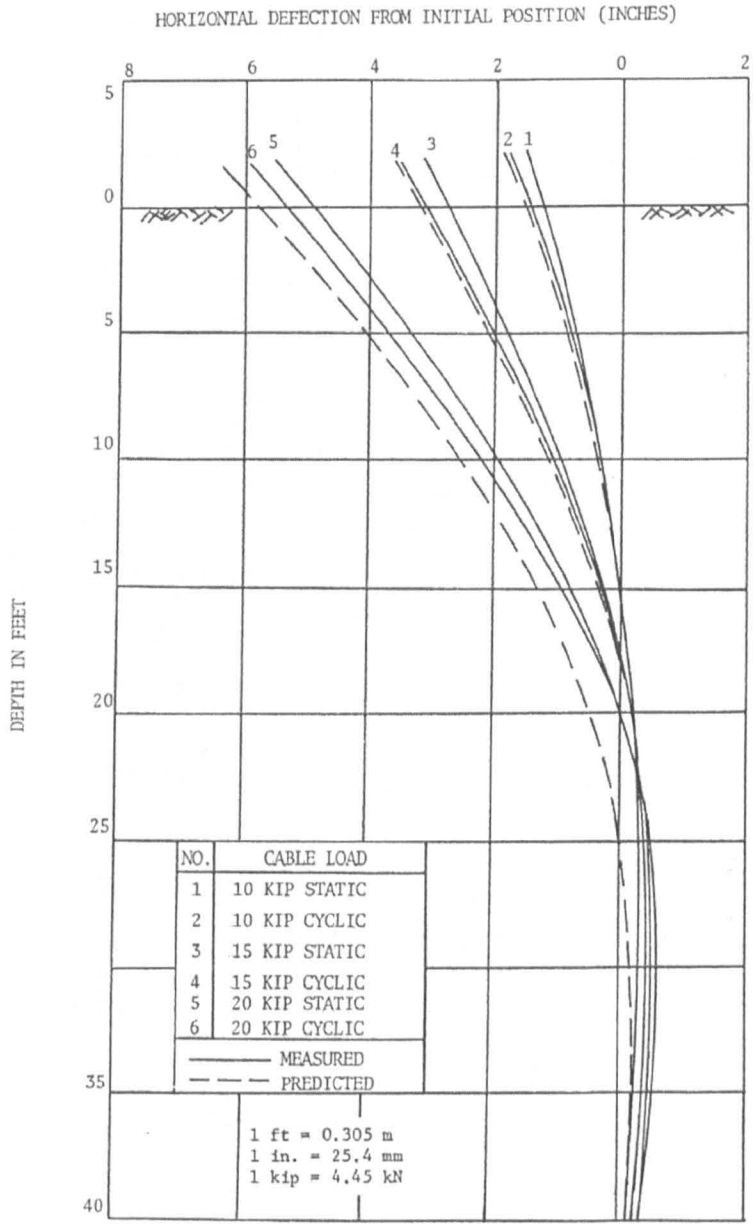

Fig. 2.11(c) Deflections along the pile under static and cyclic lateral loads (source: Lee and Gilbert, 1980).

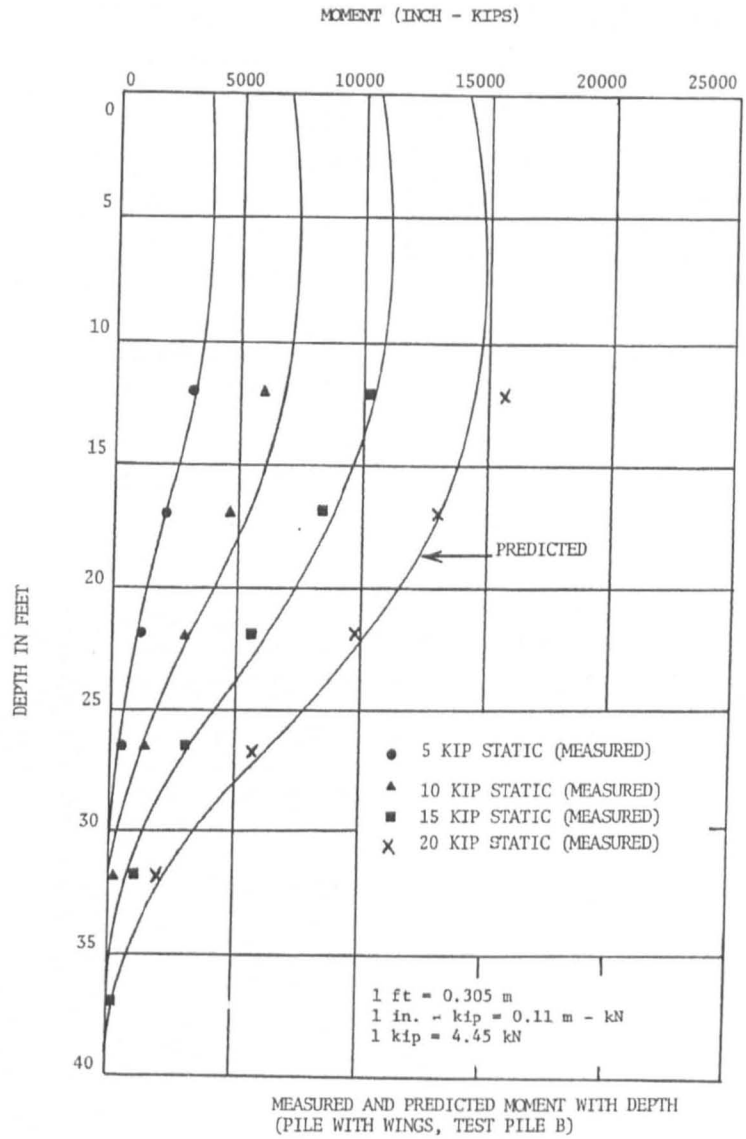

Fig. 2.11(d) Bending moments along the pile under static lateral loading (source: Lee and Gilbert, 1980).

pile. In this study, the review of these methods is restricted to free-head rigid piles in sand because most current pile foundations of offshore wind systems are free-head rigid piles, and over 80% of potential wind farms in UK are located in sand.

Brinch Hansen (1961) recommended a method for the calculation of the ultimate lateral resistance of free-head rigid piles in a single or layered soils. The ultimate lateral load acting on the pile is given by Equation 2.1. The earth coefficient is based on earth pressure theory. A trial and error procedure is used to find the point of rotation to maintain lateral force equilibrium.

$$p_u = K_q \gamma' z D \tag{2.1}$$

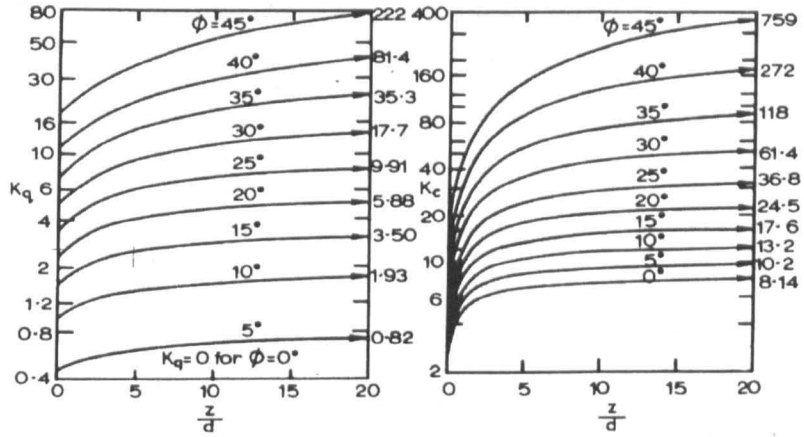

Fig. 2.12 Lateral Resistance factors, K_q and K_c (Source: Brinch Hansen, 1961)

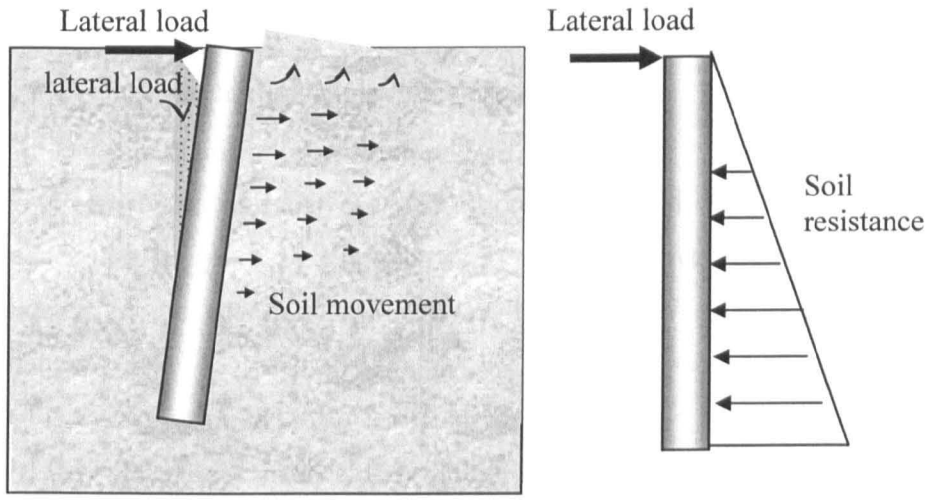

Fig. 2.13 Laterally loaded pile presented by Broms method

where p_u = ultimate resistance of the soil in the unit of force per pile length (kN/m)

K_q = Hansen earth pressure coefficient which is a function of ϕ' and $\frac{z}{d}$, values of K_q can be found in Fig. 2.12.

D = pile diameter or width of pile (m) (note: D is represented by d in Fig. 2.12)

γ' = effective unit weight of soil (kN/m^3)

z = embedded depth of pile (m)

Broms (1964 a, b) introduced an empirical method to predict ultimate lateral load by simplifying the distribution of ultimate soil resistance. Broms method can be applied to different pile head conditions (free head and fixed) and different pile flexibility conditions (rigid and flexible). In Broms method, the soil located in front of the pile moves in an upward direction (Fig. 2.13), whereas the soil located at the

rear of the pile moves downward and fills the void created by the lateral deflection of the pile. At relatively large depths, however, the soil located in front of the pile will move laterally to the rear of the pile instead of upward. Rotation of a pile is ignored. The ultimate lateral resistance in Broms method is presented in Equation 2.2. In this method, the active pressure at the rear of the pile is ignored, and the resistance equals 3 times the pressure in front of the pile. Based on observation of many field test results, Broms method is relatively conservative (Poulos and Davis, 1980).

$$p_u = 3\sigma_v' \; K_p D \tag{2.2}$$

where p_u = ultimate resistance of the soil in the unit of force per pile length (kN/m)

σ_v' = effective vertical overburden pressure (kN/m^2)

K_p = Rankine's passive earth pressure = $\dfrac{(1+\sin\phi')}{(1-\sin\phi')}$

ϕ' = internal friction angle (effective stress)

D = pile diameter or width of pile (m)

Petrasovits and Award (1972) recommended that the ultimate lateral resistance can be given by Equation (2.3). Both passive and active pressures are considered in the equation, and a shape factor of 3.7 is applied to the passive resistance.

$$p_u = (3.7K_p - K_a)\,\gamma\, z\, D \tag{2.3}$$

where p_u = ultimate resistance of the soil in the unit of force per pile length (kN/m)

K_p = Rankine's passive pressure = $\dfrac{(1+\sin\phi')}{(1-\sin\phi')}$

K_a = Rankine's active pressure = $\dfrac{(1-\sin\phi')}{(1+\sin\phi')}$

γ = unit weight of soil (kN/m^3)

z = embedded depth of the pile (m)

D = pile diameter or width of pile (m)

Meyerhof et al. (1981) proposed that the ultimate lateral load, P_u, can be expressed by the resultant net soil pressure and a shape factor (see Equation 2.4). The dimension factor of pile length to pile diameter (L / D) and the friction angle (ϕ') are used to determine the net passive earth pressure. However, the rotation point is assumed to be at the pile tip, and the resistance at the rear of the pile is ignored.

$$P_u = 0.12\gamma' DL^2K_b \tag{2.4}$$

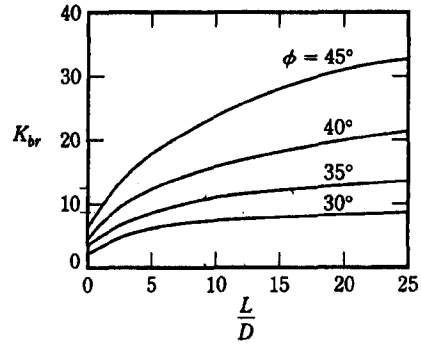

Fig. 2.14 Variation of resultant net soil pressure coefficient, K_b versus shape ratio of L/D (source: Meyerhof, 1981)

where P_u = ultimate lateral load (kN)

D = diameter of pile (m)

γ' = effective unit weight of soil (kN/m^3)

L = embedded length of the pile (m)

K_b = coefficient of net passive earth pressure (Refer to Figure 2.14)

Fleming (1992) suggested the constant shape factor 3 in Brom's method should be replaced by K_p. Fleming's method could be too conservative because K_p is higher than 3 in many cases. In addition, Patra and Pise (2001) suggest the ultimate lateral resistance in Meyerhof's method should be multiplied by a shape factor of 3 to fit the observed results.

Prasad and Chari (1999) proposed an empirical method to predict the ultimate lateral load. The lateral load is presented as a function of a rotation point shown in Equation 2.5. Importantly, it includes the side shear and passive earth pressure around a pile subjected to a lateral load represented in Fig. 2.15. The rotation point can be determined by the embedded pile length and load position (see Equation 2.6). Although Prasad and Chari's method has included the effect of rotation, the determination of the rotation point includes additional factors such as pile-soil stiffness and shape factor. A comparison of soil pressure distribution by different approaches is given in Fig.2.16. Zhang et al. (2005) completed a comparison of predicted methods and measured results. The difference between measured and predicted values varied between – 30% and 50%; Prasad and Chari's method proved to most closely predict the results.

$$P_u = 0.24\ 10^{(1.3\tan\varphi+0.3)}\ \gamma\ a\ D\ (2.7a\text{-}1.7L) \qquad (2.5)$$

$$a = \frac{\left(-(0.567L + 2.7e) + (5.307L^2 + 7.29e^2 + 10.541eL)^{0.5}\right)}{2.1996} \quad (2.6)$$

where P_u = ultimate lateral load (kN)

a = rotation point from ground level (m)

e = eccentricity of horizontal loading (m)

γ = unit weight of soil (kN/m^3)

L = embedded length of the pile (m)

d = diameter of pile (m)

ϕ' = angle of internal friction (effective stress)

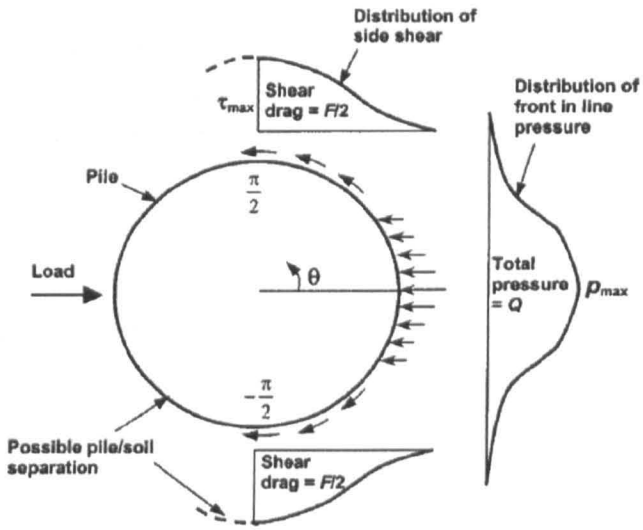

Fig. 2.15 Distribution of fount earth pressure and side shear stress around a lateral loaded pile. (source: Smith, 1987)

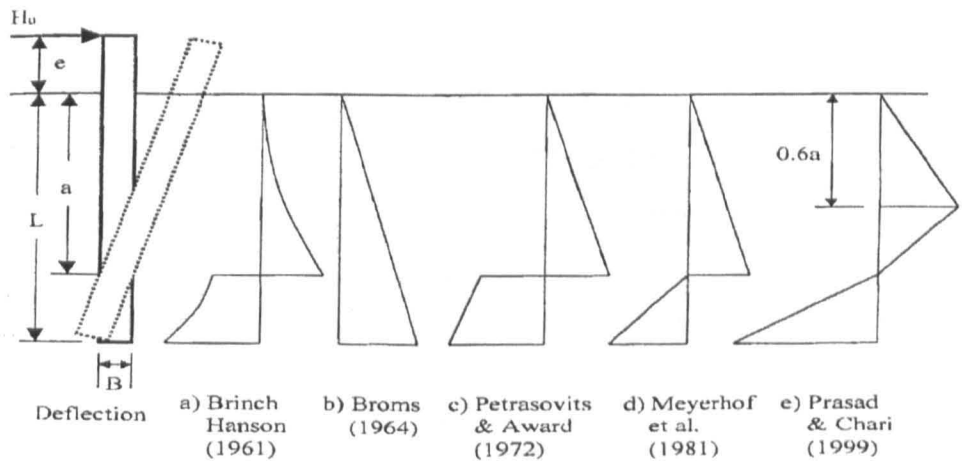

Fig. 2.16 Schematic distribution of soil pressure for a free-head rigid pile under lateral loading proposed by different studies. (source: Prasad & Chari, 1999)

API (1993) and DNV (2004) use a practical method developed by Murchison and O'Neill (1984) to determine the ultimate lateral resistance in sand which is shown in Equation 2.7(a), (b). The transition depth can be obtained from lateral force equilibrium. Reduction of soil stiffness below the transition point is considered in this method. Importantly, both shear resistance and passive pressure are presented in the equation.

$$p_u = (C_1 z + C_2 D)\gamma' z \quad \text{for } 0 < z \leq z_r \tag{2.7a}$$

$$= C_3 D \gamma' z \quad \text{for } z > z_r \tag{2.7b}$$

where p_u = ultimate resistance of the soil in the unit of force per pile length (kN/m)

z = embedded depth of the pile (m)

z_r = a transition depth (m)

γ' = effective unit weight of soil (kN/m^3)

D = pile diameter or width of pile(m)

C_1, C_2 and C_3 = coefficients determined from Fig. 2.17 as functions of ϕ'

Pile head P-Y curve methods

The ultimate lateral bearing capacity can also be determined from the pile head load displacement (P-Y) curve. Theoretically, the maximum load value in the P-Y curve can be defined as the ultimate load. Three typical P-Y curves are presented in Fig. 2.18(a). The peak load of Curve A can be easily found, and the peak load of Curve B also can be found without difficulty. However, the 'PEAK' criteria of Curve C cannot be predicted as there is no significant maximum load to be found. Unfortunately, most of P-Y curves of lateral loaded piles develop like Curve C.

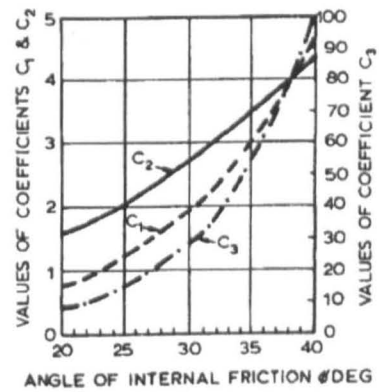

Fig. 2.17 Coefficients as functions of friction angle (source: DNV, 2004)

In order to determine the ultimate load in Curve C, Hirany and Kullhawy (1989) proposed a practical method with regard to the change of curvature in a P-Y curve. Curve C can be divided into three parts: initial linear, transition, and final linear regions which are shown in Fig. 2.18(b). Load L_1 corresponds to the load at the end of the initial linear region, and Load L_2 corresponds to the load at the initiation of the final linear region. The failure load interpreted by existing methods is located at the boundary of the transition and the final linear regions (Pan et al., 2000). The ultimate lateral load is taken as the load corresponding to the point where the curve tends towards a straight line. The tangent slopes taken from the P-Y curve can be used to determine the straight line (Fig. 2.18 (c)). Fig. 2.18(d) shows that the slope reduces with an increase in displacement, and the slope drops to a constant value. The beginning of this constant value refers to the displacement at the ultimate load. P-Y curves obtained from numerical modelling or testing can represent the pile-soil reaction. The ultimate capacity from a P-Y curve can directly reflect the real behaviour of pile and soil which can be used in foundation design.

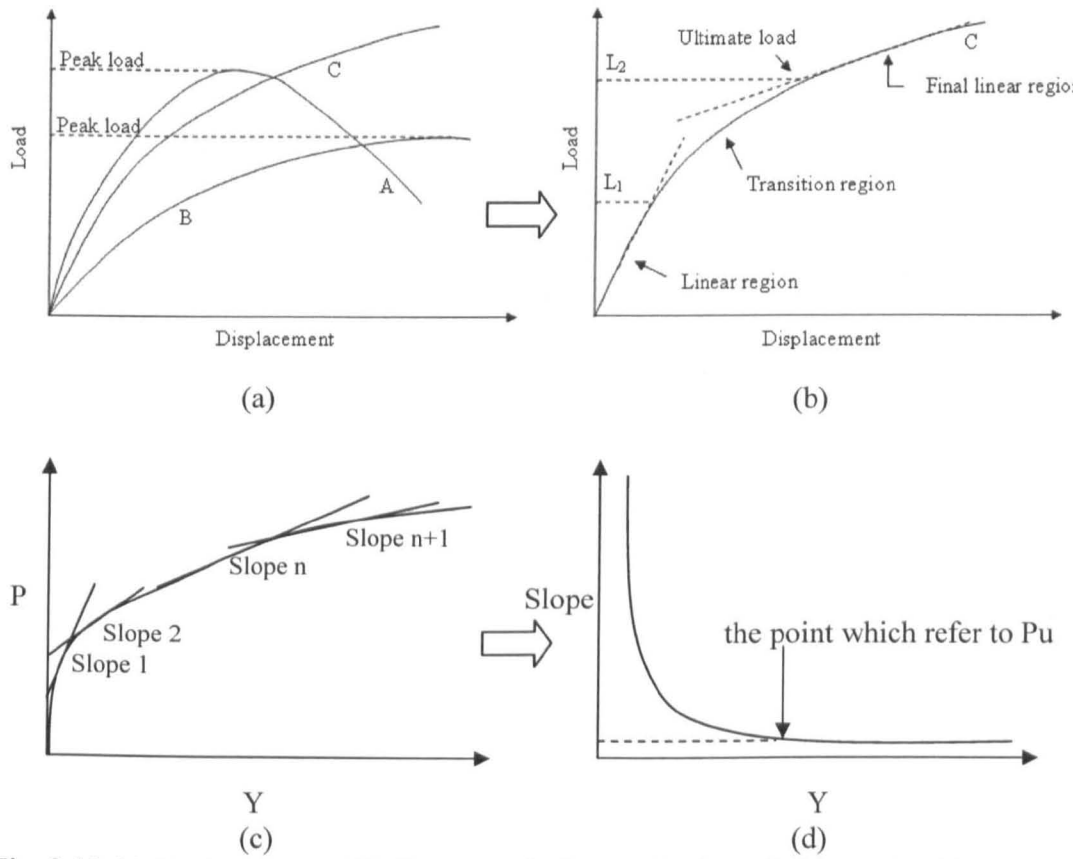

Fig. 2.18 (a) Typical types of P-Y curves; (b) Determination of ultimate load in Curve C; (c) tangent slope of P-Y curve; (d) variations of slope with displacement (after: Hirany and Kullhawy, 1989)

Serviceability limit state approach

The lateral failure load of a piled foundation can be defined as a load which causes an out of tolerance state in lateral displacement or inclination of the structure. DNV (2004) illustrates that a structure or structural component will no longer satisfy the serviceability limit states under various conditions including:

- deflections that may alter the effect of the acting forces
- deformations that may change the distribution of loads between supported rigid objects and the supporting structure
- excessive vibrations producing discomfort or affecting non-structural components
- motions that exceed the limitation of equipment
- differential settlements of foundation soil causing intolerable tilt of the wind turbine
- temperature-induced deformations

The deformation tolerances should not be exceeded for serviceability limit state (SLS) design. In offshore monopile foundations, the deformation tolerances refer to permanent deformations such as a permanent accumulated tilt of the pile head. The deformation tolerances are typically determined by visual requirements and requirements for the wind turbine operation which should be clarified with the wind turbine manufacturer. In addition, the permanent accumulated rotation is equal to the total toleration rotation minus the installation rotation.

In another definition of tolerance deformations, Prakash and Sharma (1990) suggested that the lateral displacement should not exceed 6.25mm in SLS design. This suggestion may not be accepted in all cases of pile design due to the different requirements of foundations such as various pile lengths, pile diameters and turbine tolerances.

Nowadays monopile foundations used in offshore wind farms have the ratio of pile embedded length to pile diameter of about 10. In laterally loaded monopile studies without much information on wind turbine requirements, many researchers, in practice, define service load as the load achieved when the lateral displacement reaches 10 % of outer pile diameter. This displacement tolerance refers to a rotation tolerance of 0.57°.

2.3.2. Study of pile-soil behaviour

Development of pile-soil model

Behaviour of piles under lateral loading has been studied since 1940s. Hetenyi (1946) presented the theory of a beam on an elastic foundation based on the Winkler model: the pile foundation is assumed a continuous beam supported by uniform springs along the pile surface as shown in Fig. 2.19. Based on this theory, a fourth-order differential equation is developed (Equation 2.8).

$$EI\frac{d^4y}{dz^4} + P_x\frac{d^2y}{dz^2} - p = 0 \tag{2.8}$$

where EI = pile flexural rigidity (kN-m^2)

z = embedded depth of the pile (m)

y = lateral pile deflection at depth z (m)

P_x = axial pile load per unit section (kN)

p = soil reaction in the unit of force per pile length (kN/m)

In many laterally loaded pile studies involving rigid piles, the influence of P_x is usually ignored because after integration of Equation 2.8, the value of dy/dz in the second section is very small. P_x will only be considered when the pile behaviour tends to buckling. The soil stiffness of a Winkler foundation is a function of soil resistance, p, and the lateral deflection, which can be defined as:

$$k = \frac{-p}{y} \tag{2.9}$$

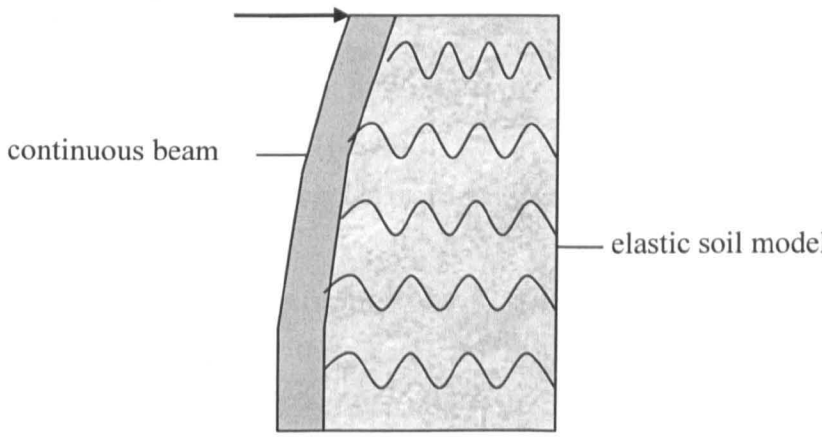

Fig. 2.19 Foundation response models for elastic continuum and Winkler Spring Medium

where k = the coefficient of subgrade reaction applied to a supported beam (kN/m^2)
(in some presentations, k is shown as E_s, soil modulus)
y = the lateral deflection (m)
p = soil reaction in the unit of force per pile length (kN/m)

In order to model layered soils, Matlock and Reese (1960) presented a generalized iterative solution. A relationship of nonlinear pile soil stiffness changing with depth which is used to predict deflection (p-y curve) has been proposed (Matlock (1970) and Reese et al. (1974)). Reese (1977) provides a computer code, COM622, based on finite difference method for analysing laterally loaded piles.

Smith (1987) interpolated the subgrade reaction, k, in Hetenyi's method as a function of pile diameter increasing linearly with depth z. Hence, the coefficient of subgrade reaction can be expressed as

$$k = n_h \frac{z}{d} \tag{2.10}$$

where n_h= constant of horizontal subgrade reaction (kN/m^2) (unit: same as k)
z = the embedded depth (m)
d = pile diameter or the width of pile (m)

A different method of calculating the soil resistance, p, has been given by Pasternak (1954). The soil model takes into account the interaction of shear stress between the springs of the Winkler model. This is obtained by linking the springs to an incompressible layer that supports only tangential deformation caused by the shear stress. The soil reaction unit force per pile length, p, is given in Equation 2.11.

$$p = k\ y + G_s \frac{dy}{dz} \tag{2.11}$$

where p = soil reaction in the unit of force per pile length (kN/m)
G_s = shear stress modulus (kN/m^2)
k = the coefficient of subgrade reaction (kN/m^2)
y = pile deflection (m)
z = the embedded depth (m)

In order to improve the quality of the analysis, studies focus on the improvement of nonlinear soil resistance, p. Seed et al. (1986) suggested that the maximum soil shear stress modulus, G_{max}, is a function of the density index and the effective unit weight of course graded soil. Fleming et al. (1992) suggested that the constant subgrade reaction, k, is a function of critical length of pile and pile stiffness.

In recent years a strain wedge model, a simplified three-dimensional model, shown in Fig. 2.20 was used to model a laterally loaded pile in layered soils (Ashour, 1998). In addition, changes in strain and stress during the lateral loading were considered within the strain wedge model in order to use the updated pile soil stiffness.

Development of p-y curve

Based on Winkler model presented by Hetenyi (1946), p-y curves have been widely used in modelling the true pile-soil interaction. Kondner (1963) interprets the p-y relationship as a hyperbolic function shown in Equation 2.12.

$$p = \frac{y}{(a + by)} \tag{2.12}$$

where p = soil reaction in the unit of force per pile length (kN/m)

y = lateral displacement (m)

a and b are derived from regressive analysis ($b = 1/p_u$, when $y \rightarrow \infty$)

unit of 'a' is 1/kN; unit of 'b' is m/kN

Matlock (1970) suggests that the p-y curve should be expressed by a cubic parabola with the equation

$$\frac{p}{p_u} = 0.5\left(\frac{y}{y_c}\right)^{\frac{1}{3}} \tag{2.13}$$

where p = soil reaction in the unit of force per pile length (kN/m)

p_u = ultimate soil reaction in the unit of force per pile length (kN/m)

y = lateral displacement (m)

y_c = lateral displacement (m) when $p = 0.5\ p_u$

In this empirical equation, the cubic p-y curve is established to include the influence of load and displacement at the ultimate limit state.

API (1993) and DNV (2004) use a hyperbolic tangent function, provided by Murchison and O'Neill (1984), to predict soil-pile behaviour shown in Equation 2.14. The soil resistance, p, is not only a function of y, but it includes the influence of the subgrade soil model, loading condition as well as pile shape.

$$p = \eta A p_u \tanh\left[\left(\frac{k_h z}{A \eta p_u}\right) y\right] \tag{2.14}$$

where p = soil reaction in the unit of force per pile length (kN/m)

p_u = ultimate soil reaction in the unit of force per pile length (kN/m)

η = pile shape factor (= 1.0 for a circular pile)

A = 0.9 for cyclic loading

= 3 – 0.8 (z/D) $\geq$ 0.9 for static loading

k_h = coefficient of soil subgrade reaction modulus (kN/m^2) which is a function of friction angle,ϕ (obtained from Fig. 2.21)

y = lateral displacement (m)

z = the embedded depth (m)

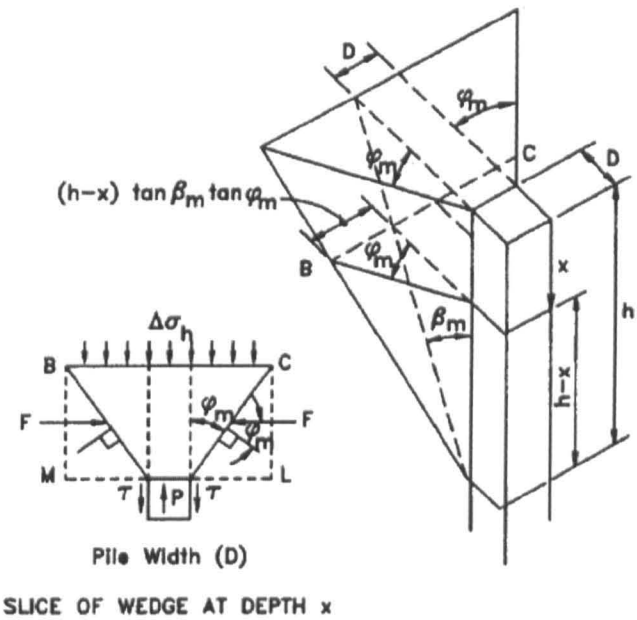

Fig. 2.20 Strain wedge model in uniform soil (source: Ashour, 1998)

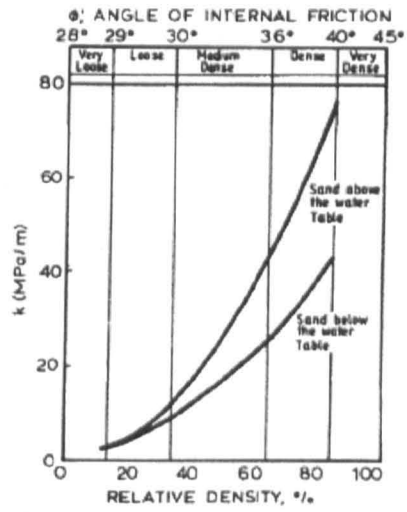

Fig. 2.21 Variation of subgraded reaction, K, with friction angle, ψ . (Source: DNV, 2004)

2.3.3. Influence of cyclic loading

Cyclic lateral loads in offshore wind farms could come from environmental loads due to waves, currents, tides and wind. The structure might be subjected to significant cyclical environmental lateral loads at a frequency of around 0.1 Hz; at critical levels and frequencies, the cyclical horizontal loads can cause a reduction in lateral resistance (Ramakrishna and Rao, 1999). The variables of cyclic loading may include: numbers of cycles; magnitude of loading; frequency of loading; and loading direction (alternating between zero load and the maximum load in one direction or alternating load in opposing directions about a mean value.) This review is only concerned with low frequency loading; foundation damage caused by high frequency loading like earthquake shaking or mechanical vibration is not covered.

Chan and Hanna (1980) proposed that pile-soil failure may be reached when the magnitude of a cyclic load is over 25% of the static ultimate load based on a series of 1G repeated loading tests in sand. Poulos (1982) defined a cyclic reduction factor by observation of quasi-static cyclic lateral loading tests for a pile embedded in clay. The total reduction factor can be expressed as a function of a soil modulus reduction factor multiplied by a rate factor. A soil modulus reduction factor is the ratio of soil modulus after cyclic loading to soil modulus for static loading; and a rate factor is a function of reference loading rate to the actual loading rate. Based on full scale test results, Little and Briaud (1988) proposed that the subgrade soil reaction after N cycles can be defined as follows:

$$k_{hN} = k_{h1} N^{-a} \tag{2.15}$$

where k_{hN} = subgrade soil reaction (kN/m^2) after N cycles

k_{h1} = subgrade soil reaction(kN/m^2) at static loading

N = number of cycles

a = a degradation parameter from the results of cyclic pressuremeter tests

Based on the regression method, Long and Vanneste (1994) suggested that the cyclic modulus ratio, R_n, can be expressed as

$$R_n = \frac{n_{hn}}{n_{h1}} N^{-t} \tag{2.16}$$

where n_{hn} = constant of horizontal subgrade reaction (kN/m^2) after N cycles

n_{h1} = constant of horizontal subgrade reaction (kN/m^2) at static loading

N = number of cycles

t = relative effect of cyclic loading on the deterioration of n_h; t is a function of pile length, relative stiffness factor, soil properties and installation method

The cyclic load ratio is defined as the ratio of the magnitude of minimum lateral load to the magnitude of maximum lateral load. Long and Vanneste (1994) collected results of loading tests and determined the cyclic effect using a cyclic strain ratio, Rs. The lateral strain, ε, can be expressed as y / (2.5d), where y is lateral displacement and d is pile diameter because over 70% of soil movement happens in a circular area with 2.5 times pile diameter surrounding the pile . Hence, the relationship between cyclic strain ratio and the number of cycles can be expressed as

$$R_s = \frac{\varepsilon_N}{\varepsilon_1} = 1 + t\ln(N) \tag{2.17}$$

where Rs = reduction of strain ratio

ε_1 = lateral loaded strain in static loading

ε_N = lateral loaded strain after N cycles

N = Number of cycles

t = relative effect of cyclic loading (degradation factor)

Ramakrishna and Rao (1999) suggested that the critical cyclic load magnitude can be defined as a load which can cause large deflection with the number of cycles; soil starts yielding and there cannot be any further resistance expected and hence the deflection never stabilizes. The critical cyclic load magnitude increases with the increase in the ratio of pile length to pile diameter.

2.3.4. Influence of combined loading

Combined loading is defined as lateral loading due to environmental loads and self weight. In an overview of lateral loaded pile studies, the influence of vertical loading is usually ignored in the fourth-order differential equation (see Equation 2.8). Many pile structures including piles in offshore wind farms are mainly designed to transfer vertical loads into deeper soil. Meyerhof has carried out research into pile foundations since 1970s' including the behaviour of vertical piles under inclined loading by observing large scale model tests. Features of combined loading include pile-soil stiffness, tilt of piles, inclined angle of loading and embedded length.

Meyerhof and Ranjan (1972) proposed that the bearing capacity reduces with the increase in inclination from observation of 1G model tests of vertical piles under

inclined loading (inclination of load, α is defined at 0^o is vertical; 90^o is horizontal shown in Fig 2.22). The soil pressure distribution along the pile under inclined loading is presented in Fig. 2.22 showing:

- The major portion of the load is transmitted through the base for an axially loaded vertical pile in sand, and the load transmitted from the shaft is small.
- The load transmitted through the base decreases with the increase in load inclination, and the pile rotates as a rigid body while the load taken by the pile shaft increases.
- As the pile rotates with load inclination, the passive pressure is on one side and active pressure is on the other side above the point of rotation; below the rotation point, stress states are reversed.

In addition, the ratio of the inclined failure load to the vertical failure load is reduced from 100% to less than 50% according to the changes of load from vertical to horizontal. This reduction is more apparent with flexible piles than with rigid piles.

Furthermore, the ultimate capacity of an inclined load can be expressed as an empirical equation shown in Equation 2.18(a); the lateral load component can also be replaced by a moment shown in Equation 2.18(b) (Meyerhof and Purkayatha, 1985).

$$\left(\frac{Q}{Q_u}\right)^2 + \left(\frac{P}{P_u}\right)^2 = 1 \qquad 2.18(a)$$

$$\left(\frac{Q}{Q_u}\right)^2 + \left(\frac{M}{M_u}\right) = 1 \qquad 2.18(b)$$

where Q, P = vertical and lateral component of inclined loads, respectively

Q_u, P_u = ultimate vertical and lateral load, respectively

M, M_u = moment at inclined load, ultimate moment, respectively

Byrne and Houlsby (2003) presented a three dimensional model showing in Fig. 2.23 for the comnbined loads (M, V and H). Concepts of elastic-plastic soil behaviour including flow rule, hardening law and yield surface have been included in the analysis.

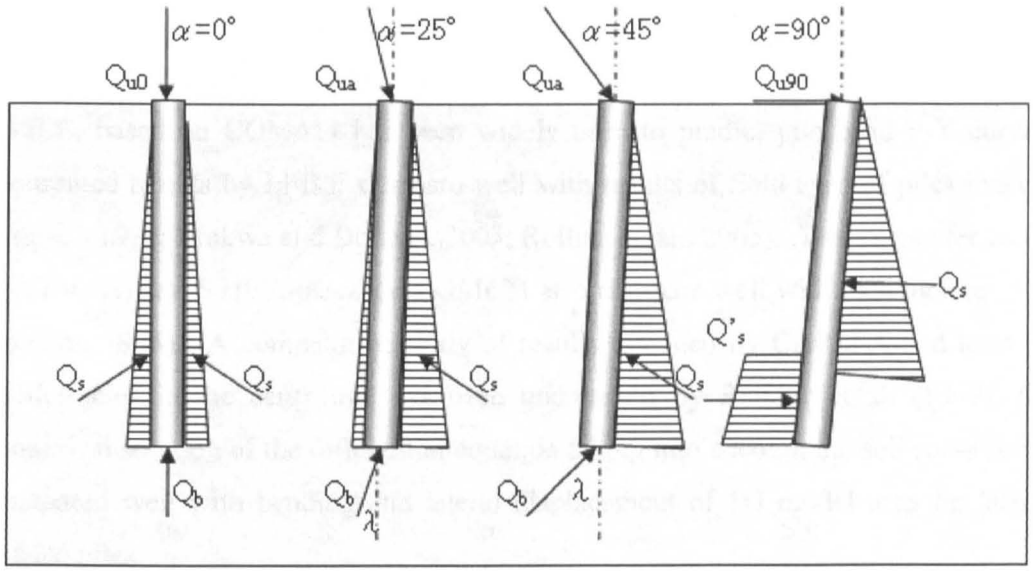

Fig. 2.22 Force distribution on a pile under inclination loading (after Meyerhof and Ranjan, 1972)

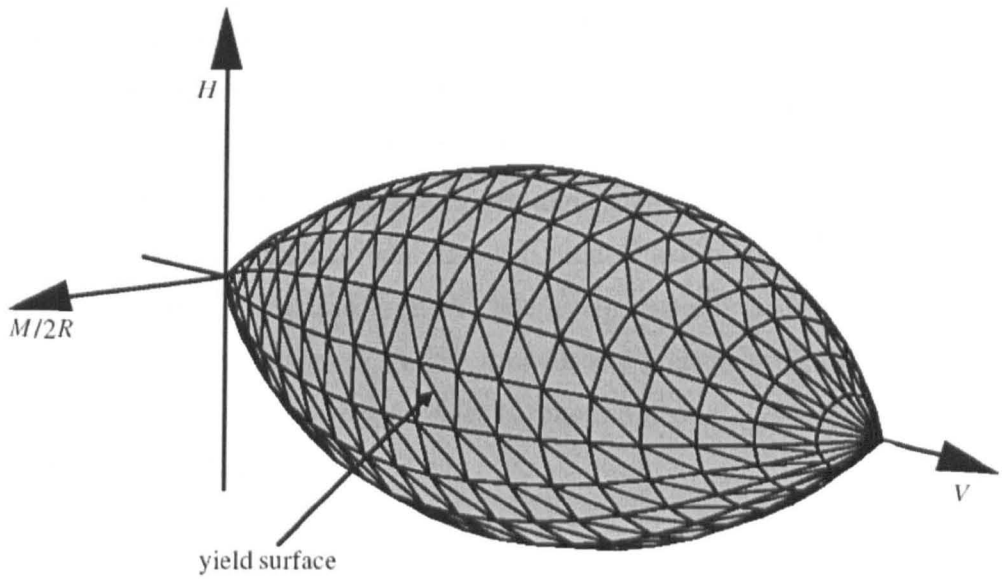

Fig. 2.23 Typical yield surface for footing under combined loading (Source: Byrne and Houlsby, 2003)

2.3.5. Computer modelling (LPILE and LUSAS)

FDM

Since the development of Heteny's theory of beam-on elastic foundation based on the Winkler model in 1946, the finite difference method (FDM) has been widely used to illustrate the fourth order pile-soil differential equation. Reese (1977) successfully developed a FDM computer code, COM622, to cover pile-soil

differential equations. Many computer programs for solving lateral loaded piles have been developed using COM622 and its updated COM624. A computer program, LPILE, based on COM624 has been widely used to predict pile head P-Y curves. Computed results by LPILE compare well with results of field tests of piles in sand (Ismael, 1991; Mokwa and Duncan, 2003; Rollins et. al., 2005). Two computer codes, INCPILAU and STIFF, based on COM624 also compare well with inclinometer data (Brown, 1994). A comparative study of results obtained by CAPELA and tests on model piles in the centrifuge has been undertaken by Belkhir et al. (1999); the numerical solution of the differential equation taking into account the soil shear stress compared well with bending and lateral displacement of 1G model tests on lateral loaded piles.

The development of a strain wedge model for pile-soil interaction has included a computer program, SWM; soil response in this model is computed over the full stress-strain range instead of being projected from known empirical data as in traditional FDM programs (Ashor, et al., 2002). Traditional FDM analyses require a significant amount of time to compute the calculation. Simple Winkler models are limited in modelling pile-soil-pile interaction for nonlinear materials (Klar and Frydman, 2002). Recently, advanced three-dimensional (3D) FDM programs have been developed which include nonlinear soil models and pile-soil interface. A 3D FDM code, $FLAC^{3D}$, was used to model pile group response under vertical loading, laterally loaded sleeved piles in sloping ground, and pile deformation due to lateral slope movement (Fig. 2.24), respectively (Comodrmos et al., 2003; Ng and Zhang, 2001; Martin and Chen, 2005).

FEM

Compared to the progress of FDM, the development of FEM was faster due to developments in structural engineering. Since the 1980s, an axisymmetric FEM model containing elastic-perfectly plastic material behaviour has been used in pile-soil analysis (Pressley and Poulos, 1986); a 3D FEM model with a hyperbolic constitutive law for soil pile interface has been used in a battered pile analysis (Muqtadir and Desai, 1986). Trochanis et al. (1991) studied the pile-soil interface conditions, bonding and slippage, by a 3D FEM of ABAQUS, with pile-soil interface behaviour represented as a function of the frictional angles and elastic stiffness. El Naggar and Bentley (2000) divided the soil field into inner field and far field

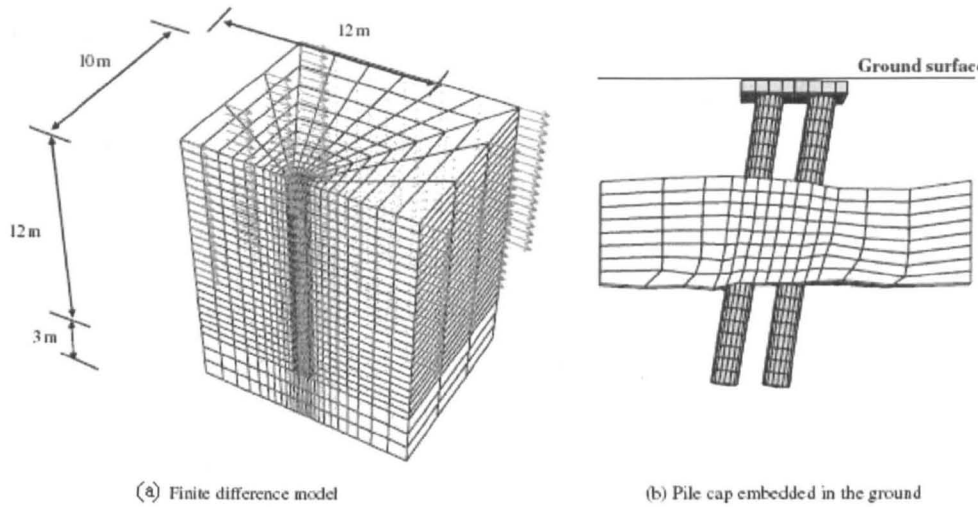

Fig. 2.24 3D FDM modelling of piles subjected to soil movement (Source: Martin, G. R. and Chen, C., 2005)

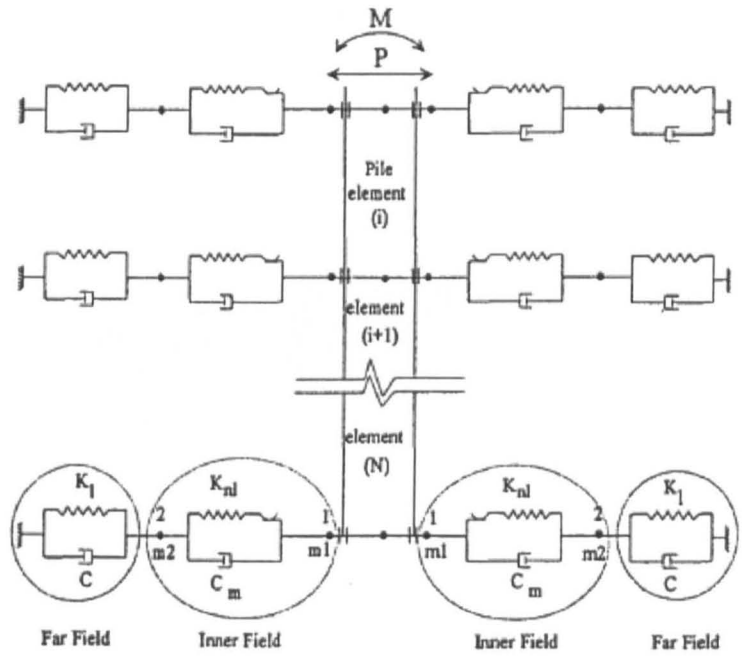

Fig. 2.25 Elements of pile-soil model for nonlinear dynamic analysis of a single laterally loaded pile (Source: El Naggar and Novak, 1996)

(Fig. 2.25) by using different soil hyperbolic stress-strain relationships to investigate the influence of the boundary. This model applied in a FEM code, ANSYS, successfully modelled dynamic lateral loaded piles. Ng and Zhang (2001) used a nonlinear 3D FEM code, FLPIER, to model pile behaviour under cyclic loading (Fig.

2.26); the relationship of subgraded soil reaction, n_h, and N values of Standard Penetration Test (SPT) were found through back-analysis of pile tests.

2.4. Review of model pile tests

The lateral resistance of laterally loaded finned piles will be assessed through a series of 1G model tests. Piles will be tested under static, cyclic and combined loadings to simulate the influence of environmental loads. The assessment of loading systems provides the design guideline for an appropriate cyclic loading system. The review of test measurement provides many examples and techniques to measure the pile and soil response. The study of various loading tests and analyses methods will be used in the assessed of behaviour of finned piles.

2.4.1. Loading systems

A number of loading devices based on mechanical, electro mechanical and hydraulic principles have been developed. The most common devices are shown in Fig. 2.27. The gravity, the gear drive and the hydraulic drive systems (Fig.2.27 (a), (b)

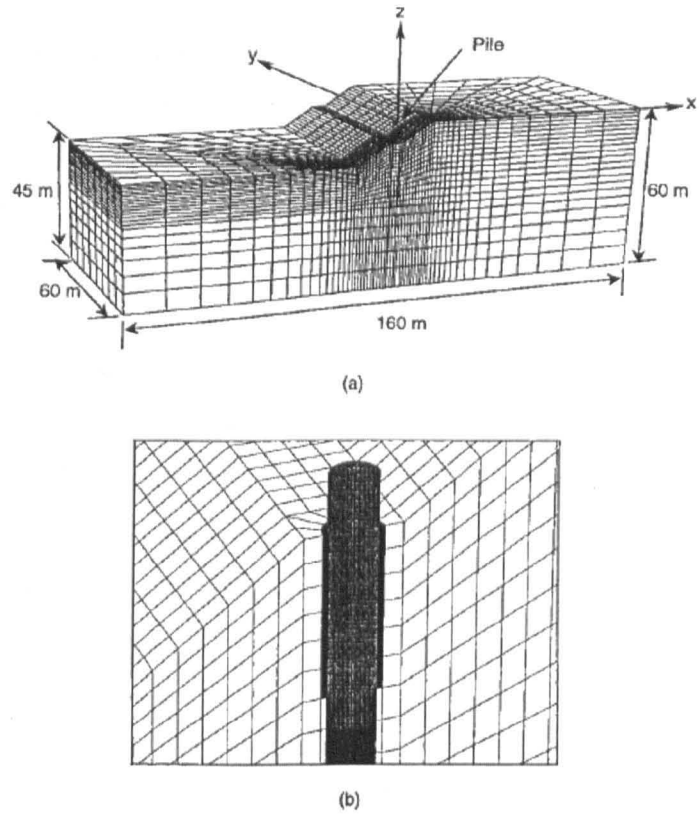

Fig. 2.26 3D FEM modelling of a laterally loaded pile in a slope (Source: Ng and Zhang, 2001)

and (c)) are commonly used for static loading. They have been used in limited number of cyclical loading tests by manual controlling the loading systems (Peng et. al., 2004; El Naggar, 1999, 2000). The statnamic device in Fig.2.27 (d) has been successfully used in a field test with a low loading frequency ranging from 0 to 10 Hz (Janes, et. al., 1991), but the method has yet to be applied in laboratory tests. The vibration system in Fig. 2.27 (e) has been used to provide cyclic loading with high frequencies ranging from 5 to 50 Hz which is not appropriate for modelling wind farm loading (Blaney and O'Neill, 1989). The pneumatic loading device in Fig. 2.27 (f) has been successfully used in one-way cyclic loading with up to 500 cycles in each test (Ramakrishna and Rao, 1999). The mechanical loading system (Fig. 2.27 (g)) uses a gear box to control one-way or two-way cyclic loading at different frequencies (Purkayastha and Basack, 1999). A three degree-of-freedom loading ring has been used to provide combined loading (Fig.2.27 (h)); cyclic vertical and horizontal loads as well as moments can be applied at the same time (Byrne and Houlsby, 2004). Although these devices have been widely used in model tests, an assessment (see Table 2.3) shows that improvements could be made.

2.4.2. Test measurements

There are some basic instruments commonly used in model pile tests to measure pile displacement, pile head load magnitude, pile deformation and soil reaction. With the rapid development in data loggers, readings of these measurements can be recorded automatically. A brief introduction to measuring systems follows:

Displacement measuring

Displacement at the pile head can be measured by a dial gauge or displacement transducer (LVDT). Fig. 2.28 shows a schematic diagram of an LVDT which is widely used in geotechnical laboratories. LVDTs can be used for both static and cyclic loadings. The recording capability depends on the data logger (Rao et al., 1998).

Load measuring

Lateral loading at the pile head is usually measured by a load cell or a proving ring. A proving ring (Fig. 2.29(a)) is made of tool steel; a dial gauge or LVDT measurement is set in the middle of the ring (Sastry and Meyherhof, 1994). A linear

Table 2.3 Comparison of loading devices

Loading type	Features	Assessments
(a) Gravity loading device	• A simple gravity theory is applied; the lateral load is given in increments by placing weights on the load hanger • The wire in titan attached to the pile cap can maintain the load in the same direction	• The load incensement is not constantly corresponding with time especially while the weight is imposed • Manual place and remove the weight may not a practical method to carry out one-way cyclic loading
(b) Gear thrust device	• A mechanic thrust drive is used to apply loads which have a same loading rate • Pile head deflection increases slowly and constantly (1 mm/min); a clear pile head load-deflection curve can be developed	• The tested pile tilted may cause the change of loading position on the pile surface • The loading rate is fixed; various frequencies can not be assessed • Manual unloading is needed in one-way cyclic loading; number of cycles would be limited
(c) Hydraulic drive device	• Lateral force acting on the pile is applied by extending hydraulic jack incrementally • Pile can be push-forward or push-backward depending on pressure inside the jack	• Hydraulic loading systems are normally applied in high load conditions but not suitable for loading under 100 N • Manual control the pressure; hence, a feedback pressure control unit is needed for cyclic loading
(d) Statnamic device	• The acting and reacting theory is adopted; fuel burned to push the pile moving. The test lasts 100ms with a low loading frequency ranging from 0 to 10 Hz • Preparation and test take 1/3 time of static loading test	• Lateral load of pile could be estimated by the Statnamic test while the Statnamic load is large enough to reach the pile capacity • It can only be applied in one-way cyclic loading due to Statnamic load direction
(e) Vibrated load system	• A vibrator supplies horizontal excitation; there is no limit of cycles	• It is usually applied for cyclic loading with high frequency • The load quality is hard to control
(f) Pneumatic load device	• The lateral force is applied by weights; frequency and load level are controlled by pneumatic ram. • Features of a feedback unit and low frequency loading are suitable to model environmental loads	• It can only be used in one-way cyclic loading test • The device has been used in loading tests of 500 cycles; its reliability should be proved in a test of large cycles
(g) Mechanic gear driven device	• Forces is applied by a gear rotation system which can provide either one-way or two-way cyclic loading • The frequency and the load level are adjustable; the loading rate is based on either load control or displacement controlled unit	• A slight variation from sinusoidal wave loading is occurred due to mechanical interaction between various components of the unit
(h) Three degree-of-freedom loading device	• A three degree-of-freedom loading rig is able to provide a composed load including vertical load, lateral load and moment • The load level, the number of cycles and the frequency are changeable	• The consistency of a load amplitude may not stable • Reliable for large number of cycles should be assessed

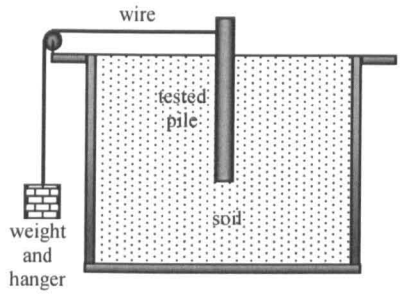

(a) Gravity loading device (after Rao, 1998)

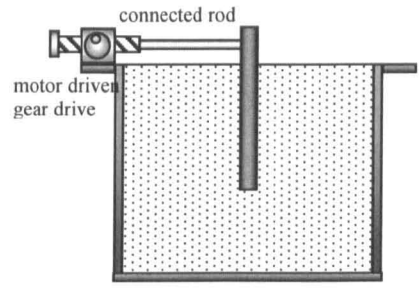

(b) Gear drive device (after Peng, 2004)

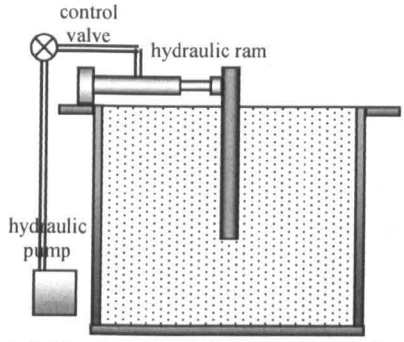

(c) Hydraulic drive device (after El Naggar, 1999)

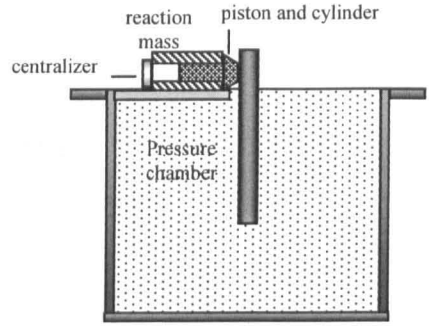

(d) Statnamic device (after Janes, 1991)

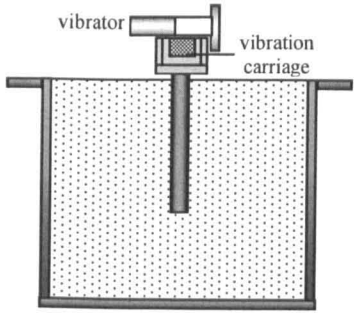

(e) Vibrated load system (after Blaney and O'Neill, 1989)

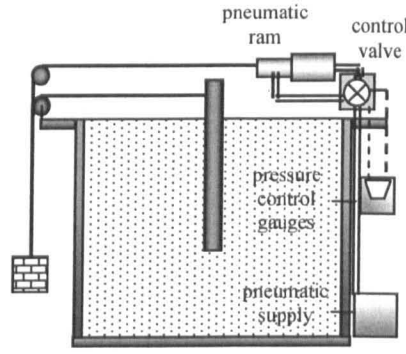

(f) Pneumatic load device (after Mahmoud, 1994; Ramakrishna, 1999)

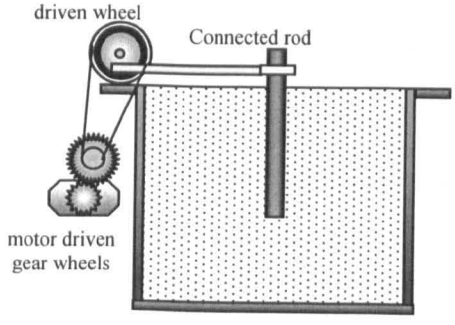

(g) Mechanical gear driven device (after Purkayastha, 1999)

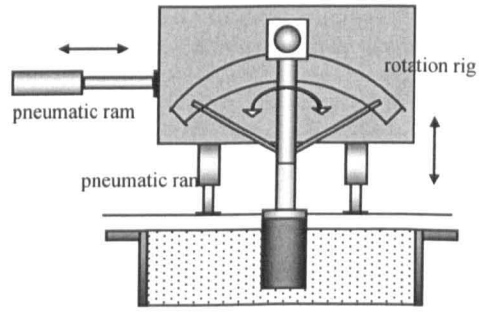

(h) Three degree-of-freedom loading device (after Byrne and Houlsby, 2004)

Fig. 2.27 Main devices of the lateral loading system in laboratory

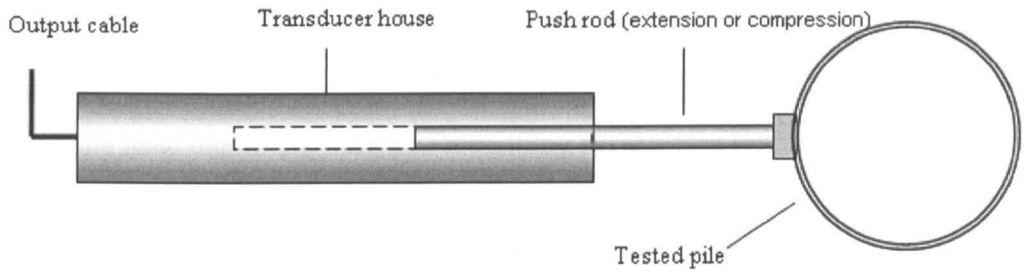

Fig. 2.28 Schematic diagram of displacement transducer LVDT

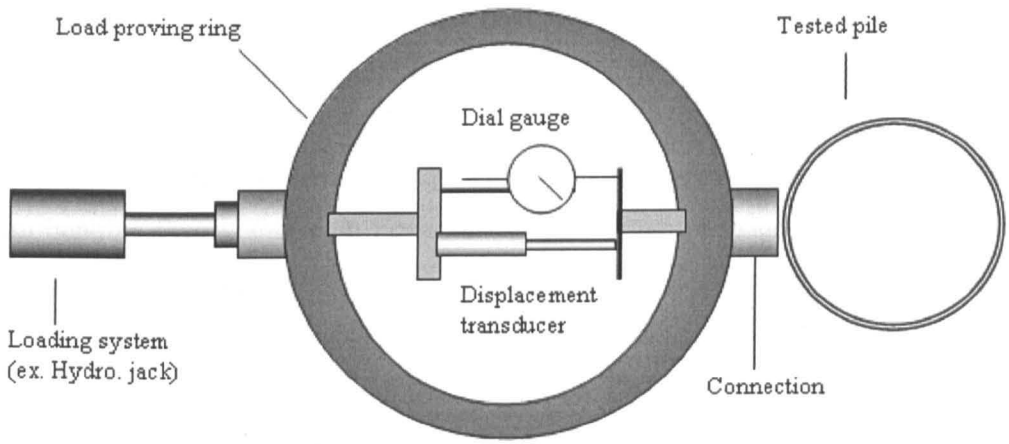

(a) Proving ring

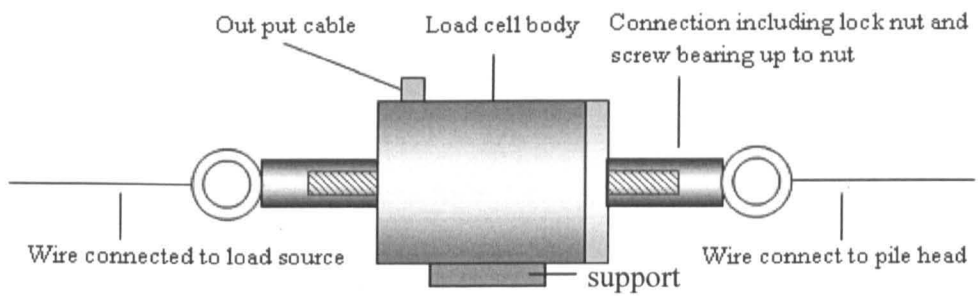

(b) Load cell

Fig. 2.29 Schematic diagrams of load measurements

relationship exists between the deformation of the proving ring and the force acting on it.

There are a number of types of load cells. For example, the cell can comprise a cantilever which bends on load. Strain gauges are used to measure the deflection

which is linearly related to the applied load (Mahmoud and Burley, 1994; Rao, et al., 1998; RDP, 2002). The load cell can be placed on a cable between the load source and the pile, and the magnitude of tensile force can be obtained. It is normally used to measure lateral cyclic loading with the load cell supported to avoid vertical loading on the pile head due to the weight of measuring system (see Fig. 2.29 (b)).

Deformation measuring

The deformation and soil resistance along the pile can be indirectly measured using strain gauges. Based on the theory of the Wheatstone-Bridge circuit presented in Fig. 2.30 (a), the strain on the surface of an element can be measured by a strain gauge (GWI, 1997). In order to measure the deformation of the pile, strain gauges are attached along the inner surface of the pile on both active and passive sides as shown in Fig. 2.30 (b).

The bending moment is a function of strains which can be found by elastic beam bending theory shown in Equation 2.19(a). If soil resistance is assumed to be distributed uniformly, the bending moment can be represented as a cubic polynomial function shown in Equation 2.19(b). Pile deflection, tilt, shear force and soil resistance can be derived through the polynomial function of bending moments (EI Nagger and Wei, 1999, Gere and Timoshenko, 1990). The relative relationships of these values are given from Equation 2.19(c)-(f).

$$M_i = \frac{\varepsilon_i EI_i}{(d/2)_i} \qquad 2.19(a)$$

$$M_i = az^3 + bz^2 + cz + d \qquad 2.19(b)$$

$$S(z) = \frac{dM}{dz} = 3az^2 + 2bz + c \qquad 2.19(c)$$

$$p(z) = \frac{d^2M}{dz^2} = 6az + 2b \qquad 2.19(d)$$

$$\theta(z) = \frac{1}{EI}\int M(z)dz = \frac{1}{EI}\left(\frac{a}{12}z^4 + \frac{b}{6}z^3 + \frac{c}{2}z + dz + e\right) \qquad 2.19(e)$$

$$y(z) = \frac{1}{EI}\int\left(\int M(z)dz\right)dz = \frac{1}{EI}\left(\frac{a}{20}z^5 + \frac{b}{12}z^4 + \frac{c}{6}z^3 + \frac{d}{2}z^2 + ez + f\right) \qquad 2.19(f)$$

where M_i = bending moment at i section

ε_i = strain at i section

EI_i = pile flexural rigidity at I section

S(z) = reaction force at z position

p(z) = soil resistance along the pile shaft at z position

θ(z) = tilt at z position

y(z) = pile lateral deflection at z position

a, b, c, d, e and f are parameters. a, b, c and d can be determined by regression analysis; e = EI θ(0) and f = EI y(0).

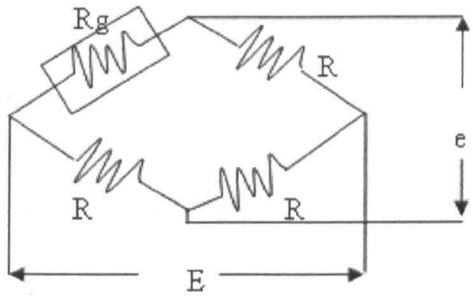

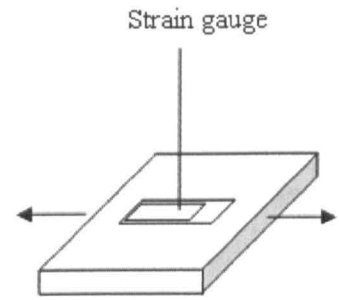

$e = E/4\ K_s\ \varepsilon$

where

K_s = gauge factor e = output voltage

ε = strain, Rg = gauge resistance

E = input voltage, R = resistor

(a)

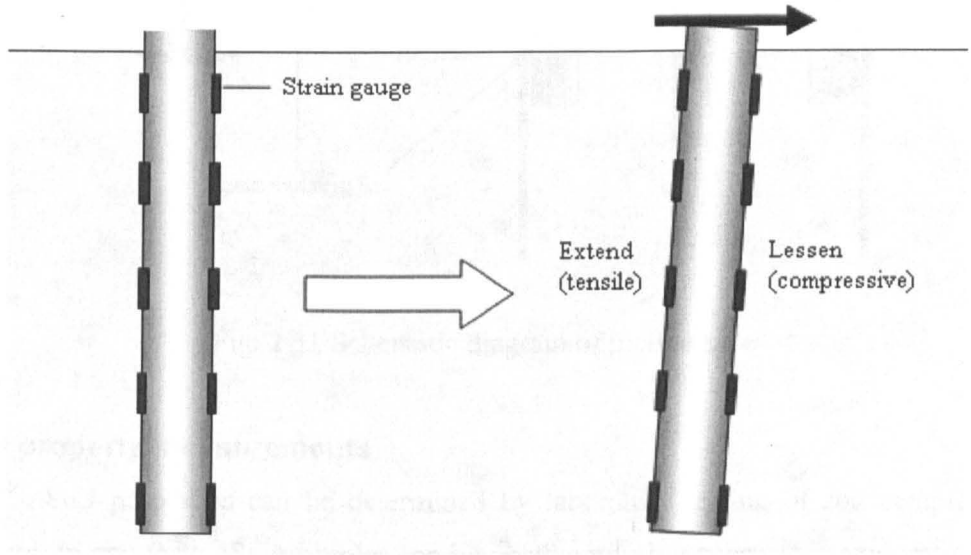

(b)

Fig. 2.30 Schematic diagram of strain gauges (a) strain gauge unit, and (b) strain gauges on a pile

These equations may not predict the real pile behaviour because the soil resistance may not be linear. In addition, the pile EI value is assumed constant which may not reflect the true pile properties. In order to improve the quality of regression in y(z), the higher order polynomial equation (10^{th}) has been proposed by Hameed et al. (2000). The accuracy of modelling also depends upon quality and quantity of strain data.

An inclinometer can be used to measure the changes of strains along the pile (Brown et al., 1994; Rollins et al., 1998). An inclinometer is composed of a slope indicator tube, strain sensing bar and position device shown in Fig 2.31. The slope indicator tube with position device controls the position of the strain sensing bar. Four strain gauges are attached on the bars 90^{o} to each other in order to measure the pile strain under loading. Equation 2.19 is used to calculate pile deformation and pile-soil reaction.

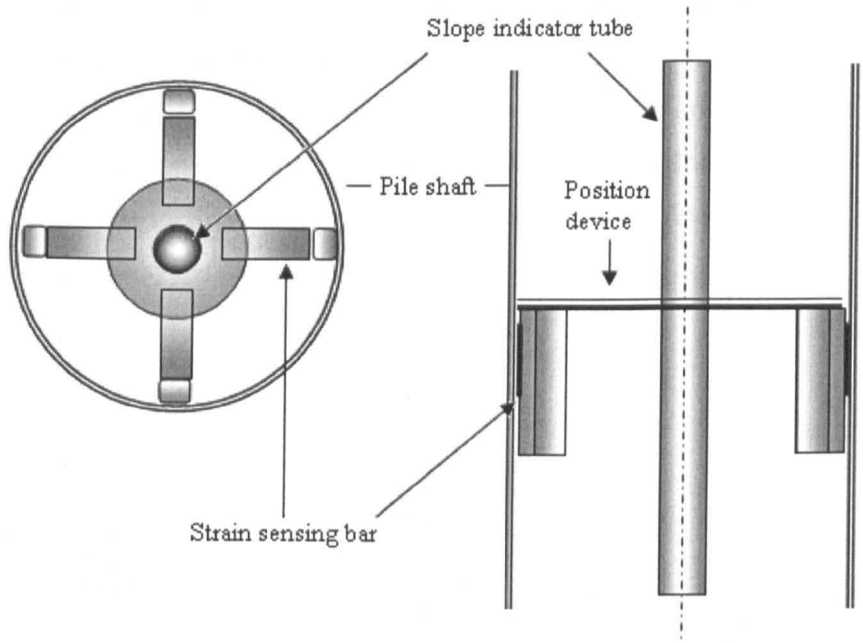

Fig. 2.31 Schematic diagram of inclinometer

Soil property measurements

Soil properties can be determined by laboratory testing of soil samples or through in situ tests. Soil samples can be obtained during subsurface exploration by disturbed and undisturbed methods. Disturbed samples can be collected from a split-spoon sampler and a spring core catcher; samples can be used for measuring some of the soil properties such as soil classification. Undisturbed samples can be obtained by

using a piston sampler and a thin wall tube; the completed sample may be used to measure a soil strength parameter, stiffness as well as permeability.

In addition to laboratory methods, soil properties can also be obtained through in situ tests such as standard penetration test (SPT), cone penetration test (CPT), vane shear test, dilatometer test (DMT) and pressuremeter test (PMT). These are normally used in sand because of the difficulties in retrieving undisturbed samples. The objective was to review the methods in order to develop an appropriate test to characterise the soil used in the model tests in this research.

The standard penetration test (SPT) is used for measuring the soil resistance at the base of a borehole (Fig. 2.32). BS 1377-9 (1990) for in situ tests of soils recommends that the SPT method is mainly used in sand and gravely sand. A hammer (63.5 kg) is freely dropped on to a driven head from a height of 0.76 m. The number of blows, N, is recorded when the penetration of the split sampler reaches 0.3 m. Based on the N values, the relative density and friction angle can be obtained through empirical formulae provided by Marcuson and Bieganousky (1977) and Wolff (1989), for example. Basically, sand or gravel with an N value less than 10 can be classified as loose soil. Sand and gravel with an N value between 10 and 30 can be classified as medium density soil. When the N value is greater than 30, the sand and gravel is very dense.

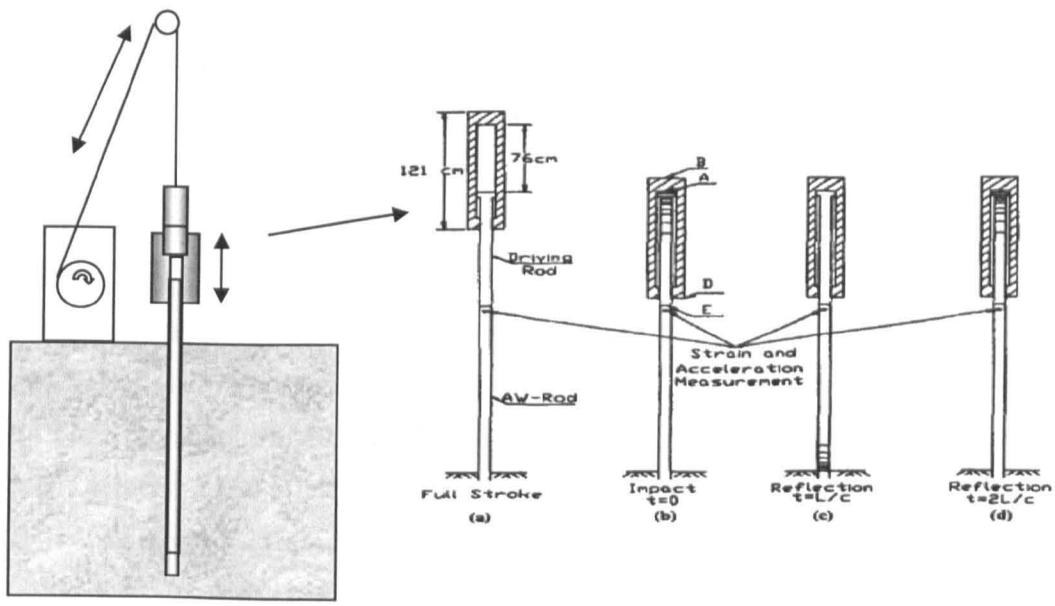

(a) (b)

Fig. 2.32 Standard penetration test (SPT) (a) schematic diagram of test and (b) loading procedure (Source: Abou-matar, H. and Gole, G.G., 1997)

The cone penetration test (CPT) is a versatile sounding method used for determining a profile of soil properties (Fig. 2.33). A 60° cone with a base area of 10 cm^2 is pushed into the ground at a steady rate of 20 mm/s; both point resistance and frictional resistance to penetration are recorded. Test procedures and calculation of point and frictional resistances are described in BS 1377-9 (1990). The CPT can be used in sand or clay. A relationship between relative density and cone resistance was recommended by Jamiolkowski et al. (1985). Kulhawy and Mayne (1990) built a correlation between effective stress, cone point resistance and peak frictional angle for granular soil. In clayey soil, a correlation between undrained cohesion, preconsolidation pressure and overconsolidation ratio was given by Mayne and Kemper (1988).

The vane shear test is used to determine the in situ undrained shear strength of soft clay soil. Four blades 90° to each other on the end of a rod are subjected to a torque force and are rotated as shown in Fig. 2.34. The torque at failure can be converted to the undrained shear strength. The vane shear test is a rapid and economical method to determine the properties of soft clay but is not used in sand.

The dilatometer test (DMT) (Fig. 2.35) is composed of a flat-plate with a thin flat circular steel membrane in the middle. The circular plate is expanded by gas pressure. Based on the values of pressure, soil properties including coefficient of at-rest earth pressure, overconsolidation ratio and modulus of elasticity can be obtained (Marchetti, 1980).

The pressuremeter test (PMT) is an instrument which allows the determination of the in situ soil properties by measuring displacement with applied load. The standard pressuremeter test (PMT) and results are shown in Fig 2.36 (Briaud and Shields, 1980). The tests are carried out at various depths in order to obtain soil modulus with depth which can be used in computer modelling. Meyerhof and Sastry (1987) proposed that the theoretical pile capacities under lateral load, P_0, or pure moment, M_0, can be estimated by using the results of full-displacement pressuremeter (FDP) tests; these relationships in sands can be expressed by the following empirical formulae:

$$P_0 = 0.125\sigma_b DL \qquad 2.20(a)$$

$$M_0 = 0.09\sigma_b DL^2 \qquad 2.20(b)$$

where σ_b = lateral pressure at base level

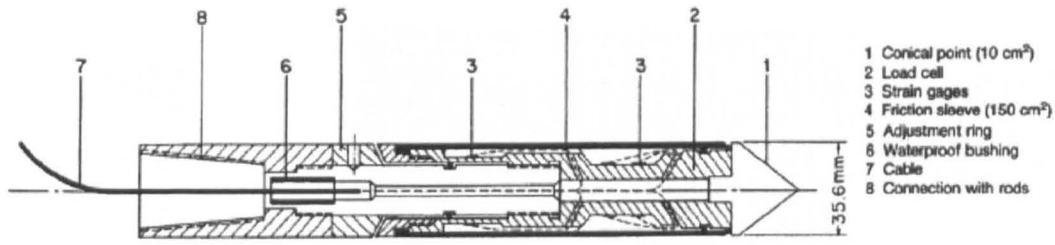

(a)

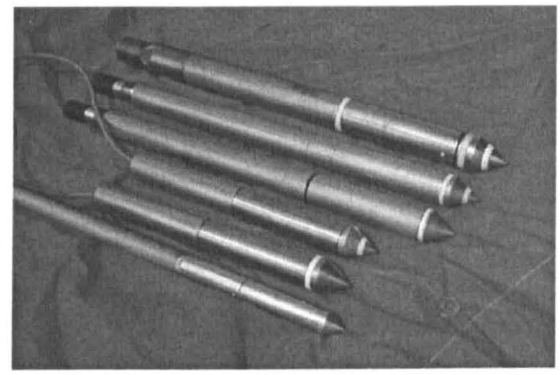

(b)

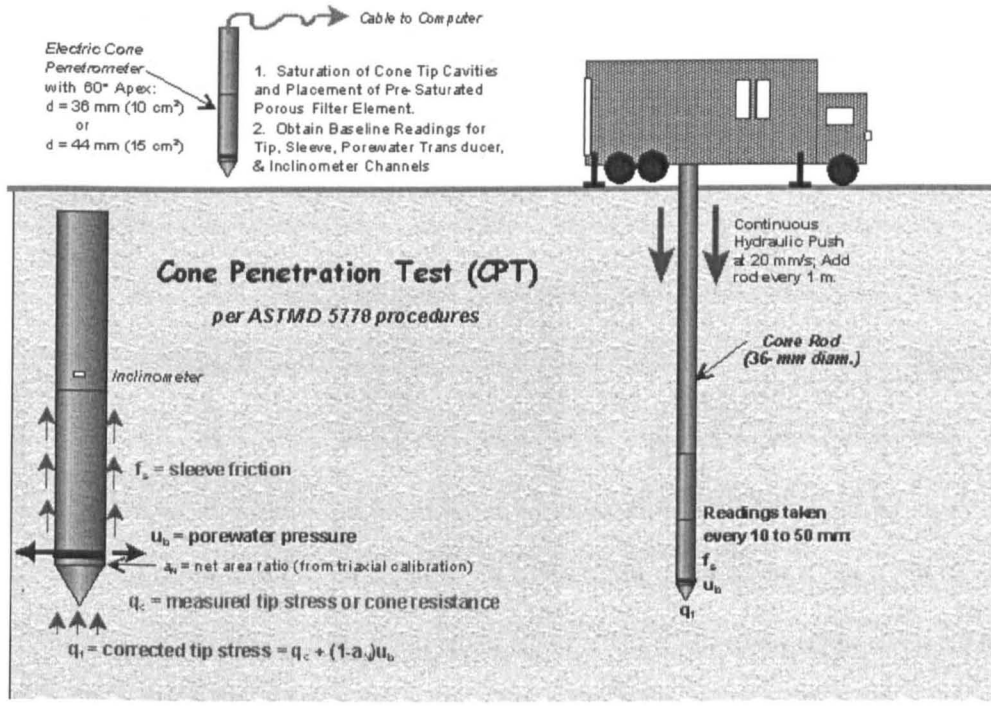

(c)

Fig. 2.33 Cone penetration test (CPT) showing (a) the electric friction-cone penetrometer, (b) a range of cones and (c) schematic diagram of the test equipment (Source: ASTM, 1992 and http://www.ce.gatech.edu, 1995)

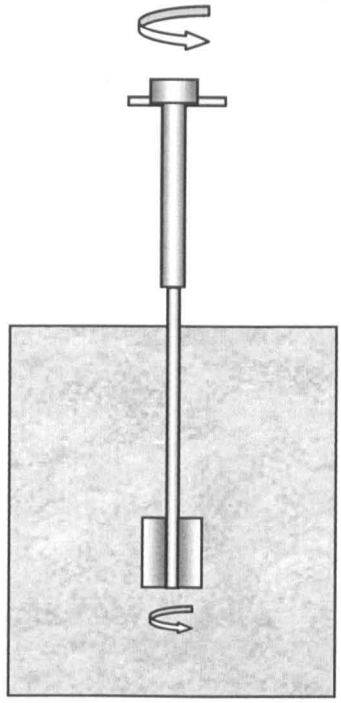

(a)

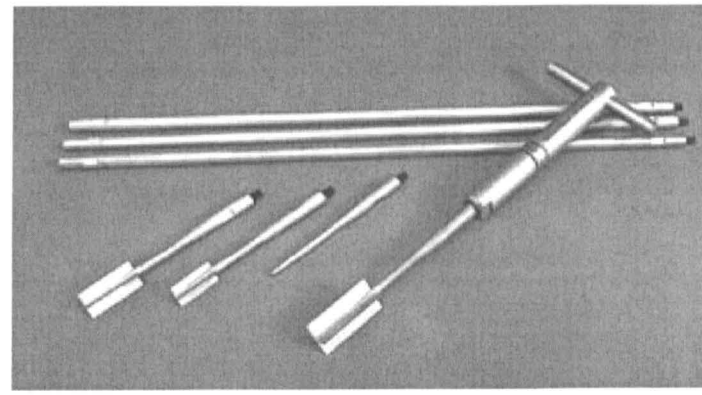

The Field Vane Shear Tester includes:

- Torque Head Assembly
- Six Extension Rods, 50 cm long by 1 cm diameter
- Three Vanes, 16 x 32 mm, 20 x 40 mm, 25.4 x 50.8 mm, (0.63 x 1.25 in, 0.79 x 1.58 in, 1 x 2 in)
- Skin Friction Probe
- Double Ended Wrench and Leather Carrying Pouch

(b)

Fig. 2.34 Vane shear test showing: (a) schematic diagram of the test and (b) the vane shear tester (Source: http://www.durhamgeo.com/, 2003)

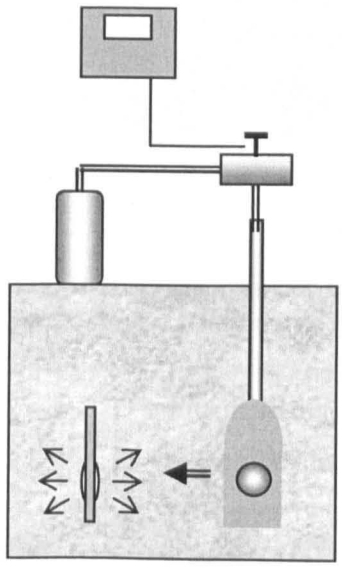

(a)

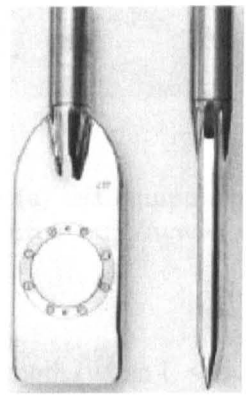

(b)

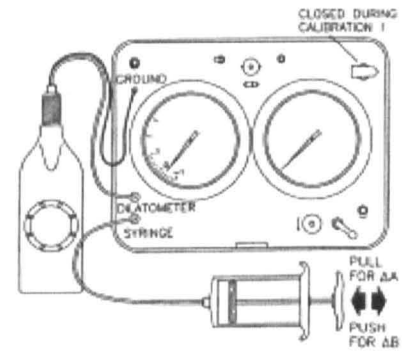

(c)

Fig. 2.35 Dilatometer test (DMT) showing (a) schematic diagram of test, (b) the flat-plate dilatometer, (c) and the test equipment (Source: Marchetti, 2001)

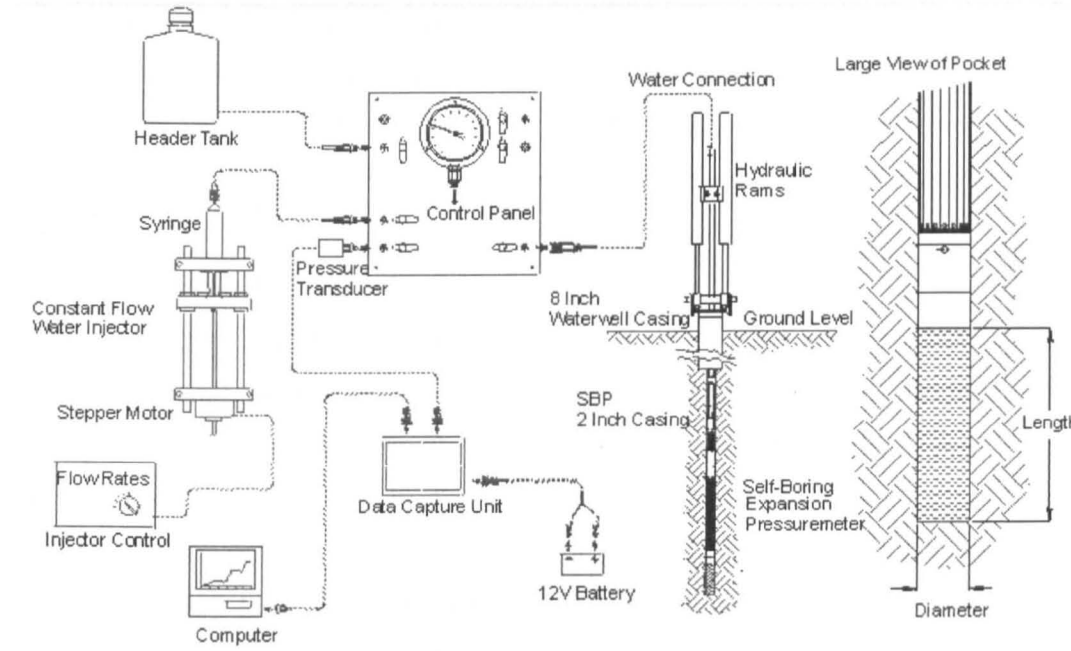

(a)

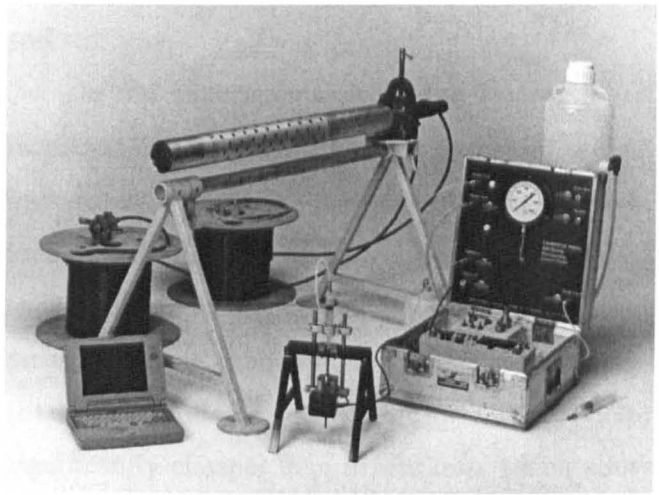

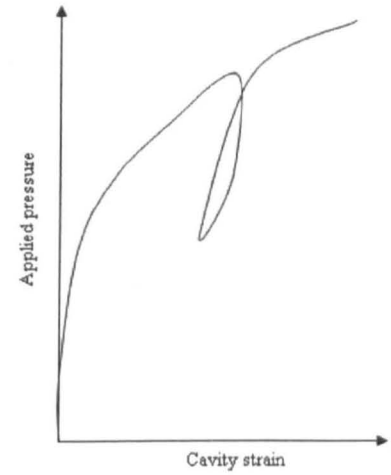

(b) (c)

Fig. 2.36 Pressuremeter test (a) test equipment, (b) the test equipment and (c) typical pressure and strain curve (Source: http://www.cambridge-insitu.com, 2005)

D = pile diameter

L = pile embedded length (when $L < L_{critical}$(critical depth), capacity should be reduced)

Although the FDP can measure the soil properties, the influence of the pile flexural rigidity, EI, still cannot be taken into account. Hence, numerical modelling involving soil properties obtained from PMT and pile properties from standard tables should be carried out in the analysis of pile-soil interaction. An analysis of in situ tests by

Wroth and Wood (1976) and Clarke (1981) suggests that the pressuremeter test would provide soil parameters through theoretical interpretation of the test. Empirical methods are used with the other in situ tests for sands. Thus it was proposed to develop a laboratory pressuremeter to characterise the sand used in the research.

2.4.3. Static loading tests

Static lateral loading tests including full-scale and model tests have been carried out to understand pile-soil response, verify various soil conditions and test innovative pile structures (Rao et al.,1999, Dunnavant and O'Neill, 1989, EI Nagger and Wei, 1999). The ultimate lateral load capacity can be determined from pile head P-Y curves (Matlock, 1970). Pile-soil interaction including bending, and soil resistance can be estimated from measured strains along the pile (EI Nagger and Wei, 1999). The effect of factors such as the shape, depth of the pile and changes of soil stiffness can be evaluated through observing the change in ultimate lateral resistance or pile-soil stiffness.

In the experimental tests, the load acting at the pile head can be gradually increased by use of weights or hydraulic pressure in order to provide a stepped increase in load or displacement (Rao, et al. 1998; El Naggar and Wei, 1999). The load direction should be horizontal; and the contact area of load source and pile head should be constant. In order to study the influence of soil stiffness, a confining pressure can be applied by an air bag surrounding the soil or by a centrifuge system (El Naggar and Wei, 1999, McVay, et al., 1996). Model static loading tests are significantly cheaper than in situ tests which allows parametric studies to be carried out to provide validation data for numerical analyses and means of extrapolatory results from limited full scale tests.

2.4.4. Cyclic loading tests

Cyclic loading tests may be carried out to model a pile subjected to environmental loading. The increase in displacement with the number of cycles is the main feature to be determined. Other features which may affect pile-soil behaviour include: magnitude, frequency and direction of the load; possible load directions have been described by Lin and Liao (1999). Frequency of cyclic loading should be set according to the real conditions; the frequencies of environmental loads (not

including earthquakes) are normally between 0 and 1Hz (Ramakrishna and Rao, 1999).

Two types of loading stages are used to model loading history: single load level and multiple load level. In the multiple type, the load level is gradually increased, and cyclic loading is applied at every load level (Lee and Gilbert, 1980; Byrne and Houlsby, 2004). In the single type, cyclic loading is only carried out at an assigned load magnitude (Ramakrishna and Rao, 1999; El Naggar and Wei, 2000). Loading under multiple load levels to assess particular pile behaviour means that the influence of load levels and number of cycles can be investigated. Loading under a single load level is used to compare the response of different pile types.

Many of the published cyclic loading tests have been carried out within 2000 cycles because the failure condition is achieved or the allowable displacement is reached. Only a few tests have been used to investigate the long term influence of cyclic loading (Meimon et al., 1986).

2.4.5. Review of combined loadings

Pile-soil behaviour under combined loading becomes more complicated than vertical or lateral loading alone acting on a pile as presented in Section 2.3.4. In order to verify the pile-soil behaviour under inclined loading, a static load at an inclined angle is applied at the pile head representing both vertical and lateral loads imposed on the pile together (Meyerhof and Ranjan, 1972). A schematic diagram shown in Fig. 2.37 presents the relationship between the inclined load and inclined angle for vertical piles. Model tests including combined loads and a moment acting at the pile head have been carried out by Sastry and Meyerhof (1986).

For an offshore wind structure, however, lateral loads are applied by environmental loads after the gravity load is applied. A combined loading test is presented by Robertson, et al. (1985); vertical loading is initially applied up to the ultimate limit state then lateral loading is applied. The test procedure used by Robertson should be modified because a pile is defined as failing when the ultimate condition is reached. This ultimate state can come from either the vertical or lateral component.

In recent years, research in cyclic combined loading has only been carried out at the Norwegian Geotechnical Institute and Oxford University. Using a combined loading system shown in Fig. 2.27(h), Byrne and Houlsby (2004) investigated cyclic

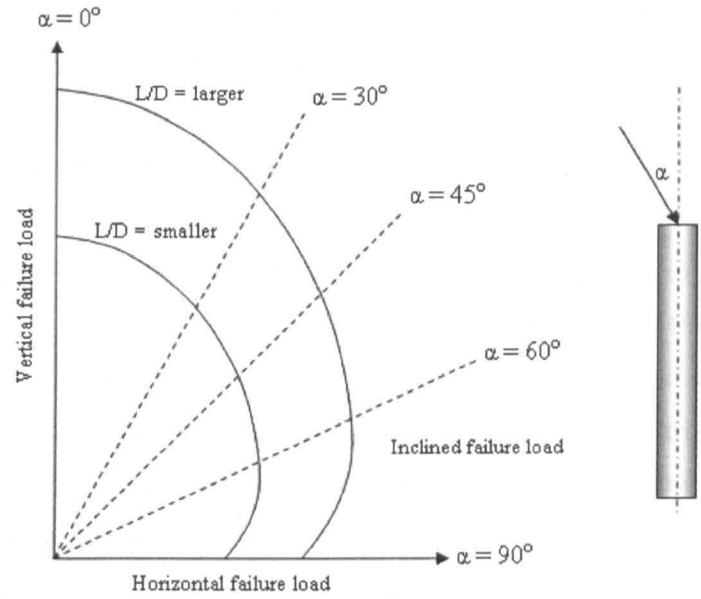

Fig. 2.37 Failure envelope of bearing capacity for vertical piles in dense sand (after Meyerfoh and Ranjan, 1972)

loading of a caisson: cyclic vertical loading has been first applied at certain load levels until a rapid degradation of soil resistance, and then cyclic lateral loading (moment or horizontal) is applied under a prescribed vertical load. Based on these results, the three dimensional yield surface for footings under combined loads can be built (see Fig.2.23).

2.5. Summary

Innovative piles

The importance of the development of offshore wind foundations has been emphasised because of the rapid expansion of global offshore wind market and UK energy target. The selection of suitable foundations to accommodate different environmental features as well as reduce the cost of offshore construction has yet to be developed. Typical types of offshore foundations and some innovative piles used to resist lateral loading have been introduced which suggested that finned piles offered the best opportunity to increase lateral resistance and reduce cost.

Empirical methods

Other studies have investigated laterally loaded piles using empirical approaches, numerical analyses as well as experimental testing. Using empirical approaches, different researchers proposed equations which could be used to predict ultimate lateral soil resistance or ultimate lateral load at the pile head. Broms (1964 a, b) ignored pile rotation and assumed that soil lateral resistance was distributed opposite to the load direction along the pile. Although the rotation of laterally loaded pile has been considered in methods proposed by Brinch Hanson (1961), Petrasovits and Award (1972) and Meyerhof et al. (1981), the assumed soil resistance distributions are different from the actual soil resistance observed from testing. The distribution of soil resistance proposed by Prasad and Chari (1999) is well predicted in the simulation of the soil pressure of a laterally loaded pile according to test results. API (1993) and DNV (2004) methods are the only approaches which consider both normal and shear stresses around a laterally loaded pile. In the following chapters, the empirical approach of finned piles is based mainly on API (1993) and DNV (2004) methods because these two methods are widely used in offshore pile design and the soil stresses (normal and shear) are considered.

All these empirical methods are established from a two-dimensional section which is unable to reflect the cross section of the fins including the increase in flexural stiffness in the fin section. In order to use these equations to predict the ultimate lateral resistance of finned piles, some assumptions have to be defined such as the pile area in the fin section, the appropriate lateral soil coefficient as well as pile to soil stiffness.

Numerical methods

Numerical methods including FD and FE analyses using laterally loaded piles have been introduced in this chapter. Two-dimensional FD software like LPILE has been widely used to predict the behaviour of laterally loaded straight piles, and it provides approximate solutions in the lateral load and displacement curve of the pile head. The unchanged soil stiffness and the two-dimensional model in LPILE could reduce the accuracy to simulate the behaviour of laterally loaded finned piles.

The applications of 3D FEM like ABAQUS and FLPIER in laterally loaded piles have been assessed by Trochanis et al. (1991) and Ng and Zhang (2001); these

advanced 3D FE and FD software give better prediction of pile behaviour than the traditional 2D software especially with regards to pile soil interaction.

In the numerical modelling of laterally loaded finned piles, 2D LPILE was used to predict the behaviour of finned piles based on simplified fin area and stiffness in the fin section. Initial analysis using LPILE was a benchmark for advanced numerical analyses by 3D FE. The 3D FE software LUSAS was used in finned pile modelling. LUSAS software contains many elements which can be used to model different materials like fin, pile, soil and pile soil interface; it also has powerful functions to process nonlinear problems. Therefore, LUSAS was applied in the 3D modelling of finned piles in this research.

Experimental methods

1G model test is one of the efficient approaches to determine the lateral resistance of piles especially for innovative piles. Many static and cyclic loading tests have been carried out to investigate the lateral resistance of piles by using the loading systems shown in Fig. 2.27. A pneumatic load device provided by Mahmoud (1994) and a mechanical gear driven device provided by Purkayastha (1999) are able to provide constant one-way cyclic loading. However, multiple load directions and load magnitudes cannot be provided in these loading systems. Based on the loading devices produced by Mahmoud (1994) and Purkayastha (1999), a new cyclic loading system was built to produce different loading conditions for the investigation of finned pile behaviour under cyclic loading.

Compared to other methods like vane shear, CPT and DMT to determine the in situ soil condition in 1G model test, the pressuremeter test, which may not disturb the soil as the shear box test does, is the most appropriate method to determine the soil property. Taking into account its diameter and length, a simple pressuremeter was built especially for measuring the soil stiffness inside the soil chamber.

LVDT transducer and load measurements introduced in Fig. 2.29 were used to measure the displacement and the load at the pile head, and these data were used to generate the pile head load and displacement (P-Y) curve. Strain gauges described in Fig. 2.30 were used to record changes in strain while the tested pile was subjected to lateral loading. These data can be transformed into moment, shear force, soil resistance and pile deformation along the pile (El Natter and Wei, 1999), and the behaviour of laterally loaded finned piles could be assessed.

In this thesis, 1G model tests of laterally loaded finned piles were carried out to investigate fin efficiency. Empirical methods were used to predict the ultimate lateral resistance of finned piles, and numerical analyses including LPILE and LUSAS were used to generate pile head P-Y curves and to investigate the behaviour of finned piles. Numerical studies were used to verify 1G modelling which could provide more reliable understanding of laterally loaded finned piles.

Applications

The analysis of laterally loaded piles was studied. Empirical methods for calculation of ultimate lateral load were used to estimate the ultimate lateral load of fin piles with different fin dimensions (Chapter 3 and 7). Concepts of serviceability limit state are applied to determine the serviceability load of finned piles based on the pile head load and displacement (P-Y) curve (Chapter 3, 5, 7). The various methods of developing P-Y curve were used to predict the P-Y curve of the model test, and modified methods based on these approaches are suggested in order to simulate the model test (Chapter 7). The influences of cyclic and combined loading were used in the analysis of cyclic and combined loading tests to develop the failure envelope of a finned pile subjected to a combined loading (Chapter 5, 6 and 7).

A review of computer modelling including finite element (FEM) and finite different (FDM) using in lateral loaded pile analysis was completed. Studies using different computer software to simulate lateral pile-soil behaviour provide important information and techniques to explore the behaviour of laterally loaded finned piles (Chapter 3). Important features such as mesh geometry and the determination of pile-soil interface were investigated in order to create an appropriate model for the analyses of the pile soil behaviour (Chapter 3).

A review of model tests included the test methods, test equipment and measuring instruments. Different methodologies mentioned in the review provided the blueprint for the model tests of finned piles (Chapter 5 and 6). The review of loading systems helped develop the principles for the static and cyclic loading systems (Chapter 4). The review of measuring equipment produced guidelines for instrumentation of the model tests (Chapter 4, 5 and 6).

3 Numerical analysis

Compared to different pile foundations like monopile, tripod or tapered foundations for offshore wind farms, *finned piles* offer the best option to increase lateral resistance and to reduce cost as suggested in Chapter 2. Therefore, this study focuses on investigating the behaviour of laterally loaded finned piles and on evaluating fin efficiency.

Although the shape of finned piles has been primarily described by Lee and Gilbert (1980) as shown in Fig. 2.11, a finned pile, in this study, is defined as a pile that has four rectangular plates welded to the top of a traditional monopile at 90° to each other. The geometry of finned pile is illustrated in Fig. 3.1 with the properties shown in Table. 3.1. The dimensions of model finned piles were approximately 1/100 in scale with reference to current offshore monopile foundations in UK and in other European countries. The following analyses including numerical and experimental approaches are based on the properties shown in Fig. 3.1 and Table 3.1.

The six empirical equations used to predict the ultimate lateral resistance of a monopile have been introduced in Chapter 2; their features and constraints have also been described in the summary of the last chapter. In this chapter, these empirical equations are first applied in the calculation of the ultimate lateral load of piles MPS and FPS210. The ultimate load of a series of finned piles with different fin dimensions are calculated according to the method recommended by AIP and DNV. Calculations here are based on the original definitions of these equations. The assessment of those empirical equations is given in Section 7.3.2.

Among all FD and FE software introduced in Chapter 2 for pile analyses, LPILE and LUSAS were chosen to predict the behaviour of laterally loaded finned piles. Two dimensional LIPLE has been widely used to predict the behaviour of a single straight pile subjected to lateral loading. Results from LPILE can be easily generated and used as a benchmark for advanced analyses. LUSAS has functions of three dimensional mesh which are able to simulate the four fins on the pile. The powerful nonlinear functions and the various element types could generate proper finned pile meshes to carry out nonlinear analyses.

A finite difference (FDM) analysis using the LPILE program was carried out to determine the pile head P-Y curves of different finned piles. The deflection,

bending moment, shear force as well as soil resistance along the pile are presented. To gain an understanding of fin behaviour during initial loading, the different pile-soil reactions of MPS and FPS210 were investigated.

Finite element analysis (FEM) was carried out using the LUSAS program. Analysis included features such as 3D modelling of full scale and small scale tests, the selection of pile-soil interface, and a comparison of the behaviour of MPS and FPS210. The pile head P-Y curves were used to show the effect of fins on lateral resistance. Pile and soil movements were presented by 3D deformation meshes; the difference of soil movement in front and behind the side fins was observed. In addition, stresses distributed on the pile and the strains within the soil are shown.

The outcome provides an overview on using finned piles to improve lateral resistance and the pile-soil interaction of finned piles.

3.1. Empirical equations

The limit state of finned piles was calculated using the different equations given in Section 2.3.1. The soil in the analysis was assumed to be uniformly distributed with a unit weight of 16.4 kN/m^3 and a friction angle of 35°. A schematic finned pile is shown in Fig. 3.1, and the properties of the model piles are shown in Table 3.1. It is assumed that the pile was installed inside the soil, and the pile head was subjected to a static lateral load.

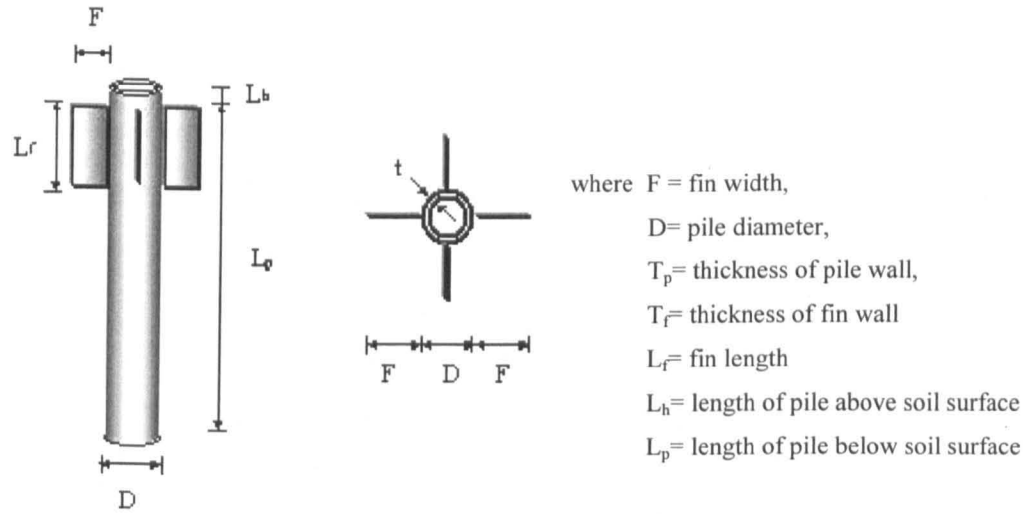

Fig. 3.1 Schematic finned pile

Table 3.1(a) Properties of model piles

Material	Steel
Modulus of Elasticity, E (GPa)	200
Pile length, L_p (mm)	400
Pile outer diameter, D (mm)	44.5
Pile wall thickness, t_p (mm)	2.1
Fin wall thickness, t_f (mm)	2.9

Table 3.1(b) Parameters of model piles

Pile Type	Fin length L_f (mm)	Fin width F (mm)	Moment inertia I *** (mm^4)	Cross section area A *** (mm^2)
MPS, MPC	0	0	64262	285.9
FPS105	50	11	114080	413.5
FPS110	100	11	114080	413.5
FPS120	200	11	114080	413.5
FPS205	50	22	210568	541.1
FPS210, FPC210	100	22	210568	541.1
FPS220, FPC220	200	22	210568	541.1
FPS405	50	44	605311	796.3
FPS410	100	44	605311	796.3
FPS420	200	44	605311	796.3
FPS240*, FPC240**	400	22	210568	541.1

Note: * FPS240 is applied in the numerical analysis and the second stage of model tests but not in the first stage of static loading tests
** 'S' means the pile subjected to static loading; 'C' means the pile subjected to cyclic loading
*** Values of moment inertia, I, and cross section area, A, presented here are taken in the section with fins on the pile

Table 3.1(c) Properties of full scale piles

Material	Steel
Modulus of Elasticity, E (GPa)	200
Pile length, L_p (m)	40
Pile outer diameter, D (m)	4
Pile wall thickness, t_p (m)	0.05
Fin wall thickness, t_f (m)	0.05

Table 3.1(d) Parameters of full scale piles

Pile Type	Fin length L_f (m)	Fin width F (m)	Moment inertia I * (m^4)	Cross section area A * (m^2)
MPF	0	0	1.21	0.62
FPF210	10	20	3.08	1.02
FPF220	20	20	3.08	1.02
FPF240	40	20	3.08	1.02

Note: *Values of moment inertia, I, and cross section area, A, presented here are taken in the section with fins on the pile.

The area and the length of a pile are two important factors to resist lateral force in the empirical methods. In the calculations, the effective area to resist soil resistance is the area perpendicular to the load direction. In the example of a monopile, the effective area is the pile diameter multiplied by the pile length. For a finned pile, the section above the fin tip has an effective area of the pile diameter plus the width of the fins multiplied by the length of the fins.

Two sets of analyses were carried out. The different methods of analysis were compared; a preferred method was used to calculate fin efficiency. In order to compare the ultimate lateral load suggested by various researchers, typical piles, a monopile (MPS) and a finned pile (FPS210), were used in the analysis. The position of rotation, the ultimate load and the ratio of ultimate load for the finned pile to that for the monopile are shown in Table 3.2. The ultimate lateral load, P_u, can be calculated using simplified equations provided by Meyerhof et al. (1981), but the position of rotation is not provided by this method. This is also the case for the methods proposed by Broms (1964) and API (1993) and DNV (2004) which assume that lateral soil resistance is distributed along the whole rigid pile, and the point of rotation is at a position far below the pile tip.

Generally, the ultimate lateral capacity of the finned pile, FPS210, is 2%-18% higher than that of the monopile, MPS. There is no significant difference in the point of rotation between MPS and FPS210. Compared to other methods, the API and DNV methods are relatively conservative. The ultimate load depends on the coefficient of earth pressure, K. The Petrasovits and Award method used a K value of 10, whereas a K of 4 was used in the API and DNV methods. With a similar coefficient of earth pressure, K, in API and DNV methods, the Brinch Hansen method gave results which were one-third of those from the Broms method. In the Broms method, the soil passive pressure was all distributed at the front of the pile; however, in the Brinch Hansen method, the moment equilibrium was considered, and soil stress below the rotation point was distributed on the rear of the pile (see Fig.2.16).

Table 3.2 Ultimate lateral loads calculated by empirical methods

Method	MPS	FPS210	MPS	FPS210	$\frac{P_{u(FPS)}}{P_{u(MPS)}}$
	Ultimate lateral load, P_u (N)		Distance of rotation point below the soil level (m)		
Brinch Hansen (1961)	178.2	204.1	0.3231	0.3222	1.146
Brom (1964)	534.3	564.6	-----	-----	1.056
Petrasovits and Award (1972)	481.6	567.2	0.3165	0.3152	1.171
Mayerhof (1981)	141.7	145.6	----	----	1.028
Prasad and Chari (1999)	108.1	128.5	0.32	0.32	1.185
API (1993) and DNV (2004)	60.0	64.7	----	----	1.078

Table 3.3 Ultimate lateral loads of different piles calculated using the methods provided by API (1993) and DNV (2004)

Pile number	Ultimate lateral load, P_u (N)	$\frac{P_{u(FPS)}}{P_{u(MPS)}}$
MPS	60.0	1
FPS105	60.4	1.007
FPS110	62.1	1.035
FPS120	69.6	1.16
FPS205	60.9	1.015
FPS210	64.7	1.078
FPS220	85.4	1.423
FPS405	62.4	1.04
FPS410	71.2	1.187
FPS420	118.2	1.97
FPS240*	128.8	2.147
Note: * FPS240 is applied in the numerical analysis and the second stage of model tests but not in the first stage of static loading tests.		

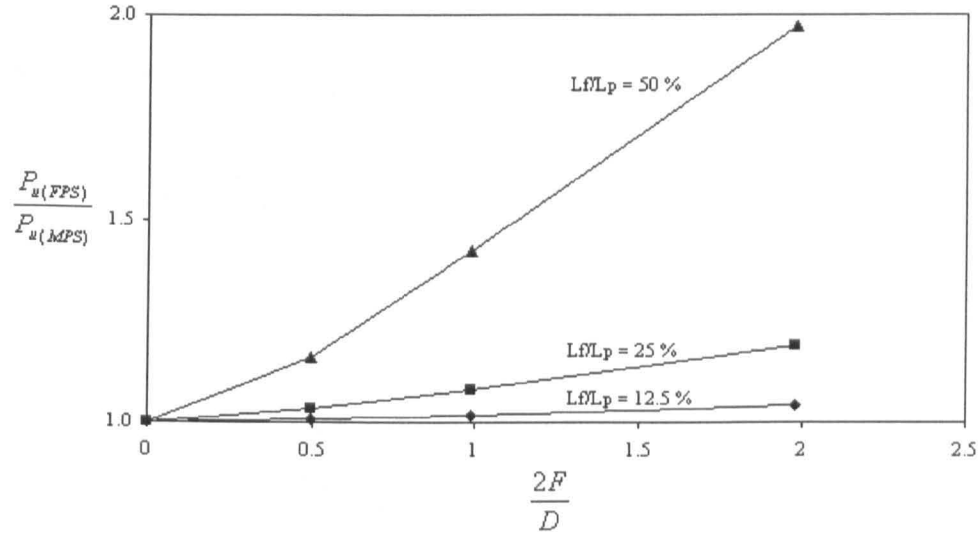

Fig. 3.2 The effect of fin dimensions on the ultimate capacity of the pile predicted by DNV method where F is the width of the fin and D is the diameter of the pile

The following analysis is based on the methods provided by API and DNV. These two codes are specifically for offshore foundation design. In this study, one monopile and ten finned piles with different fin dimensions were used to verify fin efficiency. The dimensions of the piles are shown in Table 3.1 (c) and (d). The ultimate load for each type of pile and the ratio of the ultimate load of finned pile to that of monopole $\frac{P_{u(FPS)}}{P_{u(MPS)}}$ are presented in Table 3.3. The ultimate lateral load increases with an increase in fin dimensions. Based on these results, a normalised relationship between $\frac{P_{u(FPS)}}{P_{u(MPS)}}$ and $\frac{2F}{D}$ is presented in Fig. 3.2 showing the influence of fin width and fin length on lateral capacity. The load ratio $\frac{P_{u(FPS)}}{P_{u(MPS)}}$ increases slightly when F < 0.5 D but the effect of the fins becomes increasingly significant at greater values when F > 0.5 D especially if L = 0.5 L_p. It can be concluded that the fins do increase the lateral capacity of the pile and that effect is most marked when L > 25% L_p and F > 0.25D.

3.2. FDM analysis

3.2.1. Methodology

The 2D FDM program, LPILE, was used to predict the lateral capacity of the piles. A fourth-order differential equation represented in Equation 2.8 was used to predict the behaviour of the laterally loaded pile. In the beam formulae, the behaviour of the beam can be expressed as:

$$EI\frac{d^2y}{dz^2} = M \tag{3.1a}$$

$$EI\frac{d^3y}{dz^3} = S \tag{3.1b}$$

where EI = the flexible rigidity of the pile

z = distance below the ground surface

y = lateral displacement at depth z

M= bending moment at depth z

S = shear force at depth z

Substituting Equation 3.1(a) into Equation 2.8 and using Equation 2.9 results in

$$\frac{d^2M}{dz^2} + P_x\frac{d^2y}{dz^2} + ky = 0 \tag{3.2}$$

The pile length was divided into many small sections which had a constant increment, h (Fig. 3.3(a)). Reese et al. (1977) suggested that the FD expressions for the first two terms of Equation 3.2 at point i are

$$\begin{aligned}(\frac{d^2M}{dz^2})_i = [&y_{i-2}(EI)_{i-1} + y_{i-1}(-2(EI)_i - 2(EI)_{i-1}) + y_i(4(EI)_i \\ &+ (EI)_{i-1} + (EI)_{i+1}) + y_{i+1}(-2(EI)_i - 2(EI)_{i+1}) + y_{i+2}(EI)_{i+1}]\frac{1}{h^4}\end{aligned} \tag{3.3a}$$

$$P_x(\frac{d^2y}{dz^2})_i = \frac{P_xy_{i-1} - 2y_i + y_{i+1}}{h^2} \tag{3.3b}$$

Substituting Equation 3.3 into Equation 3.2, a differential equation in FD form is presented as follows:

$$\begin{aligned}&y_{i-2}(EI)_{i-1} + y_{i-1}(-2(EI)_i - 2(EI)_{i-1} + P_xh^2) + y_i(4(EI)_i \\ &+ (EI)_{i-1} + (EI)_{i+1} - 2P_xh^2 + k_ih^4) + y_{i+1}(-2(EI)_i - 2(EI)_{i+1} \\ &+ P_xh^2) + y_{i+2}(EI)_{i+1} = 0\end{aligned} \tag{3.4}$$

The boundary conditions at the pile head and pile tip were given to solve Equation 3.4, and these bending conditions depended on the constraint of the pile head and the pile length. For example, the bending moment at the pile tip was assumed to be zero.

The generation of the p-y curve in sand was based on the empirical method proposed by Reese et al. (1974) where p is soil resistance and y is the lateral displacement along the pile. The change of non-linear soil resistance, p, with deflection, y, can be represented by a four-segment curve shown in Fig. 3.3(b). The ultimate soil resistance per unit length, p_u, is determined at the point where lateral deflection reaches 0.0375 D (D is pile diameter). The p-y curve in Fig. 3.3(b) is based on known p_u and deflection y.

The soil of unit weight 16.4 kN/m^3, was set as 1 m in depth to model the laboratory tests. The soil was assumed to have a friction angle of 35° and a soil resistance of 3000 kPa/m. Properties of the piles are shown in Table 3.1(a) and (b). The diameter of the pile above the fin tip was assumed to be (D+2F) where F is the fin width. A maximum iteration of 300 and a tolerance of 10^{-8} m were adopted to control the calculation.

3.2.2. Ultimate lateral load of finned pile

Pile head lateral load-displacement curves (P-Y curves) shown in Fig. 3.4 were used to determine the ultimate lateral load which is taken as the load corresponding to the point where the P-Y curve tends towards a straight line (Hirany and Kullhawy, 1989), and the definition of straight line is described as the ratio of Δ(P/Y) to P/Y less than 0.05. Table 3.4 presents the relationship between ultimate lateral capacity and fin dimensions. Ultimate lateral loads of finned piles increase with the increase in fin dimensions, in particular with the increase in fin length. Fig. 3.5 shows the increase in lateral capacity corresponds with the increase in the ratio of fin length to pile length, L_f/L_p. Further, the relationships are similar to those given by the empirical methods (Fig. 3.2).

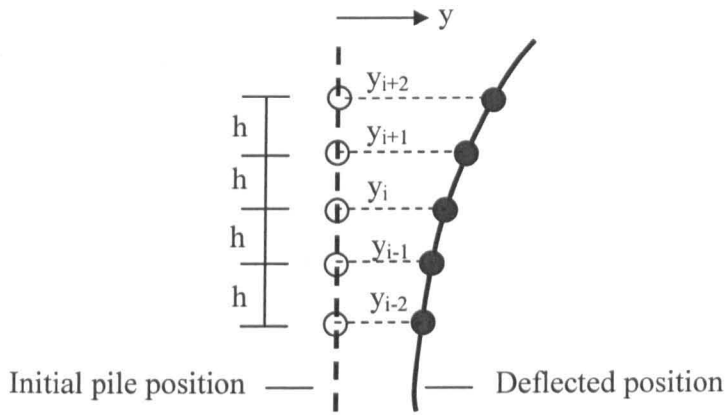

(a)

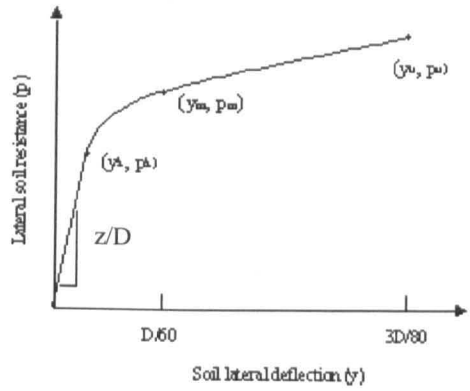

p_u = ultimate resistance per unit length

$y_u = (3/80)\ D$ (D is pile diameter)

$p_m = (B/A)\ p_u$ (B and A are empirical adjustment factors for static and cyclic loading)

$y_u = (1/60)\ D$

$p_k = (z/D)\ k_1\ y_k$ (z is depth, k_i is initial soil modulus)

$$y_k = \left[\frac{Dp_m}{k_i z y^{1/n}}\right]^{\frac{n}{n-1}} \qquad \left(n = \frac{p_m(y_u - y_m)}{y_m(p_u - p_m)}\right)$$

(b)

Fig. 3.3 (a) Representation deflected pile (b)p-y curve for sand (based on Reese, 1974 and 1977)

Table 3.4 Ultimate lateral loads of different piles by LPILE

Pile number	Ultimate lateral load, P_u (N)	$\frac{P_{u(FPS)}}{P_{u(MPS)}}$
MPS	246	1.00
FPS105	250	1.02
FPS110	262	1.07
FPS120	302	1.23
FPS205	253	1.03
FPS210	278	1.13
FPS220	356	1.45
FPS405	262	1.07
FPS410	305	1.24
FPS420	458	1.86
FPS240*	405	1.65

Note: * FPS240 is applied in the numerical analysis and the second stage of model tests but not in the first stage of static loading tests.

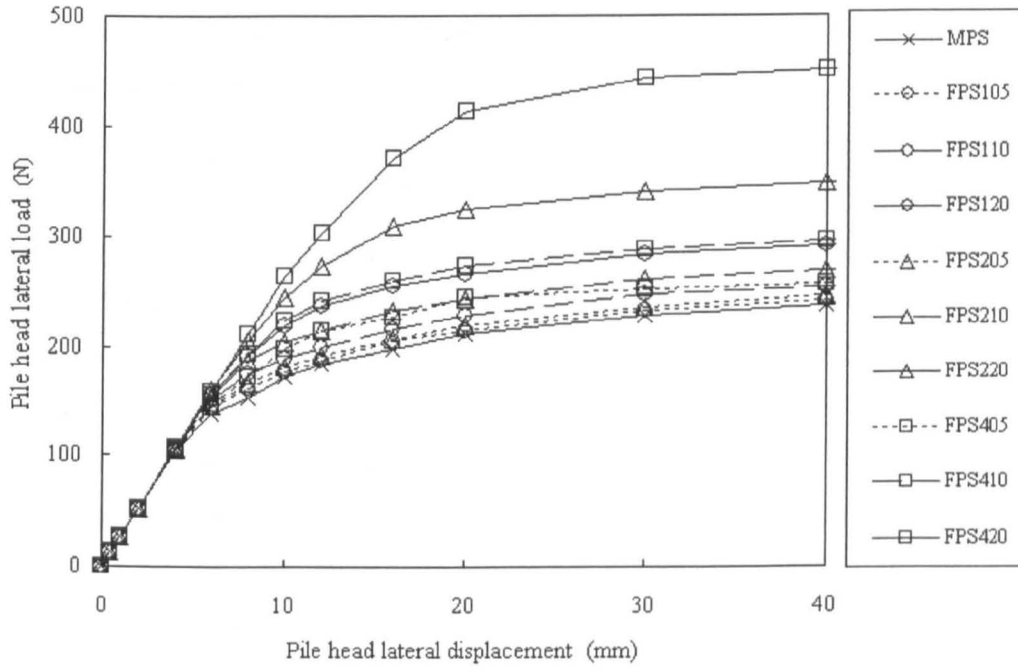

Fig. 3.4 Computer modelling of pile head P-Y curves by LPILE

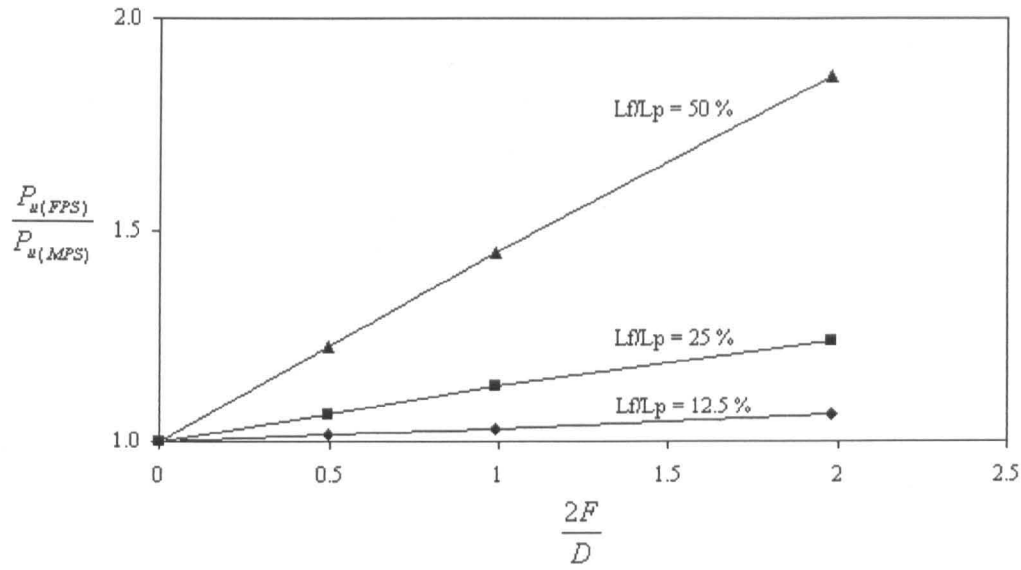

Fig. 3.5 The effect of fin dimensions on the ultimate capacity of the pile predicted by LPILE modelling where F is the width of the fin and D is the diameter of the pile

3.2.3. Pile-soil behaviour of finned pile

Typical behaviour

Pile and soil behaviour can be represented by the change in deflection, bending moment, shear force and soil resistance along the pile. In order to study pile-soil behaviour, two model piles, MPS and FPS210, were selected. The piles were subjected to increased static lateral displacements: 0.5, 1, 2, 4, 6, 8, 10, 12, 16 and 20 mm at the pile head to represent static lateral loads acting at the pile head.

Fig. 3.6 shows pile deflection with depth for MPS and FPS210. The near rigid behaviour of piles is evident from the absence of significant deformation in the pile body. Instead of deformation, piles rotate in the direction of the load with the increase in loading. A rotation point is observed at about two-thirds of the pile length from the point of load application; the point of rotation moves down from the depth of 0.3 m to 0.32 m when the pile head deflection increases from 0.5 mm to 20 mm. Since an incremental 2 mm of the movement of the pile head was used in both MPS and FPS210 to control the displacement. There is no difference in the displacement of the pile head for MPS and FPS210. Each curve represents a different load.

The variation of bending moment in the piles, MPS and FPS210, with depth is shown in Fig. 3.7. Generally, there is no moment at the pile head and the pile base; the maximum moment is located at about the middle of the pile. The moment

increases with an increase in lateral loading, and the position of the maximum moment moves down when the load increases. This is because the upper soil reaches failure first due to the large pile-soil movement.

The change in shear force along the pile is shown in Fig. 3.8. The positive and the negative shear force acted on the upper and the lower part of the pile, respectively; the transition point is the position at which maximum bending moment occurs. The shear force at the pile head is the load at the pile head. The curves of change in shear force with depth for MPS are smooth; the discontinuity of the curves for FPS210 can be observed at 0.1 m depth at the base of the fin.

Fig. 3.9 shows the soil reaction along the piles: MPS and FPS 210. The transition position between the passive resistance of the pile is at the pile rotation point. The maximum soil reaction at the pile tip increases with the increase in lateral loading. The fin contribution is obvious since there is a step change in soil resistance above the bottom of the fins. Note that this distribution is similar to that assumed by Prasad and Chari (1999) (Fig. 2.16).

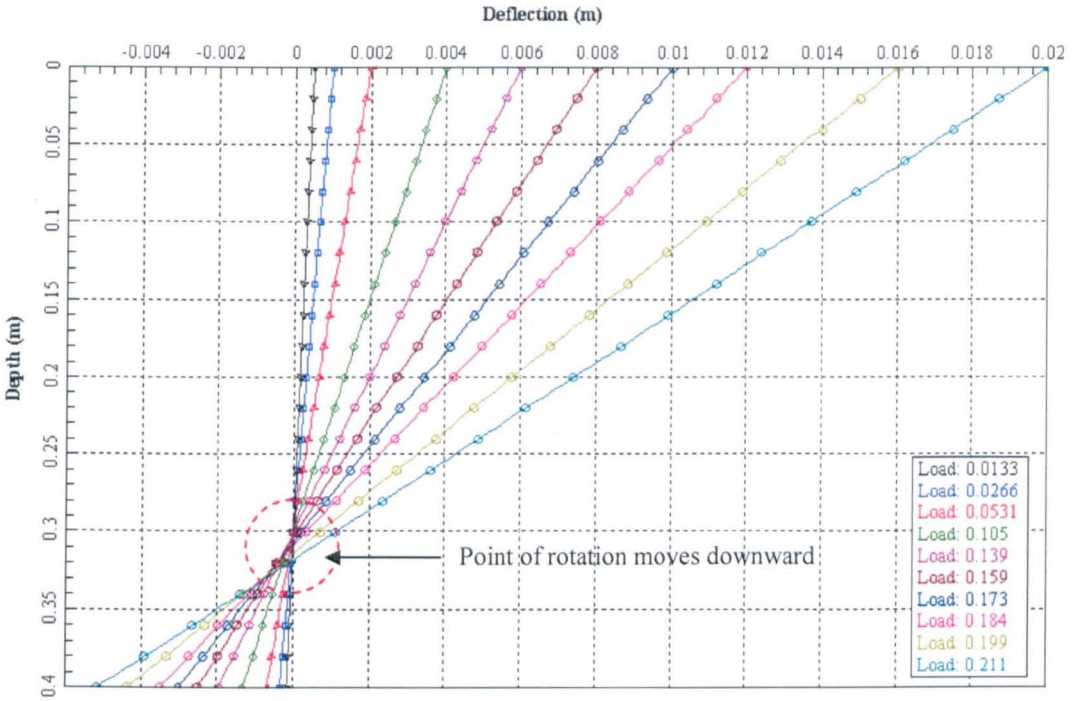

(a)

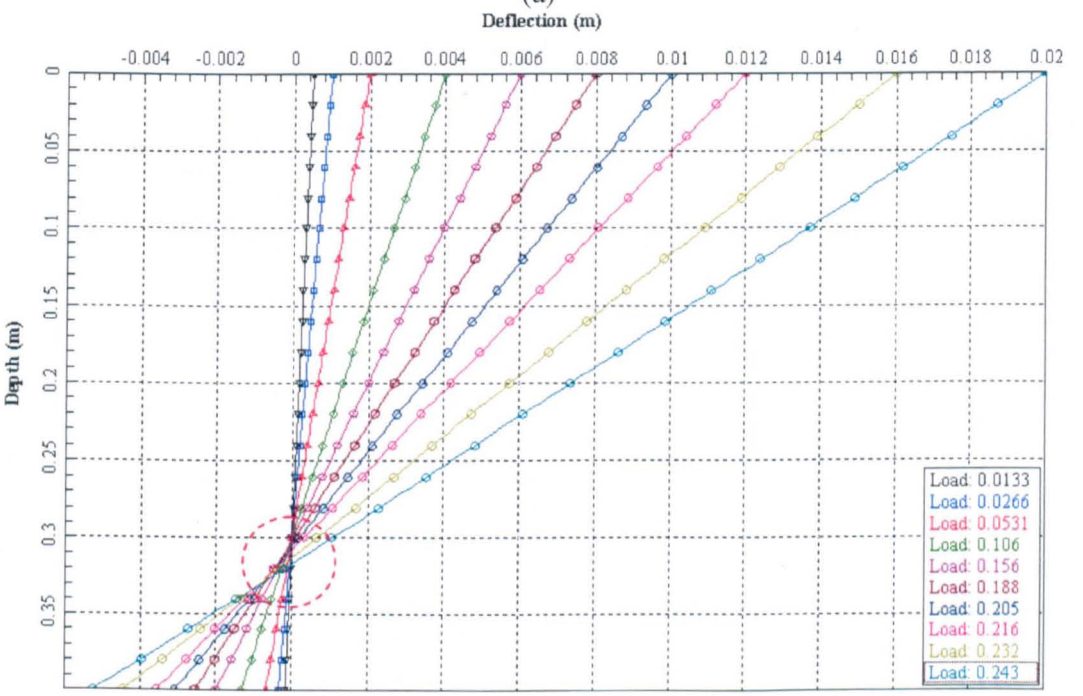

(b)

Fig. 3.6 Variation of lateral deflection with depth for (a) MPS; (b) FPS210 generated by LPILE

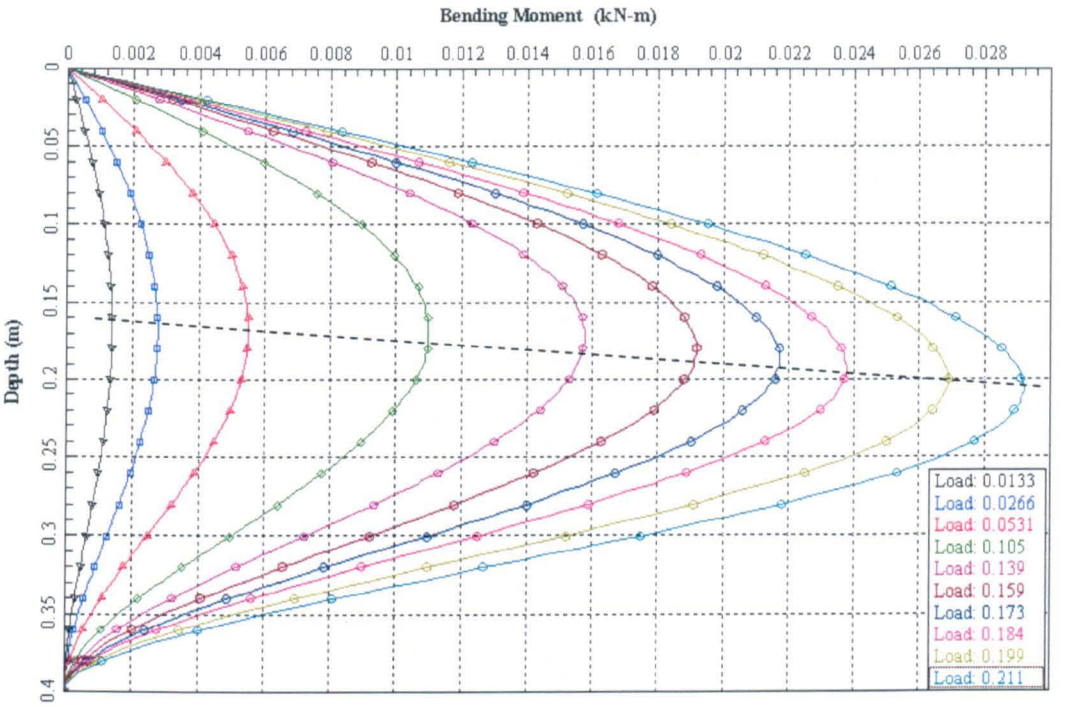

(a)

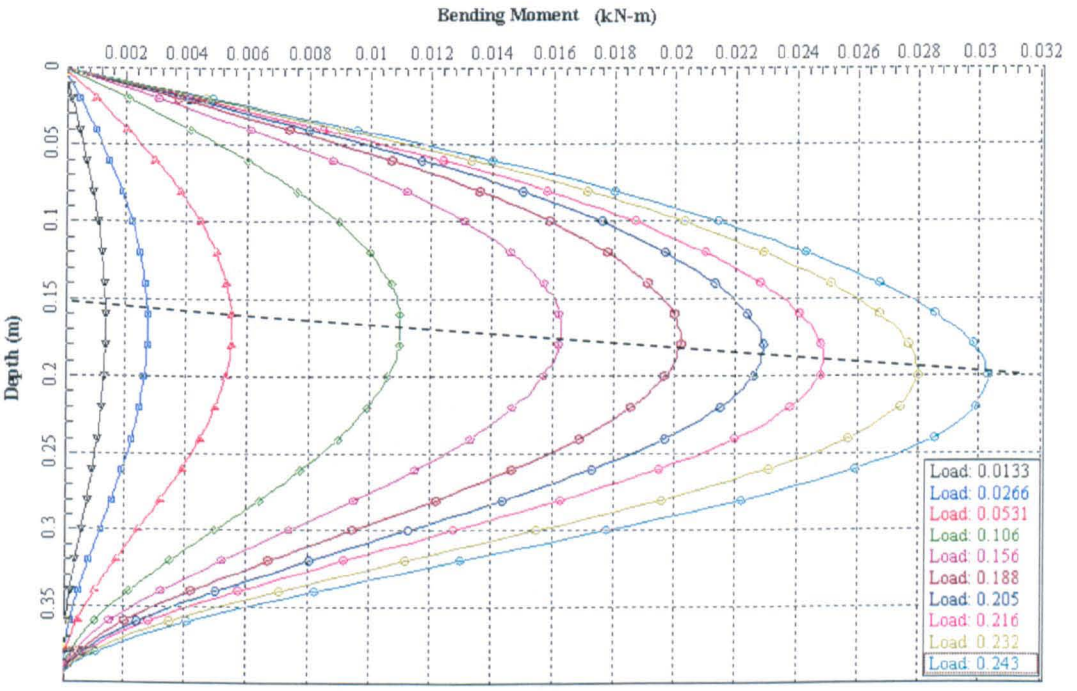

(b)

Fig. 3.7 Variation of bending moment with depth for (a) MPS; (b) FPS210 generated by LPILE

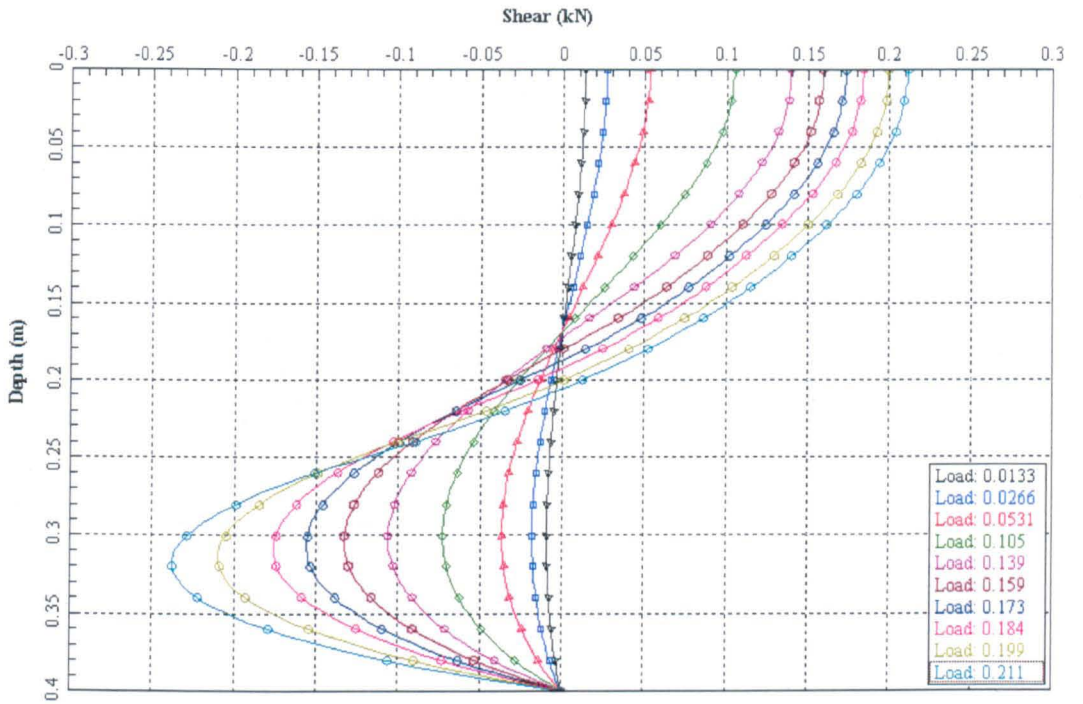

(a)

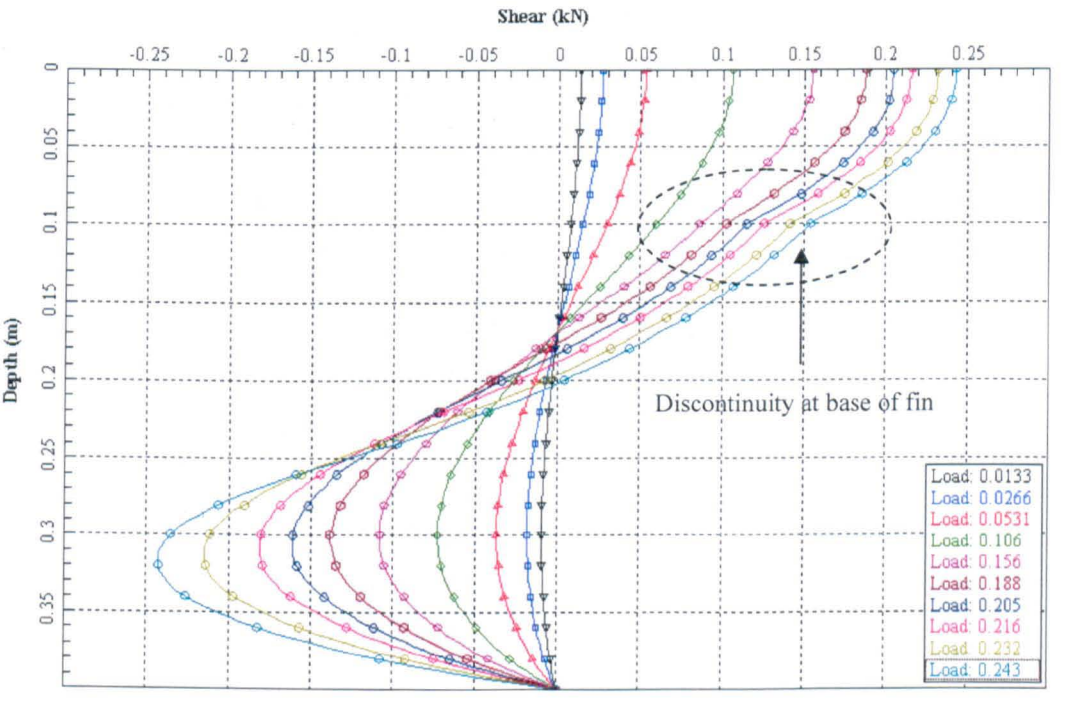

(b)

Fig. 3.8 Variation of shear force with depth for (a) MPS; (b) FPS210 generated by LPILE

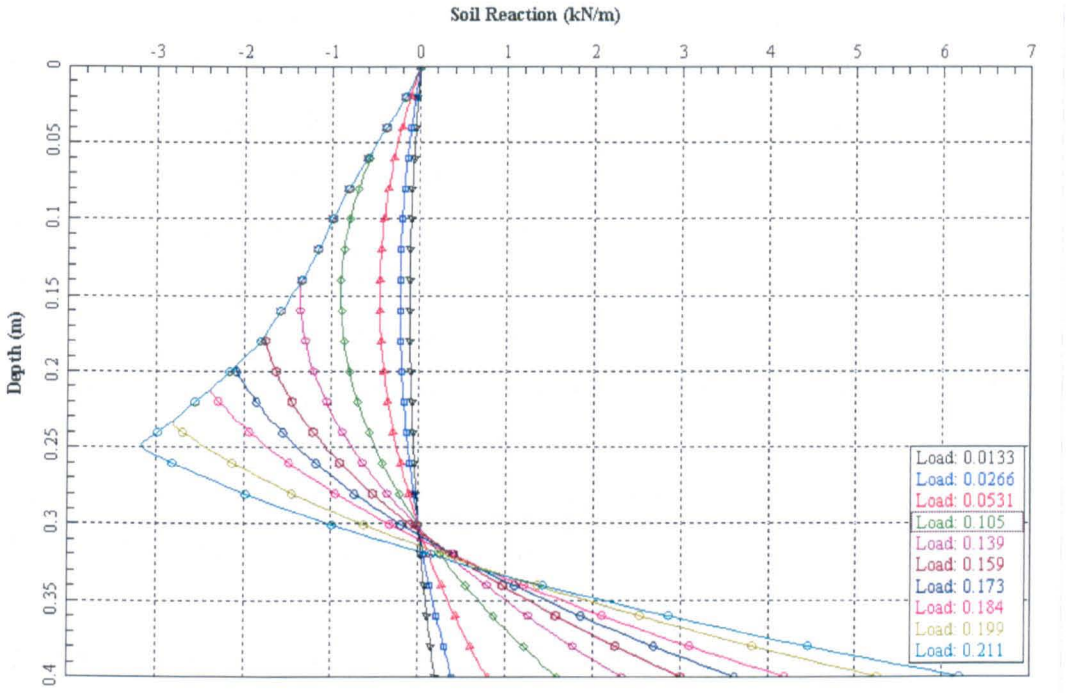

(a)

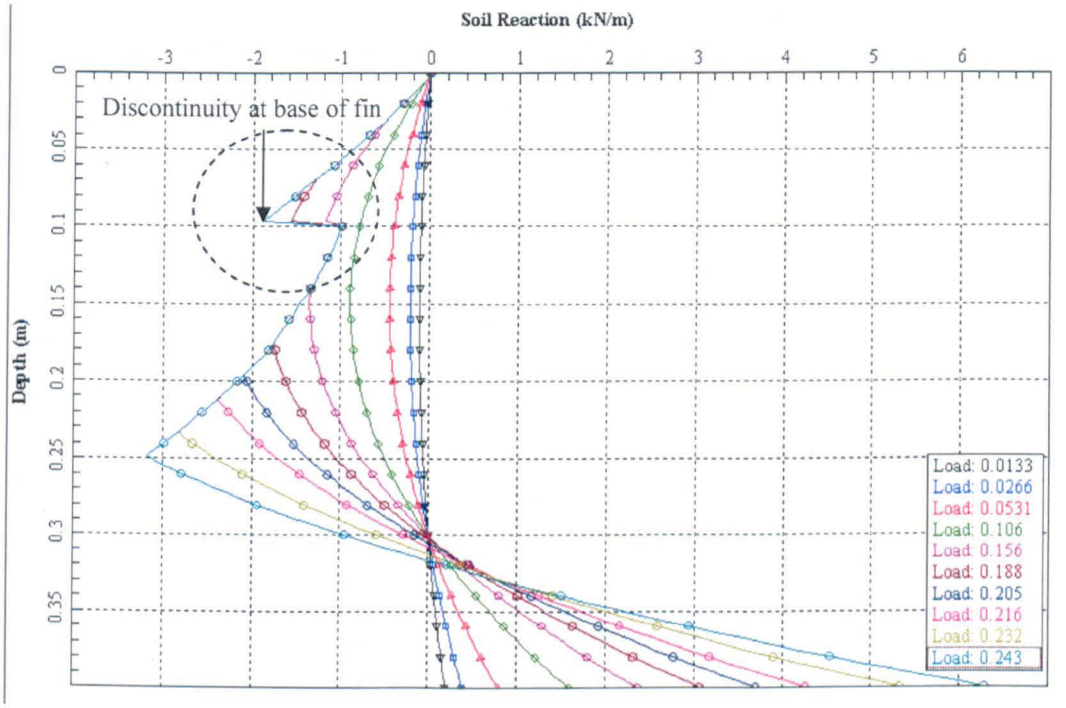

(b)

Fig. 3.9 Variation of soil resistance with depth for (a) MPS; (b) FPS210 generated by LPILE

Fin contribution

In the previous section, the response of piles, MPS and FPS210, was demonstrated by applying displacements. The effect of fins could not be observed since factors such as bending moment, shear force and soil reaction are directly related to displacement. In order to understand the influence of fins on deflection, bending moment and soil reaction, a static lateral load of 200 N was applied at the pile head of model piles, MPS and FPS210.

Lateral displacement along the pile was greatly reduced by the use of fins as shown in Fig. 3.10. The pile head deflection of FPS210 is only 60% of that of MPS. In addition, the point of rotation of FPS 210 is 0.04 L_p higher than that of MPS. The bending moment of FPS210 is less than that of MPS (Fig. 3.11), and the maximum bending moment was reduced by 15% due to the presence of fins. Fins also reduced both the shear force along the pile (Fig. 3.12) and the maximum soil resistance (Fig. 3.13). The additional soil resistance over the fin section is a result of the increase in pile rigidity and effective area. The shear force increase in this section is due to the increase in both soil reaction and reaction area.

Although true soil movement could not be examined near the fin region, the basic pile-soil reaction can still be observed through two-dimensional finite difference analysis. The contribution of fins in increasing lateral resistance has been proven by FDM modelling.

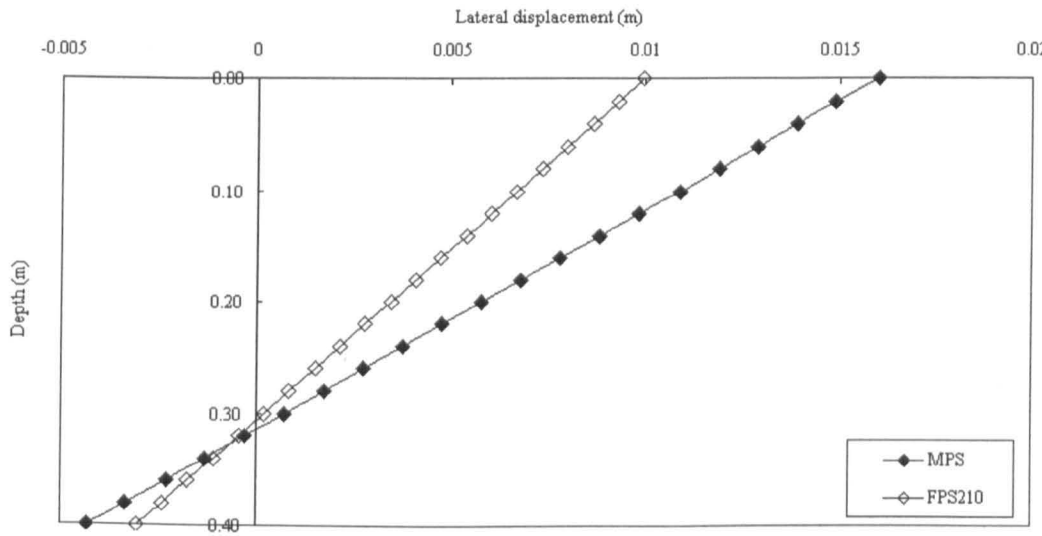

Fig. 3.10 Lateral deflection of piles subjected to a lateral load of 200 N by LPILE

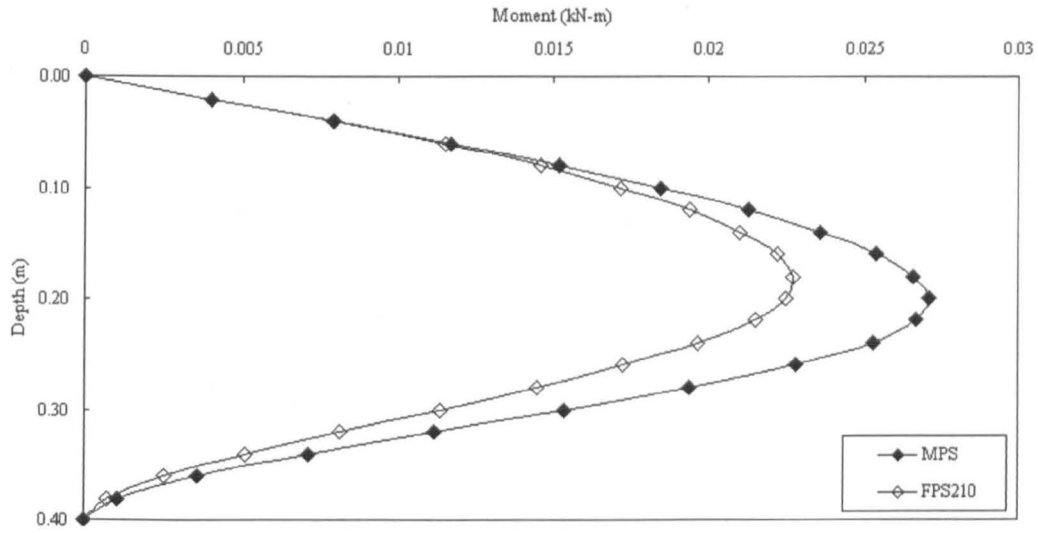

Fig. 3.11 Distribution of bending moment of piles subjected to a lateral load of 200 N by LPILE

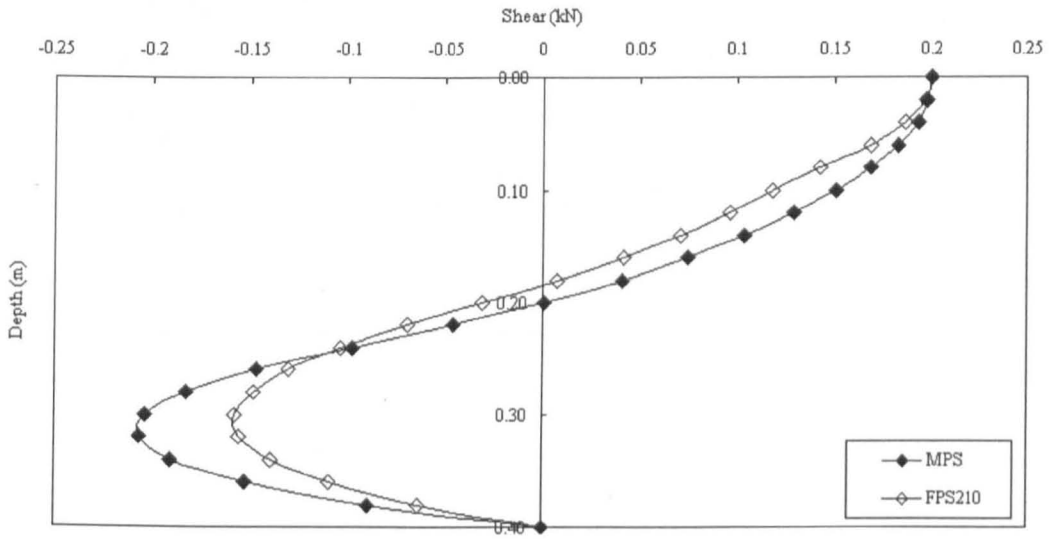

Fig. 3.12 Shear force distribution along the length of the piles subjected to a lateral load of 200 N

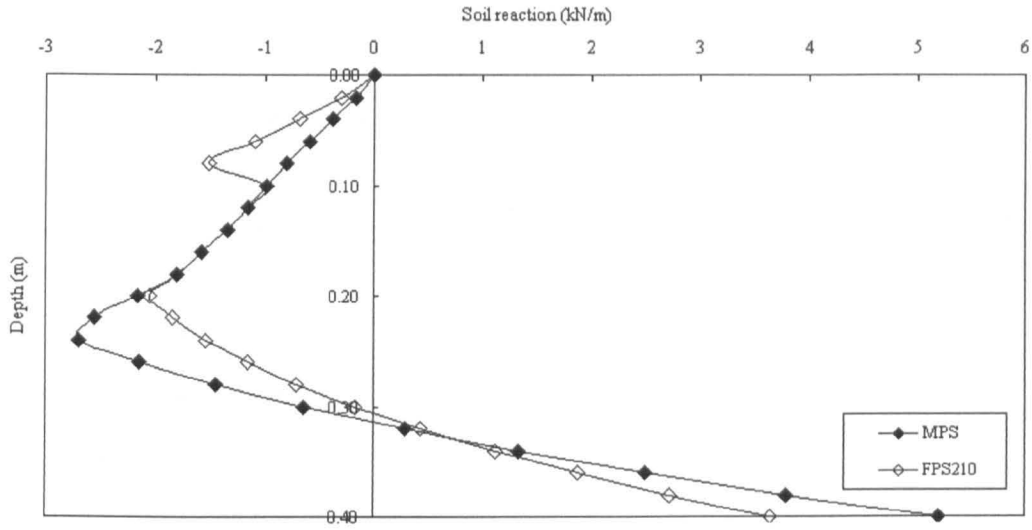

Fig. 3.13 Distribution of soil resistance of piles subjected to a lateral load of 200 N

3.3. FEM analysis

3.3.1. Introduction (based on LUSAS manuals 1996)

Main theory

In an FEM analysis, a 3D body may be subjected to surface forces, body forces and concentrated loads; and the body will move from its original position by a distance of $\underline{\mu}$ which gives rise to strain $\underline{\varepsilon}$ and the corresponding stress $\underline{\sigma}$. The principle of virtual work can be utilised in the equilibrium equation and the relationship between the total internal work and the total external work is shown in Equation .3.5.

$$\int_V \delta \underline{\varepsilon}^T \underline{\sigma} dv = \int_V \delta \underline{u}^T \underline{f} dv + \int_S \delta \underline{u}^T \underline{t} ds + \sum d\underline{u}^T \underline{F} \tag{3.5}$$

where $\underline{t}$ = surface forces

$\underline{f}$ = body forces

$\underline{F}$ = concentrated loads

$\underline{\mu}$ = displacement of the element

$\underline{\varepsilon}$ = strain of the element

$\underline{\sigma}$ = stress of the element

In an FEM analysis, each body is an assemblage of discrete elements interconnected at nodal points. Equation. 3.6 is the relationship of the element displacement and the nodal displacement.

$$\underline{u} = \underline{N}\underline{a} \tag{3.6}$$

where $\underline{u}$ = displacement of the element

$\underline{a}$ = displacement of the nodal

$\underline{N}$ = displacement interpolation or shape function matrix

In addition, strains within an element can be related to the nodal displacement by Equation. 3.7.

$$\underline{\varepsilon} = \underline{\underline{B}}\,\underline{a} \tag{3.7}$$

where $\underline{\varepsilon}$ = strain within an element

$\underline{\underline{B}}$ = the strain-displacement matrix

$\underline{a}$ = displacement of the nodal

Here strains are split into an elastic part and a plastic part:

$$\underline{\varepsilon} = \underline{\varepsilon^e} + \underline{\varepsilon^p} \tag{3.8}$$

where $\underline{\varepsilon^e}$ is elastic strain and $\underline{\varepsilon^p}$ is plastic strain. Elastic stress uses Hooke's law to relate to the elastic strain:

$$\underline{\sigma'} = \underline{\underline{D^e}}\,\underline{\varepsilon^e} = \underline{\underline{D^e}}(\underline{\varepsilon} - \underline{\varepsilon^p}) \tag{3.9}$$

where $\underline{\sigma'}$ is the stress and $\underline{\underline{D^e}}$ is elastic material stiffness matrix.

Using Equations 3.6, 3.7 and 3.9, the virtual work Equation 3.5 can be described as:

$$\sum_{e=1}^{n} \delta\underline{a}^T \int_V \underline{\underline{B}}^T \underline{\underline{D}}\,\underline{\underline{B}}\,dv\,\underline{a} = \delta a^T \left[\sum_{e=1}^{n} \int_V \underline{N}^T \underline{f}\,dv + \sum_{e=1}^{n} \int_s \underline{N_s}^T \underline{t}\,ds - \sum_{e=1}^{n} \int_V \underline{\underline{B}}^T (\underline{\sigma} - \underline{\underline{D}}\,\underline{\varepsilon})dv + F \right] \tag{3.10}$$

where $\underline{a}$ = displacement matrix

$\underline{\underline{B}}$ = the strain-displacement matrix

$\underline{\underline{D}}$ = material stiffness matrix

$\underline{N}$ = displacement interpolation

$\underline{f}$ = body force matrix

$\underline{N_S}$ = interpolation functions for the surface of the elements

$\underline{t}$ = surface force matrix

$\underline{\sigma}$ = stress of the element

$\underline{\varepsilon}$ = strain of the element

n = the number of elements in the analysis

F = concentrate load

In the virtual displacement theorem, the equilibrium equations of the element assemblage become

$$\underline{\underline{K}}\,\underline{a} = \underline{R} \tag{3.11}$$

where $\underline{a}$ is nodal displacement and $\underline{R}$ is structure force vector including body loads, surface tractions, concentrated loads as well as initial stresses and strains. The structure stiffness matrix, $\underline{\underline{K}}$, is defined as:

$$\underline{\underline{K}} = \sum_{e=1}^{n} \int_V \underline{\underline{B}}^T \underline{\underline{D}}\,\underline{\underline{B}} dv \tag{3.12}$$

Nonlinear properties

Nonlinear material properties can be represented by two types of elasto-plastic models based on continuum and consistent formulations. In the continuum formulation, the plastic strains are integrated according to a strict interpretation of the flow rule. This formulation is applied in older models like von Mises, Tresca, Mohr-Coulomb and Drucker-Prager models. In the consistent formulation, the older models have been reinterpreted in a search for greater numerical efficiency, and the stability for large load steps is improved. In addition, quadratic convergence in the global Newton-Raphson interactions improves the convergence problem.

In this study, the Mohr-Coulomb criterion accompanied with consistent formulations has been used. Based on the Coulomb friction law, the Mohr-Columb yield criterion as shown is defined as

$$F(\underline{\sigma}, k) = \tau - (c - \sigma_n \tan\phi) = 0 \tag{3.13}$$

where τ is shear stress, σ_n is normal stress, c is cohesion, and ϕ is friction angle. Furthermore, the Mohr-Coulomb yield function can be expressed as

$$F(\underline{\sigma}, k) = \sigma_n \sin\phi + (J_2)^{1/2}\left[\cos\theta - \frac{1}{\sqrt{3}}\sin\theta\sin\phi\right] - c\cos\phi \tag{3.14}$$

where θ is the lode angle approaches $\pm 30°$, J_2 is second stress deviator invariant. Fig. 3.14 shows the 3D Mohr-Coulomb yield function.

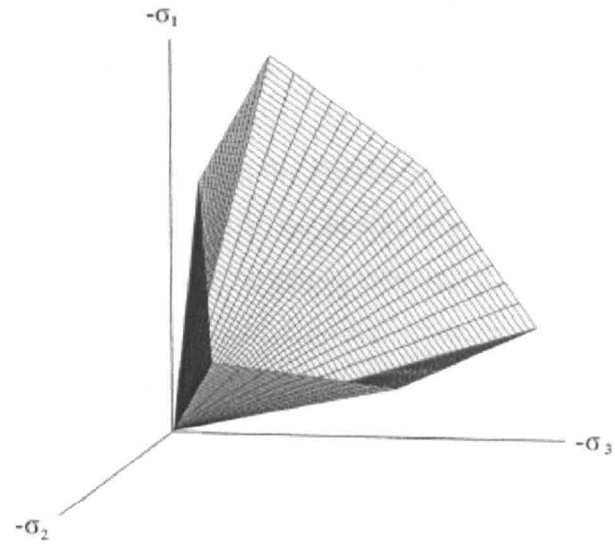

Fig. 3.14 Mohr-Coulomb yield surface (Source: Plaxis, 2001)

Nonlinear static analysis

Nonlinearities include material and geometrical nonlinearities as well as deformation dependent boundary conditions. Material nonlinearity should be specifically considered when the material stress-strain relationship is significantly nonlinear, and yielding causes a large decrease in material stiffness. Geometrical nonlinearity is due to large structural deformations and changing of equivalent nodal forces transformed from load vectors; the applied load vectors on the elements may change significantly when the deformation or angle of inclination becomes large. Instability of a deformation dependent boundary may occur due to the deformed shape of the structure; the soil is modelled as a bilinear stiffness material to take account of the initial gap between the pile and the soil (see Fig. 3.15).

In order to prevent a failure to converge or a false convergence of the results due to the nonlinear properties, LUSAS uses a variety of iteration procedures with small increments of load and displacement. The nonlinear load-displacement curve may be optimised through different iteration procedures, in which, the Newton-Raphson method has been widely used in FEM analysis because it can make the results stable and converges gradually. In this procedure, the tangent stiffness matrix needs to be inverted during each iteration, and failure to converge may occur when critical nonlinear material properties are reached. The modified Newton-Raphson method having a constant stiffness improves the calculated efficiency, and Fig 3.16 shows the variable and the constant stiffness models. In addition, the linear result-

searching method is also applied which provides a constant increase in load step. Iterative procedures can be carried out in each load step which can improve the convergence rate of the Newton method.

Convergence of the solution in the iterative procedure is based on appropriate convergence criteria, which decides if the iterations should be carried on. A tight tolerance may result in unnecessary iterations; whereas, a slack tolerance may lead to an incorrect answer. Relatively tight converge criteria should be applied in the analysis of geometrical nonlinearity to maintain the solution on the correct equilibrium path. Slack criteria, however, may be applied in material nonlinear analysis, because high local residuals may be tolerated. In LUSAS, many criteria are available to monitor convergence; and their definitions and tolerances are given in Table. 3.5. The selection of tight, reasonable or slack tolerances of these criteria is based on the type of nonlinearity of the problem.

There are two types of incremental (iterative) procedures: constant load level increment and modified arc length increment; convergence iteration is carried out at each load level. In constant load level iteration, the load level increment can be assigned by multiplying load factors manually or automatically. In the modified arc length method, the increment in load level can be proportional or non-proportional loading. The convergence near the limit points can be easily achieved as a result of flexible loading. In addition, the constraint of the arc-length method is in the stabilisation of the iterative process due to the rule of automatic load adjustment.

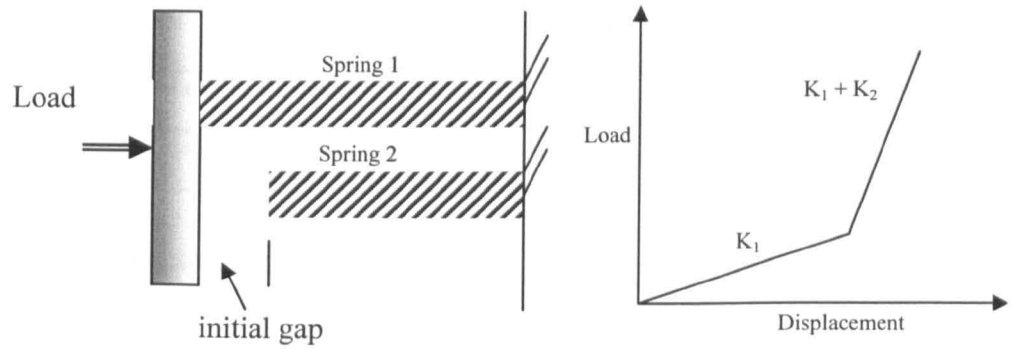

Fig. 3.15 Nonlinear support condition

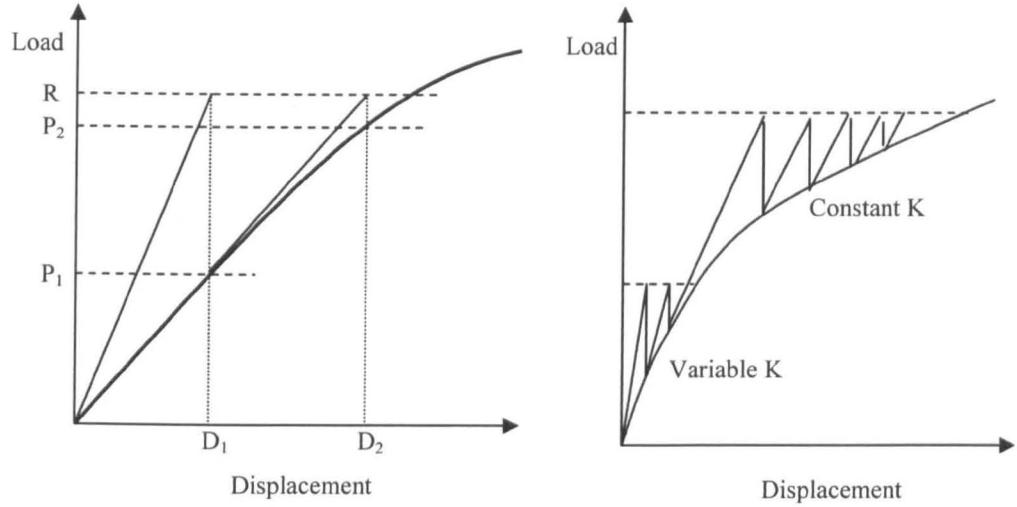

Fig. 3.16 Newton-Raphson iteration procedures (a) standard; (b) modified with constant K.

Table 3.5 Convergence criteria in LUSAS (source: LUSAS,1996)

Criteria	Definition	Tolerance
Euclidian residual norm (rdnrm)	Ratio of the norm of the residuals to the norm of the external forces shown by percentage	0.1< rdnrm <5: flexible tolerance rdnrm < 0.1: tight tolerance for geometric nonlinearity
Euclidian displacement norm (dpnrm)	Ratio of the norm of the iterative displacement to the total displacement represented by percentage	0.1< dpnrm < 1: reasonable tolerance 0.001< dpnrm < 0.1: tight tolerance
Euclidian incremental displacement norm (dtnrm)	Ratio of the norm of the iterative displacement to the norm of the displacement for that increment represented by percentage	0.1< dpnrm < 1: reasonable tolerance 0.001< dpnrm < 0.1: tight tolerance
Work norm (wdnrm)	Ratio of the work done by the residual forces on the current iteration as a percentage of the work done by the external forces on iteration zero represented by percentage	10^{-3}< wdnrm <10^{-1}: slack tolerance 10^{-6}< wdnrm <10^{-3}: reasonable tolerance 10^{-9}< wdnrm <10^{-6}: tight tolerance
Root mean square of residuals (RMS)	The root mean square value of all the residuals in the problem	depending upon the unit of the problem
Maximum absolute residual (MAR)	The maximum absolute residual in a problem	depending upon the unit of the problem

3.3.2. Methodology

Establishment of 3D geometry

A three-dimensional axisymmetric model including pile and soil has been built; details of the geometry are shown in Fig. 3.17. The boundary is a cylinder with a diameter twenty times that of the pile, and with a depth 1.25 times of the pile length in order to eliminate the boundary effect under lateral loading. The model pile is set

in the middle of the cylinder, and the pile head is located at the top of the cylinder. In the surface cross section (x-y plane), the geometry is divided into 6 columns, and each column is defined by 16 points. The space between two layers from the inner to the outer zone varies from 2 up to 5 times of the pile diameter in order to model soil and pile models. In the vertical (z-direction) cross section, the geometry is divided into 10 layers with constant spacing of 0.25 pile length. Pile dimensions are given by both full scale and small scale models (Table 3.1). Based on this arrangement, all the surface meshes are quadrilateral in shape defined by 4 points and all the volume meshes are hexahedral in shape defined by 8 points. In these arrangements, pile and soil mesh geometries are satisfied such that the shape ratio of length to width is less than 10. A small gap of 1% of the pile diameter between the pile and soil is assigned to the interface element.

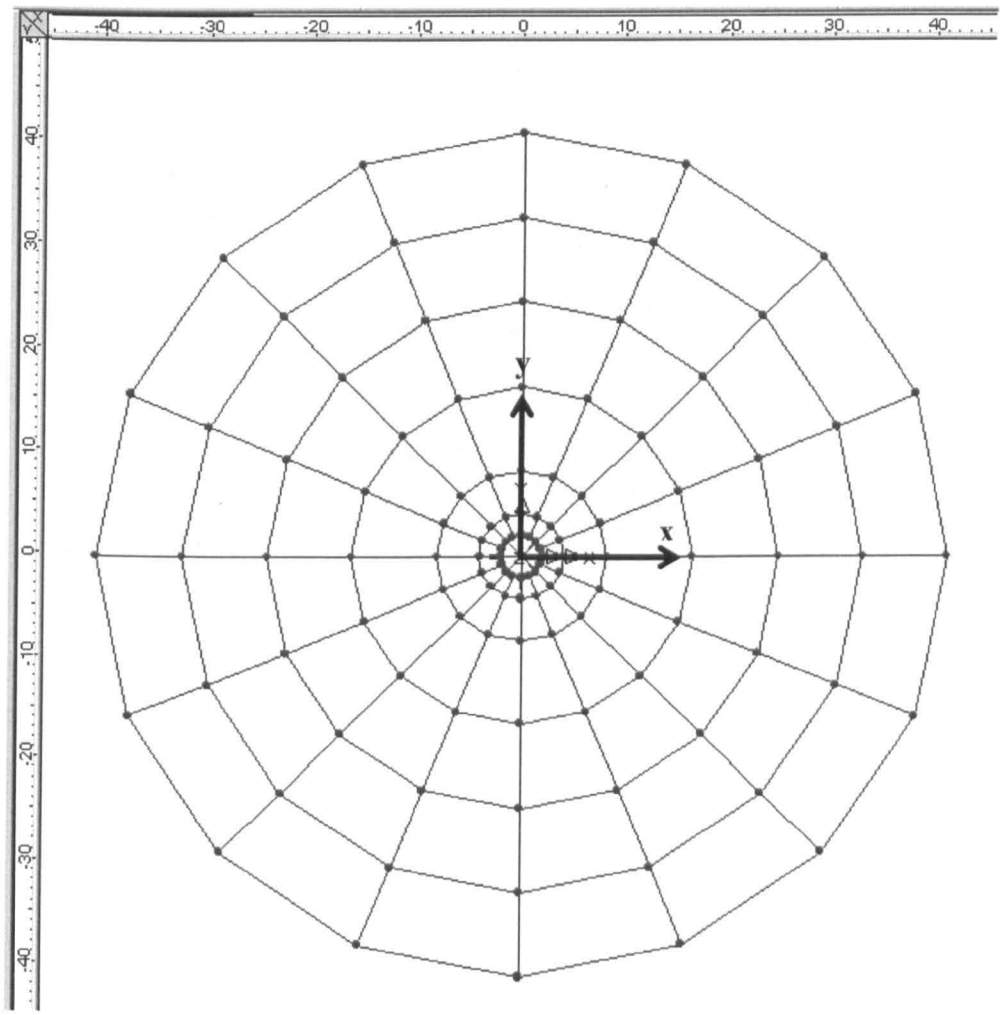

(a)

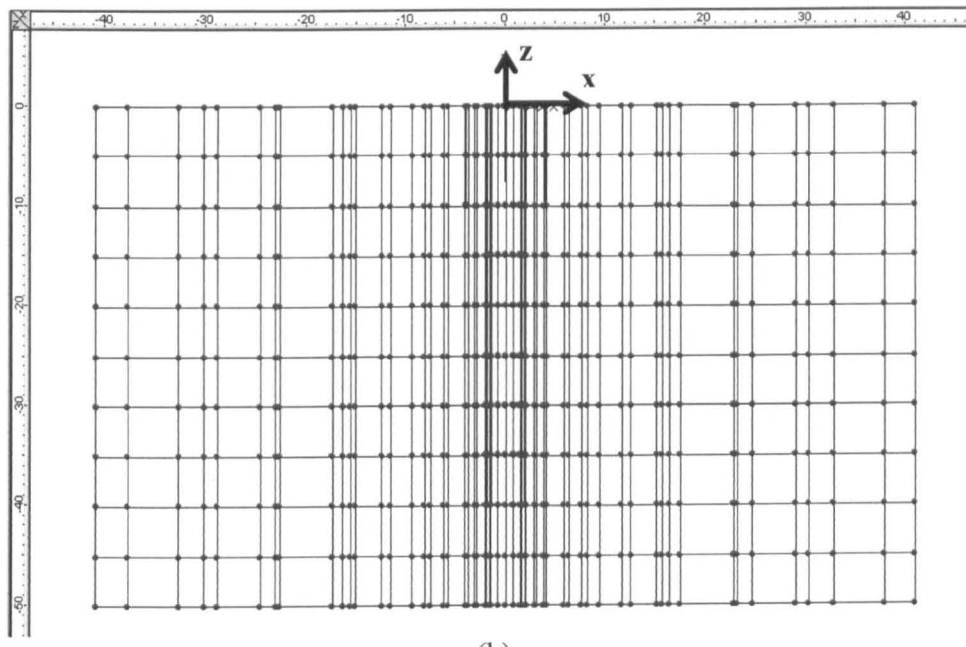

(b)

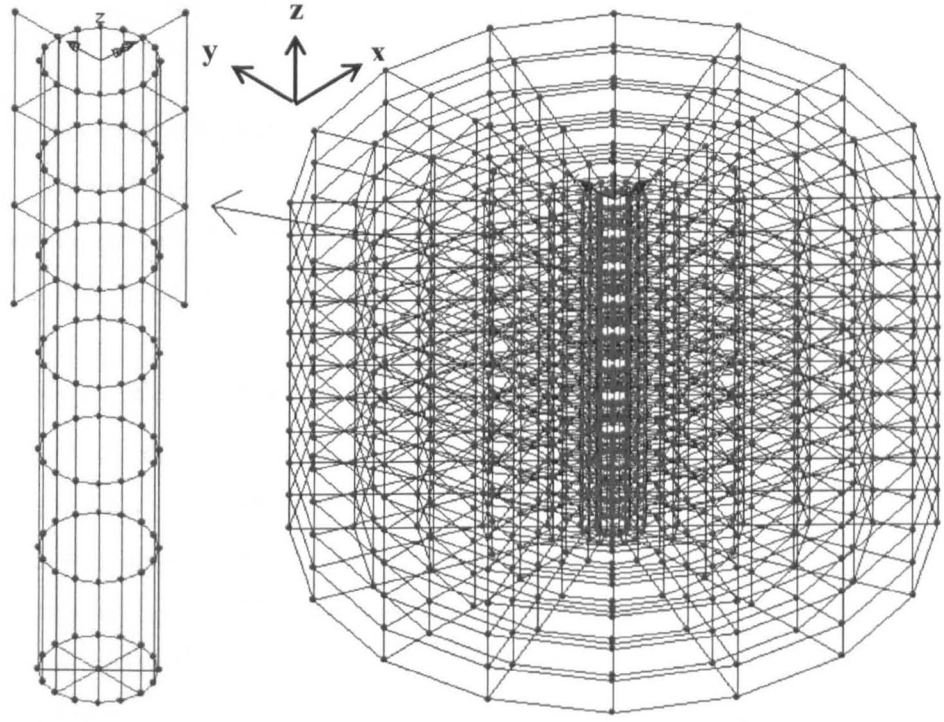

(c)

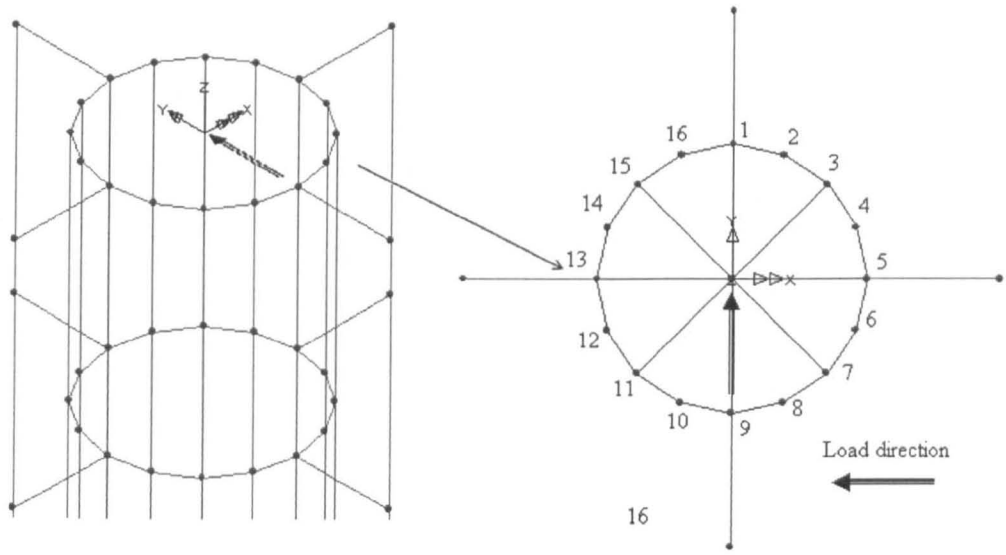

(d)

Fig. 3.17 Geometry of pile and soil (a) plan view (x-y plan); (b) front view (y-z plan, and z is depth); (c) 3D view of the whole mesh including a finned pile mesh. (d) points at the pile head

Assignment of 2D and 3D meshes

Three different meshes: soil, pile, and interface, were assigned to model pile and soil behaviour. Instead of a solid mesh, one of the 2D meshes, thin shell mesh (QSI4), illustrated in Fig. 3.18(a), was used to model pile and fins due to the geometric properties of the fin: the ratio of fin length to thickness should not exceed 10 (LUSAS, 1996). Thin shell meshes were assigned to quadrilateral surfaces of a finned pile; the thickness represented a 3D pile wall. A three-dimensional mesh using solid continuum elements in 3D with enhanced strains (HX8M), as shown in Fig. 3.18(b), was used to model soil, and this kind of mesh was assigned to all soil hexahedral volumes. The interface was modelled by a 3D joint element (JNT4) which was assigned between pile and soil surfaces as represented in Fig. 3.18(c) and (d). This joint element acting on the pile-soil surface is able to provide 3D material properties.

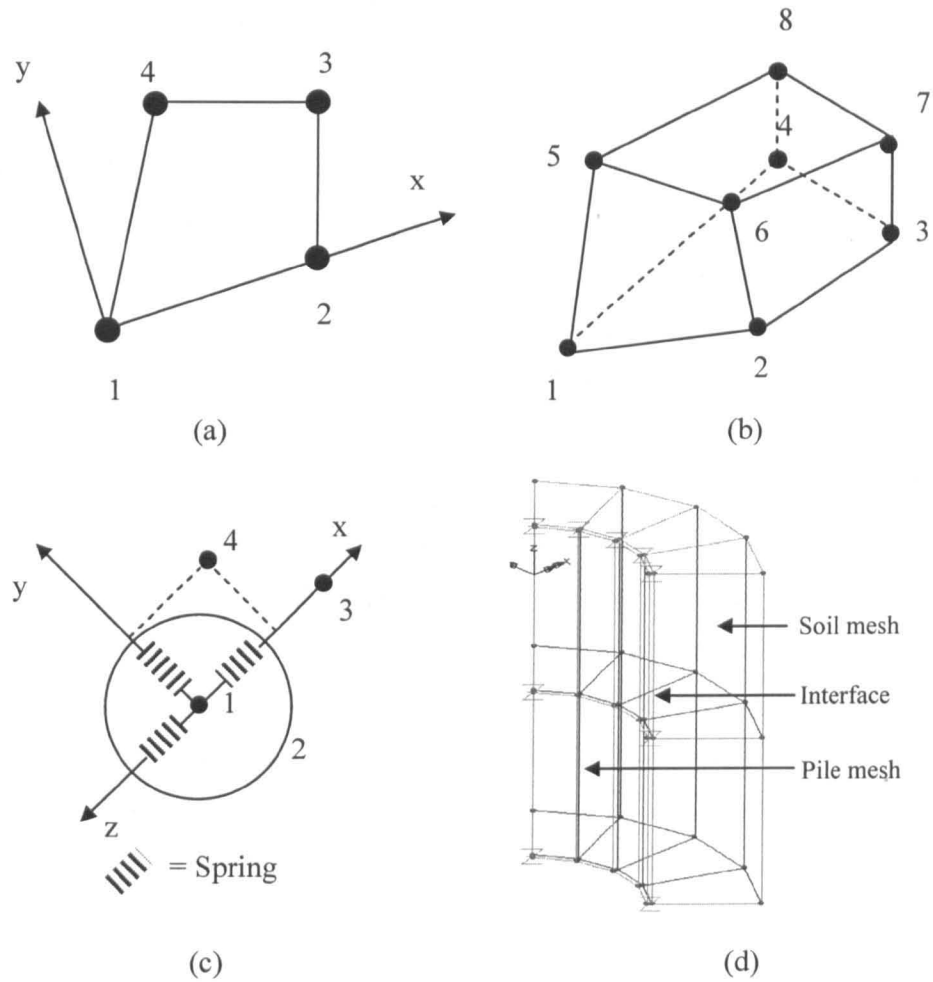

Fig. 3.18 Elements used in the pile soil analysis: (a) 3D flat box thin shell element (QSI4); (b) 3D solid continuum element with enhanced strains (HX8M) and (c) 3D joints for bars (JNT4) (d) interface element

Assignment of material properties

The pile and the fins are mild steel. The basic pile properties are: Young's modulus E_p = 200 GPa, Possion ratio ν_p = 0.3, and unit weight γ_p = 78 kN/m^3 (typical mild steel values). The yield of steel is not considered in this study, because the pile rigidity is much higher than that of soil stiffness.

Two types of soil properties were used in the modelling of the full-scale and the small-scale piles. In the full-scale analysis, the elastic soil properties, corresponding to dense sand, were: Young's modulus E_s = 30000 kPa (Das, 1995); Possion ratio ν_s = 0.33, dry unit weight γ_s = 16.5 kN/m^3. When yielding of the soil was considered, the Mohr-Coulomb model was used with a friction angle ϕ' = 35°

and cohesive strength c' = 0. In the small-scale analysis, all factors were the same as those in full-scale modelling except for the modulus of elasticity of soil E_s. According to the simple pressuremeter test in the model tank, the average E_s of the model test was about 300 kPa. The soil modulus in the small scale model was only one hundredth of that in full scale model because of the in situ stress level.

For interface material properties, a frictional coefficient μ = 1.0, and an elastic stiffness k = 30000 kPa were assigned to the interface elements when those were incorporated into full scale analysis. Interface elastic stiffness k = 300 kPa was used in small-scale tests.

Assignment of loading and boundary condition

Self-weight was modelled by applying the gravity factor of 9.81 (m/sec^2) to the whole element. Effective stress and lateral stress were modelled by applying the initial stress factor to the soil meshes. Static lateral loads were assigned uniformly to all nodes at the pile head (Fig. 3.17(c)), and the load magnitude was gradually increased by 1 N and by 1 MN in small scale and in full scale tests, respectively. The fully fixed boundary condition was assigned to the surface of the outer soil layer and the base of the model.

Analysis

In order to carry out nonlinear analysis, initial conditions including self weight and initial stress were applied to the whole mesh. In the first stage, the nonlinear analysis was based on the initial soil-pile condition to find the initial balance. In the second stage, the nonlinear analysis was based on the application of the lateral load. The total required load was applied in a number of increments, and the load increment of 0.5 was adopted in each iterative calculation up to the load factor of 10. The iterative procedure was based on the standard Newton-Raphson iteration, and the incremental solution was based on the tangent stiffness from incremental displacement.

In this study, the manual method was used in the initial stage where the loading data in each load increment was specified separately; the automatic method was used in the lateral load stage where the lateral load case was factored using fixed or variable increments. In order to obtain good convergence for geometrical

nonlinearities, the maximum iteration number was assigned as 50. In order to estimate how much the structure has moved during an iteration, Displacement Norm (dpnrm) was defined as the sum of the squares of all the iterative displacements as a percentage of the sum of the squares of the total displacements; in order to predict how much residual force was within the whole mesh, Residual Force Norm (rdnrm) was defined as the sum of the squares of all the residual forces as a percentage of the sum of the squares of all the external forces (LUSAS, 1996). Displacement Norm (dpnrm) was assigned as 1.0 while Residual Force Norm (rdnrm) was assigned as 0.1 in full-scale pile analysis; whereas dpnrm was 0.01 and rdnrm was 0.001 in small-scale modelling. The calculation was terminated when the failure state was reached or when the design maximum load was achieved.

3.3.3. Modelling variables

FE analysis has very strict rules for convergence, and the correct outcome depends upon the following parameters:

- The number and scale of meshes may affect the calculation and the accuracy. Problems with few and simple meshes may fail to simulate the soil particles around the pile; whereas, complicated meshes could waste computation time and cause iteration problems. Ideally, the number of meshes should be limited to a value which is able to represent the change of geometry. In addition, it is better to adopt a regular mesh shape.
- Lateral loads can be modelled by applying incremental displacements or loads. This is known as displacement or load control. The P-Y curve can be obtained at Point 1 and Point 9 of the pile head as shown in Fig. 3.17(d). The displacement control achieves convergence with an acceptable incremental displacement. The load control is relatively efficient and time saving. All load conditions are demonstrated in this section.
- Pile-soil interface is an important factor in the modelling of pile-soil interaction. The soil and the pile have different material properties, and they are not fully fixed together. An interface between the soil and the pile allows each to move according to its own material properties. Force and friction can still be transmitted through the interface. The interface can be modelled as a spring joint or as a joint with frictional contact. The

stiffness and the friction between pile and soil surfaces can be controlled by the use of different frictional coefficients.

- Pile-soil stiffness is one of the main factors that affect the shape of pile deformation. Based on the ratio of pile stiffness to soil stiffness with the length of pile, piles can be divided into a rigid pile or a flexible pile. A practical pile wall thickness of 0.05 m was used in most full scale modelling. A larger wall thickness of 0.2 m was also used to model a strong pile subjected to an extremely high vertical loading of wind turbine.
- Most of the modelling was carried out at full scale. In order to verify the experimental results, a small-scale model was created. Features of this small-scale model are based on the experimental tests.

A series of analyses were carried out on different piles subjected to different conditions as shown in Table 3.6, and all variables are summarised in Table 3.7. Descriptions of these follow:

Mesh assignment

Fig. 3.19 shows a model that has four times the density of meshes in x-y plane compared to the original one (Fig. 3.17) and the soil depth underneath the pile tip extends from 10 m to 60 m. This complicated model dramatically increased the time of calculation and the steps of iteration. Fig. 3.20 shows that the P-Y curves obtained from the standard model and the complicated model are nearly identical. The complicated model had better convergence and resolution especially in the initial load increment compared to those of the standard model. The P-Y curve in the standard model is very similar to that of the complicated model. The standard model shown in Fig 3.17 was used instead of the model shown in Fig. 3.19 in order to save time and memory.

Table 3.6 Summary of FE analysis

Pile type	Mesh property	Loading condition	Frictional coefficient of interface	Pile wall thickness (m)	Scale
MPF	Normal	Load control	1.0	0.05	Full-scale
MPF	Complicated	Load control	1.0	0.05	Full-scale
MPF	Normal	Disp. Control	1.0	0.05	Full-scale
MPF	Normal	Load control	0.7	0.05	Full-scale
MPF	Normal	Load control	0.7 -frictional contact	0.05	Full-scale
MPF	Normal	Load control	No interface	0.05	Full-scale
MPF	Normal	Load control	1.0	0.2	Full-scale
FPF210	Normal	Load control	1.0	0.05	Full-scale
FPF220	Normal	Load control	1.0	0.05	Full-scale
FPF240	Normal	Load control	1.0	0.05	Full-scale
MPS	Normal	Load control	1.0	0.002	Small-scale
MPS	Normal	Load control	No interface	0.002	Small-scale
FPS210	Normal	Load control	No interface	0.002	Small-scale
FPS220	Normal	Load control	No interface	0.002	Small-scale
FPS240	Normal	Load control	No interface	0.002	Small-scale
FPS210	Normal	Load 45° to fins	No interface	0.002	Small-scale
FPS210	Fins at middle	Load control	No interface	0.002	Small-scale
FPS210	Fins at bottom	Load control	No interface	0.002	Small-scale
FPS210	L'_p = 375 mm	Load control	No interface	0.002	Small-scale
FPS210	L'_p = 350 mm	Load control	No interface	0.002	Small-scale
MPS	D'_p= 2.00 D_p	Load control	No interface	0.002	Small-scale
MPS	D'_p= 1.75 D_p	Load control	No interface	0.002	Small-scale
MPS	D'_p= 1.50 D_p	Load control	No interface	0.002	Small-scale
MPS	D'_p= 1.25 D_p	Load control	No interface	0.002	Small-scale
* dimensions are based on experimental tests					

Table 3.7 Features to determine convergence and accuracy

Control	Features
Mesh density	▪ Complicated mesh: time and memory consuming
	▪ Simplified mesh: may lose accuracy if error of tolerance is high
Loading condition	▪ P-Y curves obtained from load control are higher than from displacement control
	▪ P-Y curves obtained at the front of the pile (at Node 1) are higher than P-Y curves obtained in the rear of the pile (at Node 9)
	▪ Load control has better shape (P-Y curves) than displacement control
Pile-soil interface	▪ Without interface: simplify calculation and easy to achieve convergence, but accuracy not lost since pile and soil are assigned to the same node
	▪ With interface: pile-soil interaction can be presented and it can be controlled by a frictional coefficient
Pile-soil stiffness	▪ High ratio of pile to soil stiffness: tend towards rigid pile behaviour
	▪ Low ratio of pile to soil stiffness: tend towards long pile behaviour
Scale of modelling	▪ Full scale model: general pile and soil parameters are applied, modelling close to real problem, but lose data for comparison
	▪ 1G small scale model: difficult to obtain right parameter of soil, lack of modelling of soil stiffness

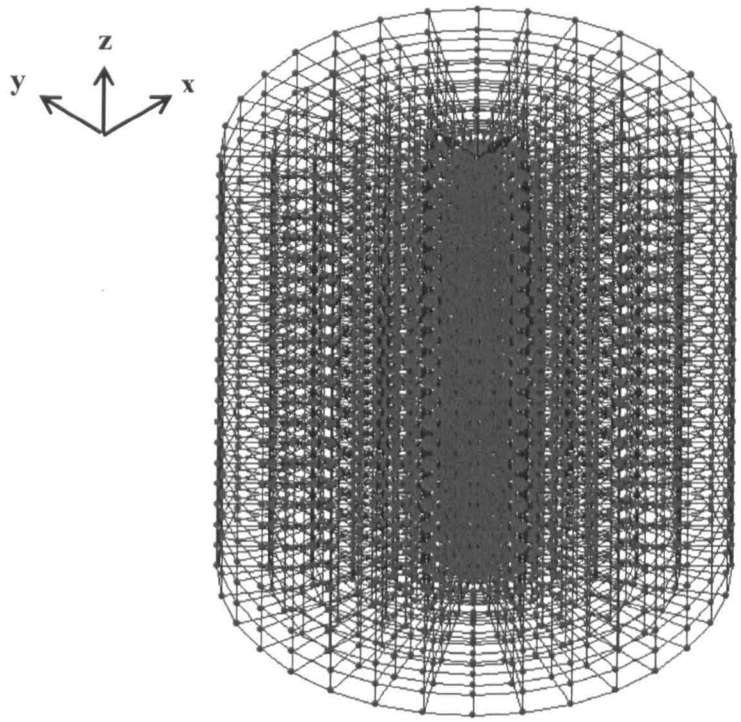

Fig. 3.19 A complicated model which has 4 times the meshes of the standard model (Fig. 3.17)

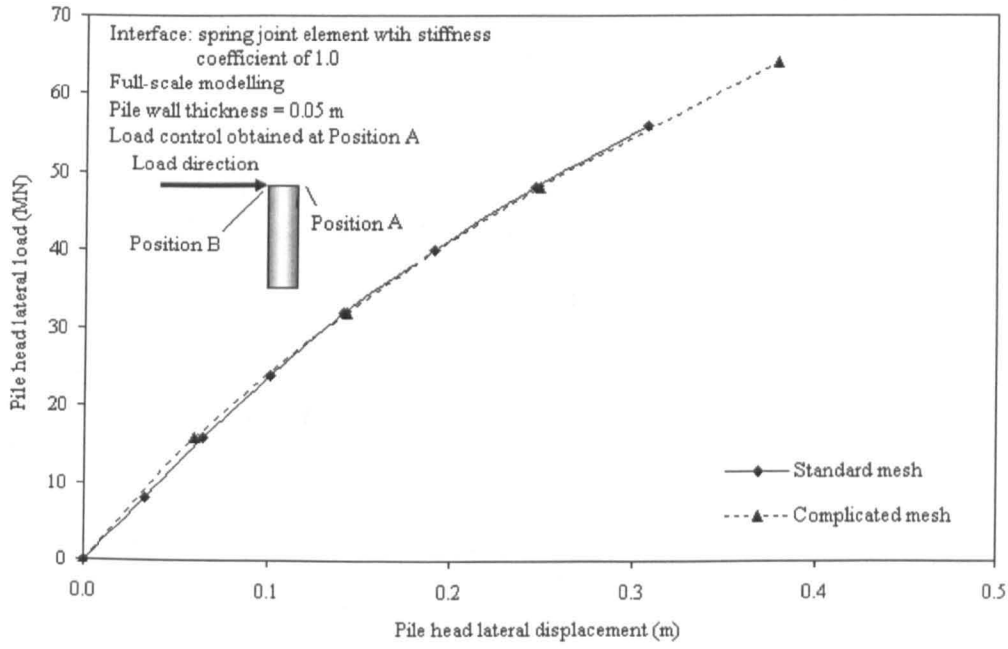

Fig. 3.20 P-Y curves obtained from a standard model and from a complicated model by using LUSAS

Loading condition

In order to verify the suitable loading position and loading method, a monopile subjected to different loads was analysed, and pile head P-Y curves generated as shown in Fig. 3.21. In the load control modelling, a constant lateral load increment was given at all nodes (Nodes 1-16 in Fig. 3.17(c)); whereas in the displacement control modelling, a constant lateral displacement was given at all nodes at the pile head. Readings in each case were obtained from both Node 1 (Point A) and Node 9 (Point B) which represented positions at the front and the rear of the pile head, respectively.

Fig. 3.21 shows that curves obtained from load control are higher than those from displacement control. Point A gives a higher value of loading than Point B at the same displacement indicating that the lateral movement at the rear of the pile (Point B) is higher than that at the front of the pile (Point A). This is expected since the load was applied at B and the tubular pile would have deformed. At Position B, the convergence in load control is more stable than that in displacement control. In view of the good convergence and smaller difference, the following analysis was carried out based on load control and displacement readings taken from Position A. The direction of the load with respect to the plane of the fin is discussed in the section on small scale modelling.

Interface

Fig. 3.22 shows P-Y curves with various interface conditions. The curve with a frictional contact with stiffness coefficient of 1.0 is very close to the curve with a spring joint interface with frictional coefficient of 1.0, but the convergence for the former stopped is 0.32 m and for the later 0.45m. The model with no interface has a similar P-Y curve to that of a model with a spring contact interface with a stiffness coefficient of 0.7. A change in the frictional coefficient does not cause a significant reduction in lateral resistance.

Pile rigidity

The increase in pile wall thickness creates an increase in pile rigidity EI. Two wall thicknesses, 0.2 m and 0.05 m, were used to represent two different pile rigidities. The EI of the wall thickness of 0.2 m is three times that of the wall thickness of 0.05 m. Fig. 3.23 shows that the lateral load for a wall thickness of 0.2 m is 1.6 times that

for a wall thickness of 0.05 m for the same displacement. The increase in wall thickness resulted in an increase in a 60% lateral resistance. This is not an efficient way to improve lateral resistance by 60% because much of the extra material is not used to full given the variation of resistance down the pile.

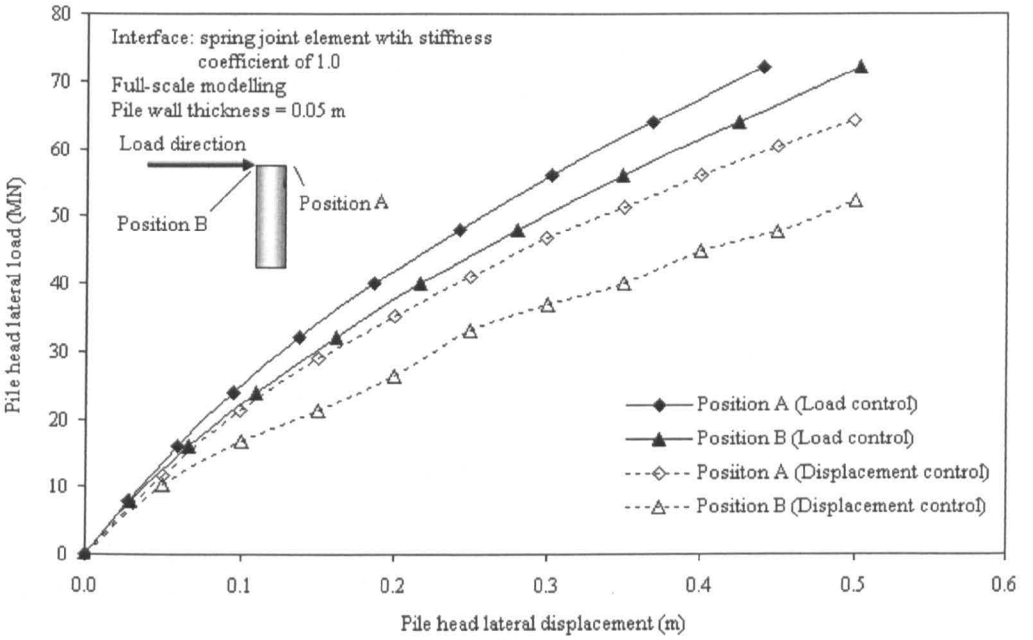

Fig. 3.21 Pile head P-Y curves generated from LUSAS of MPF under various loading conditions

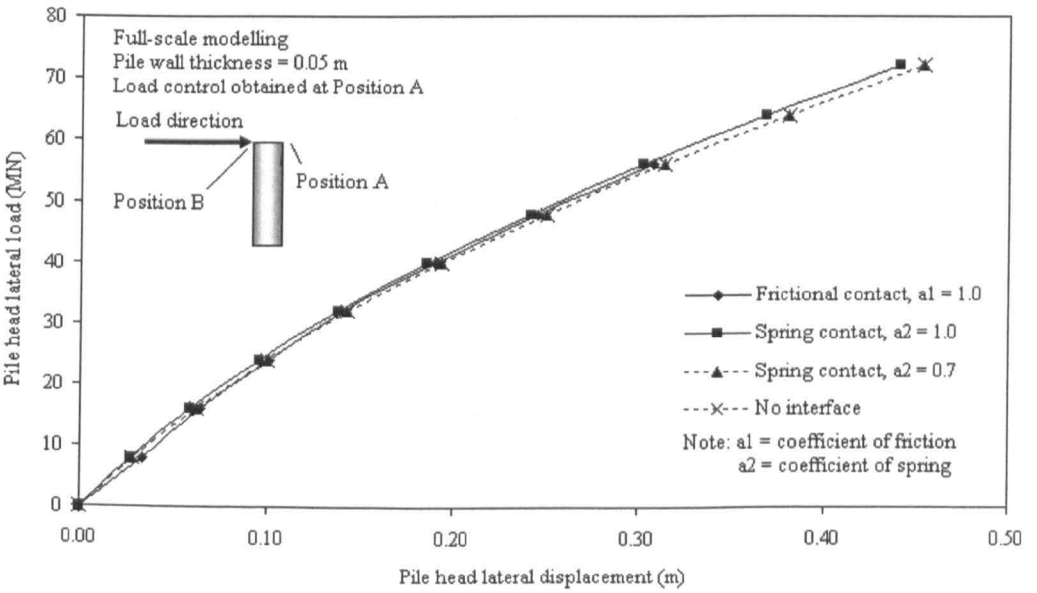

Fig. 3.22 Pile head P-Y curves o generated from LUSAS of MPF under various interface conditions

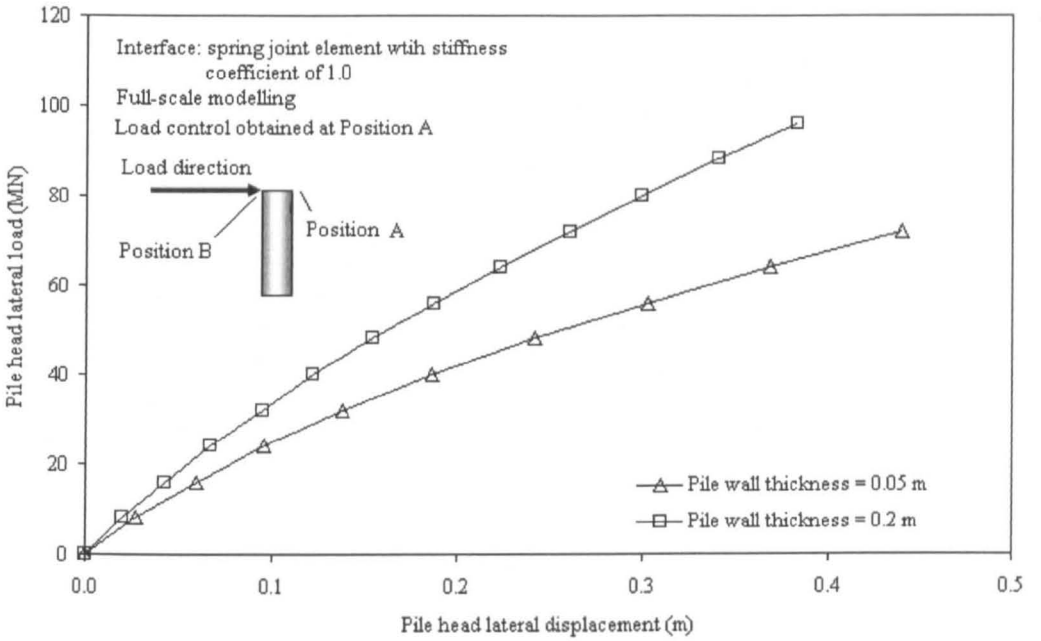

Fig. 3.23 Pile head P-Y curves generated from LUSAS of MPF with different pile wall thicknesses

Model scale and mesh limitation

A 1/100 small-scale model was built to verify pile soil behaviour in the model tests; pile dimensions are given in Table 3.1. The P-Y curve of the small-scale model is shown in Fig. 3.24, and the comparison with experimental results is discussed in Chapter 7. The reduction in soil parameters like soil modulus and effective stresses directly affected convergence and resolution especially when the ratio of the dimensions of soil mesh to the dimensions of pile mesh was high. For a high ratio, the pile passed through the soil meshes which caused a very small movement of the soil. For a low ratio, the soil meshes were pushed forward by the pile. The low ratio of soil mesh dimension to pile mesh dimension is more realistic to model pile soil movement. In order to carry out small-scale model tests by using a standard mesh instead of a complicated mesh, a strong interface was used. The movements of the pile and the surrounding soil were restricted by the use of a strong interface. Details are described in Chapter 7.

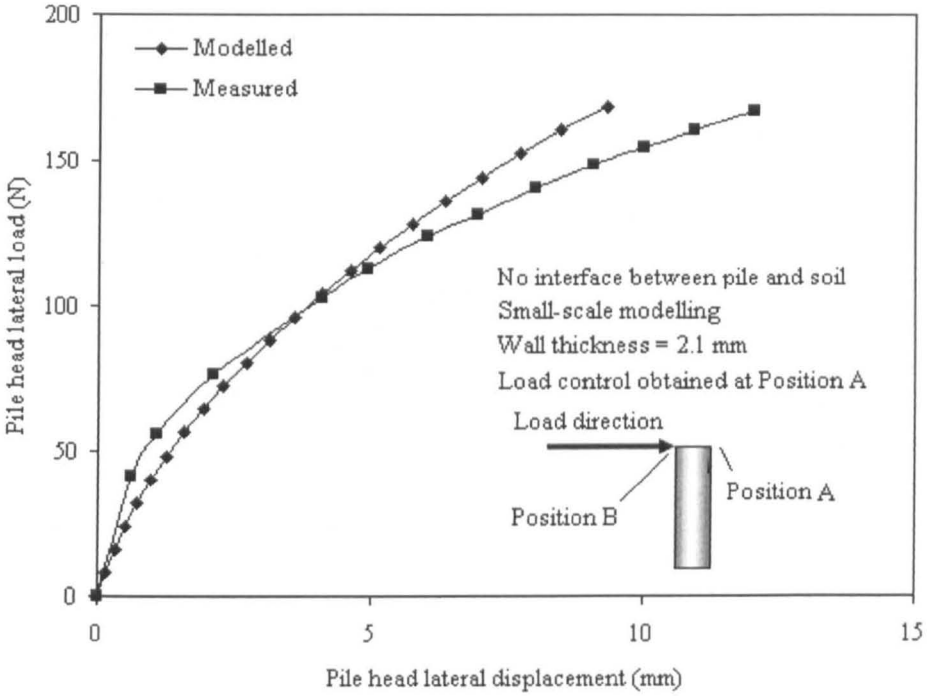

Fig. 3.24 Pile head P-Y curves of a small scale pile from 1G laboratory tests and modelled by LUSAS

3.3.4. Analysis of lateral capacity of finned piles

Pile head P-Y curves for various piles obtained from full-scale and small-scale modelling are shown in Fig. 3.25 (a) and (b), respectively. Lateral load increases with an increase in fin length at the same displacement. The ultimate load is taken at the point where the P-Y curve turns to a straight line with slope ratio less than 0.05 (see Section 6.3.2 for definition), and the serviceability load is taken at displacement 10% of pile diameter. Table 3.8 shows lateral loads at ultimate state and at serviceability state. The increase in load by using finned piles is presented in Fig. 3.26. Table 3.8 shows that the increase in lateral capacity at the serviceability limit state is almost the same as that at the ultimate limit state. Fin efficiency demonstrated by the small scale model is significantly smaller than that by full scale model. Such a difference could arise from the use of different ratio of pile to soil stiffness.

In the cross section of a finned pile, the critical load directions are at 45° and 0° to the major fin axis as shown in Fig. 3.27. A small scale finned pile, FPS210, was used in these analyses. Fig. 3.27 shows that the load-displacement curves of FPS210 subjected to 0° and 45° lateral loading to the fins are very close and both exceed these of the monopile.

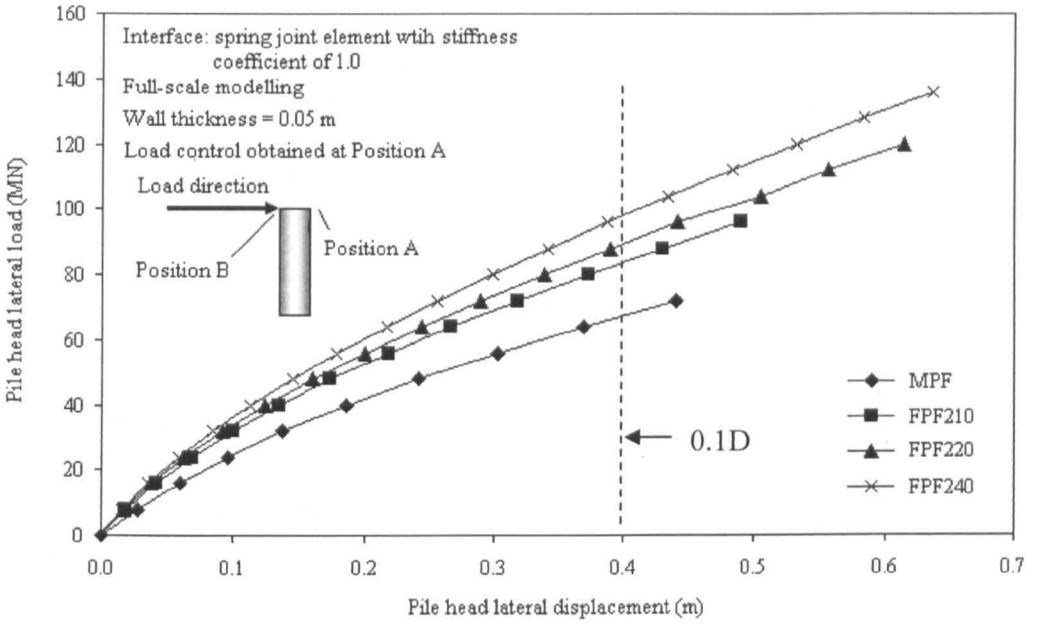

(a)

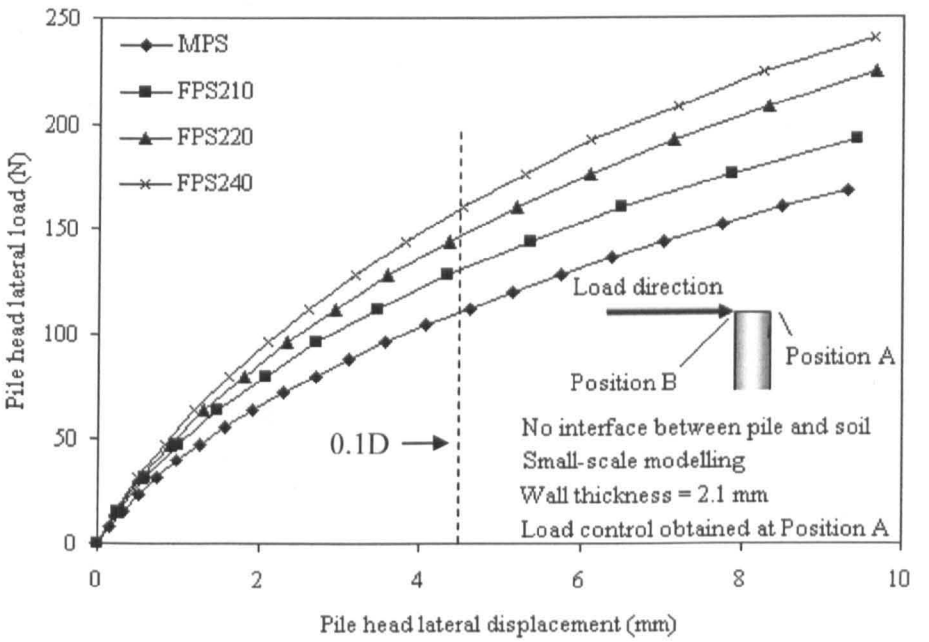

(b)

Fig. 3.25 Pile head P-Y curves generated from LUSAS for different fin dimensions (a) full-scale (b) small-scale modelling

Table 3.8(a) Lateral loads of full-scale pile modelling by LUSAS

Pile number	Serviceability lateral load, P_s(MN)	$\frac{P_{S(FPF)}}{P_{S(MPF)}}$	Ultimate load, P_u (MN) **	$\frac{P_{u(FPF)}}{P_{u(MPF)}}$
MPF	42	1	72.0	1
FPF210	55	1.31	96.0	1.33
FPF220	70	1.67	120.0	1.67
FPF240	80	1.90	136.0	1.89
Note: ** Ultimate load is taken at the final point of each P-Y curve where it stops converging				

Table 3.8(b) Lateral loads of small-scale pile modelling by LUSAS

Pile number	Serviceability lateral load, P_s(N)	$\frac{P_{S(FPS)}}{P_{S(MPS)}}$	Ultimate lateral load, P_u (N) **	$\frac{P_{u(FPS)}}{P_{u(MPS)}}$
MPS	110	1	168	1
FPS210	130	1.18	192	1.14
FPS220	146	1.33	224	1.33
FPS240 *	160	1.45	240	1.42
Note: * FPS240 is applied in the numerical analysis and the second stage of model tests but not in the first stage of static loading tests ** Ultimate load is taken at the final point of each P-Y curve where it stops converging				

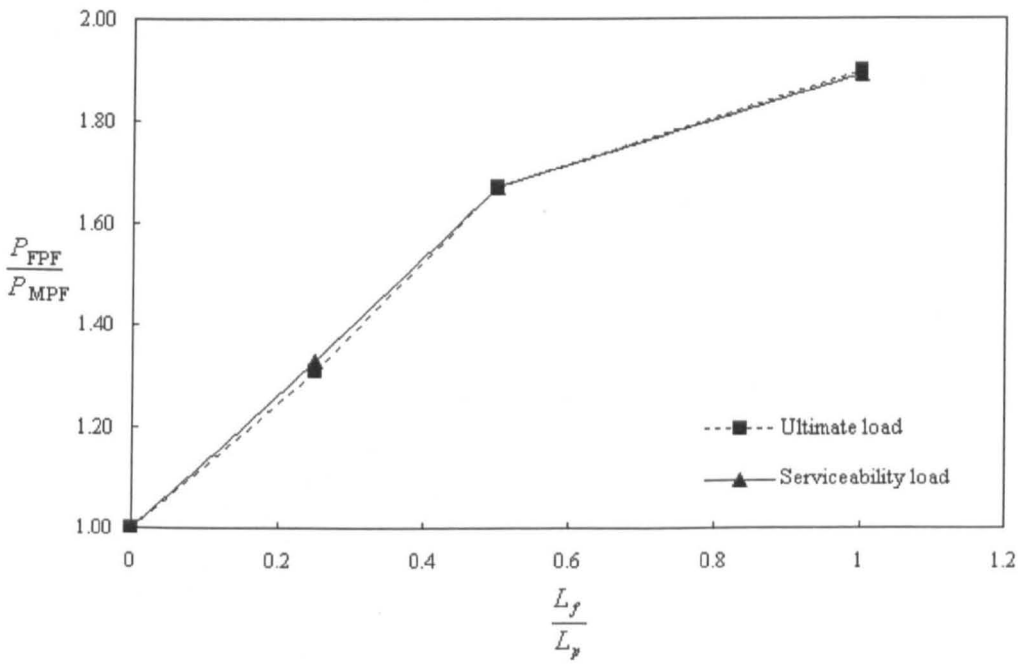

(a)

Fig. 3.26 Increase in lateral load with the increase in fin length for ultimate and service state design (a) full-scale by LUSAS

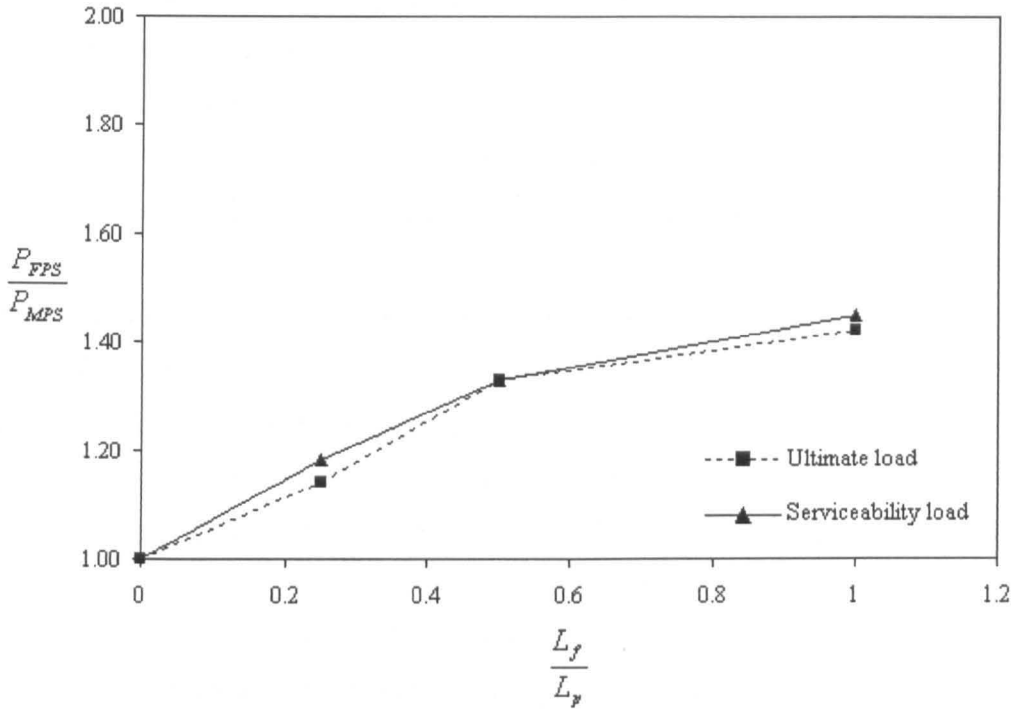

(b)

Fig. 3.26 Increase in lateral load with the increase in fin length for ultimate and service state design (b) small-scale by LUSAS

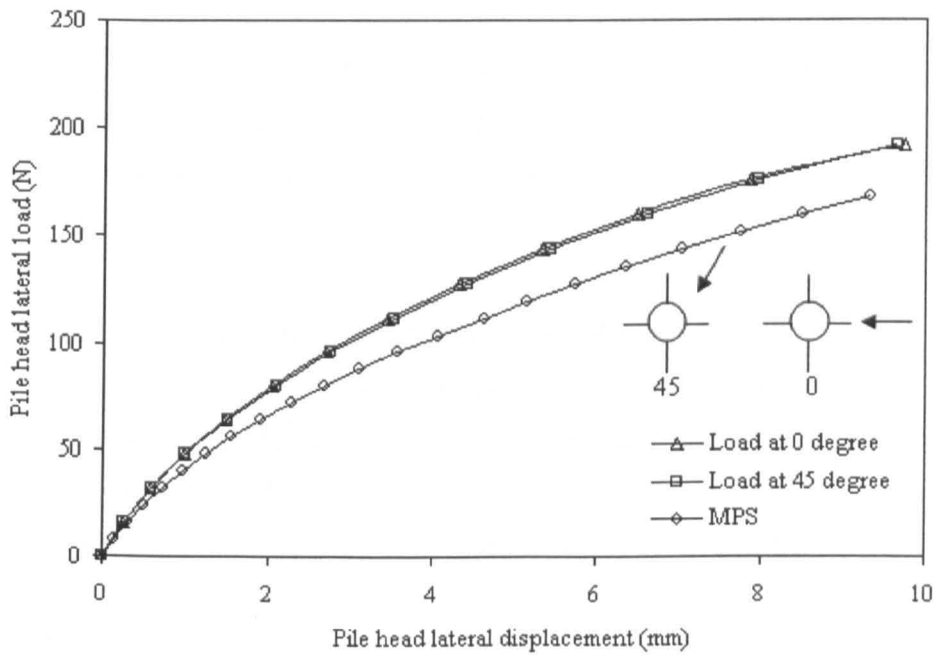

Fig. 3.27 P-Y curves for a finned pile, FPS210, subjected to different load directions by LUSAS

Fig. 3.28 shows load-displacement curves for finned piles with fins at the top, the middle and the bottom of the piles. One small scale monopile MPS and three finned piles FPS210 were used in these analyses. The pile with fins at the top has the largest lateral resistance; whereas, the one with fins at the bottom has the smallest resistance. Resistance of all finned piles are greater than that of the monopile. The improved resistance could be the result of an increase in pile rigidity and an increase in the effective area perpendicular to the load direction.

The embedded length of a monopile foundation can be reduced by the use of fins. The influence of the reduction in pile length on lateral resistance is shown in Fig. 3.29. One small scale monopile MPS and three small scale finned piles FPS210 were used in these analyses. The resistance of FPS210 with a pile length of 350 mm is almost the same as that of MPS with the pile length of 400 mm, indicating that the pile length can be reduced by 12.5% yet retain the lateral resistance.

The diameter of a monopile, similarly, can be reduced by the use of fins to maintain lateral resistance. One finned pile, FPS 210, and three monopiles with different pile diameters were used in small-scale computer modelling. Pile head P-Y curves in Fig. 3.30 show that the lateral resistance of MPS increases with an increase in pile diameter. The P-Y curve for FPS210 is between those of MPS with diameters of 44.5 and 66.75 mm. According to the P-Y curves in Fig. 3.30, the lateral resistance of a monopile MPS with a diameter of 55.625 mm should be the same as that of a finned pile FPS210 with a diameter of 44.5 mm and the fin width of 22 mm. The amount of material for FPS210 is only 60% that of MPS. The use of fins reduces the diameter of the core monopile yet maintains the resistance.

3.3.5. Pile-soil behaviour of a full scale finned pile FPS210

The aim of this analysis was to understand the pile-soil interaction of finned piles. Computer modelling was carried out using a full scale finned pile, FPF210, subjected to a static lateral load. Pile dimensions are given in Table .3.1 (c) and (d), and results are presented when the lateral displacement of the pile head is 0.4 m, that is 10% of the core diameter.

Pile-soil deformation

The movements of the pile FPF210 and the soil in the model are presented in Fig. 3.31. Fig. 3.31(a) shows a significant movement of soil around the pile especially at the front of the pile. The zone of soil movement when the lateral

displacement exceeds 1% of the pile diameter was seven times the pile diameter in the front of the pile; a zone twice the pile diameter was also affected at the rear of the pile. Importantly, the maximum lateral displacement of soil was just behind the pile, and soil movement accompanied pile movement. Soil distributed close to the trail fin moved forward to fill the gap caused by the movement of the trail fin. The movement of soil increased with a decrease in its distance from the pile. Fig. 3.31(b) enlarges the area around the pile. The soil discontinuity was distributed at the front and at the rear of side fins due to the passive and the horizontal stresses acting on the side fins. Three-dimensional movements in Fig. 3.31(c) show that the soil moved forward in the x and y directions. In the y-z plane, the distribution of soil movement was a triangular shape. The zone of soil movement when the lateral displacement exceeds 1% of pile diameter was distributed between the ground surface and half of the pile length. Soil displacement was significant near the ground surface in particular in the zone at the rear of the pile head.

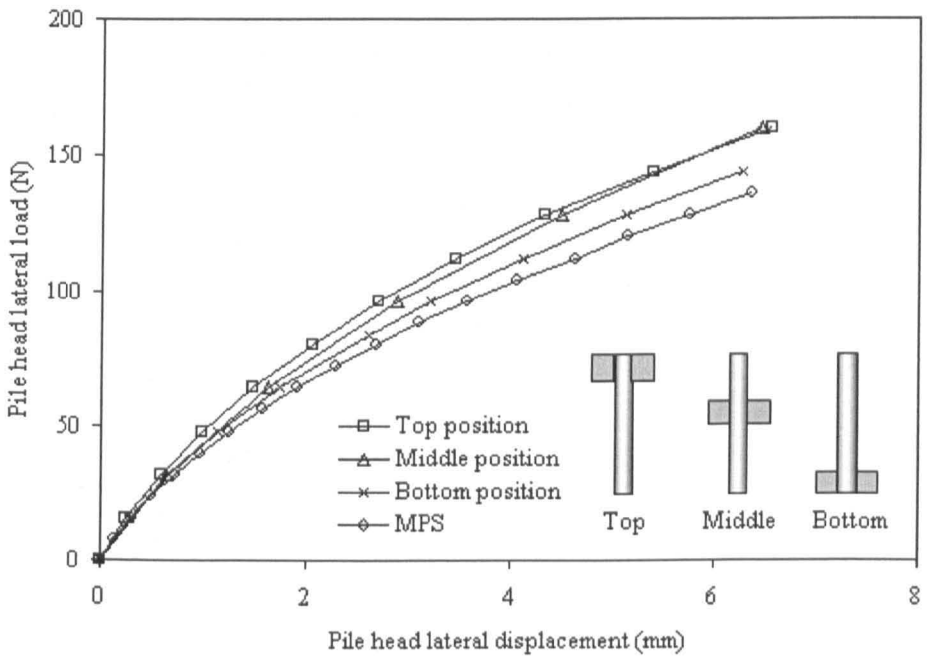

Fig. 3.28 P-Y curves generated by LUSAS for a finned pile, FPS210, with different fin positions

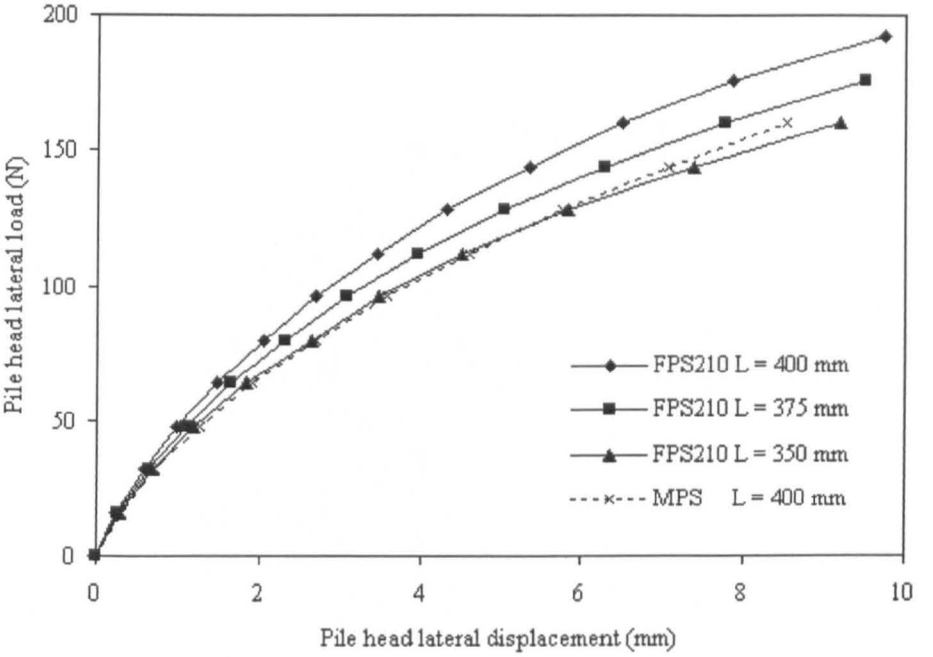

Fig. 3.29 P-Y curves generated by LUSAS for finned pile FPS210 with different pile lengths

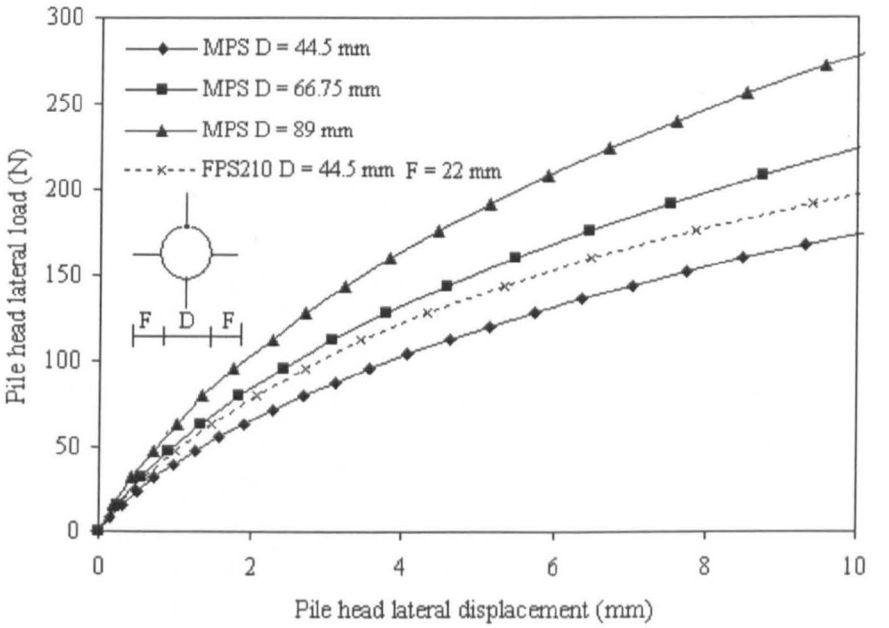

Fig. 3.30 P-Y curves generated by LUSAS for monopile MPS with different pile diameters

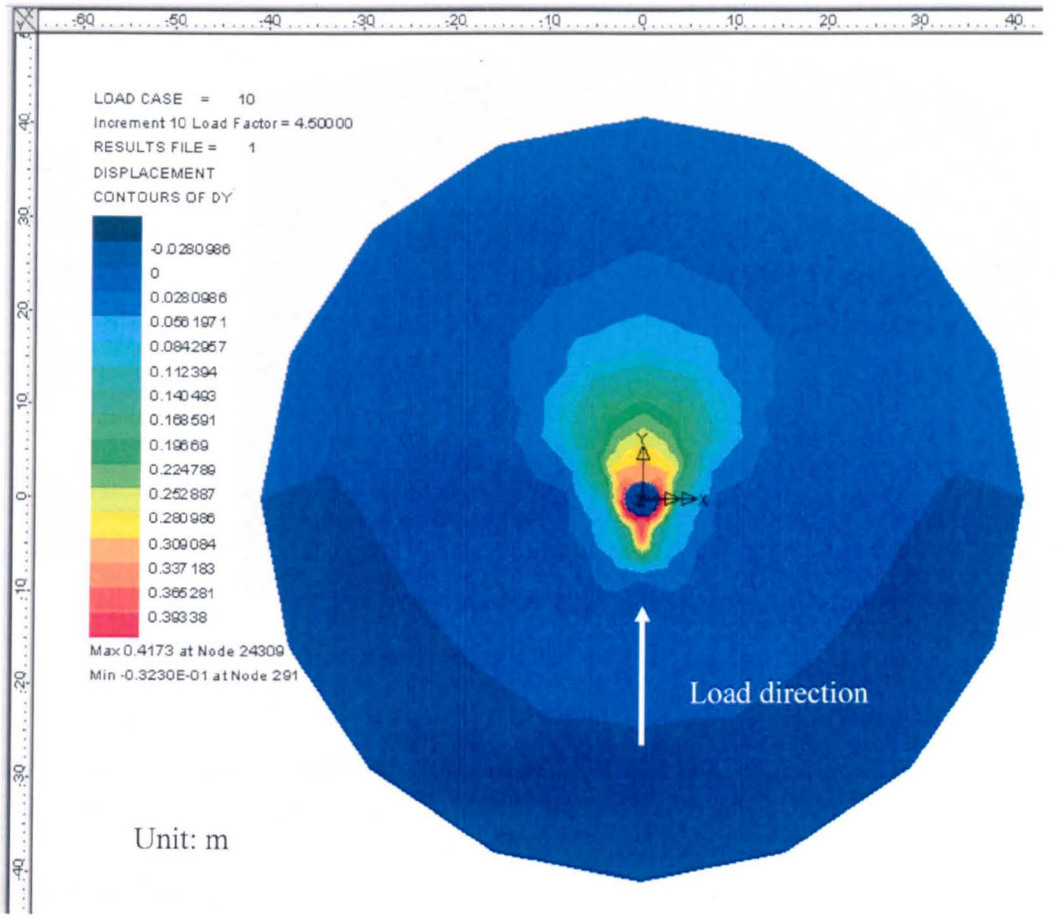

(a)

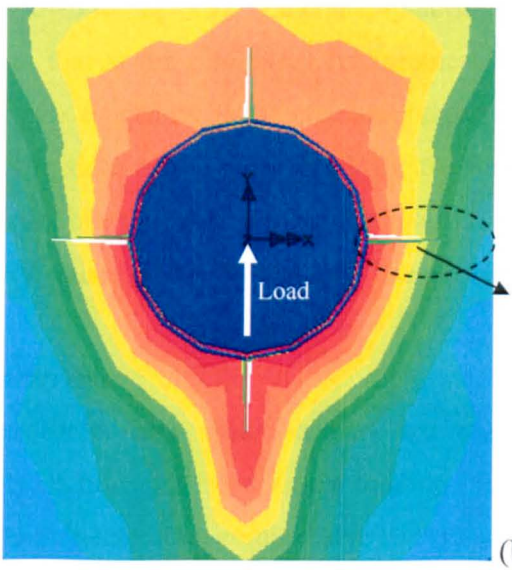

(b)

Fig. 3.31 Pile-soil deformation generated by LUSAS in the direction loading(a) on the x-y plane (z = 0) when the pile head deflection is 0.4 m (b) showing the discontunity

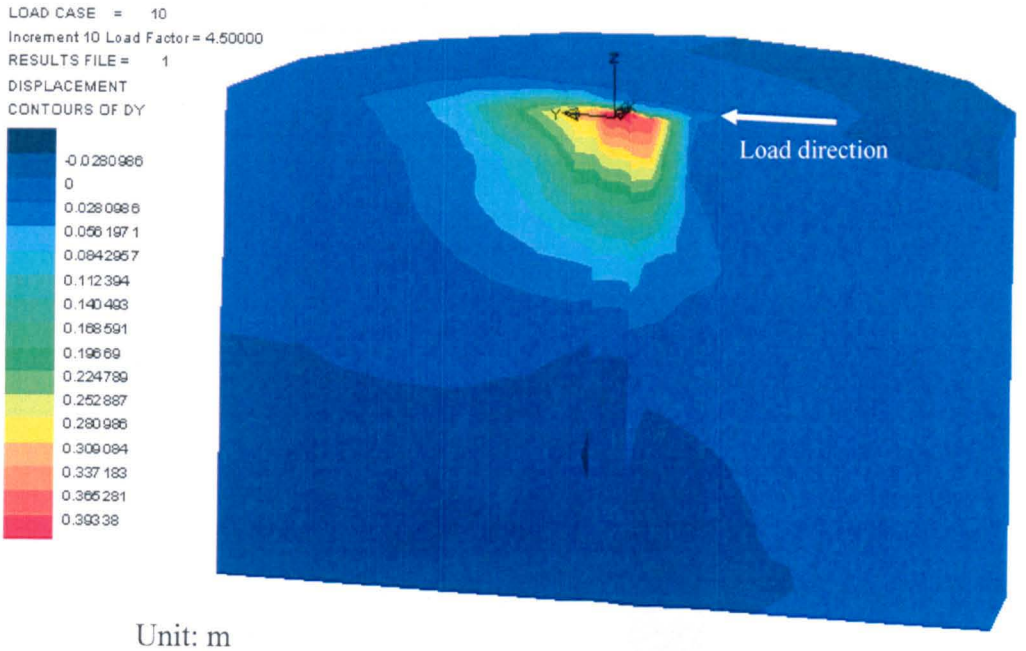

(c)

Fig. 3.31 Pile-soil deformation generated by LUSAS in the direction of loading (c) the 3D view

Pile deformation

The deformation of the finned pile, FPF210, subjected to a lateral load of 80MN is shown in Fig. 3.32. Lateral displacement at the pile head (0.4 m) was much greater than that at the pile base; displacement was mainly distributed at the upper part of the pile especially in the area around the pile head and the rear fin. Two fins welded at the sides of the pile were bent: the inner part of the side fins moved with the monopile, but the outer part of the fins did not move as much because the soil provided resistance on the fin surface. The position of rotation was near the pile base.

Stresses on pile

The direct and shear stresses are presented in Fig. 3.33 (a) and (b), respectively. Under pile head lateral loading (Fig. 3.33(a)), the front section (+y) of the pile was subjected to a compressive stress and the rear section (-y) of the pile was subjected to a tensile stress. The main direct stress was concentrated at the middle sections of the pile, and high direct stress was also distributed in the lower corners of the front and the trail fins. The maximum direct stress was at the depth of 15 m, and

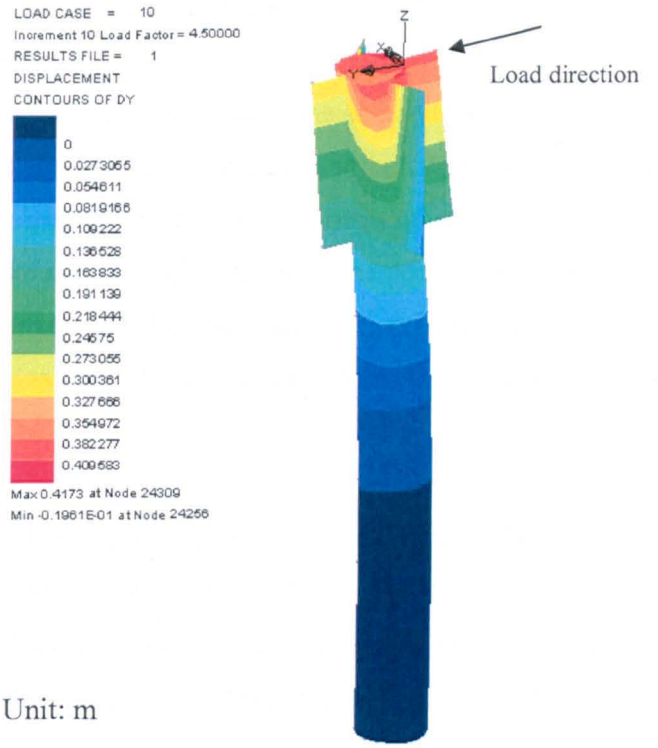

Fig. 3.32 Lateral deformation of FPF210 in the direction of loading when pile head displacement is 0.4 m

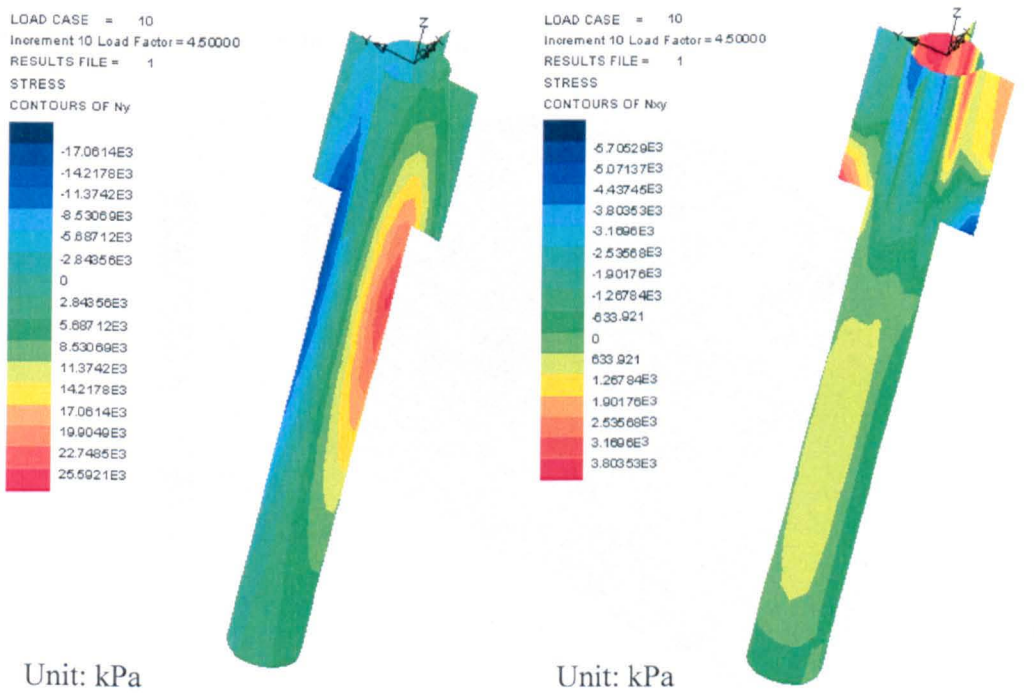

(a) (b)

Fig. 3.33 Stresses on the finned pile FPF210 (a) direct stress; (b) shear stress

the magnitude of the maximum tensile stress of 25.5 MPa was 1.5 times that of the maximum compressive stress.

Fig. 3.33(b) shows that the majority of the shear stress was concentrated near the pile head. Peak shear stresses were also distributed at the corner edges of the front and the trail fins especially in the outer corners of the trail fin. Although the middle section of the pile was also subjected to some shear stress, its magnitude was not very significant compared to the shear stress at the pile head. The maximum shear stress of 3.8 MPa was only 15% of the maximum direct stress of 25.5 MPa.

Strain of soil

The soil strain in the y direction is presented in Fig. 3.34. The compressive strain is observed at the front of the pile, and the tensile strain is observed at the rear of the pile. Soil strain increases with a decrease in soil depth. Although the zone with a strain of over 0.14 is much larger at the front of pile than at the rear of the pile, the maximum tensile strain of 0.1097 at the rear of the pile is four times higher than the maximum compressive strain of 0.027 at the front of the pile. A high tensile strain zone with strain of over 0.1 includes the area at the rear of the monopile and the side fins. The pile tip experiences very low strain due to insignificant soil movement at the lower half of the pile (Fig. 3.31).

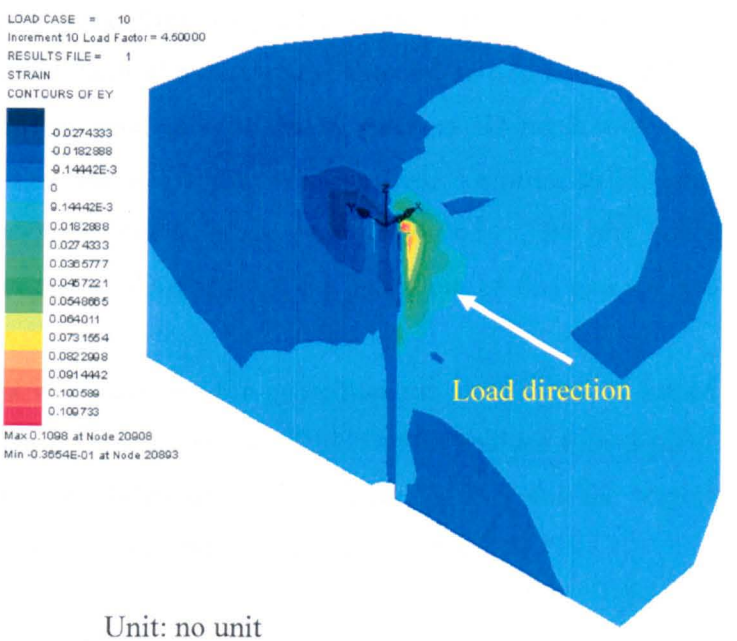

Unit: no unit

Fig. 3.34 Three-dimensional diagram for soil strain in the direction of loading when pile head displacement is 0.4m (by LUSAS)

3.4. Summary

In this chapter, the behaviours of laterally loaded finned piles were predicted using numerical analyses, including empirical equations, finite difference and finite element methods which have been introduced in Section 2.3. Empirical methods proposed by many researchers were used to predict the ultimate lateral load of the mono- and finned piles in Section 3.1. Results from empirical methods will be used to compare with those generated from the model tests, and the modification of these methods will be suggested in order to match the ultimate lateral load obtained from model tests in Section 7.3.

Computer modelling using LPILE was assessed in Section 3.2. The theory of the finite difference method using LPILE to predict the behaviour of lateral loaded pile was introduced. Pile head P-Y curves of finned piles with different fin dimensions were presented to show the efficiency of the fins on the increase in ultimate lateral capacity. The displacement, bending moment, shear force and soil resistance with depth on a finned pile were compared with those on a monopile; the influence of the use of fins to increase lateral capacity was assessed. This study gave a benchmark to investigate finned pile behaviour by mode tests (Chapter 5). The interpretation of LPILE and the possible improved methods will be presented in Chapter 7.

Computer modelling using LUSAS was carried in Section 3.3. The theory of the finite element method including the calculation and control rules was introduced. In order to model behaviour of finned piles, a 3D mesh was developed, and the properties of this pile soil mesh were verified. Similar to FD modelling, the pile head P-Y curves of finned piles were generated. The pile soil interaction was presented through the 3D diagrams; the behaviour of fins and soil around them were observed.

Results were used for the guidelines for model tests of finned piles (Chapter 5). In addition, the advanced use of LUSAS to analyse finned piles is described in Chapter 7. The reliability of analysis using LUSAS and the improved methods to predict behaviour of finned piles is discussed in Chapter 7.

4 The laboratory equipment

In order to verify the efficiency of the fins, 1/100 scale monopile and finned piles were tested. Dry dense sand contained within a steel chamber was used to simulate the ground condition. In order to carry out static and cyclic loading tests of finned piles in laboratory, both static and cyclic loading systems were developed. In static loading tests, a LVDT transducer and a proving ring were used for measuring displacements and loads on the pile head; in cyclic loading tests, the cyclic load on the pile head was measured by load cells. A simple pressuremeter was used to determine the soil modulus. Strain gauges attached on the inner surface of a pile were used to observe the strain along the pile. A data acquisition system, a Pico logger, was used to generate and process data from the electric measurements. The pile-soil properties can be obtained through integral equations. Details of these devices are presented in the chapter.

4.1. Model piles and pile caps

Ten 430 mm long steel tubes, shown in Fig. 4.1, were used. The outer diameter of the pile was D = 44.5 mm and the pile wall thickness T_p = 2.15 mm. Each finned pile consists of a pile welded with 4 fins at 90° to one another, and the fin thickness T_f = 2.9 mm. The finned pile dimensions are shown in Fig. 3.1 and Table 3.1 (a) and (b).

In order to apply the *static* load, a steel cap (Fig. 4.2(a)) 80 mm in length was installed at the head of the test pile. The cap extends 50 mm above the pile head, and the length connected to the pile was 30 mm. A 10 mm hemispherical seat in the upper part of the pile cap ensures that the lateral load was unaffected by pile tilt.

In order to apply the *cyclic* load, another steel cap (Fig. 4.2(b)) was used. This cap was divided into two parts: the main section to connect the test pile to the loading system and a top frame to seal to a vertical displacement transducer. The main section, 40 mm long, was connected to a pile by a 20 mm long cap fitting inside the tested pile. The load was applied 20 mm above the top of the pile. The top frame was 30 mm from the top of the main section, and the clear space between the top frame and the main section of the cap was high enough to connect the loading wire.

The top of the frame was a plane steel plate with a cross section of 50 x 100 mm which is large enough to ensure the vertical displacement transducer remained in contact with the pile cap. A tensile load was applied through a steel wire connected to a screw at the centre of the pile cap.

Fig. 4.1 Model monopile and nine finned piles

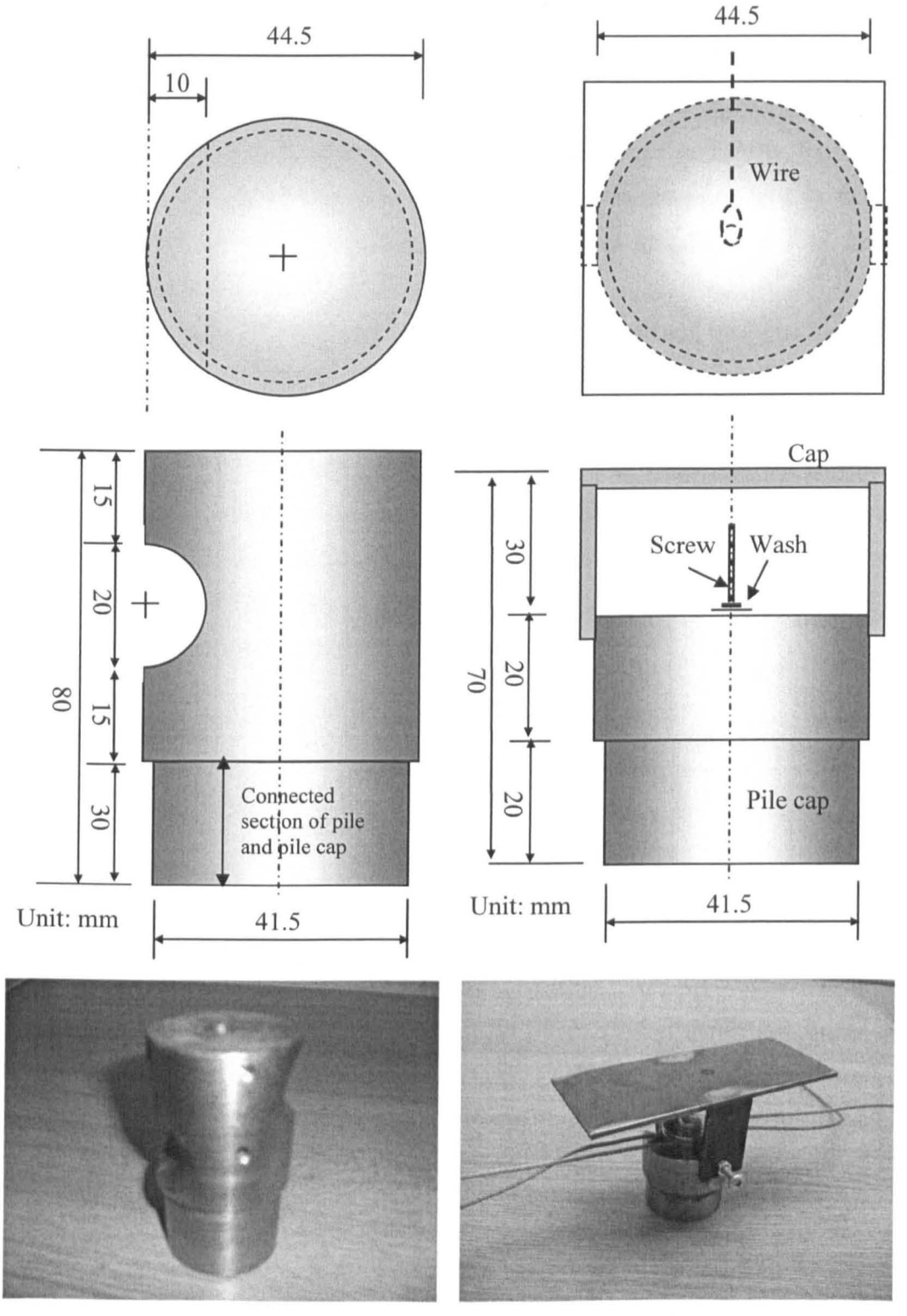

(a) (b)

Fig. 4.2 Pile caps for (a) static loading; (b) cyclic loading

4.2. Soil

The soil supporting the pile foundation was dry medium-dense sand with an internal friction angle ϕ'of 35.2° , and a dry unit weight γ_{dry} of 16.4 kN/m^3. The maximum and the minimum dry unit weight of the soil sample were 17.1 and 14.4 kN/m^3 respectively, and the relative density was 71.7% based on density distribution tests shown in Fig. 4.3. According to the grain-size distribution (see Fig. 4.4), the soil was *poorly graded Sand* with a uniformity coefficient (D_{60}/D_{10}) of 1.45, and a coefficient gradation ($D^2_{30}/ (D_{60}D_{10})$) of 0.92.

The empirical relationship of sand frictional angle and soil modulus, E_S, in Fig. 2.21 should not be used for the determination of the soil modulus of elasticity. This relationship was based on many in situ tests carried out at a depth of about 10 m. The 1G model tests were carried out at a depth of less than 1 m which may not provide as high soil modulus as in field tests even though both of their frictional angles were the same. In order to understand the distribution of the soil modulus inside the test tank, simple pressuremeter tests were carried out at different depths of the soil sample. Fig. 4.5 shows the values of modulus of elasticity with depth.

Sand Density Test

Min Density Test
Date: 07/05/03
Min. Density = **1.44 Mg/m^3**

Max Density Test
Date: 08/05/03
Max. Density = **1.71 Mg/m^3**

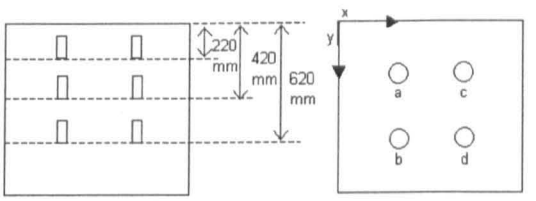

Density test for sand in the chamber
Date: 19/05/03

No.	Depth (mm)	Position (mm,mm)	W(s+c) (g)	W(w+c) (g)	W(c) (g)	W(s) (g)	W(w) (g)	D (Mg/m^3)	D_{avg} (Mg/m^3)	Dr (%)	Dr_{avg} (%)
1a	120-220	a(330,330)	908.3	569.2	19.3	889.0	549.9	1.62		65.11	
1b	120-220	b(330,660)	902.1	564.1	18.9	883.2	545.2	1.62		66.30	
1c	120-220	c(660,330)	906.1	567.4	19.4	886.7	548.0	1.62		65.62	
1d	120-220	d(660,660)	900.4	560.9	18.8	881.6	542.1	1.63	1.62	68.59	66.40
2a	320-420	a(330,330)	913.1	562.6	19.0	894.1	543.6	1.64		75.31	
2b	320-420	b(330,660)	912.7	563.1	20.5	892.2	542.6	1.64		75.14	
2c	320-420	c(660,330)	909.8	566.1	19.1	890.7	547.0	1.63		69.34	
2d	320-420	d(660,660)	911.1	567.6	20.7	890.4	546.9	1.63	1.64	69.25	72.26
3a	520-620	a(330,330)	914.2	562.3	20.1	894.1	542.2	1.65		76.85	
3b	520-620	b(330,660)	914.3	563.5	20.7	893.6	542.8	1.65		75.86	
3c	520-620	c(660,330)	916.3	565.0	20.6	895.7	544.4	1.65		75.50	
3d	520-620	d(660,660)	916.3	563.2	20.5	895.8	542.7	1.65	1.65	77.44	76.41
								D_{Avg}=	**1.635**	**Dr_{Avg}=**	**71.692**

Where W(s+c) = weight of soil and cup; W(w+c) = weight of water and cup; W(c) = weight of cup
W(s) = weight of soil; W(w) = weight of water; D = Density of soil; Dr = Relative density of soil

Fig. 4.3 Distribution of sand density inside the model test chamber

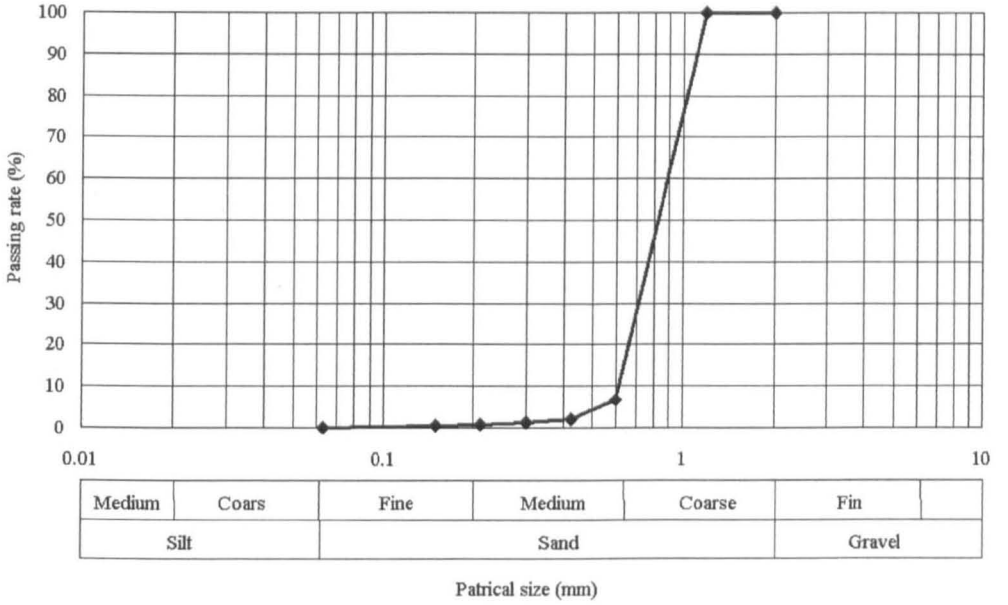

Fig. 4.4 Results from particle size test

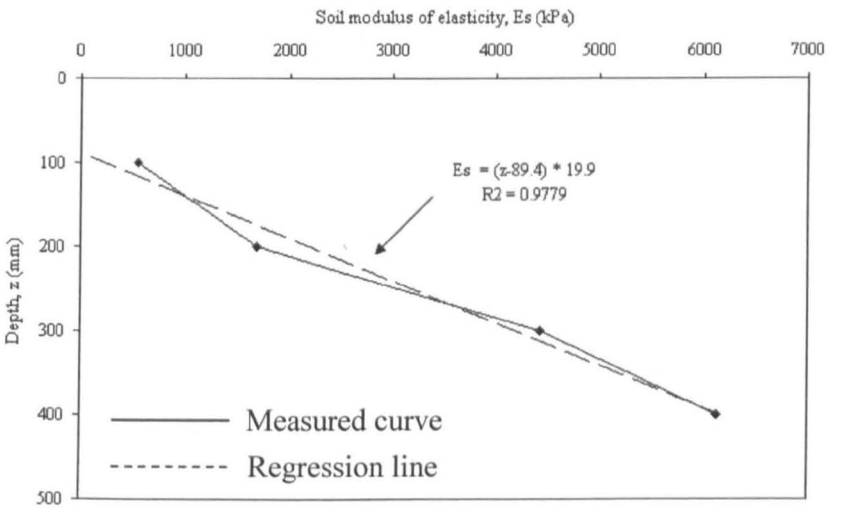

Fig. 4.5 Variation of soil modulus with depths

4.3. Chamber

The soil chamber was a 1 m^3 steel container with interior dimensions of 1 m, and a wall thickness of 25 mm as shown in Fig. 4.6(a) and (b). An angle iron flange around the top of the tank 60 mm in width and 10 mm in thickness stiffened the top of

the tank and supported the loading system and other facilities. Channels were used at third height to provide further stiffness of the tank.

In static loading tests, the pile was installed in the position shown in Fig. 4.7(a) in order to gain more area to the rear of the pile to reduce the boundary effect. The ratio of the distance between the pile and the chamber wall opposite to the point of application of the load to the pile diameter was 15. In cyclic loading, the pile was installed in the centre of the tank as shown in Fig. 4.7(b). The ratio of the distance between the pile and the wall to the pile diameter was 11 in the cyclic tests.

4.4. Pile clamping system

The pile head was clamped in place when placing the sand. The top of the pile was clamped onto a supporting frame as shown in Fig. 4.8. The clamp was released from the pile after the sand was placed leaving the pile at the design position in the sand sample. The clamping beam was a 1100 mm long L section beam with a width of 60 mm and a thickness of 5 mm.

4.5. Data acquisition system

Lateral displacement and load at the pile head were measured by transducers shown in Fig. 4.9 (a) and (b). A data acquisition system was connected to the transducers to read and to record the displacement and the applied load simultaneously. In static loading tests, the readings were recorded every 5 sec; the readings were taken every 0.1 sec in cyclic loading tests. A Pico logger system, AUT 11, is able to record readings up to 12 channels at the same time, and the maximum readings can be up to 100000. A regulated power supply and amplifiers were used to provide and to convert voltage on the transducers into a range of 0 – 2.5 V for data logging.

4.6. Device of static loading system

4.6.1. Introduction

An ideal static loading system should deliver a uniform rate of displacement at low speed, maintaining the direction of the loading. An overview of loading systems showed that some increased the load by applying weights and some used hydraulic pressure. In this series of model pile tests, the maximum loading was less than 0.5

kN for the largest finned pile, FPS240. In order to provide a constant low-speed increasing load, a static loading system was developed. The loading system developed for direct shear tests was used.

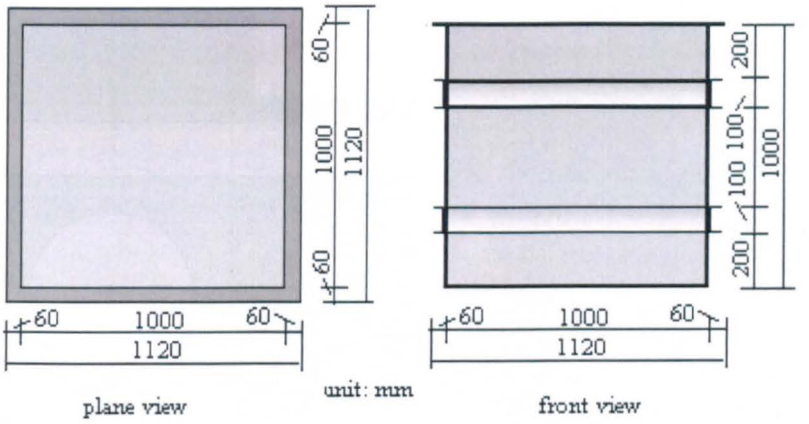

(a)

(b)

Fig. 4.6 Soil chamber (a) Schematic diagram (b) photo

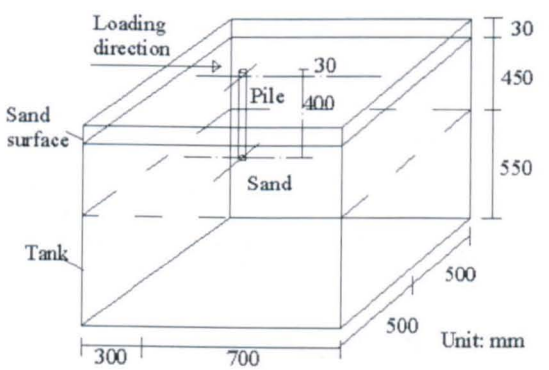

(a)

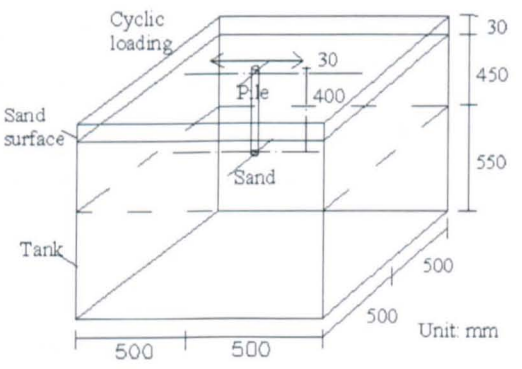

(b)

Fig. 4.7 The arrangement of test pile in (a) static loading tests (b) cyclic loading tests

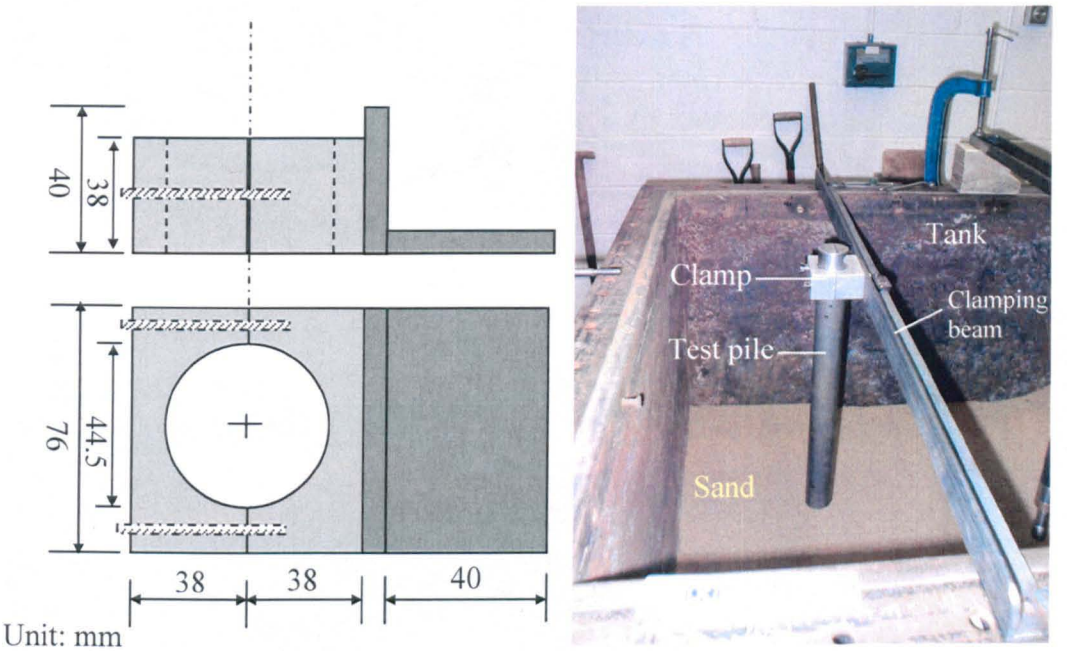

Fig. 4.8 (a) schematic of pile clamping system; (b) photograph of the pile clamping system in operation

4.6.2. Static loading device

The loading system was composed of three parts: a motor with a gearbox to provide a constant rate of displacement, a spherical seating to keep the load in the horizontal direction and a transducer to measure load and displacement (see Fig. 4.9 (a) and (b)). The motor (8) to operate the gearbox (8) drove the connecting rod (7) at a rate of 1 mm/min. The force was transmitted through the rod (7), the proving ring (6) and the spherical seating (5) to the pile head (4); the load was measured at the load ring (6 and 1). The load ring (6) was supported by a rod (7) held in place remote from the tank to ensure that there was no vertical load transmitted to the test pile. The spherical seating (5) at the front of the load ring (6) kept the applied load horizontal even when the pile tilted. The maximum movement of the pile head was 20 mm. The load ring had a capacity of 1 kN.

4.6.3. Demonstration of a static loading test

Initial sand filling

Sand was poured into the chamber at a constant rate up to a depth of 600 mm, and the surface was levelled manually. During each filling stage, four buckets of

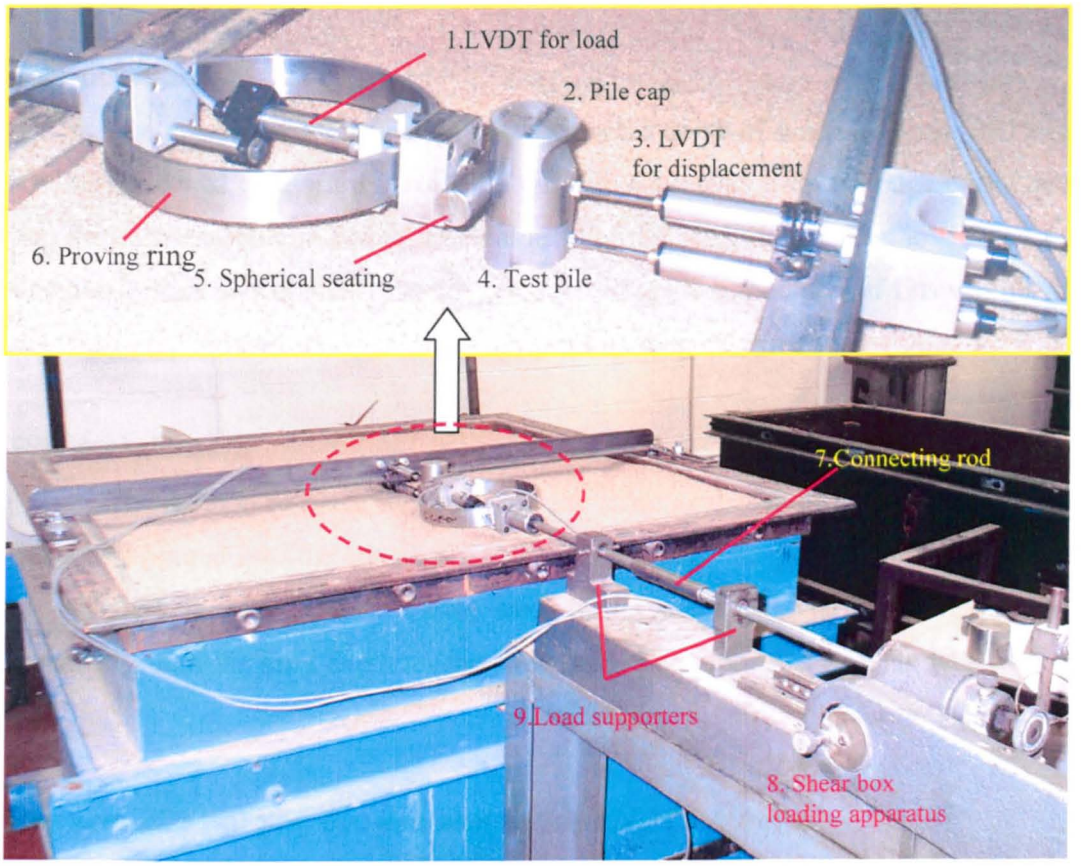

(a)

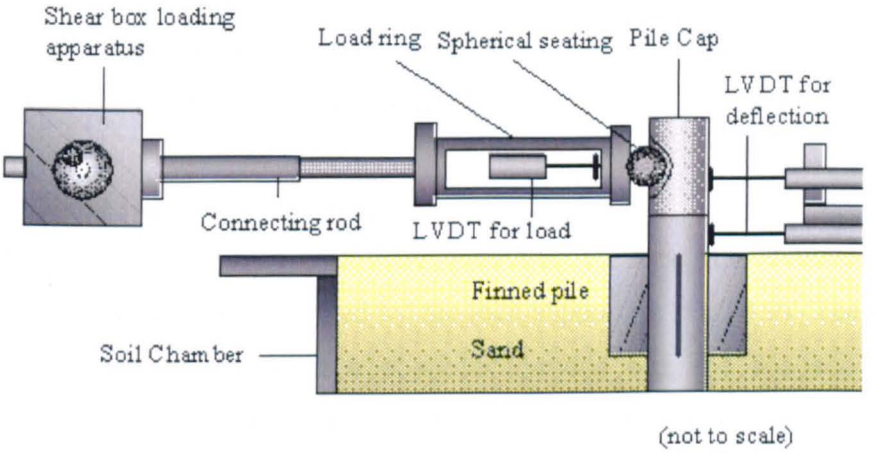

(b)

Fig. 4.9(a) Photos of static loading system; (b) schematic diagram of the loading system

sand (around 15 kg/ bucket) were poured steadily into the chamber to produce a uniform density. The depth of sand was increased by about 20 mm in each stage, and 30 layers were needed to place sand to a depth of 600mm. This process was repeated until the chamber was filled.

Pile positioning

The test pile was clamped in place when the depth of sand was about 600 mm. The test pile was temporarily fixed 300 mm for static tests from the edge of the tank and the toe was 400 mm below the final level of the sand. For normal loading cases, one pair of fins was aligned with the direction of loading; one pair of fins was set 45 degrees to the load direction for the 45 degrees loading cases.

Pile embedment

The method to place the sand was the same as that used to position the pile. Sand was poured into the chamber using a bucket, and four buckets of sand (around 15 kg/ basket) were poured during each filling process. The sand was poured constantly until the sand depth reached 970 mm. The processes were up to 20 stages of filling.

Remove pile holding system and set up LVDT

After the sand was placed, the pile clamping system was removed carefully to prevent any movement of the pile head. The deflection measuring system was then installed with the tip of LVDT directly at the rear of the loading system of the pile at 1.0 mm above the surface of the sand (Fig. 4.9).

Setting up the loading system

The proving ring with LVDT for measuring the load was connected to the connecting rod which was supported by the load supporters (Fig. 4.9) The distance between the spherical seating in front of the proving ring and the test pile was adjusted to less then 5 mm. The load ring had to be checked so that it was fully connected with the pile. Disturbance to the pile head was avoided during the setting of the load system.

Setting up the data acquisition system

Pico logger software was used to process the data from the LVDT. Firstly the generic information of the test was input. For the static loading test, a time interval of 5 sec to record the data sets was used. For the cyclic loading tests, a smaller time

interval of 0.1 sec was used so that the change in values could be monitored more closely. A test was ready to be carried out after these settings were completed.

Results presentation

Pile head displacement curves for a monopile, MPS, used in the static lateral loading test are shown in Fig. 4.10. Static loading tests of MPS were repeated three times. The difference between the P-Y curves was less than 5% at any displacement. The serviceability load, P_s, was 110 N at a displacement of 4.5 mm, and the ultimate lateral load, P_u, was 155 N.

Fig. 4.11 shows the variation of load and displacement with time. Displacement increased linearly with an increase in time which showed that the test was displacement controlled.

4.6.4. Performance of static loading system

The static loading system was able to sustain a lateral load at the pile head. The load could be gradually increased by increasing the displacement at a very low speed of 1 mm/min to represent the static loading behaviour. Both the ultimate lateral load (P_u) and the serviceability load (P_s) could be determined.

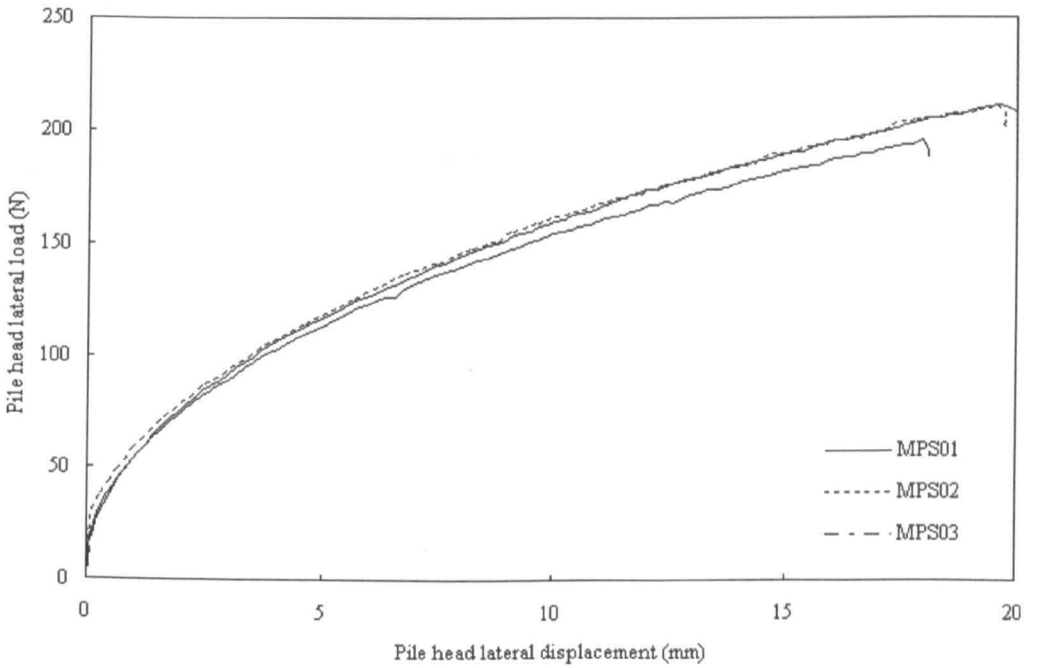

Fig. 4.10 Typical P-Y curves of MPS under static lateral loading tests

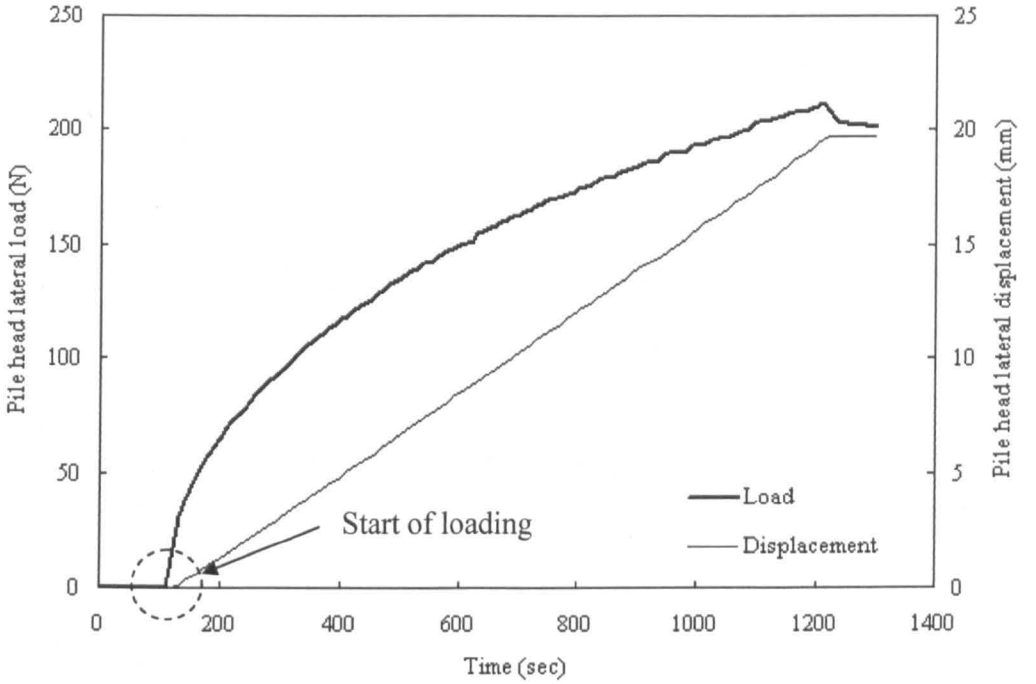

Fig. 4.11 Variation of loads and displacements with time for MPS02 under static lateral loading tests

4.7. Device of cyclic loading system

4.7.1. Introduction

As part of the research programme evaluating the lateral resistance of innovative pile foundations, a series of cyclic loading tests was carried out in the laboratory to model environmental loads for offshore wind farms. A new mechanical loading device was designed based on the principles of eccentric rotation and load distribution proposed by Ramakrishna and Rao (1999) and Purkayastha and Basack (1999), but extending it to symmetric two-way loading.

In this study, a pile was loaded by the horizontal force acting on the pile head. Either one-way or two-way cyclic loading were imposed by applying a horizontal force in one or alternating opposite directions. The magnitude and the frequency of the loads could be altered.

4.7.2. Cyclic loading device

The new loading system shown in Fig 4.12 is composed of four parts: the support frames, the power system, the control apparatus, and data acquisition units.

Supporting frames (5(a), (b)) are used to support the loading system. The support structure for the load system (5a) is composed of two steel circular columns, a rectangular frame and pulleys; all of them designed to minimise the vibration and the deformation of the loading system.

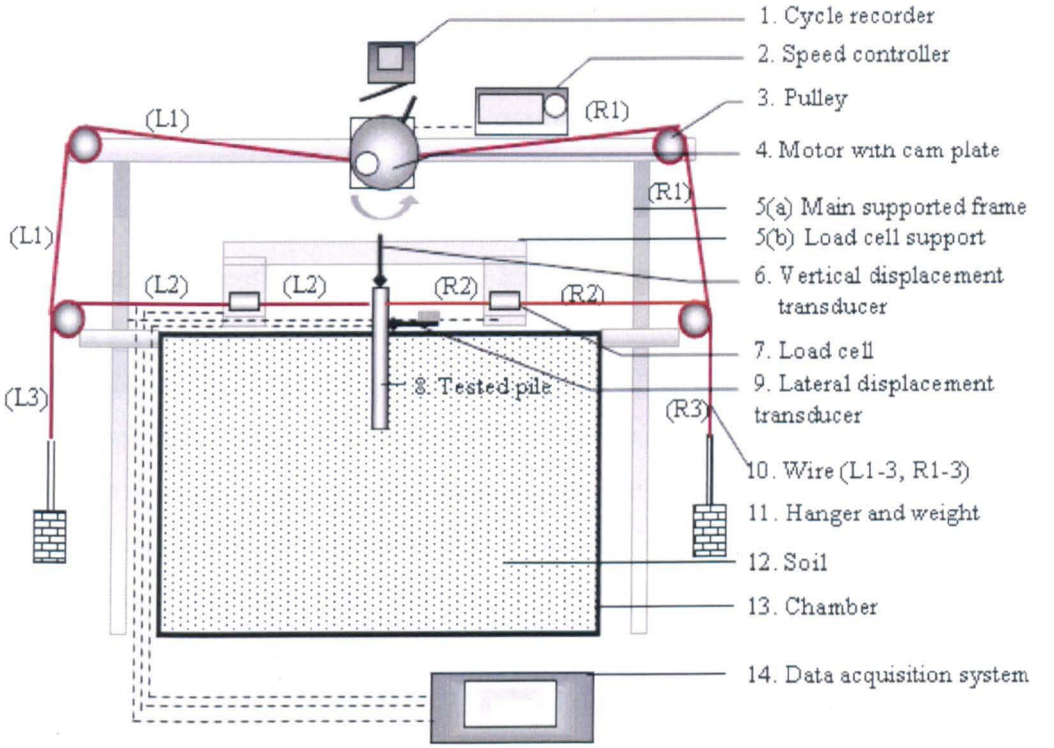

(a)

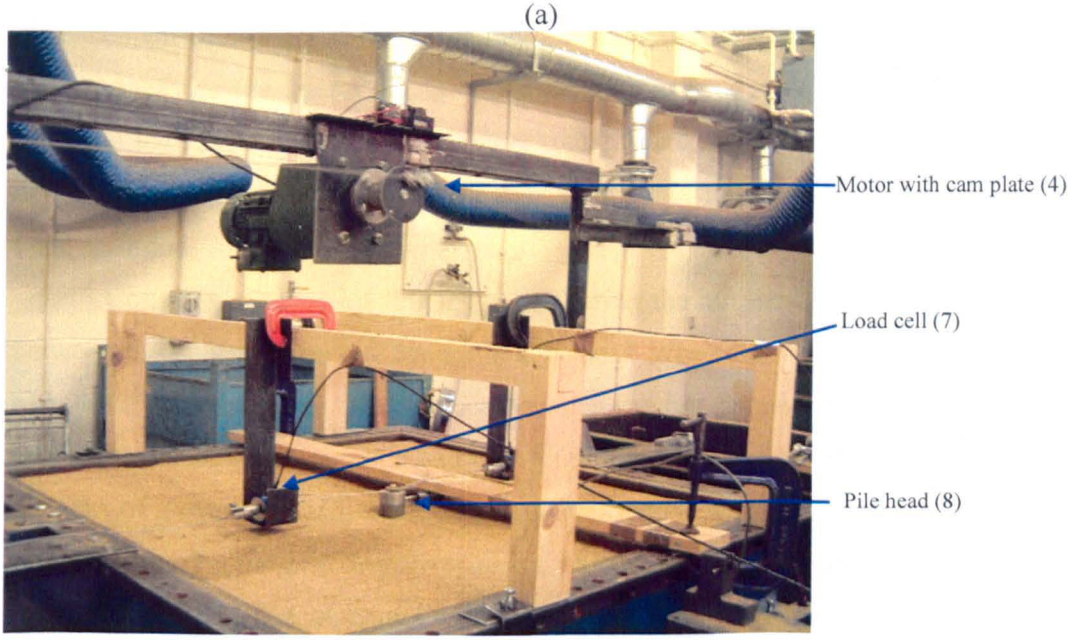

(b)

Fig. 4.12 - (a) Schematic of a new device for lateral cyclic loading; (b) a photograph of the loading system

The power system includes a motor (4) and a speed controller (transistor inverter) (2). A three phase AC motor (4) with a maximum output power of 0.35 kW was used, and its rotation speed was managed by a speed controller with a maximum output of 0.55 kW; the power system was able to operate under a torque of 4 N-m at a frequency between 0.3 and 1.5 Hz.

The control apparatus connected the loading system to the pile head. It consisted of hangers and weights (11), wires (L1-3, R1-3) and a cam plate (4). The weights (11) could be varied between 0 N to 200 N depending on the design load. The steel wires (L1-3, R1-3) were from 900 to 1500 mm in length with a diameter of 2 mm and had a tensile capacity of 2.5 kN. The cam plate (4) had a diameter of 40 mm and an eccentric diameter of 20 mm; the maximum lateral displacement in a test was determined by the plate's eccentric diameter. In line load cells (7) were mounted on a timber frame supported by steel plates (5b) to measure the tensile force applied to the pile head. The timber frame supported the weight of the cells.

The data acquisition unit included a revolution counter (1), two load cells (7) and a LVDT (9) which were used to count the number of cycles, the variation in lateral load and the lateral displacement, respectively. The revolution counter (1) was able to record over 10,000 cycles. Two load cells (7), each with a capacity of 1 kN, were used to measure the horizontal force acting on the test pile. An electronic displacement transducer (LVDT) (9) with a maximum displacement of 50 mm was used to measure the lateral displacement at the pile head. Voltage output obtained from the load cells and the LVDT were transformed and could be recorded by the data acquisition system (14) every 0.1 sec. Time, load and the pile head displacement were recorded.

Consider one way loading (Fig. 4.12) using the left hand hanger. The distance between the cam and the left hanger is constant. When the wire L1 is pulled to the right by the cam, the relative distance between the left hanger and the pile becomes shorter; the wire L2 is loosened and the weight is transferred to wires L3 and L1. At the start of a cycle of load, the weight is supported by wire L1 which means there is no load acting on the pile through wire L2. As the cam rotates, the distance between the pile and the hanger increases which means the load is transferred from L1 to L2. The weight creates a tensile force in wires L3 and L2 which is transferred onto the pile head through the load cell. The load acting on the pile is determined by the hanging weight. The cam system (4) allows a maximum pile head displacement of 20

mm. As the cam rotates the load is alternatively applied to the pile head and the cam. For two-way cyclic loading, the right hand side of the loading system is connected to the cam which causes the pile head to oscillate as the tension shifts from the wires on the right to the ones on the left.

4.7.3. Demonstration of a cyclic loading test

Test set up

Preparation of the sand bed and pile support were the same as those described for static loading (Section 4.6.3). But unlike static loading, the test pile in a cyclic loading test was placed at the centre of the tank to give the same boundary conditions for two-way cyclic loading (Fig. 4.7(b)). The support frame for holding load cells and the cyclic loading system was installed in the design positions shown in Fig. 4.12. The vertical and lateral displacement transducers were set up at the top and at the rear of the pile head, respectively. The weight, load frequency, cycle recorder were set to the design values. The cyclic loading test was carried out until the number of cycles reached 10,000 in order to model ten years of environmental loading.

Result presentation

Lateral load and displacement curves for one-way and two-way out-of-balanced loading are presented in Fig. 4.13 (a) and (b) respectively, showing the pile soil stiffness (load/displacement) increasing with the increase in the number of cycles. The pile moved significantly within the initial few cycles which replicated the results of static loading. In order to focus on the long-term influence of cyclic one-way loading, the initial ten cycles was not taken into account. This was similar to bedding error in laboratory tests and could represent the effects of pile driving for full scale piles in which the sand around a pile is compacted.

Fig. 4.14 shows the cumulative displacement of the pile head with the number of cycles demonstrating the difference between the maximum and minimum displacement for balanced and out-of-balanced loads. These indicate that there is very little displacement for balanced loads; and significant cumulative displacement for out-of-balanced loads suggesting a combination of sand heave and densification in front of the pile in the direction of the largest load, physical displacement of the whole pile and sand flowing past the pile.

Fig. 4.15 shows the relative displacement of the pile head with the number of cycles for balanced and out of balanced loads. The lines show that the relative displacement reduces with the number of cycles confirming an increase in soil stiffness.

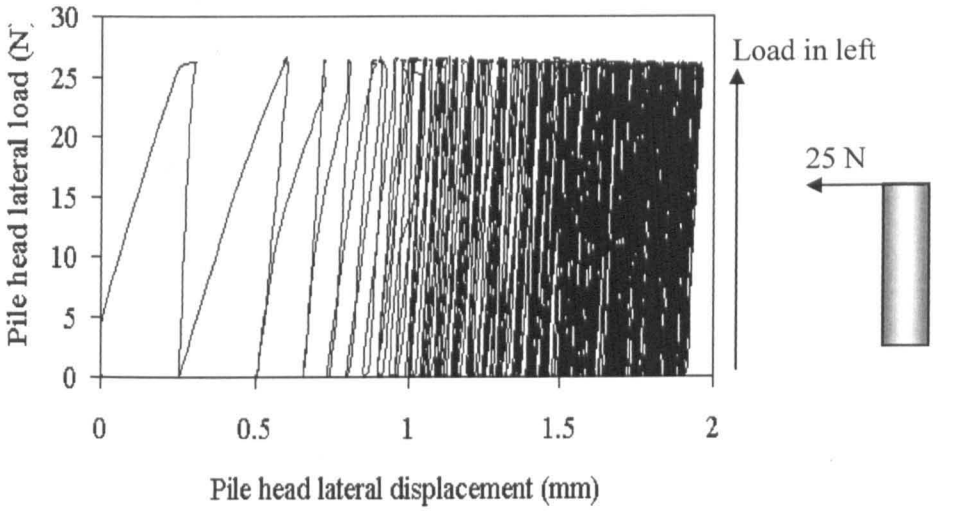

(a)

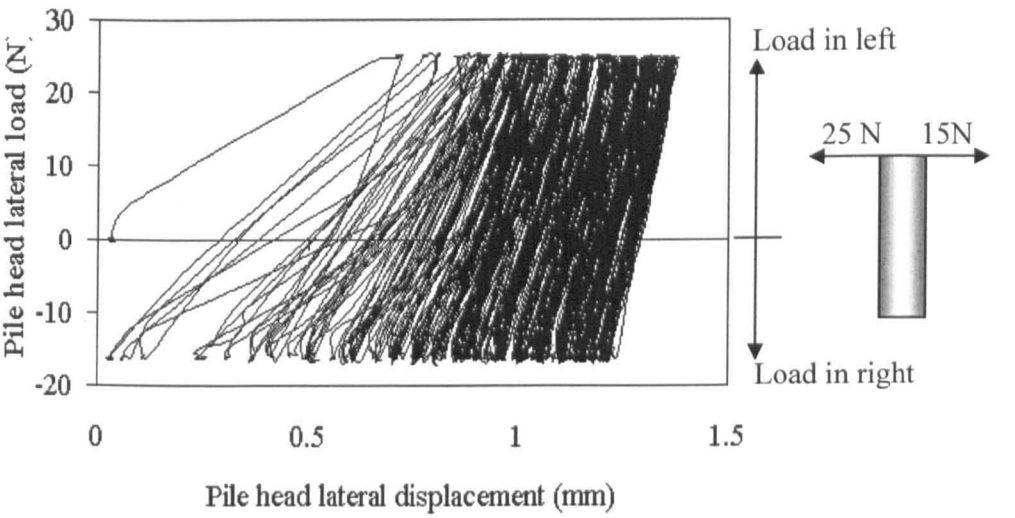

(b)

Fig. 4.13 Variation of pile head lateral load with displacement in (a) one-way loading; (b) out of balanced two-way loading (note: readings were taken every 0.1 sec)

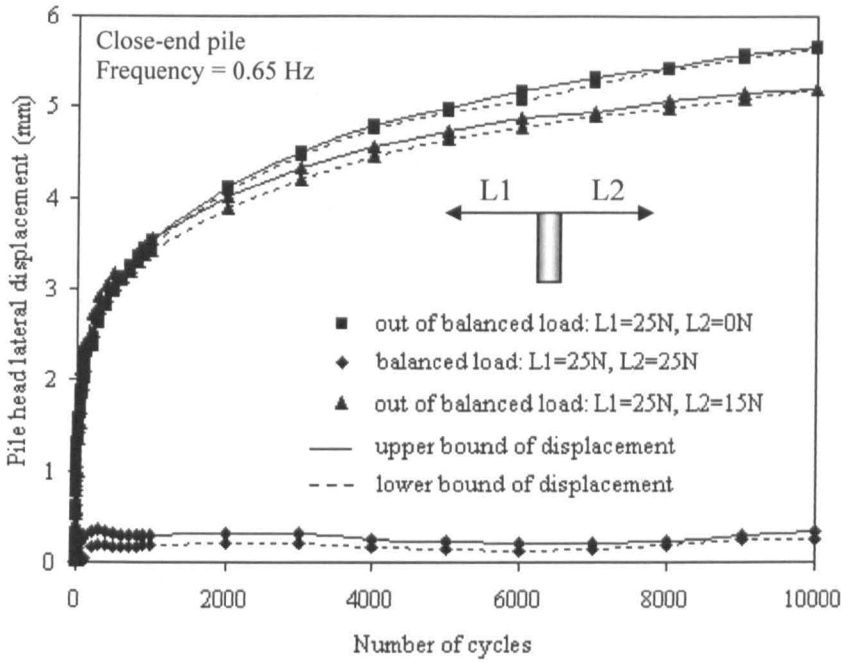

Fig. 4.14 Variation of pile head lateral displacement with the number of cycles

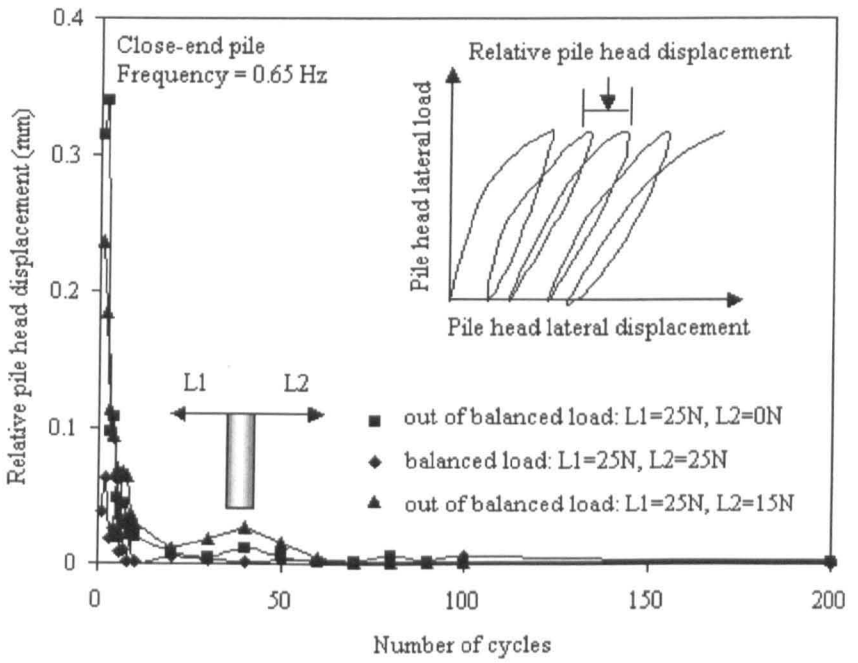

Fig. 4.15 Variation of pile head relative displacement with the number of cycles

Four sets of model tests of cyclic loading are presented here. The curves of displacement versus the number of cycles are presented in Fig. 4.16(a) for the first set

showing lateral displacement of the pile head increasing with the increase in frequency. The displacement at the highest frequency of 0.94 Hz is double that at the lowest frequency of 0.45 Hz.

The second set of results (Fig. 4.16(b)) shows a pile subjected to different load levels: 25, 50 and 75 N, representing 20%, 40% and 60% of the ultimate load of 120 N. The changes in pile head deflection with the number of load cycles are shown in Fig. 4.16(b). The lateral displacement increases with the increase in load magnitude. The third set of results in Fig. 4.16(c) shows the pile head displacements under different loading conditions: balanced and out-of-balanced loadings. The lateral displacement of a pile subjected to an out-of-balanced loading is significantly higher than that of a pile under balanced loading, even though the magnitude of an out-of-balanced load is lower than that of a balanced load. The vertical displacement of a pile under balanced loading is much greater than that of a pile under out-of-balanced loading. Under balanced loading, there is a significant increase of lateral displacement during the first cycle. There is very little further lateral displacement during subsequent cycles.

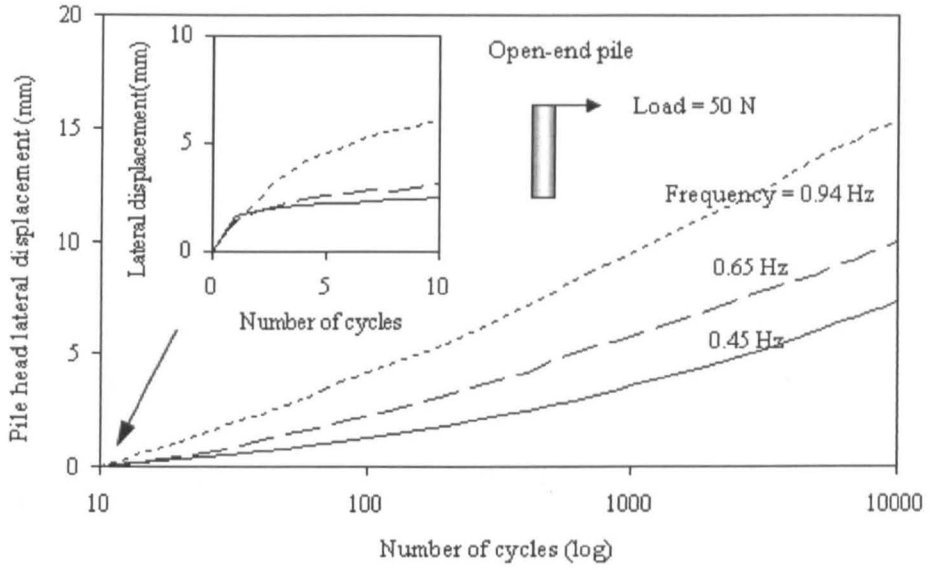

(a)

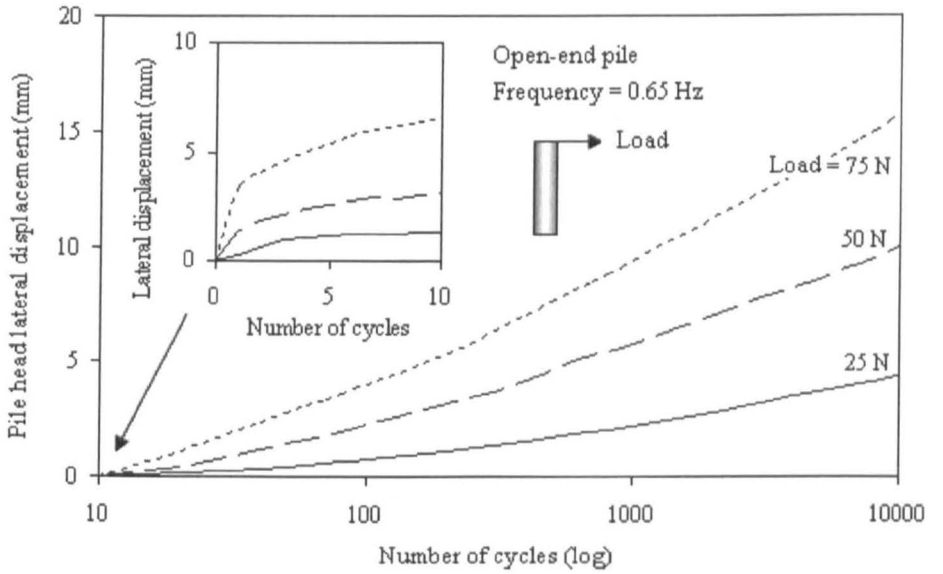

(b)

Fig. 4.16 Variation of pile head lateral displacement with the number of cycles for (a) different frequencies of loading, and (b) different levels of load (note: 75N is 0.5Pu; 50N is 0.33Pu; 25N is 0.15Pu)

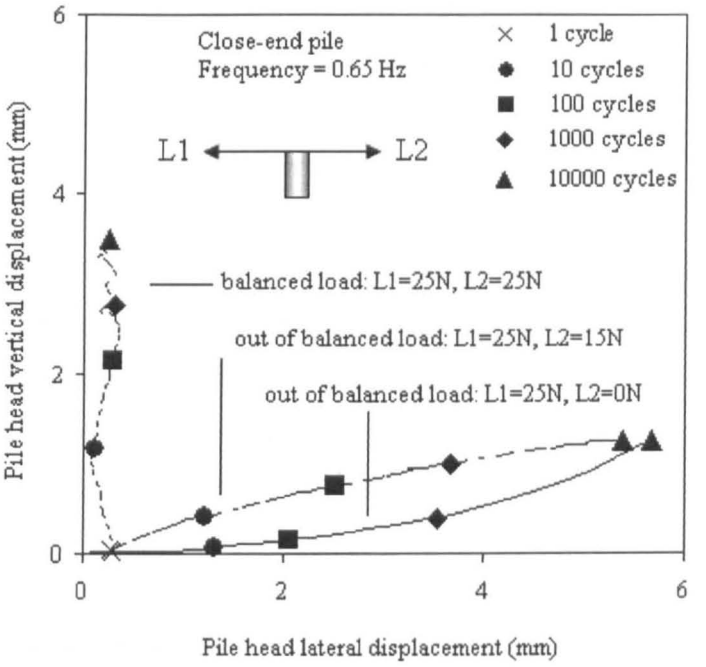

(c)

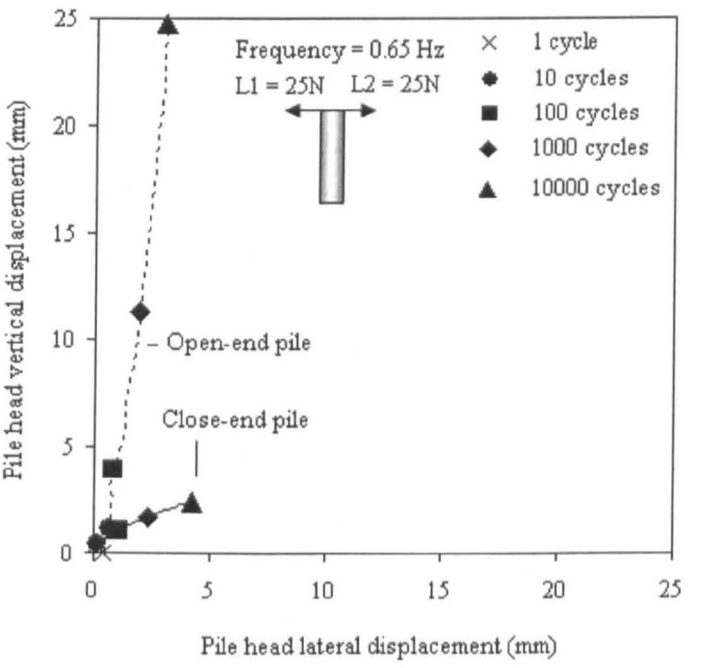

(d)

Fig. 4.16 Variation of pile head displacements with the number of cycles for (c) balanced and out of balanced loading; and (d) different tip conditions.

The fourth set of results (Fig 4.16(d)) shows the effect of a pile with different pile tip conditions: open-end and close-end. The curves of vertical versus lateral displacements are shown in Fig. 4.16(d). The lateral displacement of a close-end pile is slightly higher than that of an open-end pile; the vertical displacement of the open-end pile, however, is very much larger than that of the close-end pile. In addition, the settlement of the open-end pile occurs not only in the initial stage of loading; the pile keeps sinking with an increase in the number of cycles. The pile tip on the close-end pile brings a significant improvement in bearing capacity, corresponding to a reduction of vertical displacement.

These sets of tests demonstrate that the system can be used to alter the frequency of loading, the magnitude of the loads, the balance of the loads and the number of cycles.

4.7.4. Performance of cyclic loading system

Tests have been carried out with up to 10,000 cycles which can represent 10 years of environmental loading on a typical offshore structure with a lifetime of twenty years. This assumption was based on the number of cycles of loads developed during a hurricane (Bea et. al. in 1999) and the principle of extreme value analysis (Holmes, 2001). Horizontal loads varying from 15 N to 75 N represent a range between 10% and 50% of the ultimate lateral load of the monopile (155N). It was possible to set the load magnitude, the frequency and the direction of loading. Two-way loading could be used to model an offshore wind foundation subjected to a wind load and a wave load of differing magnitude and from opposite or the same directions. For example, wind and waves could load the wind turbine in opposite directions causing two-way cyclic loading at different load levels; the new device could provide out-of-balance cyclic loads to model this situation.

The speed of the motor was managed by a speed controller which ensured a constant rate of loading and unloading for each cycle. The frequency could be altered by adjusting the speed controller. The load was fixed by the weight on the hanger(s) which provide(s) tensile force(s) on the pile through wires and load cell(s). The actual load was measured directly with the load cells to take account of the friction in the system. This friction did not exceed 3% of the design load for that test.

The maximum cyclic load provided by the loading system was limited to 200N because of the capacity of the motor. The load of 200N is over 150% more

than the ultimate lateral load (P_u) of 155N in this study which indicates that the system is sufficient to model full-scale environmental loads from 0 to 100% of the ultimate lateral load, P_u. Values of the ultimate load could be greater than 200N for tests with a larger pile diameter. Increasing the power of the motor would increase the maximum load of the loading system to satisfy the test load.

The diameter of the cam affects the maximum movement of the pile head. This repeated process causes cyclic loading, and its maximum displacement is half of the diameter of the cam. The maximum displacement was set at 20 mm in this study because the diameter of the cam was 40 mm. Larger displacements can be obtained by increasing the radius of the cam plate.

4.8. The simple pressuremeter

4.8.1. Introduction

In order to predict the behaviour of the piles, soil properties such as density, relative density and internal frictional angle should be measured. A modulus of elasticity E_S in sand may be estimated from the friction angle ϕ; the empirical relationship between E_S and ϕ was based on field tests at depth about 10m. In model tests with a soil depth of 1m, the relationship between E_S and ϕ should be determined directly. Soil specimens in the triaxial compressive tests have to be remoulded which cannot show the real properties of the soil inside the tank. A simple pressuremeter device has been developed to obtain the soil modulus without disturbing the soil sample. This simple pressuremeter is easy to operate, and the test can be completed within 10 minutes.

4.8.2. A simple pressuremeter device

The simple pressuremeter was composed of three parts: a pressure control unit, a water volume measuring unit and a pressuremeter pipe (see Fig. 4.17 and 4.18). The pressure control unit includes an air control valve and a pressure transducer. The pressure control unit can control the value of the pressure inside the whole pressuremeter system. The pressure transducer can measure the pressure in the range of 0 – 55 kPa, and the pressure can be recorded by a data logger.

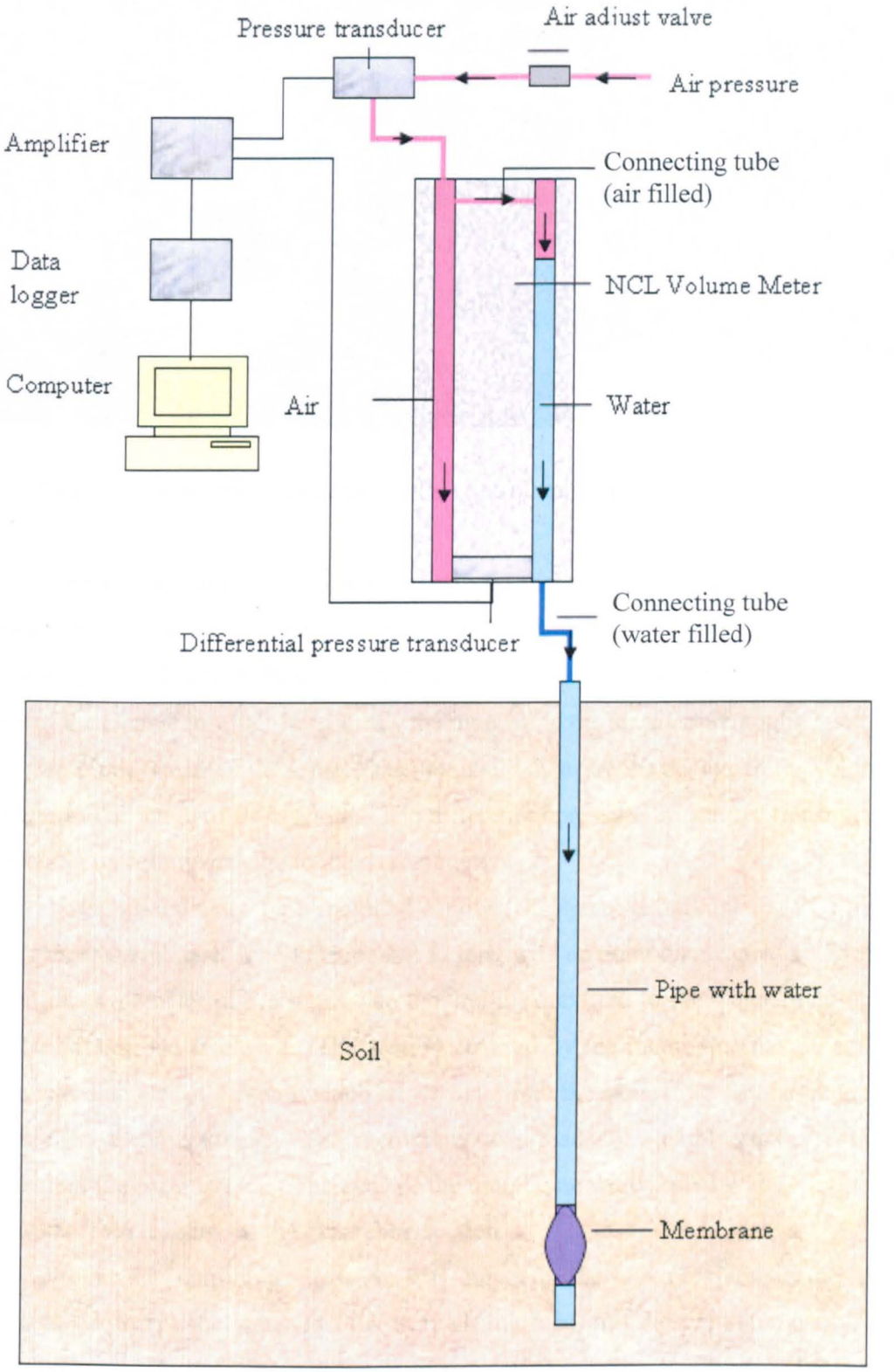

Fig. 4.17 The simple pressuremeter equipment

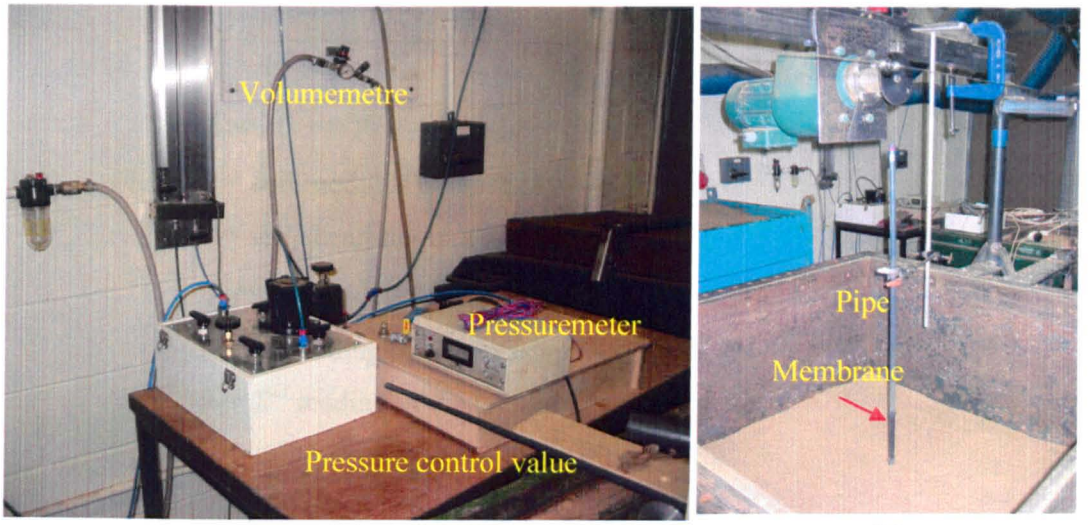

(a) (b)

Fig. 4.18 Photos of simple pressuremetre (a) control unit (b) pressure metre unit

The volume measuring unit included two pipes (one contains water and air and one contains air only) with a differential pressure transducer between the base of the two pipes. This transducer could measure the change in volume of water as a result of the change in water level inside the pipe while the air pressure applied within these two pipes remained the same. The unit could measure the change in the volume of water in the range of 0 – 150 ml. The differential pressure transducer transmitted the reading of volume change to the data logger.

The pressuremeter pipe included a Poly (Bisphenol-a Carbonate) (PC) pipe and a rubber membrane. The PC pipe is 1 m long with an outer diameter of 13.75mm and an inner diameter of 8.6 mm. The top end is connected to the water filled tube and the bottom end is closed. The section covered by the membrane has 20 small holes with diameter of 0.5 mm which allow water into the expanding section to apply pressure on the membrane. The membrane was made of flexible rubber firmly attached on the pipe surface. The ends of the membrane were sealed with O-rings to stop water from leaking for the expanding section.

When the confining pressure was applied, the air pressure inside the volumemeter forces the water to flow through the tube into the pressuremeter. The membrane expands until the soil pressure balances the water pressure. The shear modulus equals the ratio of the difference of pressure to the difference of change in volume as shown in Equation 4.1(a). In addition, the modulus of elasticity of the soil can be obtained from Equation 4.1(b).

$$G = \frac{P_2 - P_1}{(V_2 - V_1)/V_{ini}} \tag{4.1a}$$

$$E = 2(1+\nu s)G \tag{4.1b}$$

where E = soil modulus of elasticity

G= soil shear modulus

ν_s= Poisson ratio of soil

P_1= 1st reading of the pressure (see Fig. 4.19)

P_2= 2nd reading of the pressure (see Fig. 4.19)

V_1= volume reading at P_1 (see Fig. 4.19)

V_2= volume reading at P_2 (see Fig. 4.19)

V_{ini}=initial volume reading (see Fig. 4.19)

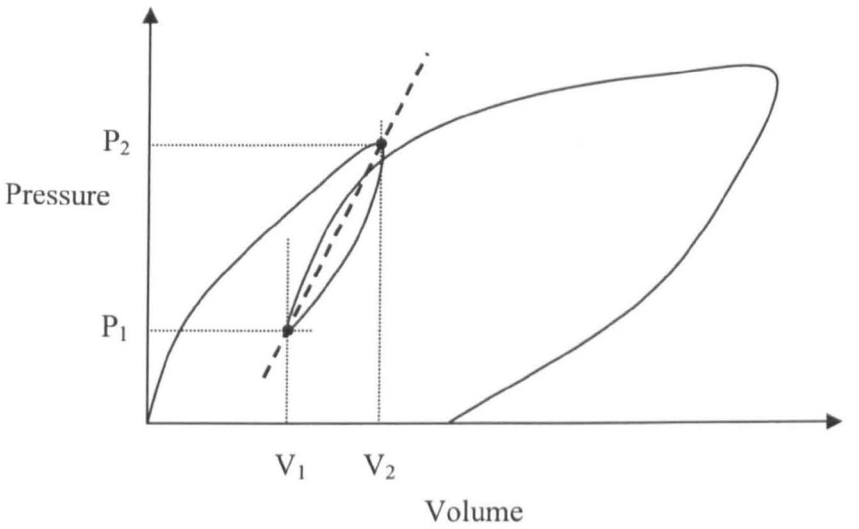

Fig. 4.19 Typical curve of pressure and volume from a pressuremeter test

4.8.3. Demonstration of a pressuremeter test

Test preparation and procedure

The volumemeter and pressure transducer were connected to the pressuremeter and the control system as shown in Fig. 4.18. The pressuremeter was set near the middle of the tank, and the installation depth was based on the position of the membrane. The sand was filled using the same procedure as a pile test until the sand depth reached 970 mm. After these preparations, the control valves on the tubes were opened, and the data logger was set.

The air control valve was opened to allow the air pressure to fill the inside of the tubes of volumeter and apply pressure to the transducer as shown in Fig. 4.17. The air pressure inside the volumemeter compressed the water forcing it to flow through the tube into the pressuremeter. The membrane of the pressuremeter expanded to balance the soil pressure. A complete cycle of pressure was carried out at five different pressure magnitudes: 100, 150, 200, 250 and 300 mmHg. When the maximum pressure of 350 mmHg was achieved, the pressure was reduced to zero. The test could be stopped when the water level in the volumemeter dropped dramatically which indicated that no more soil resistance was available.

Results presentation

Tests were carried out at four different soil depths: 100, 200, 300, 400 mm. The test curve in Fig. 4.20 shows the variation of pressure with volume change at the depth of 400 mm. The soil shear modulus and modulus of elasticity were calculated according to Equation 4.1 (a) and (b), respectively. It is assumed that the Poisson ratio, ν, is 0.33. Results of soil Young's modulus, Es, are shown in Fig. 4.5; Es increases with depth.

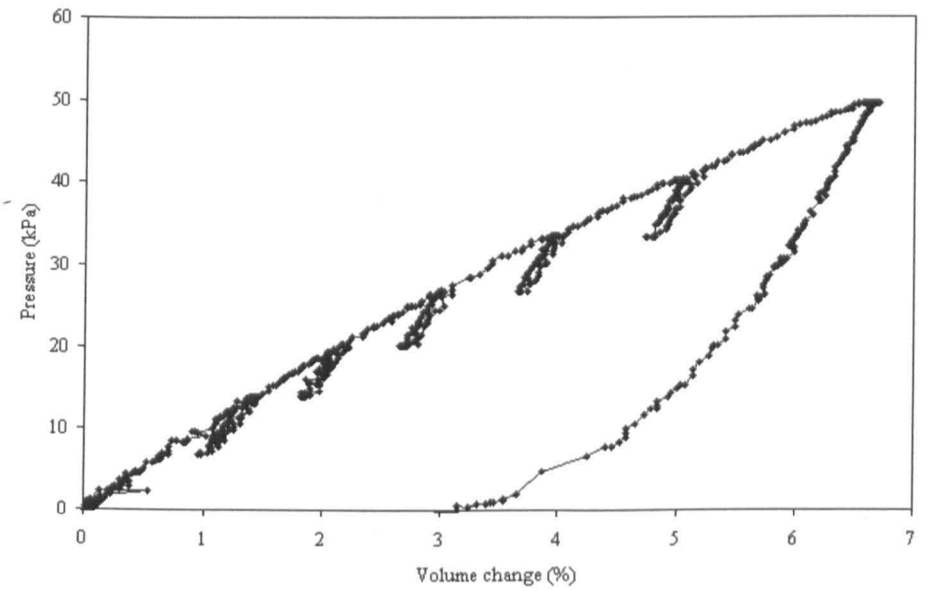

Fig. 4.20 Variation of pressure with volume change measured at depth of 400 mm

4.8.4. Performance of simple pressuremeter

In order to inspect the influence of lateral stress on the shear modulus with change in strain, a modified relationship was developed (Fig. 4.21) based on the results in Fig. 4.20. The stress function was presented as G_S / σ'_h where G_S was secant shear modulus taken from the secant slope of the unloading parts of a cycle section, and σ'_h was horizontal stress measured at the start of unloading (Clarke, 1981). The percentage of current volume strain, ε^* was the difference of volumetric strain between the start of unloading and the point on the unload curve at each load level. The values of G_S / σ'_h decreased with the increase in volumetric strain. The curves of G_S / σ'_h and ε^* measured at five different cycles are bounded in a region showing the reduction of G_S / σ'_h with an increase in ε^* at the same depth.

Results show that the simple pressuremeter can be used for predicting the soil properties in the small scale test. Compared to a commercial pressuremeter test, the simple pressuremeter has advantages of easy operation, low cost and small sample measurement. This device can also be applied to measure other kinds of soil samples. In future research, the simple pressuremeter should be automatically controlled in order to improve the consistency of the test.

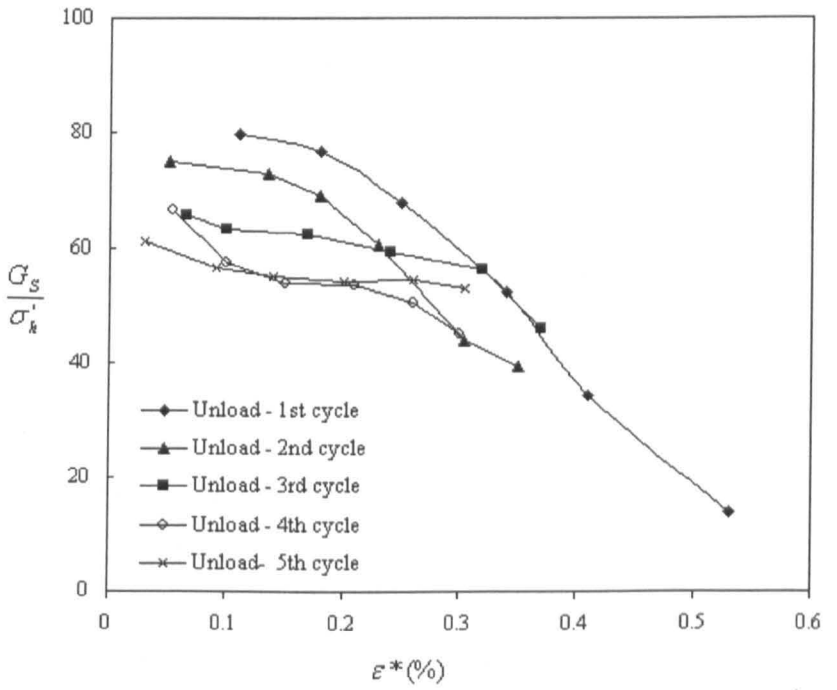

Fig. 4.21 The variation in modulus with strain

4.9. Installation of strain gauges

4.9.1. Introduction

Strain gauges attached to the pile surface have been widely used to verify pile soil behaviour. Theories of the interaction have been introduced in Section 2.4.2. In a hollow pile with a large diameter, strain gauges are usually installed in the inner wall of the pile; whereas, gauges can only be installed on the outer wall of a solid pile or on a hollow pile which has a small diameter. Friction contact between the pile and the soil on the pile outer surface may cause errors in readings; the wires and gauges could be damaged as a result of high frictional force.

Although the diameter of the model pile is small (0.045mm), the gauges should still be placed on the inner surface of the pile to protect them. A new gauge installation method has been developed to allow the gauges to be fully attached to the inner pile surface.

4.9.2. Installation method

A foam tape was bonded to thin laminate paper to improve the stiffness of the foam tape. Strain gauges were attached at the required positions on the tape as shown in Fig. 4.22(a); the wires for the strain gauges were then glued to the side of the laminate paper covered by sealing tape as shown in Fig 22(b). The composite tape was temporarily attached to a steel bar. The side with the strain gauges attached was then covered with adhesive, and the tape on the bar was immediately placed inside the test pile at the test position. The gauges were clamped to the pile wall by the steel bar which was clamped to the ends of the pile (see Fig. 22(c)). After 40 minutes, the steel bar was removed, and the installation work was completed. The same installation method was applied to the opposite side of the pile wall resulting in pairs of gauges at each level.

4.9.3. Demonstration of a test using a strain gauge pile

Calibration of a test pile

The test pile was set up in the design position as shown in Fig. 4.23 to demonstrate the effectiveness of the gauges. In the point load test, the pile was supported at either ends with clear space of 380 mm between the supports. The point load was applied at the middle of the pile. The signals of gauges were transmitted

into a channel unit box. A control unit box gave the strain reading of each gauge according to the signals from the channel unit box (see Fig. 4.22(d)).

In order to verify the efficiency of the strain gauge method, measured strains were compared with calculated strains. The calculated strains can be taken from Equation 4.2

$$\varepsilon = \frac{Md}{E_p I_p} \tag{4.2}$$

where = calculate strain

M = bending moment at the measuring point

d = the distance between the measuring point and the pile centriod which is the inner diameter of the pile

E_pI_p = pile flexural stiffness at the measuring cross section

The pile was installed according to the method described in Section 4.4.3when testing the pile.

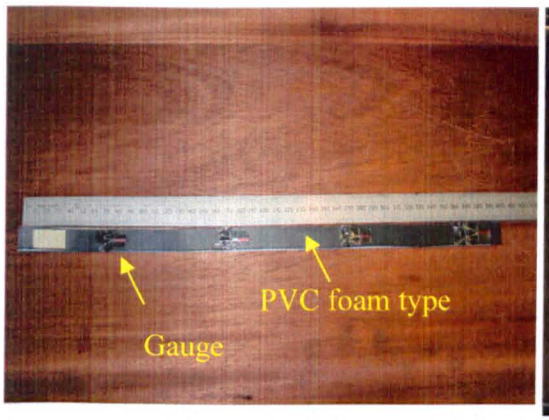

(a) gauge attached

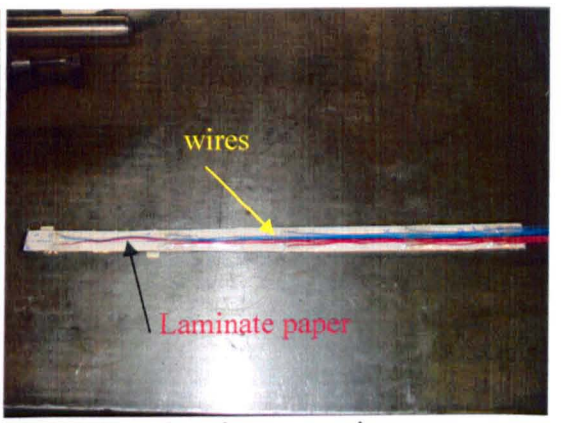

(b) wire connection

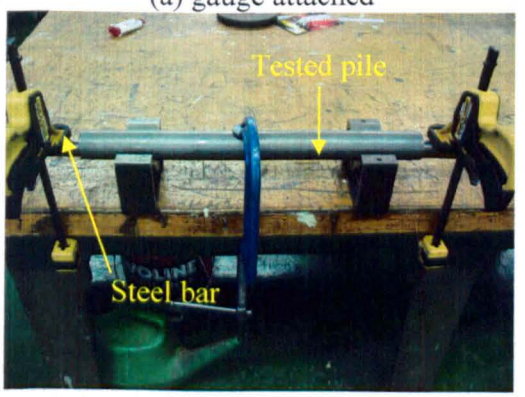

(c) gauge installed inside the pile

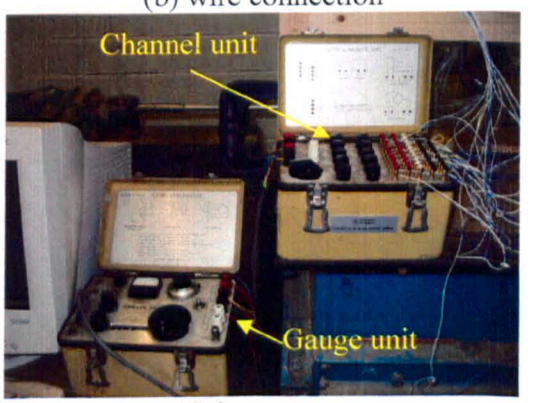

(d) instrument

Fig.4.22 Strain gauge installation

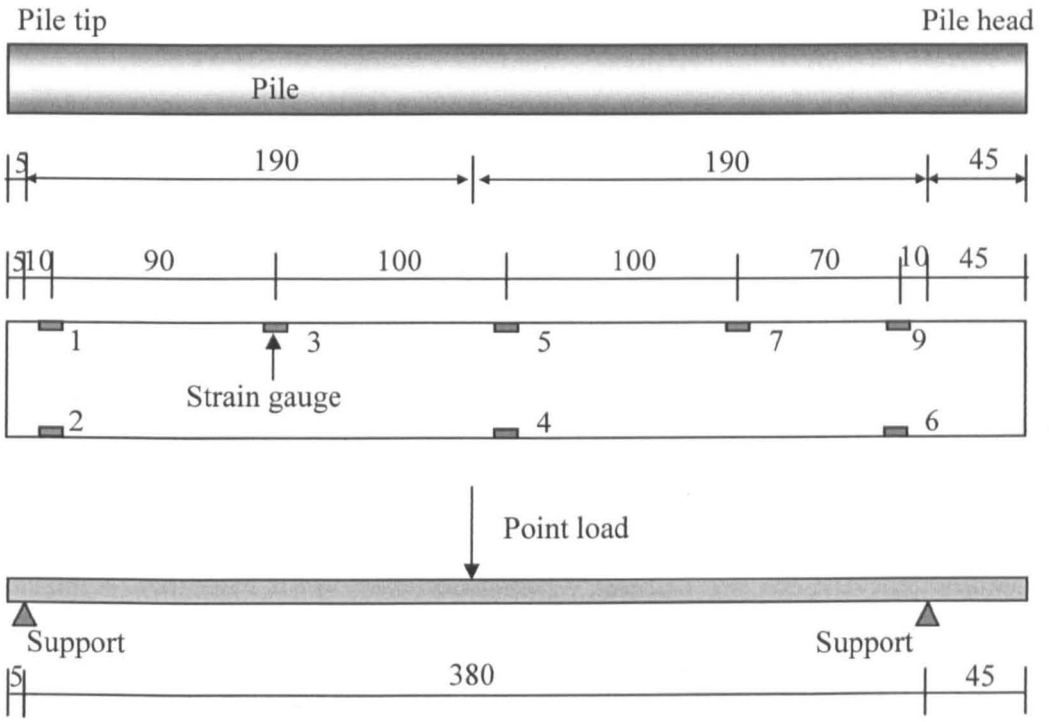

Fig. 4.23 Point load test and strain gauge positions

Table 4.1 Strain readings along the pile when the point load is 500N

Gauge No.	Position (from tip) (mm)	Strain (calculate) (no nuit)	Strain (measured) (no unit)	$\frac{Strain_{(measured)}}{Strain_{(calculate)}}$
1	15	4.14E-06	4.00E-06	0.97
2	15	4.14E-06	4.00E-06	0.97
3	105	4.14E-05	4.10E-05	0.99
4	205	7.46E-05	7.50E-05	1.01
5	205	7.46E-05	7.50E-05	1.01
7	305	3.32E-05	3.40E-05	1.03
6	375	4.14E-06	4.00E-06	0.97
9	375	4.14E-06	4.00E-06	0.97

Table 4.2 Ratio of $Strain_{(measured)}/Strain_{(calculate)}$ under different loadings

Gauge No. Load (N)	1	2	3	4	5	7	6	9
100	*	*	0.97	1.01	1.01	0.98	*	*
200	*	*	1.03	1.01	1.01	0.98	*	*
300	1.01	1.01	0.97	1.01	1.01	1.01	1.01	1.01
400	0.97	0.97	0.99	1.01	1.01	1.03	0.97	0.97
500	1.19	1.12	0.88	0.85	0.84	1.08	1.07	1.24
Avg. reading	1.06	1.03	1.01	1.00	1.00	1.00	1.01	1.01
Note: * means the reading is less the 10^{-6} strain, which is too small to measure								

Results of a calibration test and a static loading test

Results of two tests are presented here: a point load test and a pile lateral load test. In the point load test (Fig. 4.23), the point loads were given at five different load magnitudes: 100, 200, 300, 400 and 500 N. The tested pile was a monopile, MPS, with 8 strain gauges inside; positions of the strain gauges are shown in Fig. 4.23. Table 4.1 shows the measured and calculated strains of all gauges at the load magnitude of 500 N, and the ratio of measured strain to calculated strain. The ratios of measured strain to calculated strain at different load magnitudes are given in Table 4.2. The readings of Channel 1 and 2 were ignored at the load magnitudes of 100 and 200 N because the gauge values were less than 1 micro strain (the gauge unit could only read to1 micro strain). Generally the ratio is between 0.96 and 1.01, with the low ratios distributed at one end of the pile.

In a static loading test of a monopile, the strain values were measured every 2 mm of pile head displacement. The bending moment, shear force, soil resistance as well as pile deformation can be derived from strain data using Equation 2.19(a)-(f). These values are presented in Fig. 4.24 (a)-(d). Pile head shear force at the displacement of 20 mm shown in Fig. 4.24(b) is 209 N which is close to the value of 207 N obtained from the load cell reading. The soil resistances at the front and the back of the pile are shown in Fig. 4.24 (c).

4.9.4. Strain gauge performance

The gauge readings and the calculated results show a difference of up to 4% of the gauge readings. This difference could be due to:

- The gauge unit can only measure to an accuracy of 1 micro strain.
- The strain gauges near the supports were influenced by the supports (Fig. 4.23).
- The strain was determined over the whole length of the gauge, but the calculated strain was taken at the centre point of a gauge.
- In the Equation 4.2, the calculation of strain is based on the bending moments which are assumed to be the same in the compressive and tensile parts of the pile. However, the point load applied on the pile was not uniformly distributed on the cross section which could cause differential deformation along the pile. The irregular deformation is illustrated in Fig. 4.25 by 3D LUSAS analysis.

In the demonstration of static loading test, the pile soil behaviour of the monopile, MPS, was verified by investigating the bending moment along the pile. The accuracy in the estimation of shear force and soil resistance along the pile was based on fitting a curve to the output. Taking an overview on these results, the strain gauge installation method is able to set the gauges in the inner wall of the pile, and the gauge readings could be applied in the preliminary prediction of pile-soil behaviour.

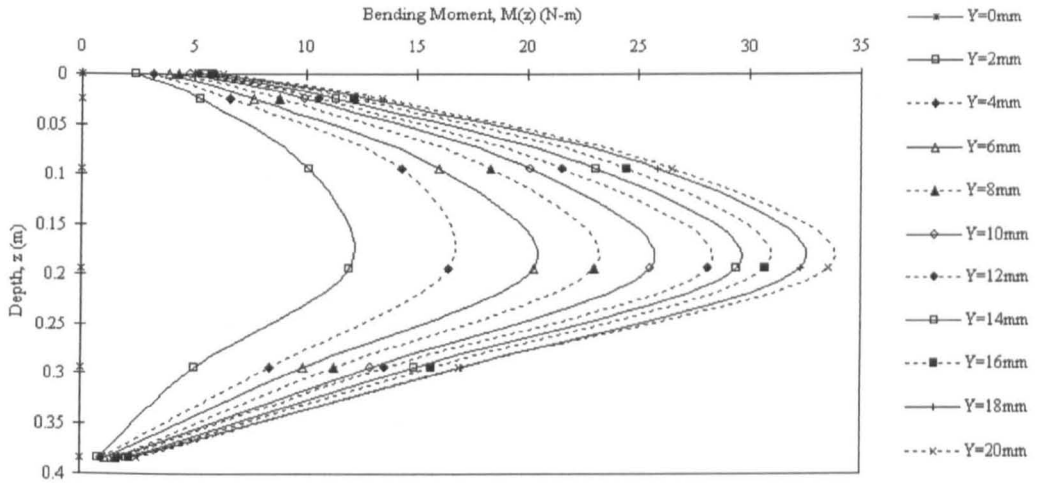

Fig. 4.24 (a) Calculated bending moment along the pile, MPS from strain gauge test

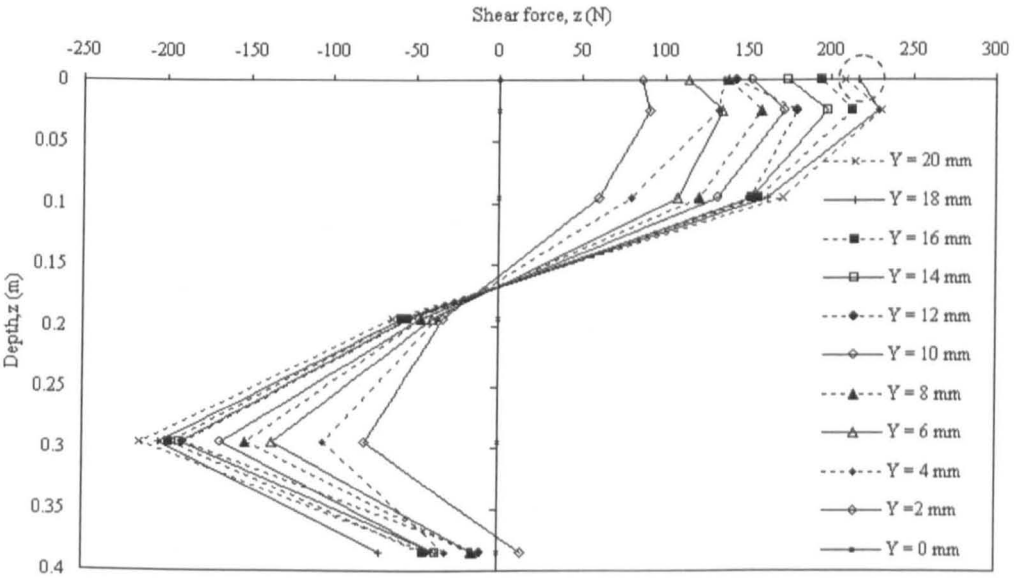

Fig. 4.24 (b) Calculated shear force along the pile, MPS from strain gauge test

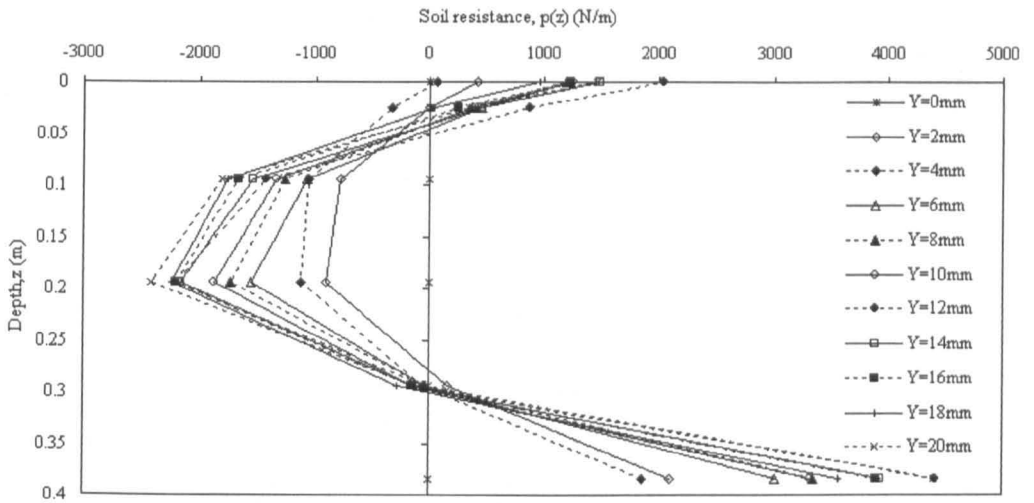

Fig. 4.24 (c) Calculated soil resistance along the pile, MPS from strain gauge test

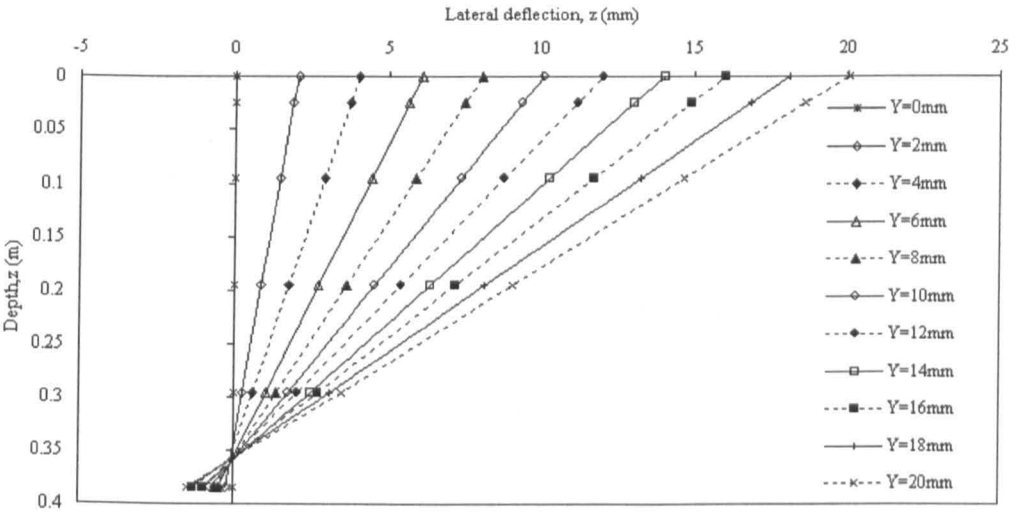

Fig. 4.24 (d) Calculated pile deformation along the pile, MPS from strain gauge test

4.10. Summary

Reviews of lateral loading tests (Section 2.2.3 and 2.2.4) provided the methodology of finned pile tests. Properties of equipment including model piles, soil, the chamber, the data acquisition system have been presented.

The device of the static loading system has been presented in Section 4.6, and its performance was assessed according to a laterally loaded monopile test. The static

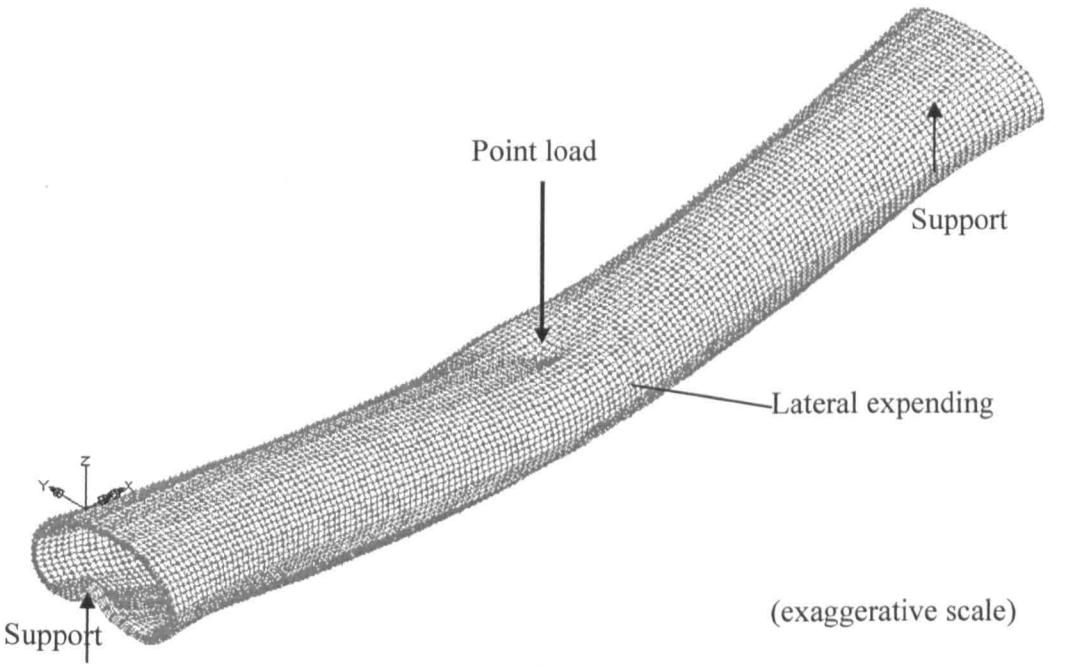

Fig. 4.25 3D Computer modelling of deformation of a tube subjected to a point load generated by 3D LUSAS analysis

loading system will be used to measure the pile head load and displacement (P-Y) curves of finned piles and to determine the ultimate lateral load of piles in Chapter 5.

The methodology of the cyclic loading system has been described in Section 4.7. A monopile subjected to cyclic loading with different load magnitude, frequency and direction was tested to investigate the performance of the loading system. The device of the cyclic loading system was used to carry a series of tests of finned piles discussed in Chapter 6.

In order to investigate the behaviour of finned piles under lateral loading, a strain gauge method was provided. A simple pressuremeter was developed to measure the soil properties which are used in the numerical modelling in Chapter 3. Assessment and improved methods of test equipment will be presented in Section 7.3.4 for the future research of finned piles.

5 Static loading tests

5.1. Introduction

In order to determine the serviceability loads, P_s, and the ultimate lateral loads, P_u, of finned piles subjected to lateral loading, a series of static loading tests were carried out. The lateral resistance was determined from the pile head load displacement (P-Y) curves. Model piles with different fin dimensions were assessed, and the load magnitudes at a displacement of 10% of the pile diameter were used to represent the improvement in lateral resistance. The values of serviceability loads, P_s, and the ultimate lateral loads, P_u, were used to describe the efficiency of the fins.

The study then looked at loading at different directions on a finned pile. The pile lateral rigidity, EI, and the effective area facing the load will change with the loading direction. The variation of load magnitude with load direction at a displacement of 10% of the pile diameter was assessed. The increase in fin dimensions of finned piles was transformed into the increase in the weight of piles because the weight of steel is a measure of the cost of the piles. A relationship between weight and lateral resistance was developed.

The position of the fins was the next parameter to be assessed. The horizontal effective stress of sand increases with depth which suggests that fins placed near the bottom of the pile may provide more soil resistance. The lateral force acting on the pile head was mainly applied near the pile head. In order to find the best position for the fins, finned piles with fins at the top, the middle and the bottom were tested. In addition, a finned pile, FPS210, with gauges inside was tested to determine the pile soil reaction. Details are given in Section 5.2.4.

Tests described above focussed on the investigation of the behaviour of laterally loaded piles. In reality, a pile is used to support both vertical and horizontal loads. Static combined load tests have been carried out to determine the failure envelope of finned piles. A constant vertical load was first applied to the pile to model the gravity load of the superstructure acting on the pile head. This was followed by a static lateral load gradually applied at the pile head until the soil reached failure. Based on the different load combinations, a failure envelope was

established. This failure envelope was used to define a safe working loading combination.

5.2. Results

5.2.1. Standard finned pile test

The methodology including the test materials and static loading procedures is introduced in Section 4.6. One monopile and nine finned piles were used in this series of tests, and the test codes are given in Table 3.1 (a) and (b). Fig. 5.1 shows the P-Y curves of static loading tests on all piles. The load P for a given displacement Y increased as the fin length or width increased. Therefore, an increase in fin area improves the lateral resistance of pile foundations. The results of finned piles, FPS205 (6650mm^2) and FPS110 (6650mm^2), were similar suggesting that fin area is a key parameter that controls the lateral resistance; the same situation was found for piles FPS405 (6650mm^2) and FPS120 (6650mm^2). However, the results of FPS220 were significantly higher than those of FPS410 even though their fin areas were equal, which suggests that the fin dimensions as well as the fin area are critical.

The P-Y curves shown in Fig. 5.1 were used to determine the serviceability lateral load, P_s, (when Y = 0.1D) and the ultimate lateral load, P_u. Results are shown in Table 5.1. The ratios of limit states of finned piles to those of the monopile, MPS, are also given in the table to show the effect the fins have upon the capacity. The increase of load varied from 5 % up to 75 % of the MPS limit states depending on the fin dimensions.

Table 5.1 Limit state of lateral capacity of finned piles based on static loading tests

Pile number	Serviceability lateral load, P_s(N)	$\frac{P_{S(FPS)}}{P_{S(MPS)}}$	Ultimate lateral load, P_u (N)	$\frac{P_{u(FPS)}}{P_{u(MPS)}}$
MPS	112	1.00	155	1.00
FPS105	120	1.07	162	1.05
FPS110	130	1.16	175	1.13
FPS120	139	1.24	192	1.24
FPS205	130	1.16	172	1.11
FPS210	142	1.27	189	1.22
FPS220	174	1.55	236	1.52
FPS405	127	1.13	175	1.13
FPS410	144	1.29	195	1.26
FPS420	197	1.76	264	1.70

Note: Ps is taken when lateral displacement is 4.5 mm
Pu is taken when the increase of P-Y curve starts to be constant

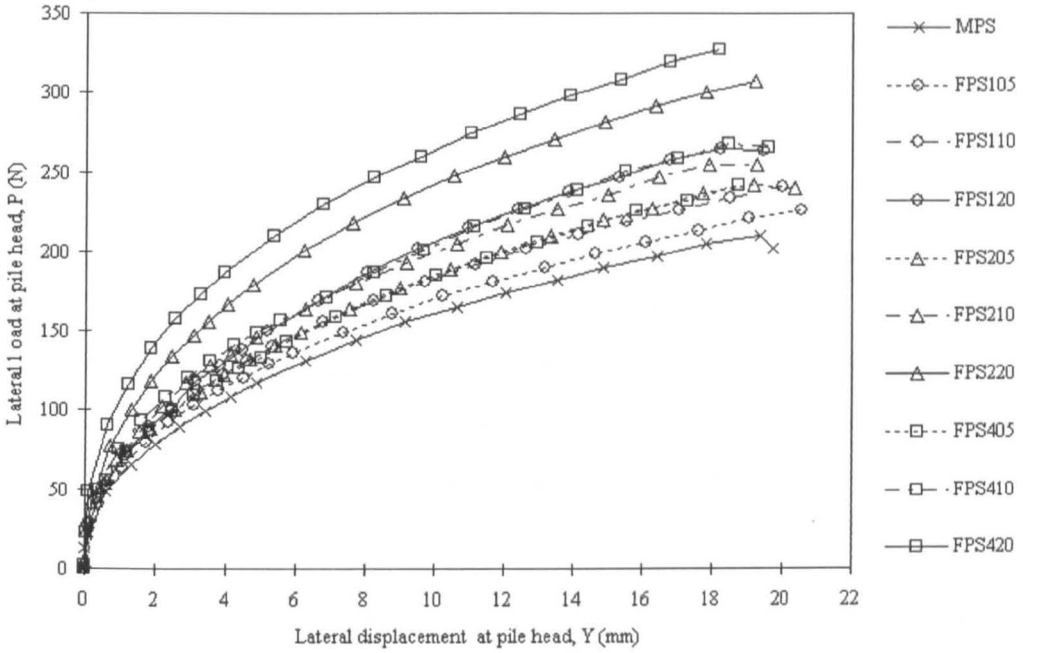

Fig. 5.1 Pile head P-Y curves from lateral static loading tests

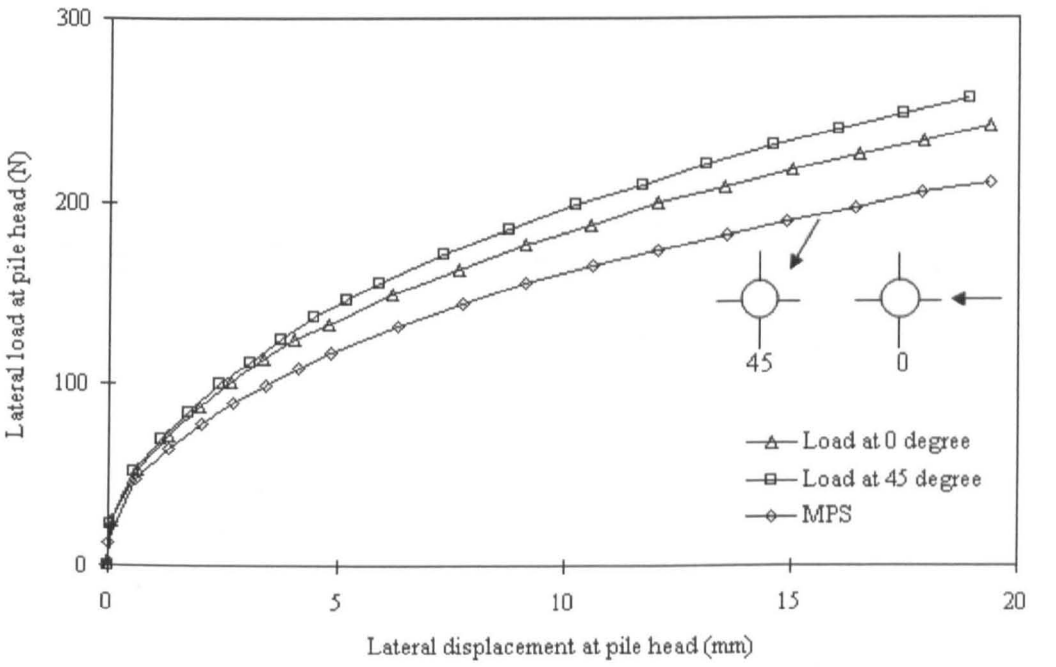

Fig. 5.2 P-Y curves for a finned pile, FPS210, subjected to different load directions

5.2.2. Change in load direction

In the cross section of a finned pile, the critical load directions were 45° and 0° as shown in Fig. 5.2. A finned pile, FPS 210, was used in these tests. The load-displacement curves, Fig. 5.2, show that the resistance at 45° to the fins is greater than that for a load applied in line with the fins for the same displacement. The curves show not much difference when the displacement is below 4.5 mm, that is 10 % of the pile diameter which suggests that in service, the fin direction may not be critical. The pile flexural rigidity, EI, was the same for both loading directions (Fig.5.3). Lateral resistance for the finned pile subjected to a load at 45° was assumed to be the block shown in Fig. 5.4(b). The pile subjected to a load in the line with the fins had the maximum effective surface perpendicular to the load direction (Fig .5.4(a)) but the shear resistance on the end of the pile was negligible. For the finned pile FPS210, the normal effective area at 45° to the fins was 70% of that at 0° to the fins, but the shear effective area was significant assuming the sand enclosed by the fins moved with the fins (Fig. 5.4). Details of distribution of soil resistance will be interpreted in Section 7.2.2.

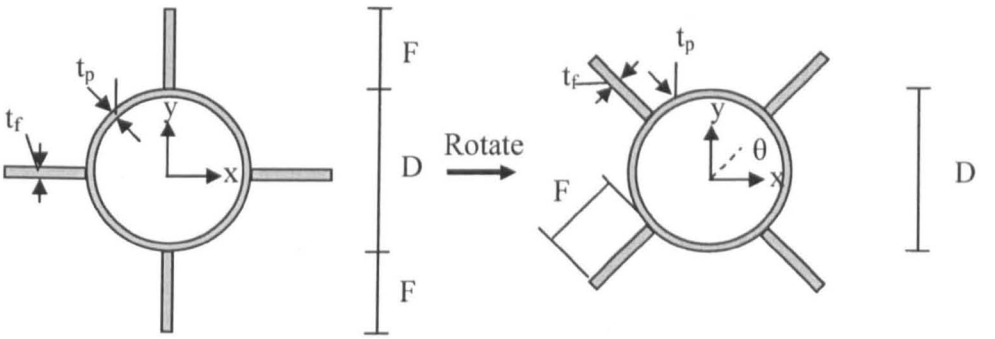

$$I_x = \frac{\pi}{8}(D^3 t_p) + 2\left(\frac{1}{12} t_f{}^3 F\right) + 2\left(\frac{1}{12} t_f F^3\right) + 2\left(t_f F\right)\left(\frac{F+D}{2}\right)^2$$

$$I_y = \frac{\pi}{8}(D^3 t_p) + 2\left(\frac{1}{12} t_f{}^3 F\right) + 2\left(\frac{1}{12} t_f F^3\right) + 2\left(t_f F\right)\left(\frac{F+D}{2}\right)^2$$

$$I_{x1} = \frac{I_x + I_y}{2} + \frac{I_x - I_y}{2}\cos 2\theta - I_{xy}\sin 2\theta$$

For finned pile: $I_x = I_y$, and $I_{xy} = 0$
$I_{x1} = I_x$ for all angles of rotation

Fig. 5.3 Moment of inertia of a finned pile

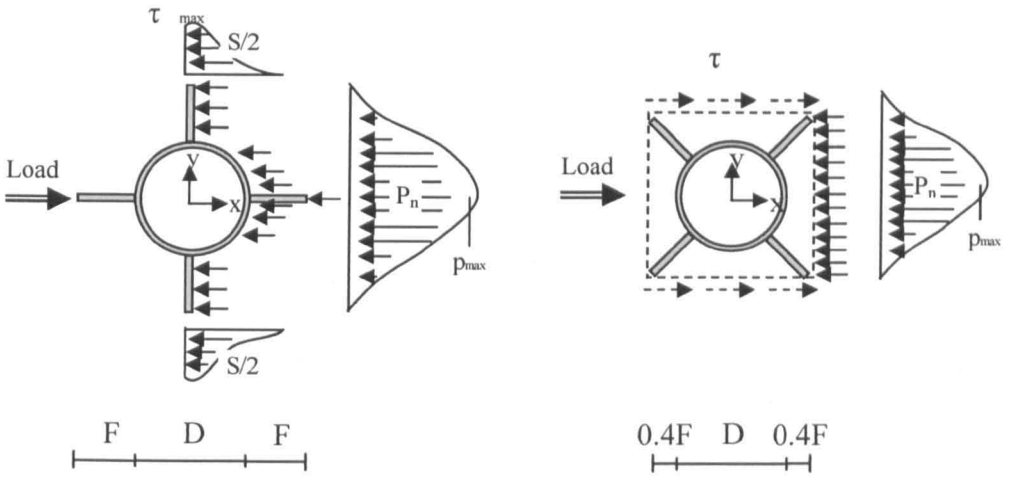

Fig. 5.4 Effective area to sustain the soil horizontal stress

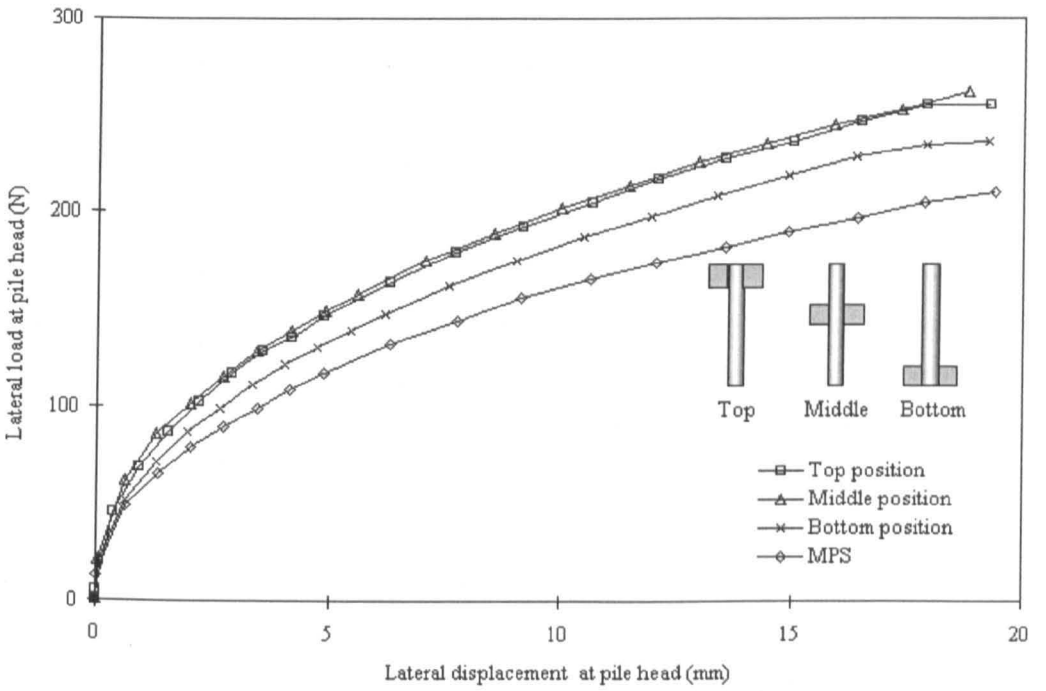

Fig. 5.5 P-Y curves for a finned pile, FPS210, with different fin positions

5.2.3. Change in fin position

For pile tests with different fin positions, that is fins at the top, the middle and the bottom of the piles (Fig. 5.5), the resistances with the fins at the top and at the middle positions were nearly the same whereas the resistance with the fins at the bottom was reduced by 10 % from that with the fins at the top and middle of the pile. The improved resistance could be the result of an increase in pile rigidity at the top

and at the middle of the pile or it could be that the effect of the fins was reduced with depth because of the reduction in displacement.

Based on these results, the fins should be placed near the top of the pile. In addition, the installation forces will be reduced when the fins are placed near the top of the pile compared to fins at the middle position.

5.2.4. Static load test with strain gauges

In order to investigate the finned pile behaviour strain gauges were used during the static loading test of a finned pile, FPS210. Ten strain gauges were placed on the inner surface of a finned pile, FPS210. The gauge positions as shown in Fig. 5.6 are different from those for MPS, Fig. 4.23, in order to determine the effect of the fin dimensions. Gauge readings were taken at every 2mm of the pile head lateral displacement. The bending moment at each point can be derived from the gauge reading using Equation 4.2. The bending moment profile along the pile was generated using graphic functions in Excel software. Curves of shear force, soil resistance and lateral displacement are generated from Equation 2.19 based on bending moment curves.

Results in Fig. 5.7(a) indicate that the bending moment along the finned pile has a similar shape to that of the monopile. There is no significant increase in the moment over the section with fins on it, but there is a change in shape at the point where the fins start. Below the serviceability limit state, the maximum bending moments for MPS and FPS210 are similar. The maximum bending moment of FPS210 (14.7 N-m) is 15 % less than that of MPS (17 N-m) (Fig. 4.24(a)) when the lateral displacement exceeds the serviceability limit state.

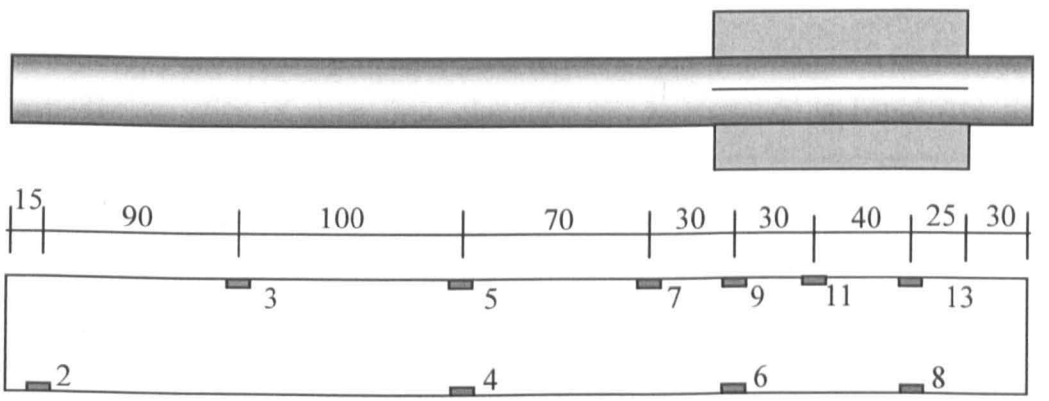

Fig. 5.6 Distribution of strain gauges on a finned pile FPS210

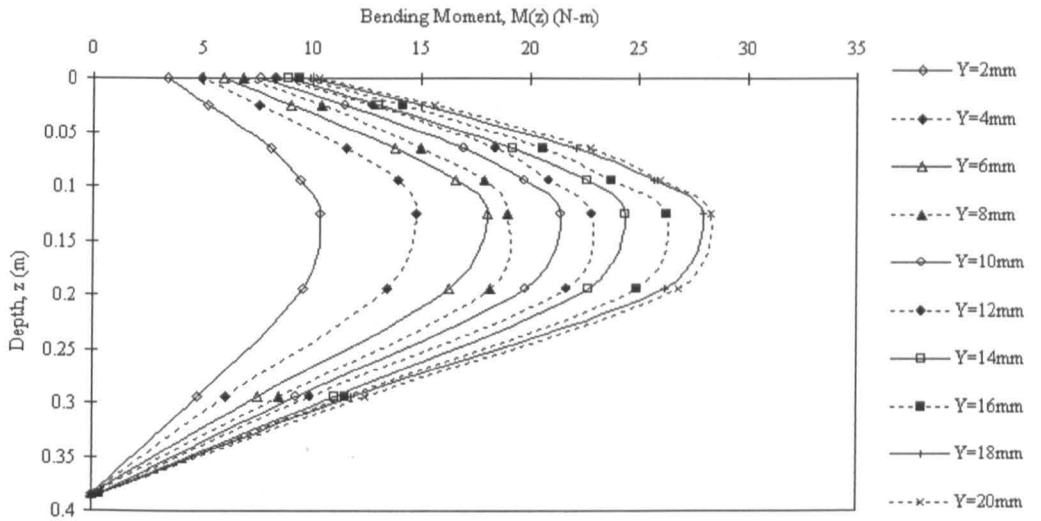

Fig. 5.7(a) Calculated bending moment along the pile, FPS210 from strain gauge test

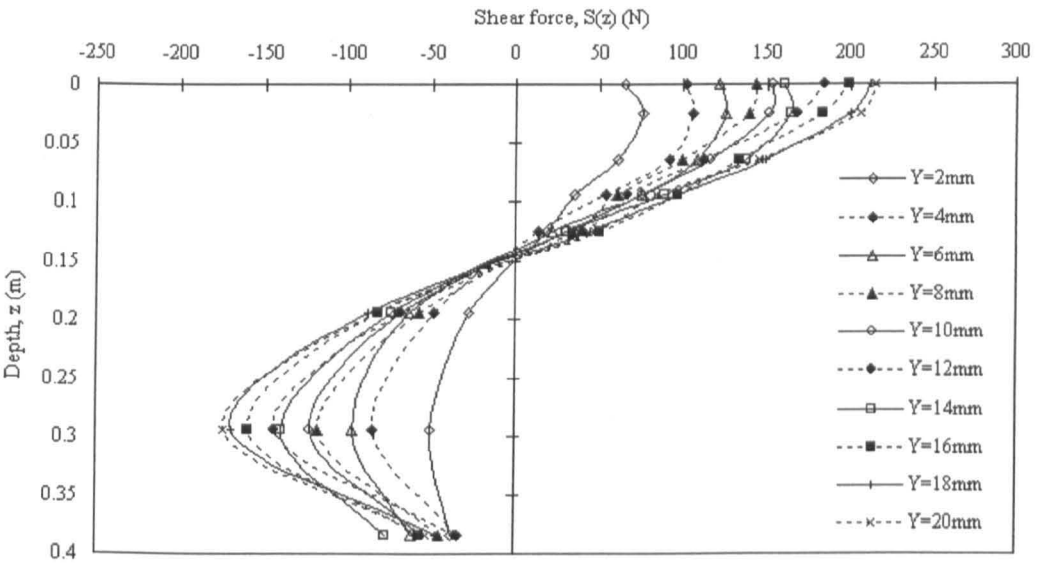

Fig. 5.7(b) Calculated shear force along the pile, FPS210, from strain gauge test

The variation of shear force along the pile is presented in Fig. 5.7(b). The transition point is defined as the point where the shear force is zero; the position of this point for MPS is just below 0.15 m below the top of the pile, and that is slightly higher than 0.15 m for FPS210. The transition point of shear force moves up 0.05 m by using a finned pile which means the higher shear resistance is in the fin section rather than in the ordinary section without fins.

The distribution of soil resistance along the finned pile is shown in Fig .5.7(c). A discontinuity in the soil resistance profile at the start of the fin section resulted in

the use of two continuous equations to model finned pile behaviour. The highest soil resistance concentrates at the bottom of the fin section (= 0.1 m in depth) which means that fins increase the resistance of the pile. The pile deformation, as presented in Fig. 5.7(d), is not significant because of the high rigidity of pile compared to soil stiffness, but the pile rotated with the increase in loads.

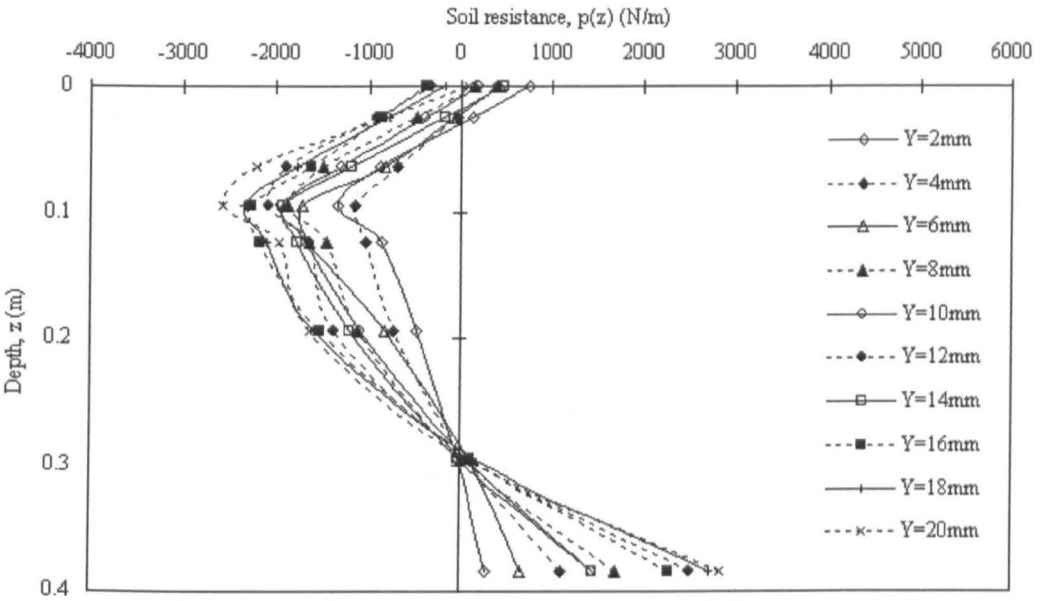

Fig. 5.7(c) Calculated soil resistance along the pile, FPS 210, from strain gauge test

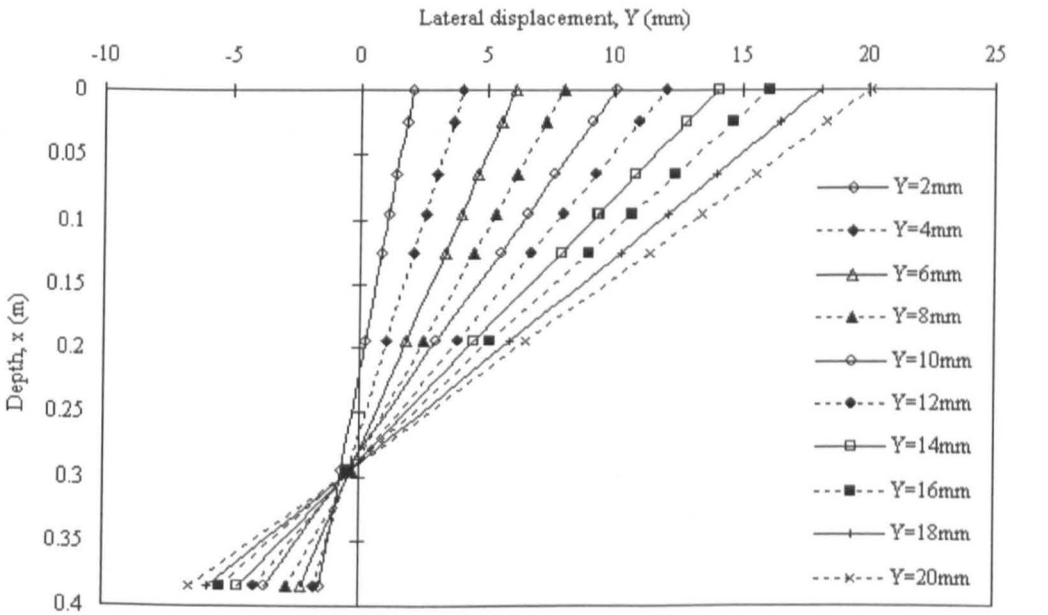

Fig. 5.7(d) Calculated displacement along the pile, FPS 210, from strain gauge test

5.2.5. Combined loading

In order to verify the failure envelope of finned piles, a monopile, MPS, and a finned pile, FPS210, were used. Both of them had pile tips to simulate closed-end pile conditions; hence, the vertical bearing capacity is a function of the pile surface friction and pile-end bearing capacities.

The ultimate lateral loads, when no vertical load was applied, were taken from static lateral loading tests in Section 5.2.1. The ultimate vertical loads for MPS and FPS210, when no lateral load was applied, were determined by vertical loading tests. The ultimate lateral load for different vertical loads was found by applying a vertical load and then increasing the lateral load until failure (see Fig. 5.8). Based on the P-Y curve, the ultimate load was defined as the starting point of the final linear region with the increase of slope less than 5% described in Fig. 6.9. Values of assigned vertical loads and the corresponding lateral loads including serviceability and ultimate states are shown in Table. 5.2.

The failure envelope for combined loading is shown in Fig. 5.9. The ultimate vertical loads (when P = 0) are about 4 times higher than the ultimate lateral loads (when Q = 0). Lateral serviceable loads, in general, are about 60% of ultimate lateral loads. Both ultimate and serviceable lateral capacities increase with the increase in vertical loads when the vertical loads are under 50% of the ultimate vertical capacity though, for design purposes the lateral loads could be considered constant with a vertical load of up to 75% of the ultimate vertical load. Importantly, the failure envelope of FPS210 is 30% larger than that of MPS in the lateral direction. In other words, the safe lateral load region is extended by 30% by placing fins on the pile.

Table 5.2 Combined loading for MPS and FPS 210

MPS			FPS210		
Q	P_S	P_U	Q	P_S	P_U
0	109	155	0	141	210
100	110	157	200	145	217
250	116	165	350	158	230
450	128	177	450	160	235
600	110	160	600	142	220
750*	0	0	800*	0	0

Note: * is the ultimate vertical load
all results are in unit of N
Q = vertical load; P_S = lateral serviceability load; P_U = lateral ultimate load

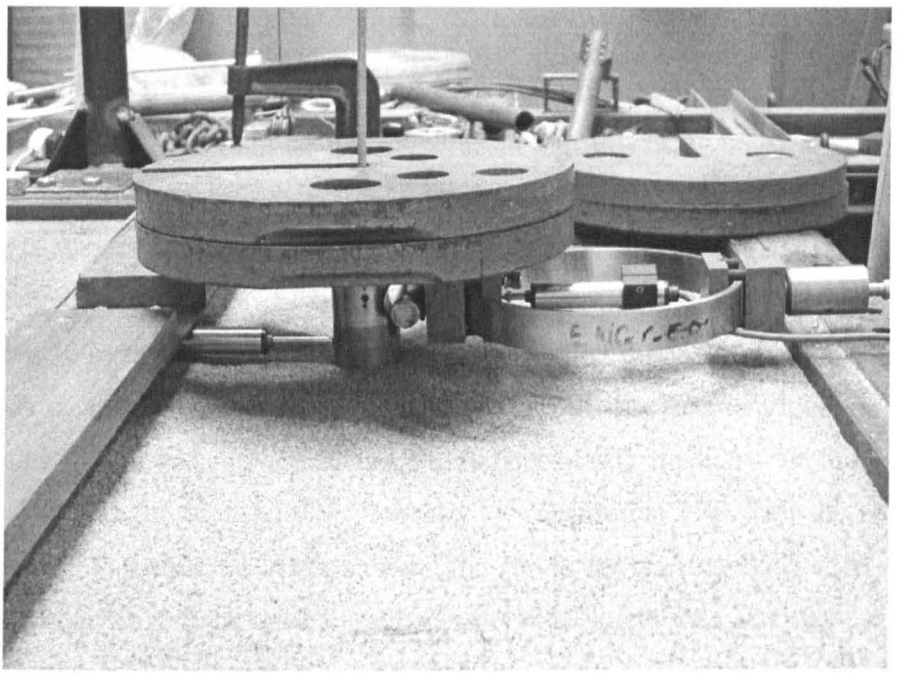

Fig. 5.8 Photograph of a pile subjected to a combined static loading

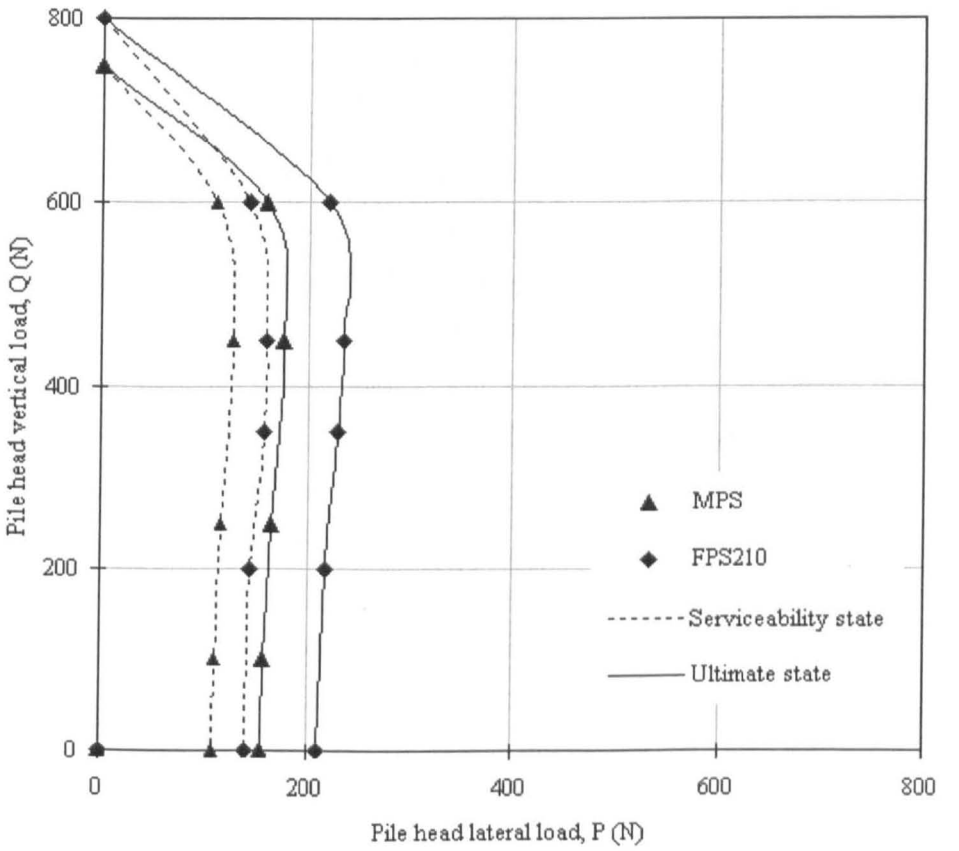

Fig. 5.9 The failure envelopes of piles subjected to combined loading

5.3. Analysis

5.3.1. Modified relationship of load and displacement

Two modified relationships are suggested in this section. One was derived from a simple hyperbolic function, and the other relationship involves more factors. In order to understand the influence of ultimate lateral load and pile diameter on load-displacement relationships, non-dimensional curves are suggested (see Fig. 5.10). Hyperbolic curves have been widely adopted to predict the lateral load-displacement relationships for soft to medium soils. The ratio of displacement/load (= Y/P) to displacement (Y) was applied in the simple hyperbolic method. In this study, a modified hyperbolic method was proposed by substituting Y/P with the new ratio P/P_u where P_u is the ultimate lateral load. The curves for the finned piles fall within a narrow band giving an approximate relation between lateral load and displacement at the pile head.

5.3.2. Relationship between ultimate load and fin dimension

In order to predict the effect of the fins including fin width and length, ultimate lateral loads of finned piles were compared to those of the monopile. Based on the results, the ratio of ultimate load $P_{u(FPS)}$ /$P_{u(MPS)}$ to 2F/D is shown in Fig. 5.11 where F is the fin width and D is the pile diameter. An increase in the ratio of fin width to pile diameter (2F/D) results in an increase in lateral resistance ($P_{u(FPS)}/P_{u[MPS]}$), which is proportional to the increase in the ratio of fin length to pile length (L_f/L_p). An increase in fin width increases the lateral resistance particularly when the ratio of 2F/D is less than 1. The increase in lateral resistance is not very significant when the ratio of 2F/D is over 1 especially for finned piles with short fin lengths. When 2F/D is less than 1, the resistance increases linearly with an increase in both fin length and fin width.

5.3.3. Relationship between ultimate load and pile weight

The weight of material is one of the important features in the evaluation of the efficiency of finned piles; the increase in weight effects the manufacture, transportation and installation of piles. Based on the ultimate loads shown in Table 5.1 and pile dimensions shown in Table 3.1, a relationship between ultimate lateral

loads and weight of pile foundations was developed (Fig. 5.12); in the figure, P_u is the ultimate lateral load and W is the weight of the test pile.

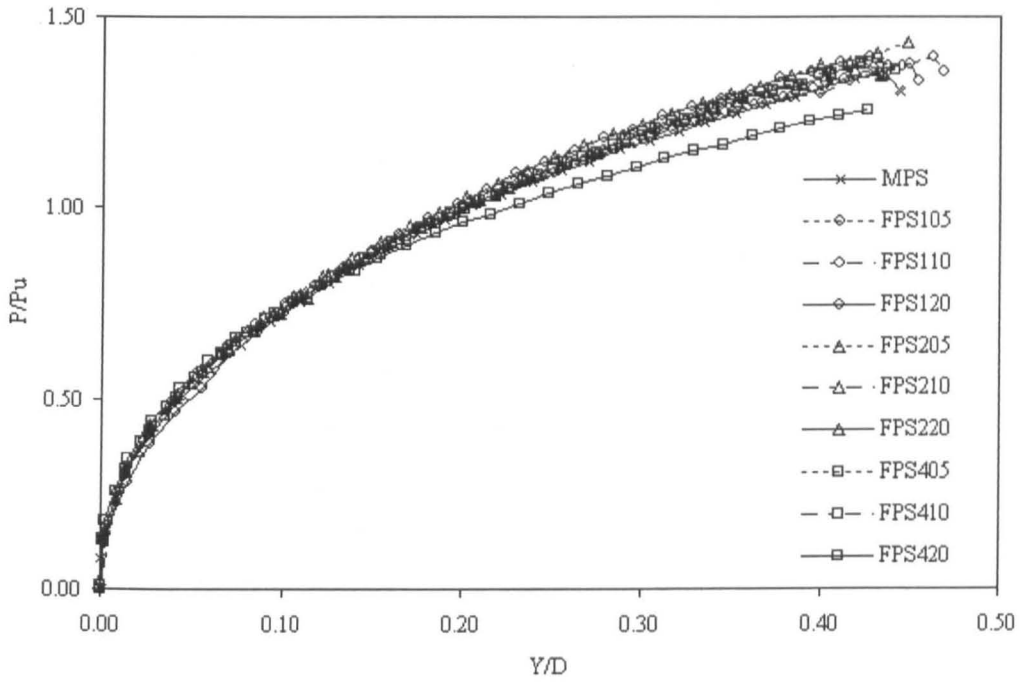

Fig. 5.10 A modified relationship of load and displacement

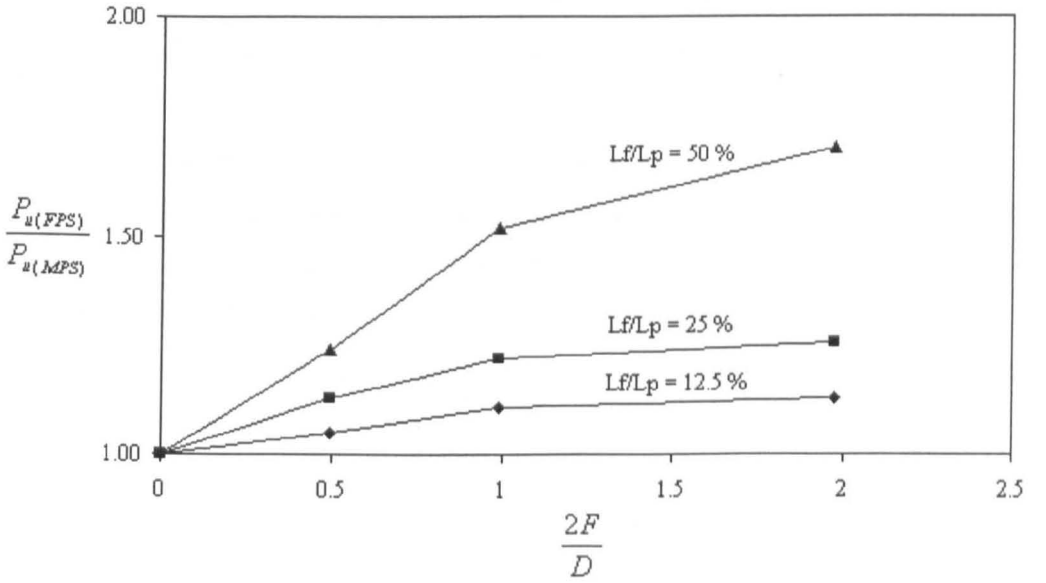

Fig. 5.11 The effect of fin dimension on the ultimate capacity of the pile obtained from model tests

All points are covered by an upper bound and a lower bound. The upper bound represents the highest efficiency of using finned piles, whereas the lower bound represents the lowest efficiency. The points (Fig. 5.12) close to the lower bound represent the pile with the largest fin width of 44 mm, and the points close to the upper bound represent the pile with a fin width equals to 50% of the pile diameter. The solid line in the middle is taken from the linear regression. Equation 5.1 represents the relationship between ultimate lateral load and selfweight.

$$\frac{P_{u(FPS)}}{P_{u(MPS)}} = 0.8044 \times \frac{W_{(FPS)}}{W_{(MPS)}} + 0.211 \qquad (5.1)$$

where $P_{u(FPS)}$ = ultimate lateral load of finned piles

$P_{u(MPS)}$ = ultimate lateral load of monopile

$W_{(FPS)}$ = weight of finned piles

$W_{(MPS)}$ = weight of monopile

According to Equation 5.1, the weight of fins can be determined when the increase in lateral resistance has been decided. If the value of fin width equals to 50% of the pile diameter, the design resistance can be raised from the regression up to the upper bound. However, Equation 5.1 may not apply to all piles since there are other factors to be considered, the ratio $\frac{P_{u(FPS)}}{P_{u(MPS)}}$ can be represented as a function of the increase in pile weight, the flexible stiffness of pile and the soil resistance. For certain pile conditions modifications to Equation 5.1 would be necessary.

5.3.4. Pile-soil behaviour along a finned pile

The pile-soil behaviour along the pile was estimated from the development of the strains. In order to match the distribution of the bending moment along the finned pile with depth, a six-order continuous equation was established according to regression analysis. This equation failed to represent the change of the pile section when it was transformed into the curves of shear force with depth (S-z) and the curves of soil resistance with depth (p-z) because there is a discontinuity between the intersection of fin and pile. The six-order polynomial equation is a continuous equation with a variable of depth, and the equation could not reflect the change in either pile stiffness or cross section.

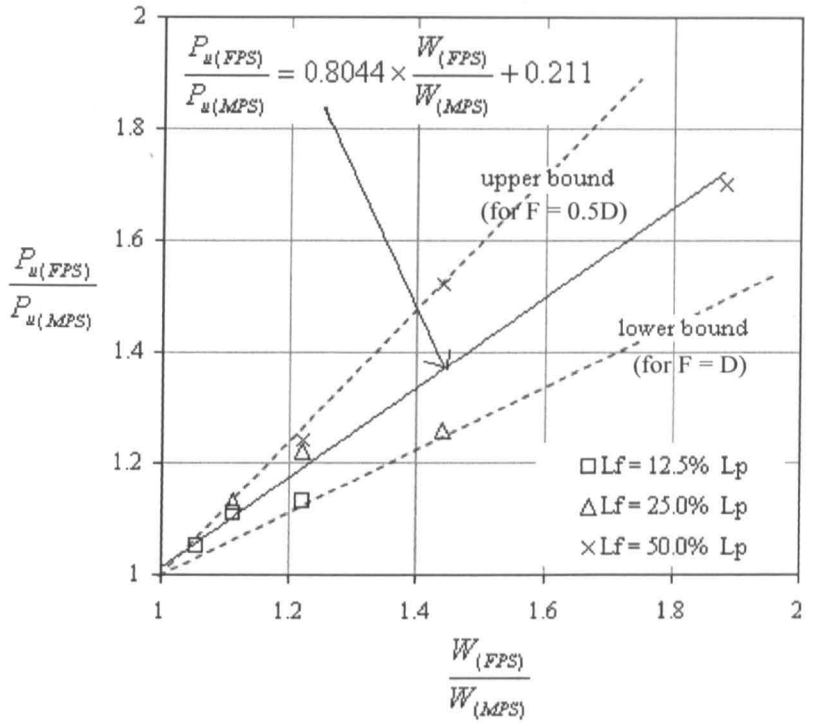

Fig. 5.12 Relationship between lateral resistance and weight of piles

Two continuous equations were used to represent the bending moment along the pile; the section with fin and the section without fin were expressed by a three-order continuous equation and a four-order continuous equation, respectively. Results are shown in Section 5.2.4; the distribution of soil resistance calculated from the test has a similar shape as that proposed by Prasad & Chari (1999) shown in Fig. 2.16.

In order to understand the fin contribution in pile-soil behaviour, a comparison is given on MPS and FPS210 at the serviceability limit state. Fig. 5.13(a) shows that the rotation point of FPS210 is 80 mm higher than that of MPS. Bending moments along the pile, Fig. 5.13(b), show that the maximum bending moment is reduced by 15% as a result of the fin section of FPS210. Similarly, Fig. 5.13(c) shows the shear force is reduced by using fins. The variation of soil resistance with depths, Fig. 5.13(d), shows that the fins increase the resistance in the fin section. The soil resistance of the finned pile FPS210 at the ground surface is not zero because the soil resistance curve is derived from Equation 2.19(d) through regression analyses.

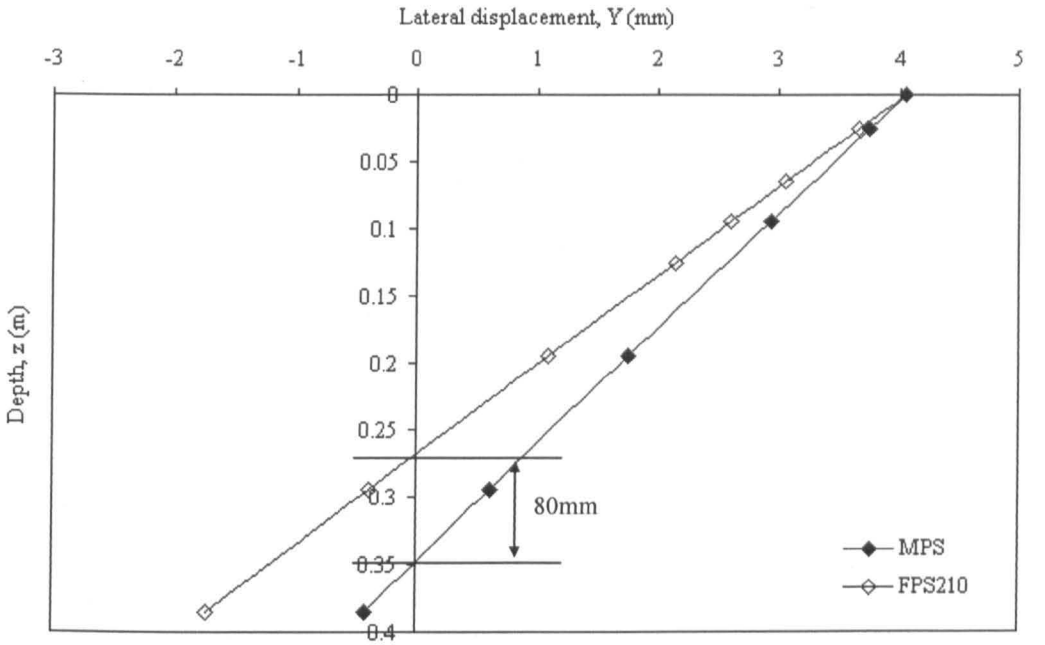

Fig. 5.13(a) Lateral deflection of piles when pile head lateral displacement at serviceability limit state

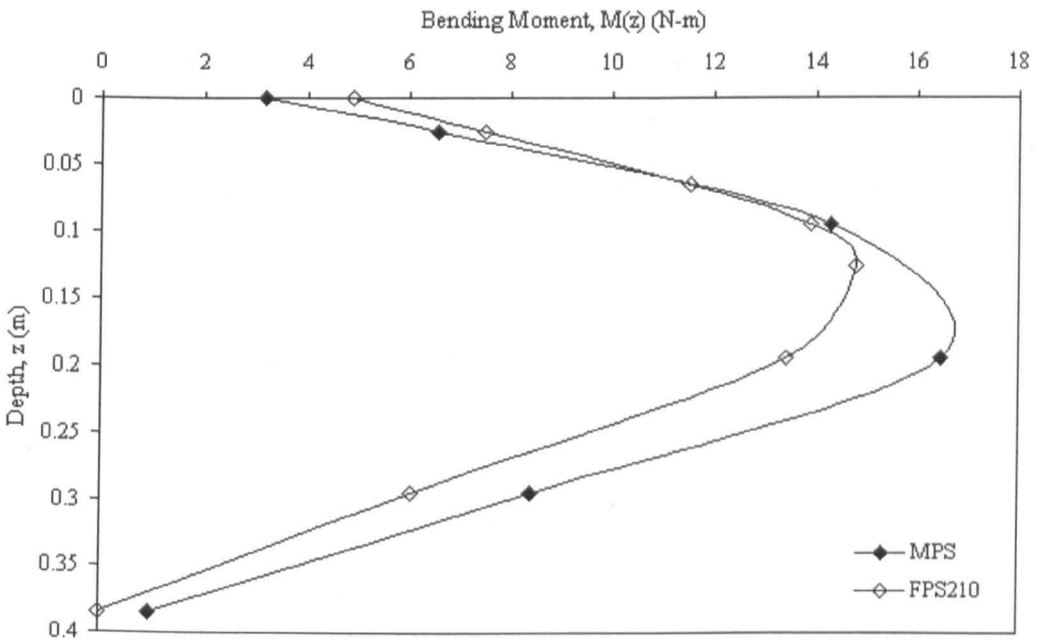

Fig. 5.13(b) Bending moment of piles when pile head lateral displacement at serviceability limit state

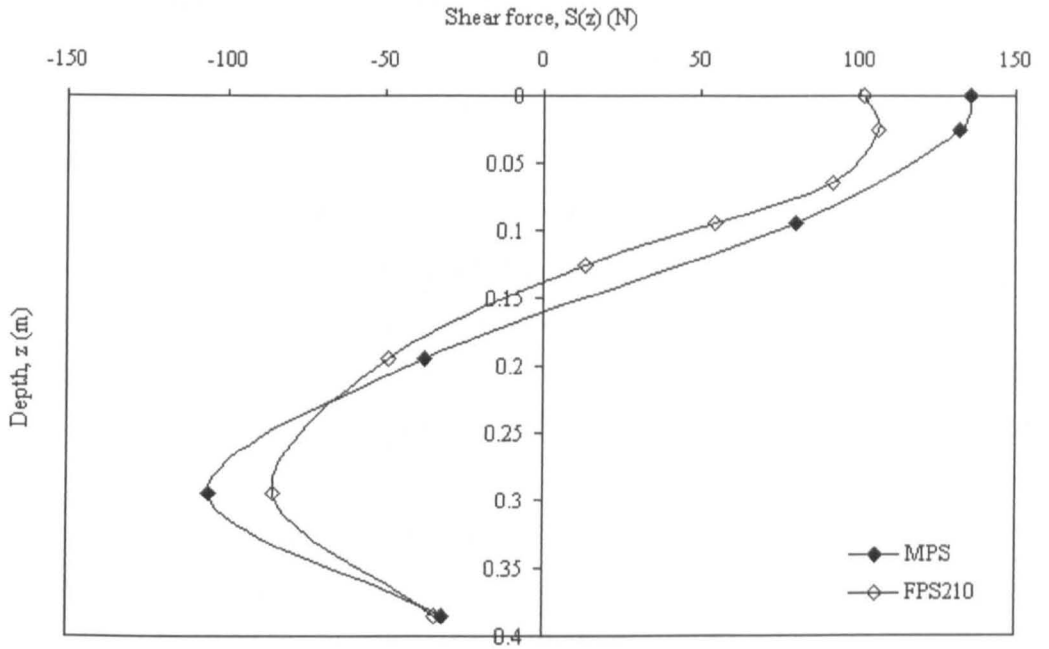

Fig. 5.13(c) Shear force of piles when pile head lateral displacement at serviceability limit state

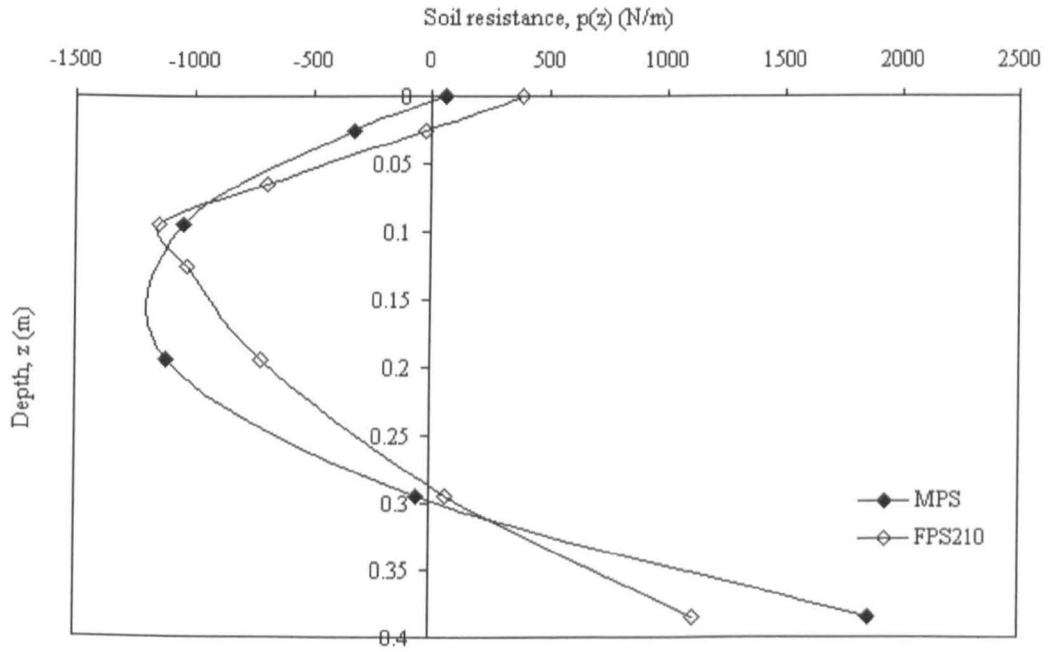

Fig. 5.13(d) Soil resistance of piles when pile head lateral displacement at serviceability limit state

5.3.5. Bearing capacity of combined loading

Based on the results in Section 5.2.5, the combined loading is presented as modified values in Fig. 5.14. All vertical loads in Fig. 5.7 were divided by the ultimate vertical load of MPS (when lateral load P = 0), and all lateral loads in the figure were also divided by the ultimate horizontal load of MPS (when vertical load Q = 0). Fig. 5.14 shows the normalised capacity of the pile subjected to combined loading. Although the envelope of serviceability state is almost half of the ultimate state, both limit states have very similar shapes. By using the finned pile FPS210, the increase in vertical capacity was not significant because the bearing capacity was mainly applied from pile tip instead of from shaft friction along the pile. The lateral capacity, however, increased from 30 to 50% depending on the vertical load by using a finned pile (FPS210).

The improvement in combined loading as a result of fin contribution was simply verified on these envelopes. According to the combined loading envelope shown in Fig. 5.14, the normalised lateral load reduces significantly when the normalised vertical load is larger than 0.75. In the region of normalised lateral load between 0.75 and 1.0, the fin efficiency does not improve lateral resistance significantly. In order to obtain maximal improvement in lateral resistance by the use of fins, the vertical loading should be under 75% of ultimate vertical bearing capacity. If a global factor of safety of 3 is used to determine the vertical bearing capacity, the lateral capacity can be increased by 90% with the use of fins.

5.4. Summary

A series of 1G model tests of finned piles have been carried out using the equipment introduced in Chapter 4. Pile head P-Y curves of finned piles with different fin dimensions were generated and their ULS were determined (Section 5.2.1). A normalised relationship between fin dimension and ULS was used to represent the efficiency of fins (Section 5.3.2). Further, the influence of pile weight to the ULS was assessed (Section 5.3.3). Behaviour of finned piles under static loading was presented through the strain gauge tests (Section 5.2.4); the comparison of behaviour of a finned pile to that of a monopile was provided in Section 5.3.4.

The features such fin position, load direction and combined loading were tested. The ideal fin position and load direction to resist lateral load were suggested

(Section 5.2.2 and 5.2.3). The influence of combined loading to lateral resistance of the finned pile was presented using a normalised diagram (Fig. 5.14).

Model tests provide useful data such ULS and SLS for the study of cyclic loading in Chapter 6. Results of model tests will be used to compare with these from numerical analyses in Chapter 7. The improvement of testing methods and the possible tests for the future study will be discussed (Chapter 7).

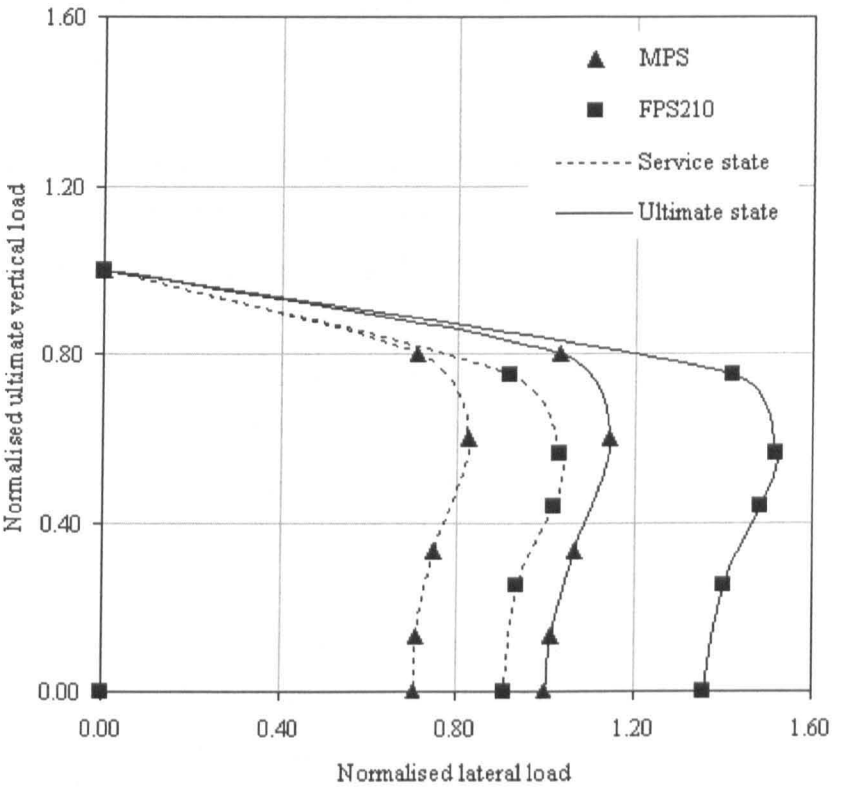

Fig. 5.14 Normalised envelopes of combined loading

6 Cyclic loading tests

6.1. Introduction

Following the presentation of static loading tests for finned piles in Chapter 5, this chapter aims to demonstrate the influence of cyclic loading on finned piles. Repeated unload-reload tests were carried out on piles, MPC and FPC210, to determine the effect of the fins on the capacity of the piles. Five unload-reload cycles at various load levels were used to generate P-Y curves to demonstrate the efficiency of the fins.

The cyclic loading device introduced in Section 4.7 was used to carry out the tests, and there were 10,000 cycles in each test. The results of static loading tests and typical environmental conditions for offshore wind foundations were used to set the test parameters:

- Fin length: finned piles with different fin lengths: quarter of, half of and the entire pile length were compared with a monopile.
- Load level (magnitude): Loads ranging from 15 to 75 N were chosen to represent 10% to 50% of the ultimate load of 155 N acting on a monopile foundation.
- Frequency: low frequencies of 0.45, 0.65 and 0.94 Hz were applied to study the influence of speed. Liquefaction at high frequencies was not included in this research.
- Direction of loading: test piles were subjected to either one-way or two way cyclic loading as shown in Fig. 6.1(a). One-way loading was used to model the foundation subjected to a repeated load in a single direction which may be caused by sustained current or wind load. Two-way loading was used to model a pile under a load acting repeatedly in opposite directions which may be caused by wave loads.
- Pile tip condition: a cap at the bottom of a test pile was used to represent a close-end pile; a pile without a cap at the bottom is defined as an open-end pile.

A series of tests was carried out on different piles subjected to different conditions as shown in Table 6.1. The open-end monopile was used mainly to

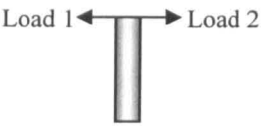

One-way cyclic loading:
Load 1 = A, Load 2 = 0
Two-way balanced loading:
Load 1 = A, Load 2 = A
Two-way out of balanced loading:
Load 1 = A, Load 2 = B
where A and B $\geq$ 0; and A$\neq$ B

(a)

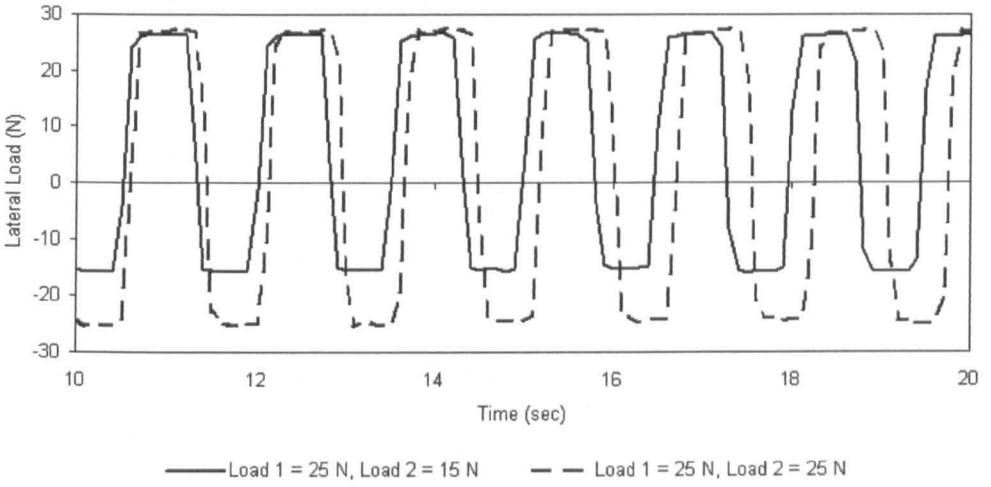

(b)

Fig. 6.1 (a) Schematic of load directions;(b) variation of load with time for a monopile subjected to two-way cyclic loading (note: 1. readings were taken between 10 and 20 sec; 2. loads are positive from the right and negative from the left)

identify the influence of load level and frequency which has been presented in Section 4.7.3. The efficiency of fin length was then measured under both one-way and two-way cyclic loading conditions for open-end piles. Other factors such as unbalanced loads and pile tip conditions were studied along with changes in fin length. Typical loading sequences are shown in Fig. 6.1(b).

In order to study the behaviour of a finned pile under cyclic loading, the strain gauge method was used. Two model piles, MPC and FPC210, were subjected to one-way cyclic load of 25 N. The strain gauge readings were recorded at specified cycles: 1, 10, 100, 1000 and 10,000. Comparison of bending moments at different load cycles is provided to verify the influence of the number of cycles.

After the assessment of cyclic lateral loaded finned piles, the study progressed to finned piles subjected to combined cyclic loading including vertical and horizontal loads. Again, model piles, MPS and FPS210, were used in these tests. Based on the results of combined static loading in Section 5.2.5 and cyclic lateral loading in Section 6.2.2, the parameters were:

- Pile types: MPC and FPC210
- Vertical load level (magnitude): Three vertical loads of 80, 160 and 240 N were chosen to represent 10%, 21% and 32% of the ultimate bearing capacity of 750 N acting on a monopile foundation.
- Lateral load level (magnitude): Three lateral loads of 15, 25 and 35 N were chosen to represent 10%, 16% and 22% of the ultimate lateral load of 155 N acting on a monopile foundation.
- Frequency: low frequencies of 0.45, 0.65 and 0.94 Hz were applied to study the influence of speed.

A series of tests were carried out on different piles subjected to different conditions as shown in Table 6.2. In the initial observation of fin efficiency, tests were carried out by one-way lateral cyclic loading only, because it caused significant lateral displacement of the pile head according to the results in Section 6.2.3. Pile behaviour under two-way cyclic loading tests is more complicated and should be assessed in a future study.

The tests were analysed to examine the influence of fin efficiency on cyclic loading, the pile behaviour under cyclic loading and lateral resistance of the finned pile subjected to combined cyclic loading.

Table 6.1. Summary of cyclic loading tests

Pile type	Pile tip	Load way	Load 1 (N)	Load 2 (N)	Freq. (Hz)	Pile type	Pile tip	Load way	Load 1 (N)	Load 2 (N)	Freq. (Hz)
MPC	Open	One	50	0	0.65	FPC210	Close	Two	25	15	0.65
MPC	Open	One	50	0	0.95	FPC210	Close	Two	25	25	0.65
MPC	Open	One	50	0	0.45	FPC220	Open	One	25	0	0.65
MPC	Open	One	25	0	0.65	FPC220	Open	One	25	0	0.45
MPC	Open	One	75	0	0.65	FPC220	Open	One	50	0	0.65
MPC	Open	One	15	0	0.65	FPC220	Open	Two	25	25	0.65
MPC	Open	One	25	0	0.45	FPC220	Open	Two	25	15	0.65
MPC	Open	Two	25	15	0.65	FPC220	Close	One	25	0	0.65
MPC	Open	Two	25	25	0.65	FPS220	Close	Two	25	15	0.65
MPC	Close	One	25	0	0.65	FPC220	Close	Two	25	25	0.65
MPC	Close	Two	25	15	0.65	FPC240	Open	One	25	0	0.65
MPC	Close	Two	25	25	0.65	FPC240	Open	One	25	0	0.45
FPC210	Open	One	25	0	0.65	FPC240	Open	One	50	0	0.65
FPC210	Open	One	25	0	0.45	FPC240	Open	Two	25	25	0.65
FPC210	Open	One	50	0	0.65	FPC240	Open	Two	25	15	0.65
FPC210	Open	Two	25	25	0.65	FPC240	Close	One	25	0	0.65
FPC210	Open	Two	25	15	0.65	FPC240	Close	Two	25	15	0.65
FPC210	Close	One	25	0	0.65	FPC240	Close	Two	25	25	0.65

Table 6.2. Summary of combined cyclic loading tests

Pile type	Pile tip	Load way	Vertical load (N)	Lateral load (N)	Freq. (Hz)	Pile type	Pile tip	Load way	Vertical load (N)	Lateral load (N)	Freq. (Hz)
MPC	Close	One	0	25	0.65	FPC210	Close	One	0	25	0.65
MPC	Close	One	80	25	0.65	FPC210	Close	One	80	25	0.65
MPC	Close	One	160	25	0.65	FPC210	Close	One	160	25	0.65
MPC	Close	One	240	25	0.65	FPC210	Close	One	240	25	0.65
MPC	Close	One	240	15	0.65	FPC210	Close	One	240	15	0.65
MPC	Close	One	240	35	0.65	FPC210	Close	One	240	35	0.65
MPC	Close	One	240	25	0.94	FPC210	Close	One	240	25	0.94
MPC	Close	One	240	25	0.45	FPC210	Close	One	240	25	0.45

6.2. Results

6.2.1. Repeated unload and reload test

An initial investigation on the improvement of lateral resistance of a finned pile (FPC210) under repeated loading was compared with that of a monopile (MPC). Various load levels were applied from 30 N to 150 N using the ultimate lateral load of 155 N for the monopile as the benchmark (Section 5.2.1). Five reload-unload loops have been completed at five different load levels (30, 60, 90, 120 and 150 N). In the repeated loading test, the lateral load was applied by the static loading device. The load was added gradually from zero until it reached the first assigned load level of 30 N. Unloading was then carried out when the load was reduced to zero. Again the load was gradually increased to the next load level of 60 N. These procedures were carried out until the 5 loops were completed.

The results in Fig. 6.2 show that the finned pile curve is always above the monopile curve at every load stage; the displacement of FPC210 is smaller than that of MPC. These indicate that fins increase the lateral load resistance of a monopile within various load levels and cycles. In addition, the slope of the P-Y curve of FPC210 is steeper than that of MPC in the same load cycle of the same load level.

Repeating loading tests was used to investigate the initial effect of cycles on the displacement at different levels of load. The influences of number of cycles and load magnitudes on the lateral resistance were investigated in the same test. In the following cyclic loading tests, each test was based on a constant load magnitude with repeated loading up to 10000 cycles. Comparison is made between tests in which the pile was subjected to different load magnitudes. In summary, repeating load tests provided a practical and efficient method for the preliminary analysis of cyclic loaded piles.

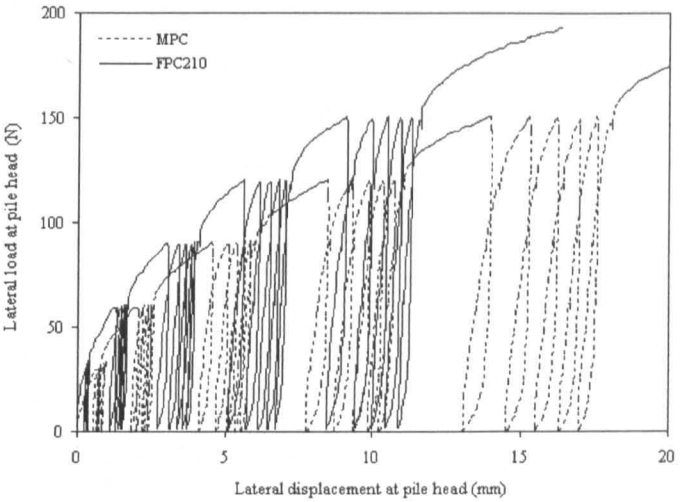

Fig. 6.2 P-Y curves obtained from repeated unload-reload test

6.2.2. One-way cyclic loading

A lateral load level of 25 N was mainly used to represent a cyclic load of 15% of the ultimate static load of 155 N corresponding to a pile head lateral displacement of 10% of the monopile diameter after 10,000 cycles. One monopile and three finned piles with various fin lengths were tested. Fig. 6.3 shows the variation of lateral displacement with the number of cycles. Displacements within the first ten cycles are not shown in the main figures for two reasons. The rate of loading was varying as the motor built up to speed; the initial response is akin to "bedding error." The "bedding error" in this case could be considered to be the difference between cast in situ piles such as those used in these tests and driven piles as used in practice. In order to investigate the long term influence of constant cyclic loading, the main figures only show displacements after ten cycles. Displacements within the first ten cycles are shown in the inset. The lateral movements of the heads of open-end piles with the number of cycles are shown in Fig. 6.3(a). In all cases, the lateral displacement reduces with increasing fin length even under cyclic loading.

The results in Fig. 6.3(b) show that the displacement of the pile reduces as the frequency decreases: the displacement at the lower frequency of 0.45 Hz is only half of that at the higher frequency of 0.65 Hz.

The variation of lateral displacement with the number of cycles for closed-end piles is presented in Fig. 6.3(c) showing that the lateral displacements of closed-end finned piles are slightly less than those of open-end piles. An increase in load causes

an increase in lateral displacement, as seen in Fig. 6.3(d). The lateral displacement at the higher load of 50 N is almost double that at the lower load of 25 N. In one-way cyclic loading, the trend of displacement increasing with the number of cycles is reduced by an increase in fin length (Fig. 6.3).

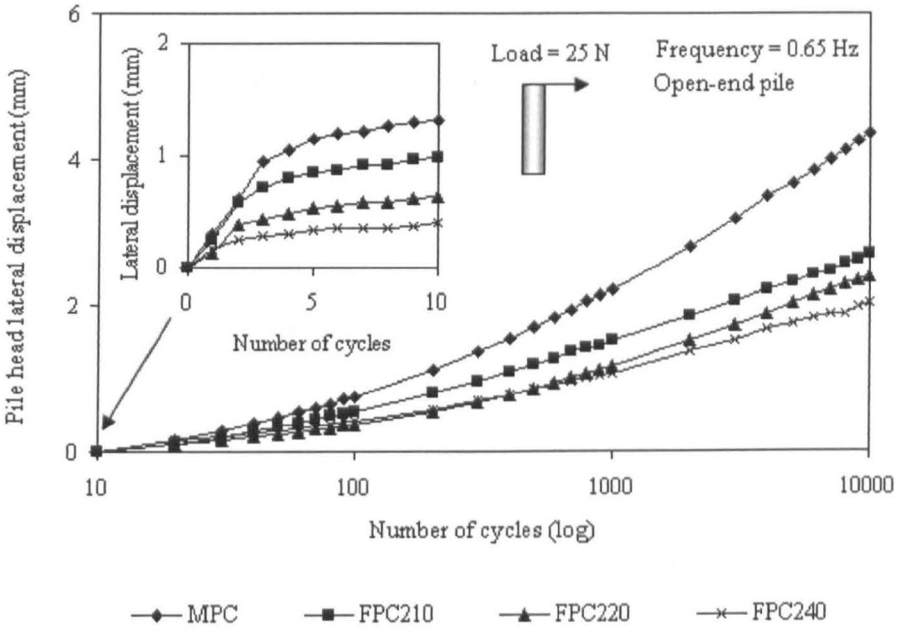

(a)

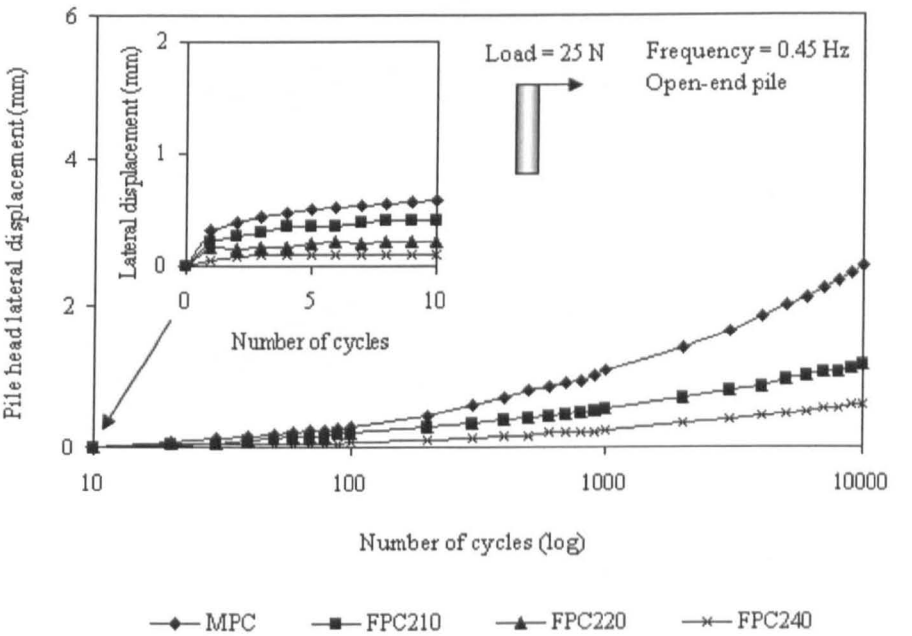

(b)

Fig. 6.3 Variation of pile head lateral displacement with the number of cycles for finned piles at (a) 0.65 Hz, and (b) 0.45 Hz.

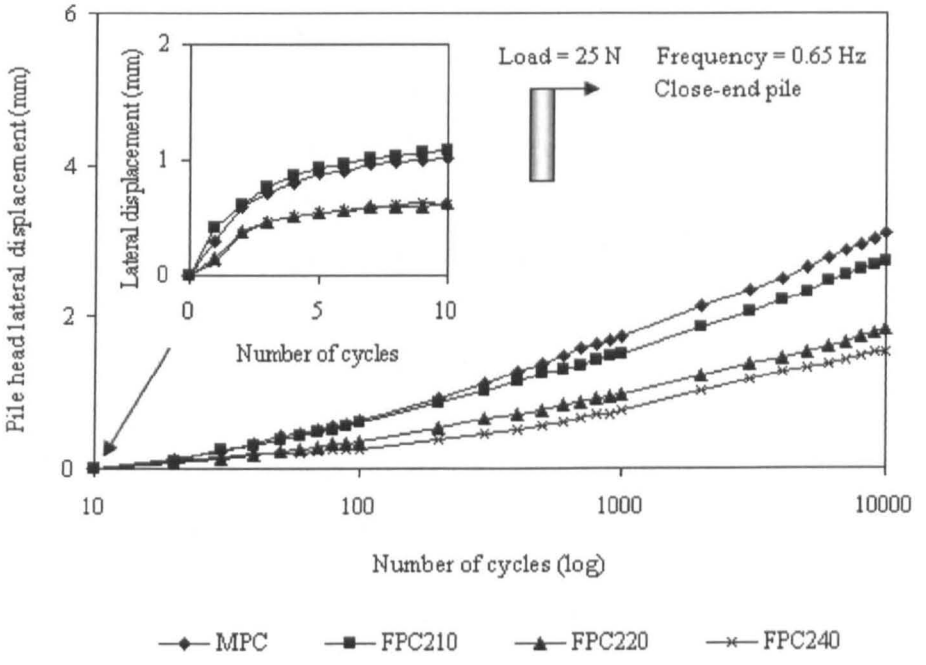

(c)

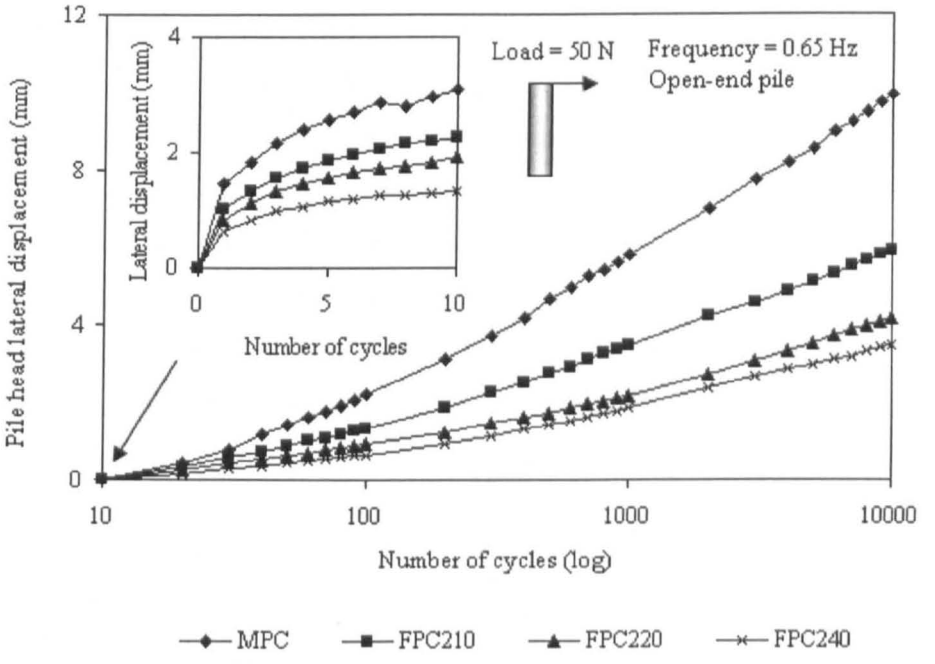

(d)

Fig. 6.3 Variation of pile head lateral displacement with the number of cycles for finned piles; (c) close-end finned piles, and (d) at higher load level

6.2.3. Two-way cyclic loading

The curves of vertical versus lateral displacement of the pile head under two-way loading for different numbers of cycles are presented in Fig. 6.4. Fig. 6.4(a) shows open-end piles under balanced loading. The vertical displacement is much higher than the lateral displacement for all test piles. Fig. 6.4(b) shows open-end piles under out of balanced loading. Again, the vertical displacement is higher than the lateral displacement but the vertical displacement in Fig. 6.4(b) is 20% less than that in Fig. 6.4(a). Both vertical and lateral displacements are reduced by placing fins on the pile.

Fig.6.4(c) shows displacements of closed-end piles under balanced loading. The vertical displacement is reduced as a consequence of the pile tip. Vertical and lateral displacements are reduced as the fin length increases. Fig. 6.4(d) shows displacements of closed-end piles under out of balanced loading. Again, the vertical displacement is less than that for open-end piles. The lateral displacement is uniformly reduced by increasing the fin length; the vertical displacement, however, is little affected by the use of fins.

6.2.4. Cyclic loading test with strain gauges

In order to investigate finned pile behaviour under cyclic loading, the strain gauge method was used. A comparison of monopile and finned pile behaviour under cyclic loading is presented in Fig. 6.5 (a) - (h). The applied load was 25N with a frequency of 0.65Hz. The deflection of piles, MPC and FPC210 in Fig. 6.5 (a) and (b) shows the reduction of lateral displacement by the use of fins; both piles remained relatively straight during cyclic loading; that is the piles performed as rigid piles.

Bending moments along the piles, Fig. 6.5 (c) and (d), show that the moments gradually increase with the increase in the number of cycles. The moments along the pile were reduced significantly by the use of fins.

Fig. 6.5 (e) and (f) present the variation in shear force along the piles. Shear forces, in general, increase with an increase in the number of cycles. The increase in shear forces in the fin section is evident from the higher lateral resistance provided by the fins.

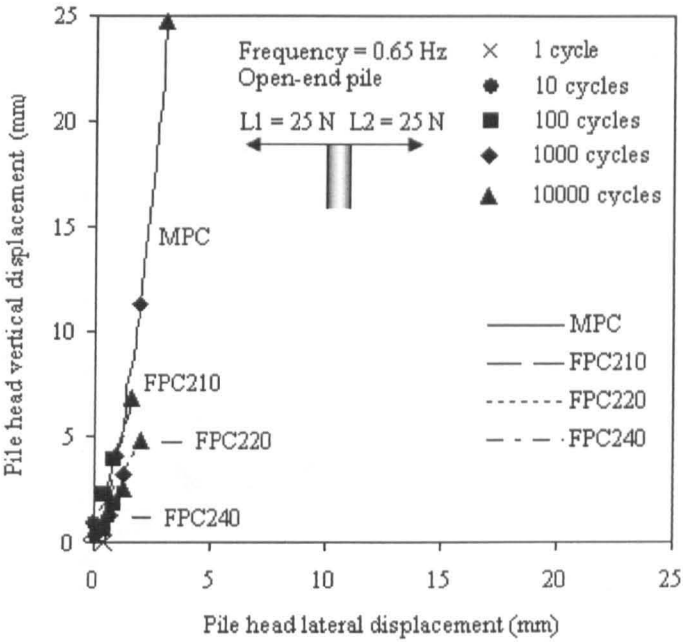

(a)

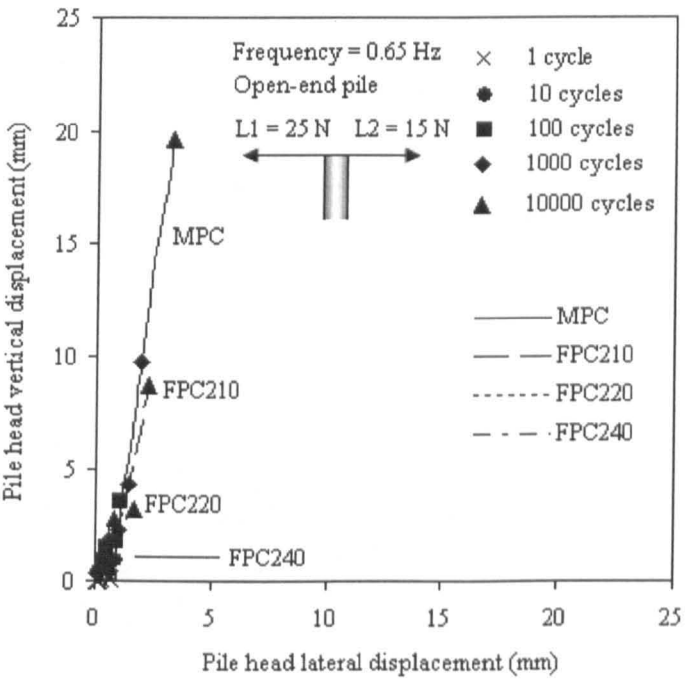

(b)

Fig. 6.4 Variation of pile head displacement with the number of cycles for open-end finned piles subjected to (a) balanced loading; and (b) out of balanced loading

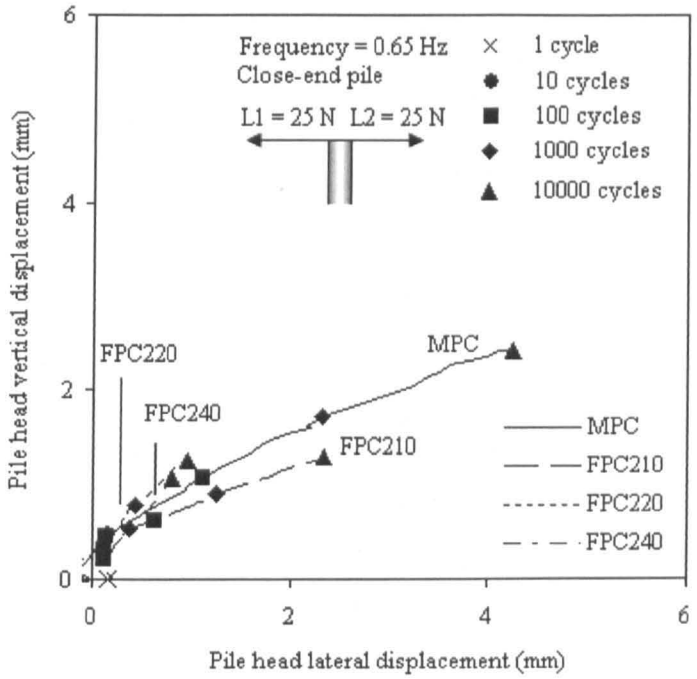

(c)

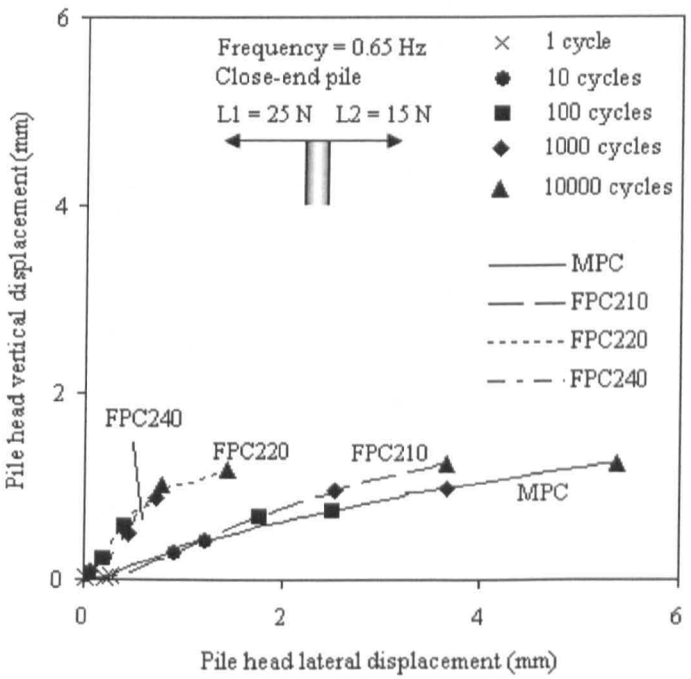

(d)

Fig. 6.4 Variation of pile head displacement with the number of cycles for closed-end finned piles subjected to (c) balanced loading; and (d) out of balanced loading

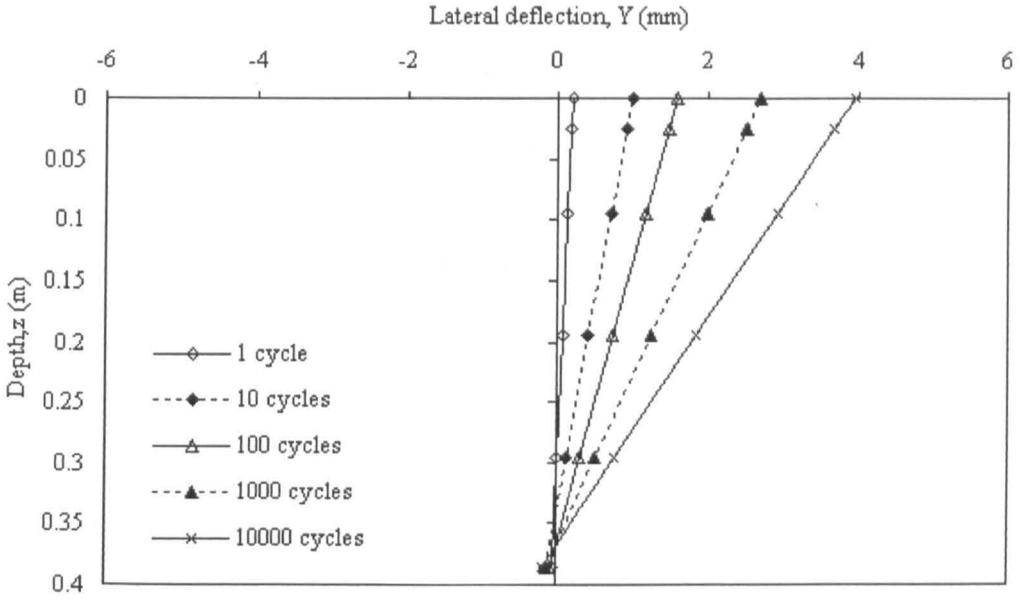

(a)

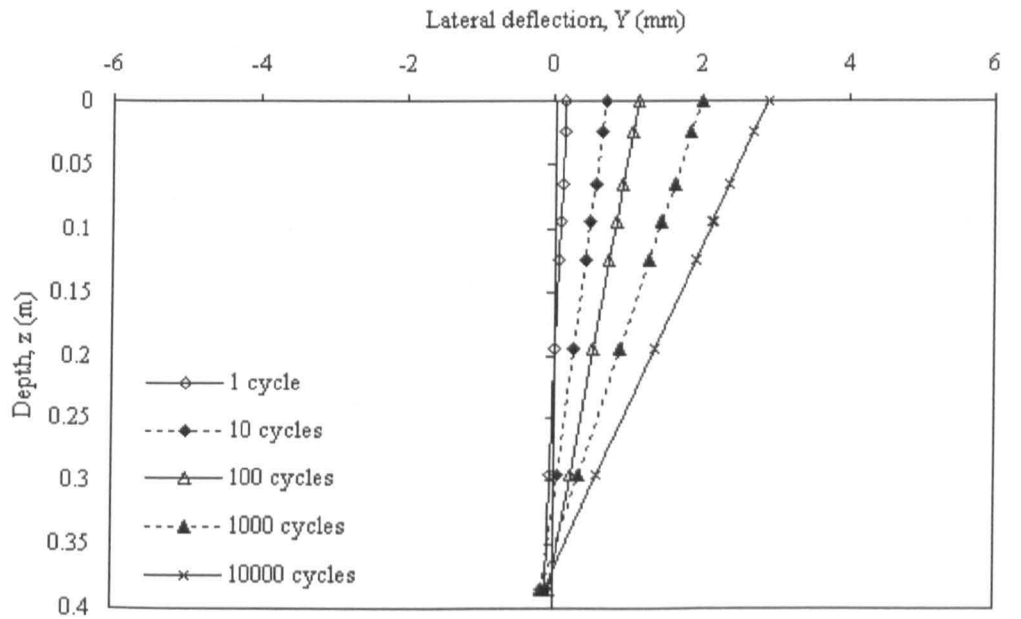

(b)

Fig. 6.5 Variation of pile deflection with depth under cyclic loading (a) MPC and (b) FPC210

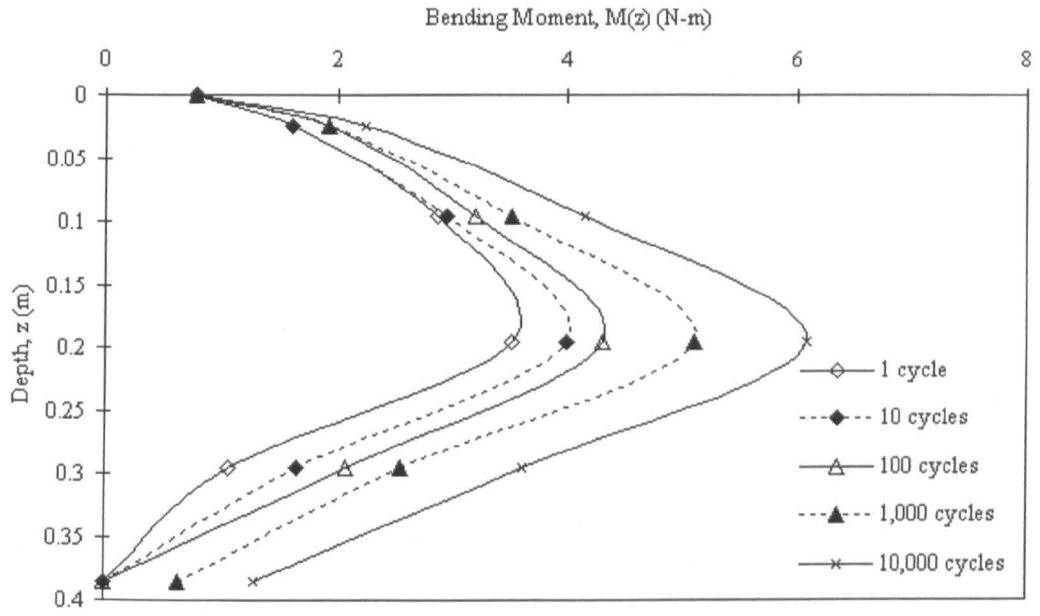

(c)

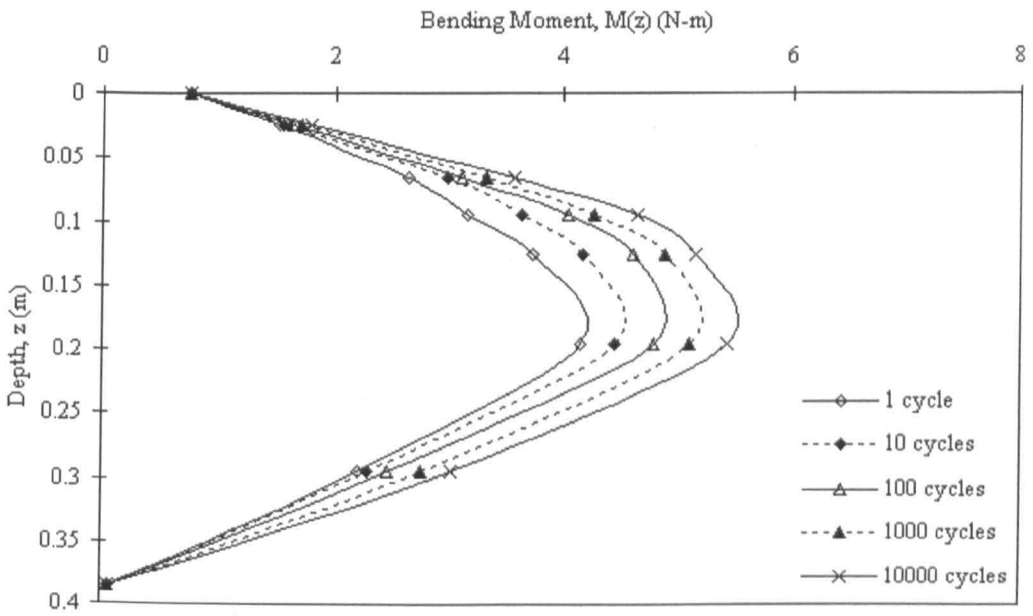

(d)

Fig. 6.5 Variation of bending moment with depth under cyclic loading (c) MPC and (d) FPC210

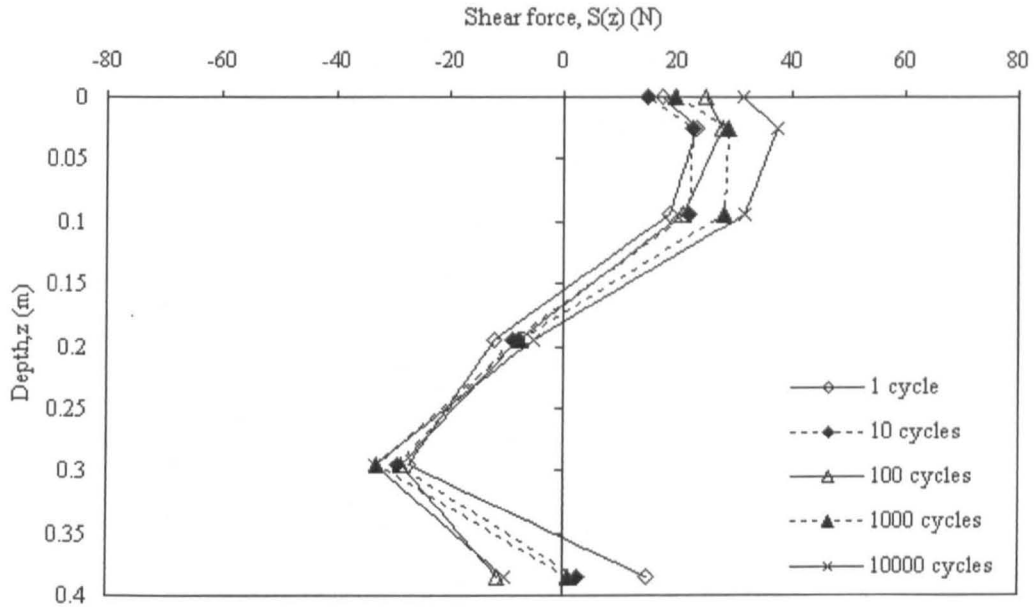

(e)

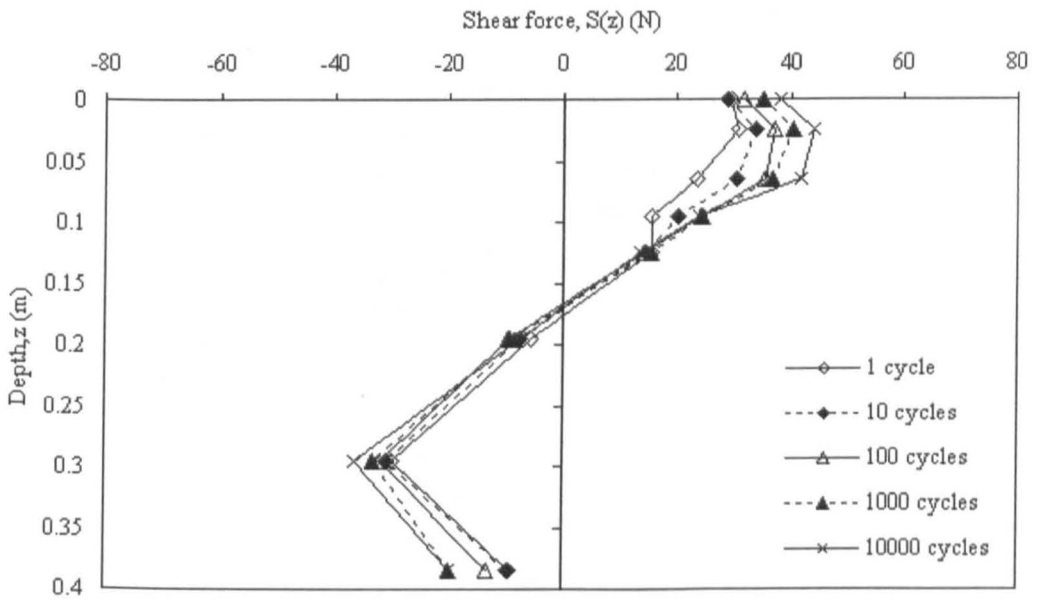

(f)

Fig. 6.5 Variation of shear force with depth under cyclic loading (e) MPC and (f) FPC210

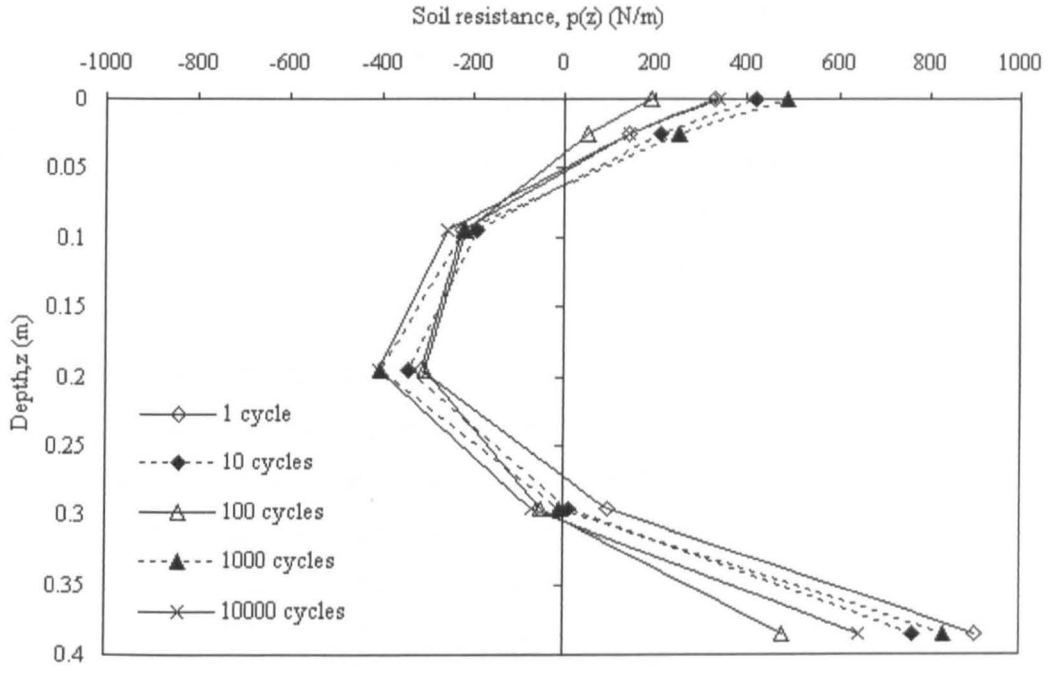

(g)

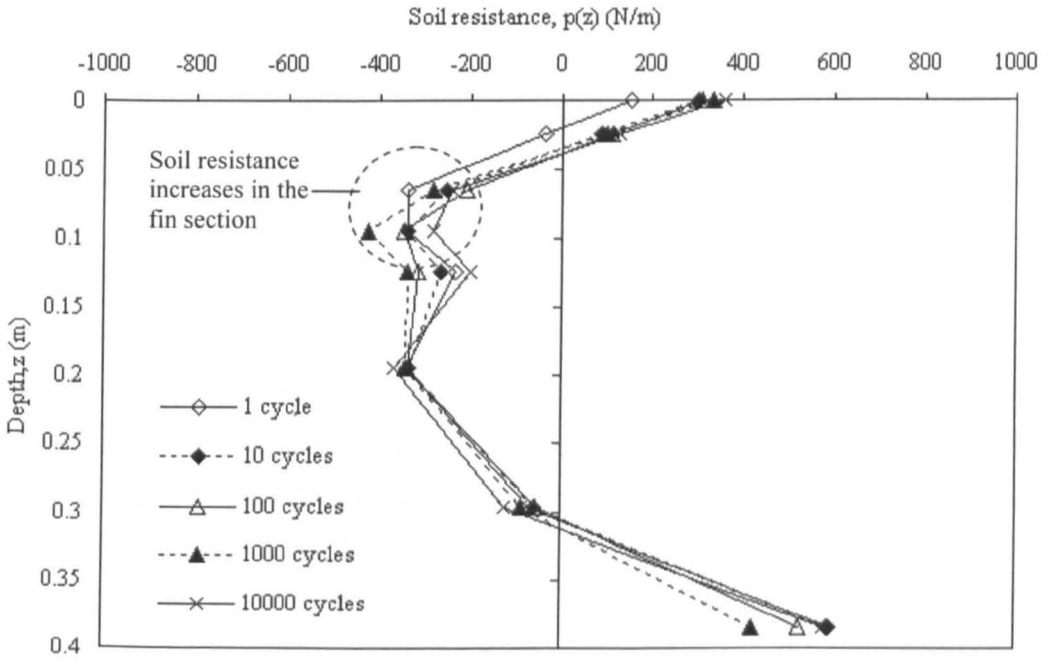

(h)

Fig. 6.5 Variation of soil resistance with depth under cyclic loading (g) MPC and (h) FPC210

A similar situation is observed in soil resistance, Fig 6.5 (g) and (h), showing that the soil resistance increases with an increase in the number of cycles. Importantly, the gain of resistance in the fin section is presented in Fig. 6.5 (h); such resistance, as observed from computer modelling, is higher than the maximum resistance of the monopile. The cyclic lateral movement makes the soil more dense and thus increases the soil resistance.

6.2.5. Combined cyclic loading

A vertical load was first applied to the top of the pile, a cyclic lateral loading test was then carried out up to 10000 cycles (see Fig. 6.6). Fig. 6.7 shows the variation of lateral displacement with the number of cycles. Lateral displacement in the first 10 cycles is presented in the inner chart because cyclic loading in these cycles, which occurred with increasing speed (Fig. 4.13), has the characteristics of static loading; the displacement from 10 to 10000 cycles represents the long term influence.

The influence of vertical loading on piles subjected to cyclic lateral loading is presented in Fig. 6.7(a). Three different vertical loads: 80, 160 and 240 N were used which represent 10%, 20% and 30% of the ultimate vertical load of MPC. Although the increase in vertical load results in a reduction of lateral displacement in the first 10 cycles, vertical loading is not directly proportional to lateral displacement after the first 10 cycles. Lateral displacement was reduced by about 50% with the use of fins.

Fig. 6.7(b) shows that lateral displacement increases with an increase in lateral loading on both monopile and finned piles. A constant vertical load of 240 N was applied to simulate a pile subjected to 30% of the ultimate vertical load. Three different lateral loads: 15, 25 and 35 N were used which represent 10%, 20% and 30% of the ultimate lateral load of MPC. Lateral displacement increased with an increase in lateral loads. The pile head lateral displacement of FPC210 was only 60% of that of MPC; and this tendency was apparent with an increase in the magnitude of lateral load.

The influence of the frequency of the cyclic lateral load on a pile under combined loading is presented in Fig. 6.7(c). In order to verify the influence of cyclic frequency on lateral displacement, cyclic lateral loading was applied on the pile at three different frequencies: 0.45, 0.65 and 0.94 Hz. In this group of tests, a constant vertical load of 240 N was applied which is about 30% of the ultimate vertical load; a

cyclic lateral load of 25 N was used which is about 20% of the ultimate lateral load. Results show that lateral displacement increases with an increase in frequency. Ignoring the displacement of the first 10 cycles, the lateral displacement of MPC at the frequency of 0.94 Hz is 9 times that at the frequency of 0.45 Hz. At the same frequency, the lateral displacement of FPC210 is reduced to only 75% of that of MPC.

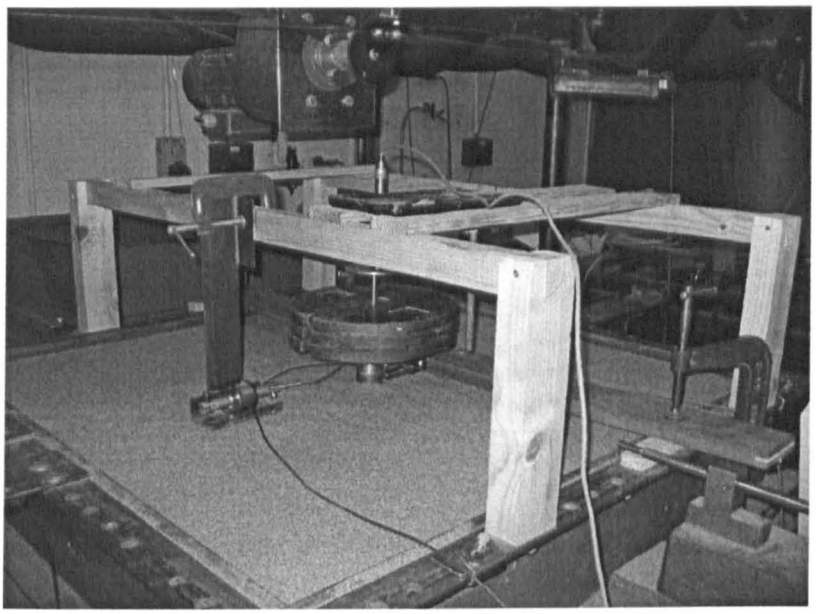

Fig. 6.6 Photograph of a pile subjected to combined cyclic loading

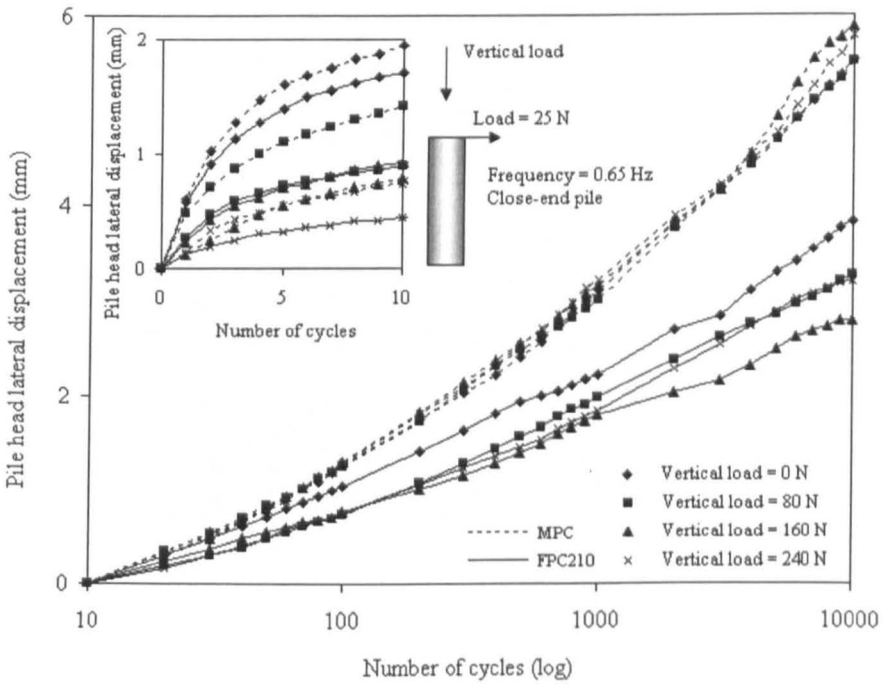

Fig. 6.7 Variation of lateral displacement with the number of cycles under (a) different vertical loads

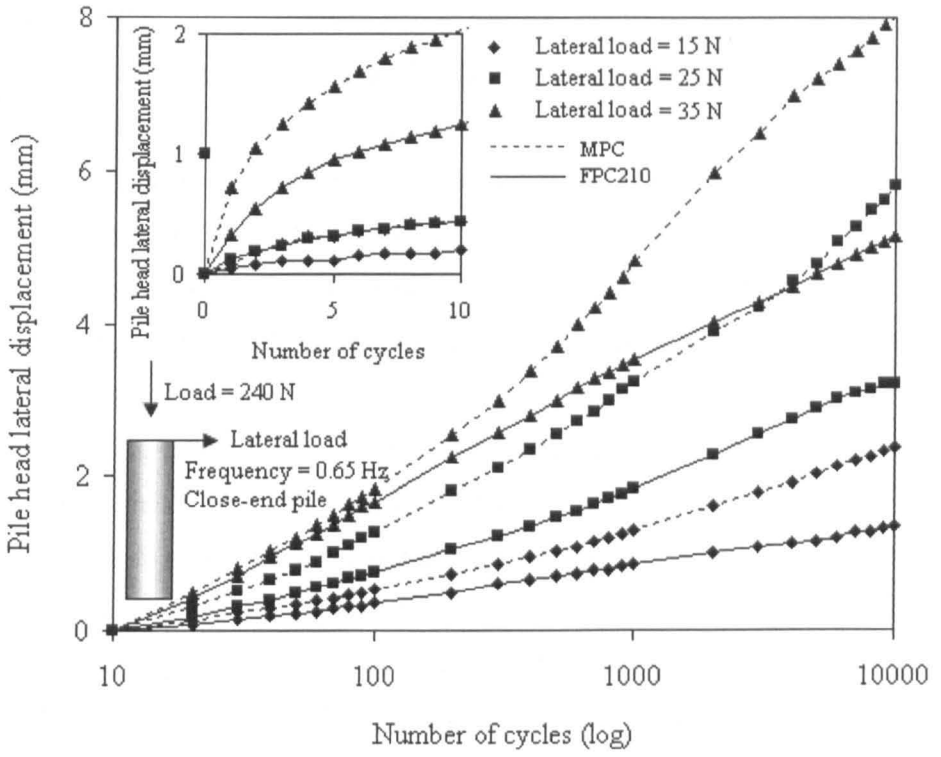

(b)

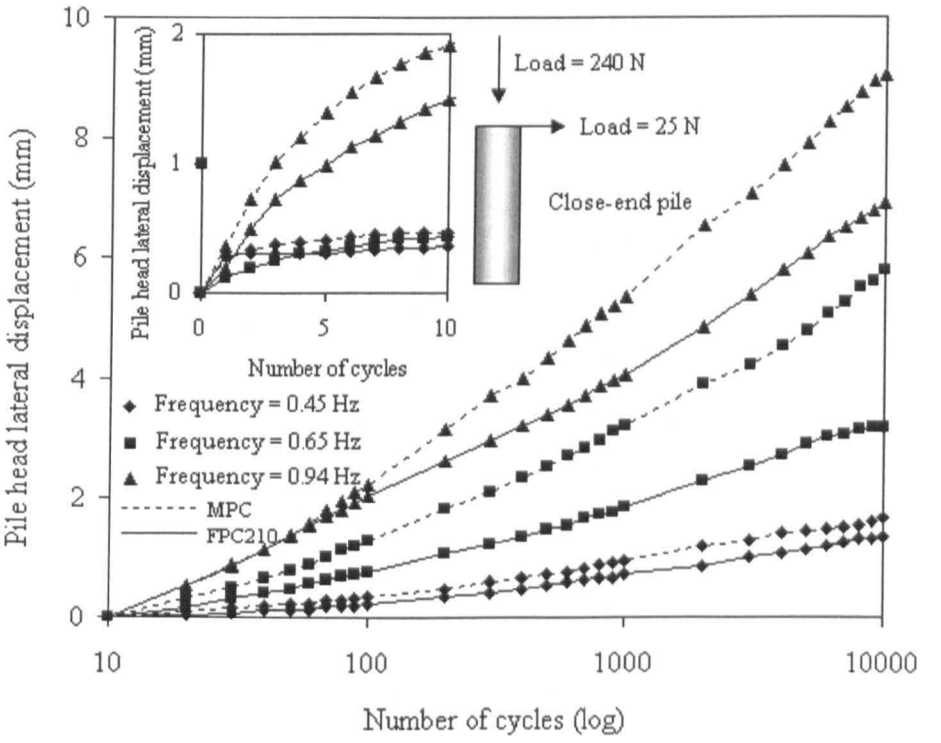

(c)

Fig. 6.7 Variation of lateral displacement with the number of cycles under different (b) lateral loads, (c) frequencies

6.3. Analysis

6.3.1. Modified relationships of P-Y based on repeated loading

The variation in the tangent slope of $\Delta P / \Delta Y$ with Y* for the loading position of a cycle can be used to compare the variation in resistance with the number of cycles (see Fig. 6.8(a)); the higher the value the stronger the soil pile resistance. The variation in resistance, $\Delta P/\Delta Y$, is plotted against the displacement expressed as a ratio of pile diameter, Y*/D, for pile FPC210 at a load of 150 N as shown in Fig. 6.8(b). It is observed that values of resistance degrade with an increase in displacement during reloading within a reloading cycle. The total resistance increased with the number of cycles, especially in the first two cycles.

Fig. 6.8(c) shows the influence of load level on resistance; the resistance, $\Delta P / \Delta Y$, was obtained at a displacement of 0.45 mm (1% pile diameter) for every reload cycle at load levels of 120 and 150 N. Y** was taken from the initial point of the first loop at each load level. Fig. 6.8(d) shows that resistance decreases with an increase in load level for the same ratio of Y**/D. The finned pile not only has higher resistance compared to monopile, but shows a greater increase in resistance with the number of cycles as well.

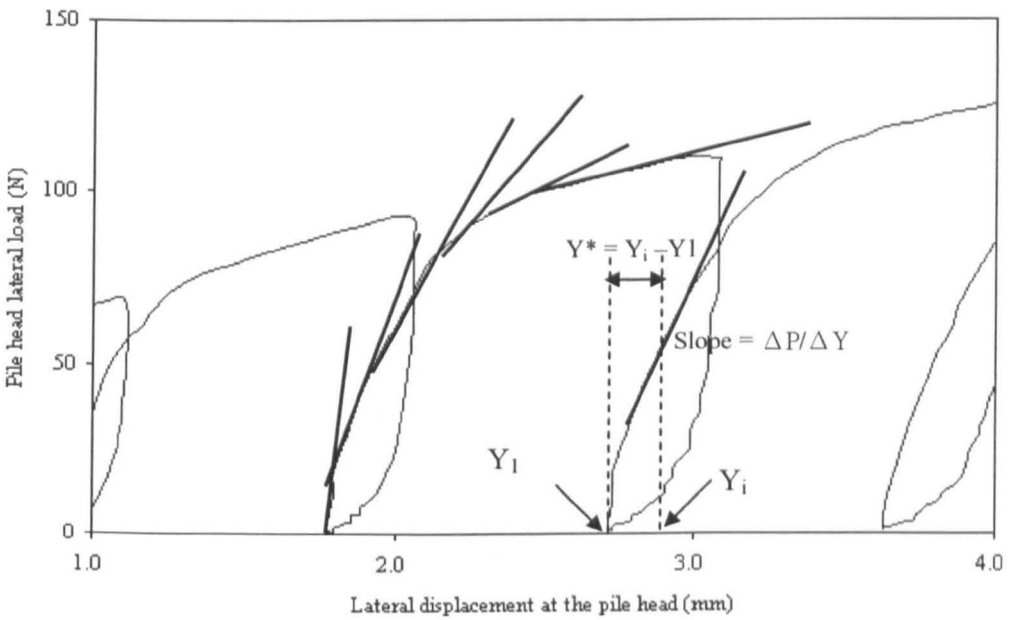

(a)

Figure 6.8 (a) Determination of slope $\Delta P/\Delta Y$ and the relevant displacement Y*

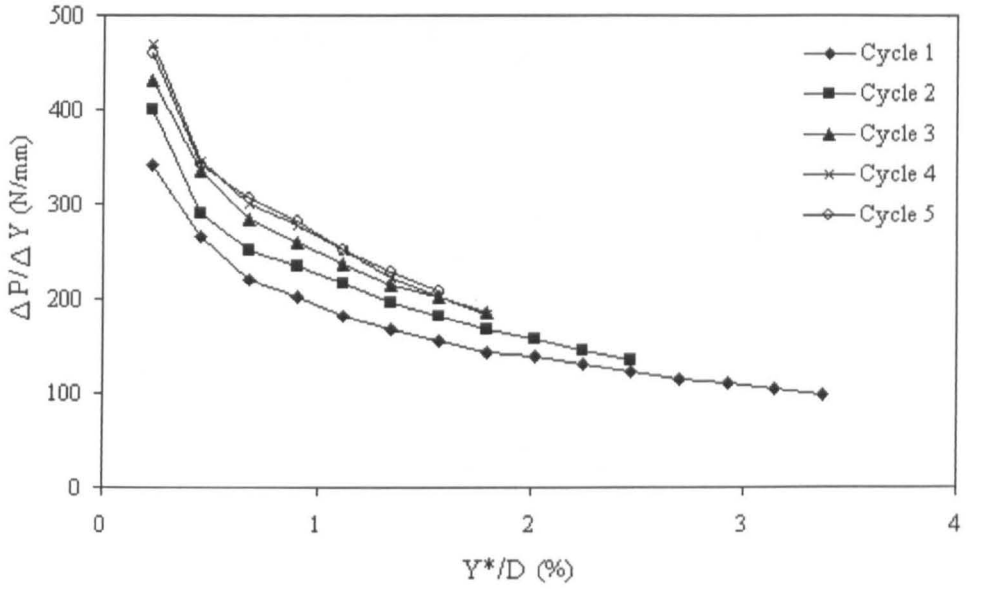

(b)

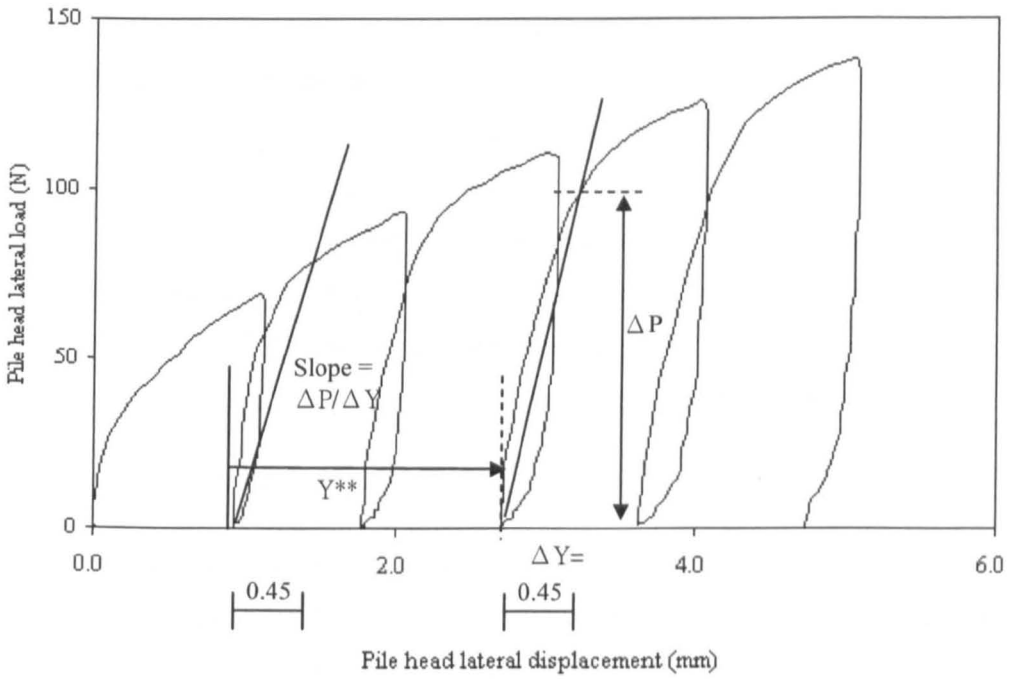

(c)

Figure 6.8 (b) Variation of resistance, $\Delta P/\Delta Y$ with the displacement ratio, Y*/D; (c) Determination of slope $\Delta P/\Delta Y$ and the relevant displacement Y**

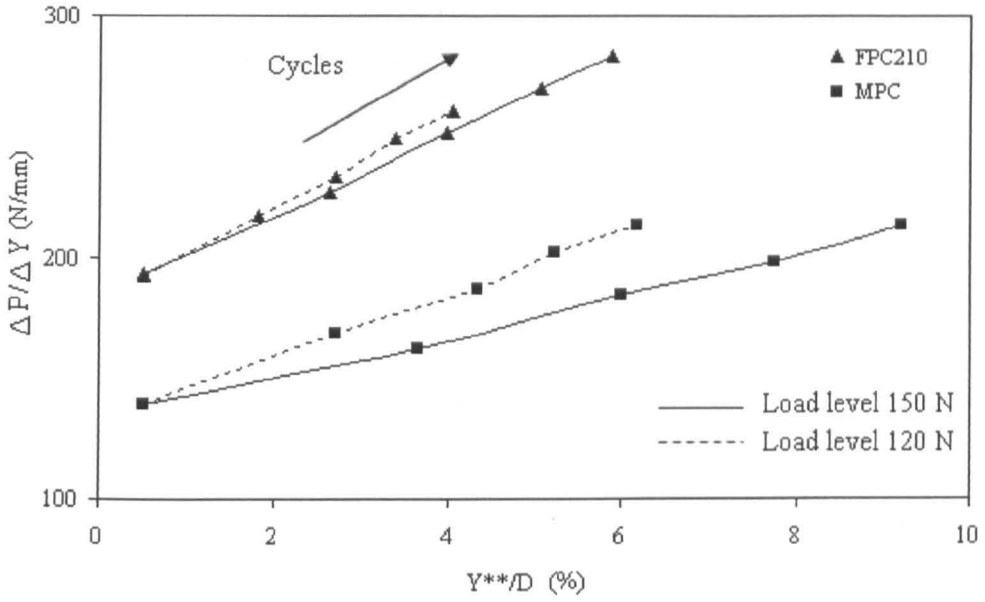

(d)

Figure 6.8 (d) Influence of the number of cycles and load level on resistance, $\Delta P/\Delta Y$

6.3.2. Influence of fin dimension

The curves of lateral load versus lateral displacement in Fig. 6.9(a) demonstrate the lateral resistance of piles under static lateral loading. For a given displacement a pile with longer fins can support a greater load than a pile with shorter fins. The normalised relationship between fin length and lateral resistance under static loading is presented in Fig. 6.9(b) where P_u, the ultimate lateral load, is taken as the load corresponding to the point where the curve tends towards a straight line; Fig. 6.9(c) that is the slope reduction ratio of $\frac{Slope_{(i)} - Slope_{(i+1)}}{Slope_{(i)}} \leq 0.05$. The slope reduction ratio of 0.05 was used to determine the point of ultimate load because the reduction ratio dropped with the increase in displacement to the value of 0.05, and it remained constant. An increase in fin length results in an increase in lateral resistance (Fig. 6.9(d)).

The increase in pile soil resistance can be estimated from the reduction of displacement which is defined as

$$\text{Reduction}, R_1\ (\%) = \frac{\text{Displacement of monopile - Displacement of finned pile}}{\text{Displacement of monopile}} \qquad (6.1)$$

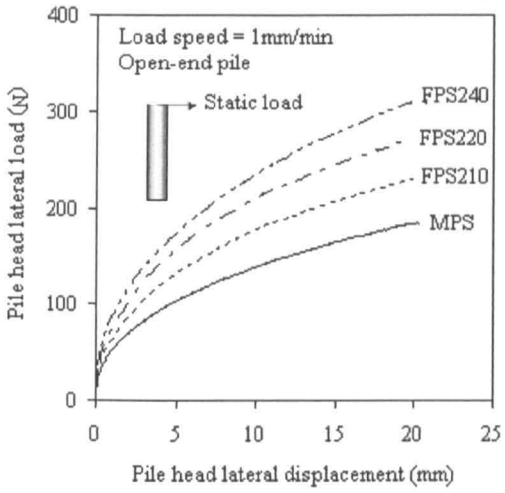

(a)

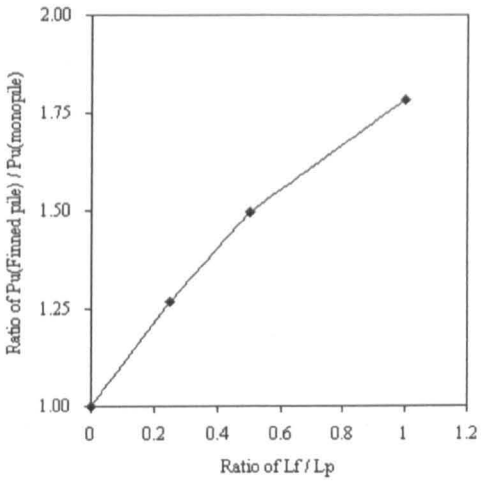

(b)

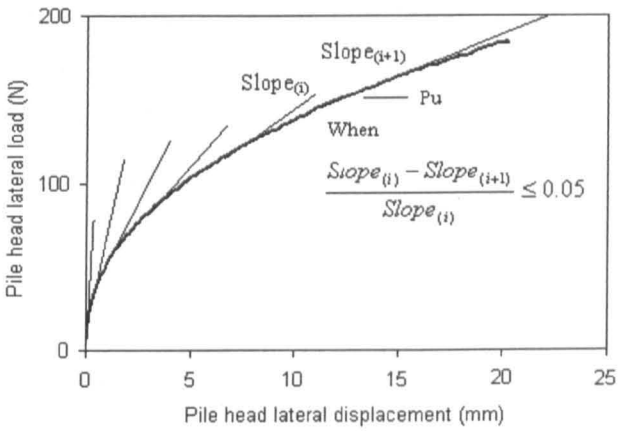

(c)

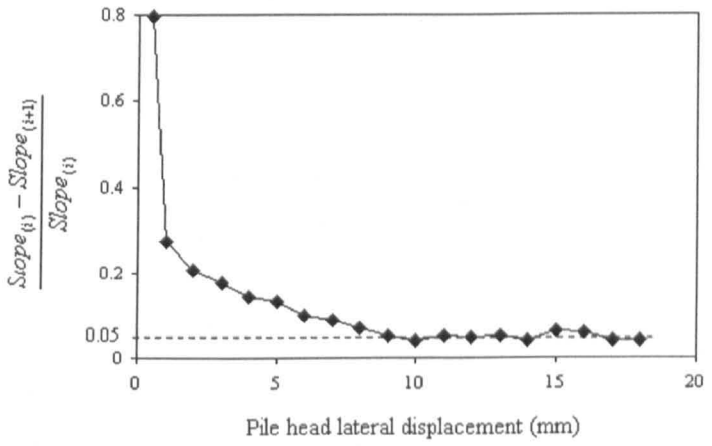

(d)

Fig. 6.9 (a) Variation of lateral load with displacement of pile head; and (b) variation of the ratio of ultimate load with the ratio of fin length to pile length (c) determination of ultimate lateral load (d) variation of slope ratio with displacement

The displacements in Equation (6.1) at 10000 cycles are used to show the variation of reduction in displacement with the ratio of fin length, L_f, to pile length, L_p, in Fig. 6.10(a)-(c).

The reduction factors, R_1, are shown for three sets of tests. The first set of tests (Fig. 6.10(a)) represents piles subjected to one-way cyclic loading. Fig. 6.10(a) shows the reduction of lateral displacement with an increase in the fin length to pile length ratio from 0.25 to 1. The reduction is most apparent when the fin length is less than 0.5 of the pile length for all cases.

The second set of tests (Fig. 6.10(b)) is based on two-way cyclic loading with balanced loads. The curves of reduction of displacement versus the ratio of fin length to pile length are presented in Fig. 6.10(b). The greatest reduction is achieved when the fin length is only a quarter of the pile length. The reduction of lateral displacement is greater than that of vertical displacement in close-end piles. In contrast, the reduction of vertical displacement is more significant than that of lateral displacement in open-end piles. The reason could be that the use of a pile tip provides high bearing capacity, with reduced settlement.

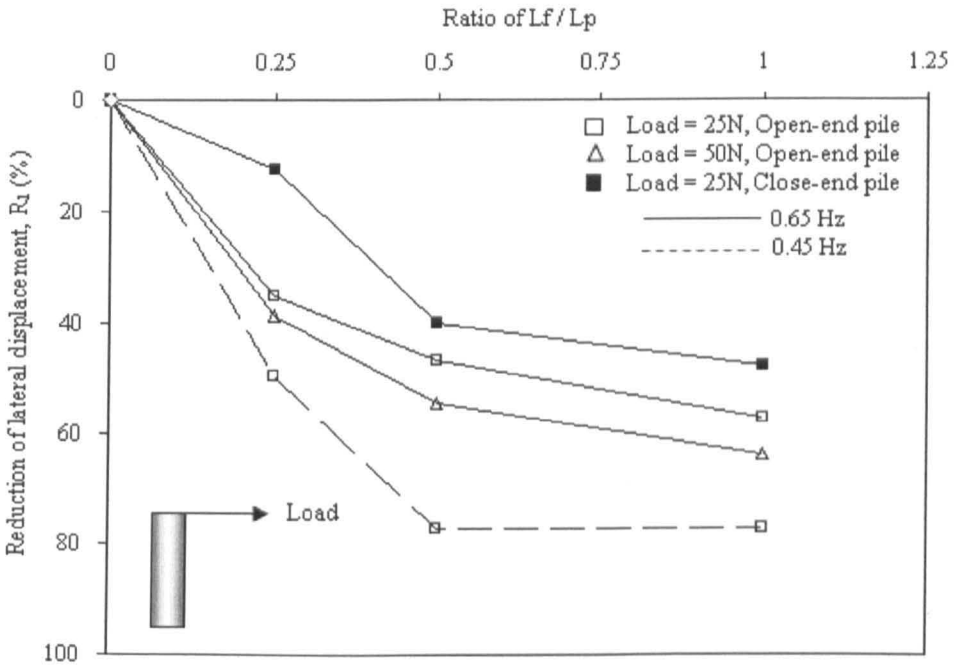

(a)

Fig. 6.10 Reduction of displacement versus ratio of fin length to pile length for (a) one-way cyclic loading

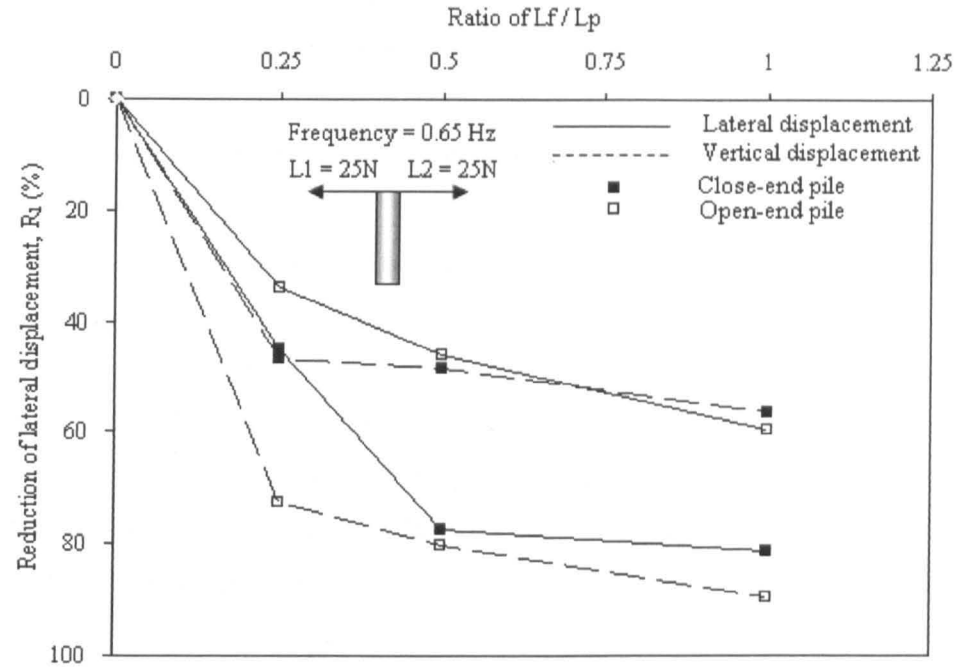

(b)

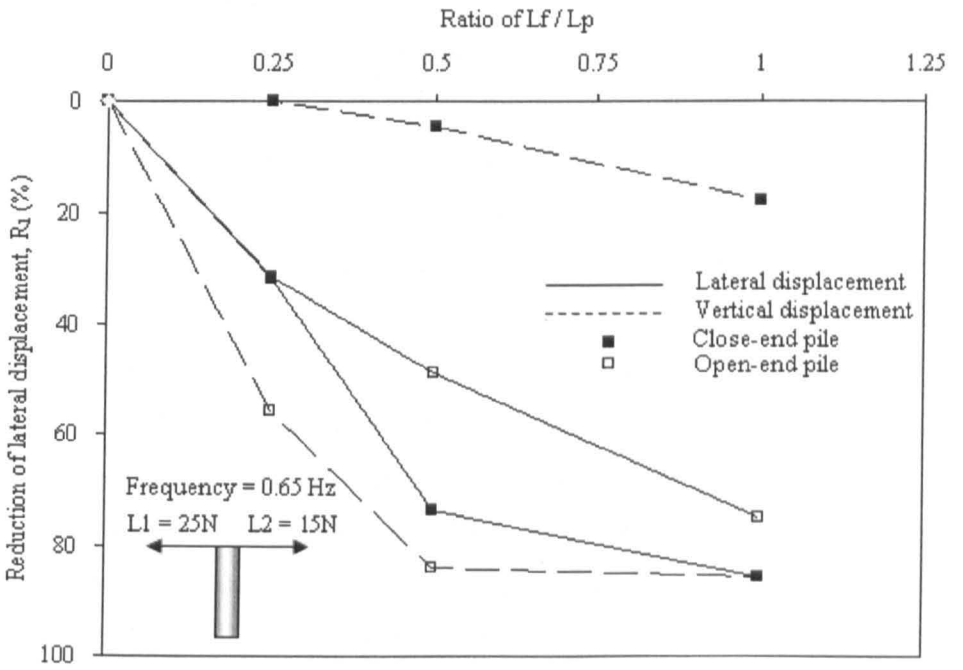

(c)

Fig. 6.10 Reduction of displacement versus ratio of fin length to pile length for (b) two-way cyclic loading with balanced loads (c) two-way cyclic loading with out of balanced loads

The third set of tests (Fig. 6.10(c)) examined piles under out-of-balanced loading. Fig. 6.10(c) again shows that the reduction of displacement increases with an increase in fin length. Tests on open-end piles show that fins provide large

reductions of both lateral and vertical displacements; in close-end piles, however, the reduction of vertical displacement is limited compared to that of lateral displacement.

6.3.3 The variation of soil resistance with cycles for a constant maximum load

Fig. 4.13 shows the load at the pile head versus the resulting displacement for the first 200 cycles in cyclic loading of a monopile. The maximum applied load is P. The resulting displacement for each cycle of the load P is Y as defined in Fig. 6.11(a).

The P/Y, ratio that is the soil resistance, increased over each cycle and increases as the number of cycles increases especially in the first 10 cycles. The P/Y ratio in one-way loading is greater than that in unbalanced two-way loading even though the lateral displacement in one-way loading is larger than that in two-way cyclic loading. In order to quantify the increase in pile-soil stiffness with the use of finned piles, the value of P/Y at the pile head after a given number of cycles is defined as the average slope of the cycle, that is:

$$P/Y = \frac{\text{Difference of lateral load}}{\text{Difference of lateral displacement within each cycle}} \qquad (6.2)$$

Values of P/Y were obtained at the following cycles: 1, 10, 100, 1000 and 10000. Variations of secant P/Y with the number of cycles are shown in Fig. 6.11 (b)-(d) for the three types of loadings: one-way; two-way balanced and two-way out of balanced. The value of P/Y generally increases with the increase in both the number of cycles and the length of the fin; that is the soil becomes stiffer or the pile/soil interaction is stiffer. P/Y for piles under one-way cyclic loading is greater than that under two-way cyclic loading, and the smallest stiffness is created by unbalanced two-way loading. It is difficult to assess the change in stiffness by measuring the displacement only. The change in stiffness, however, is easily determined through the change in P/Y derived from the load-displacement curve. This work shows that unbalanced loading could cause serious damage to the structure because of the relatively low value of P/Y compared to other loading conditions. In addition, stiffness tends to be constant for unbalanced loads after 1000 cycles which suggests that this is the critical design condition for both monopiles and finned piles. Fins apparently help to increase soil-pile resistance by over 20%, and the foundation becomes more stable than that of a monopile.

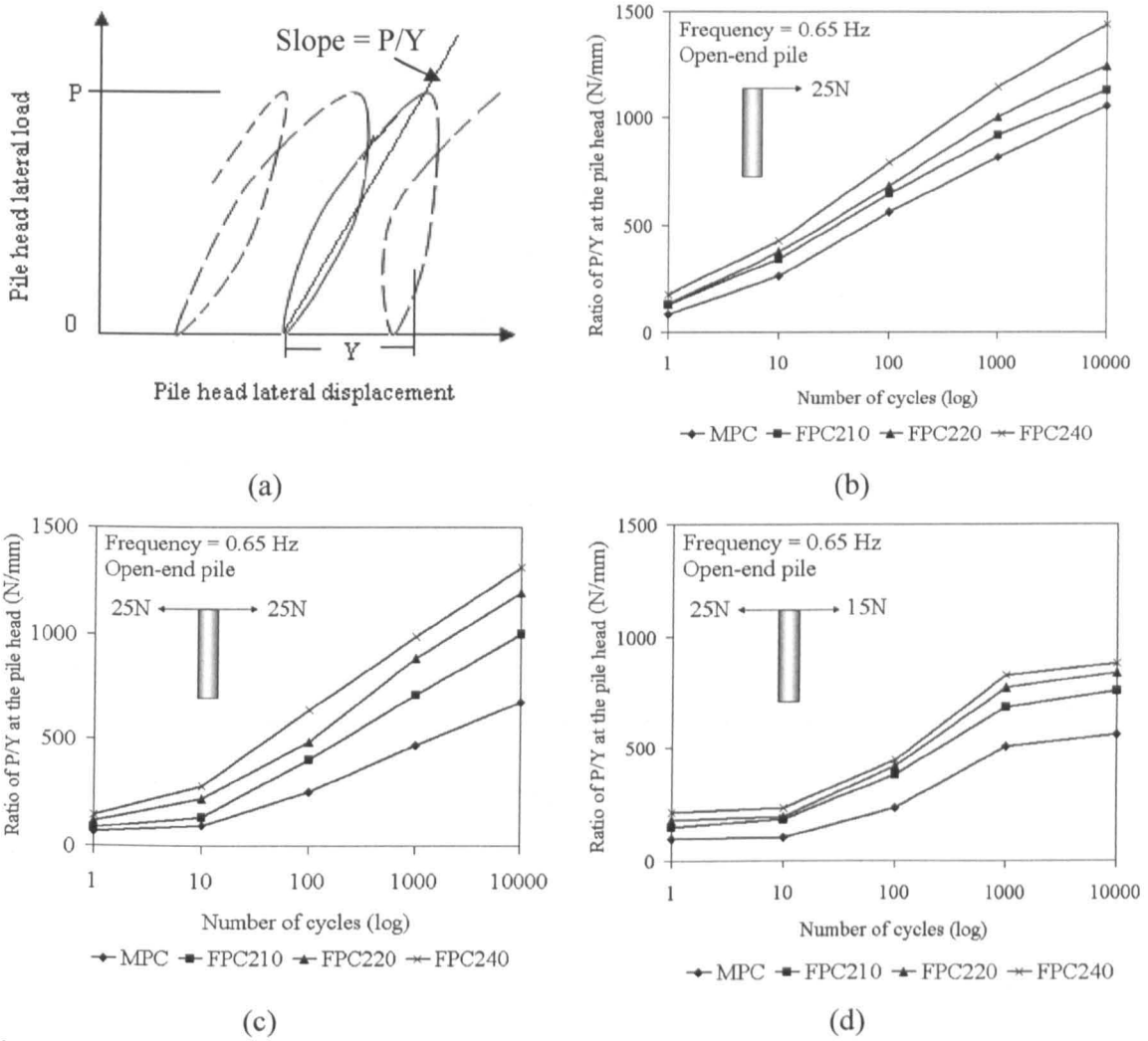

Fig. 6.11 (a) Definition of P/Y; variation of P/Y at the pile head with the number of cycles under (b) one-way cyclic loading, (c) two-way balanced cyclic loading, and (d) two-way out of balanced cyclic loading

6.3.4. Pile-soil behaviour along a finned pile

In order to verify the influence of fins under cyclic loading on the pile soil interaction, both MPC and FPC210 are compared at 10000th cycle. The pile deflections, Fig. 6.12(a), show a significant reduction in lateral displacement when fins are added to a monopile. In addition, a smaller pile tilt is observed for FPC210.

Fig. 6.12(b) presents the bending moment distribution along the piles. On the section with fins, the pile provides a greater resistance to bending as a result of the increase in pile rigidity. The maximum bending moment of a monopile is reduced by using a finned pile.

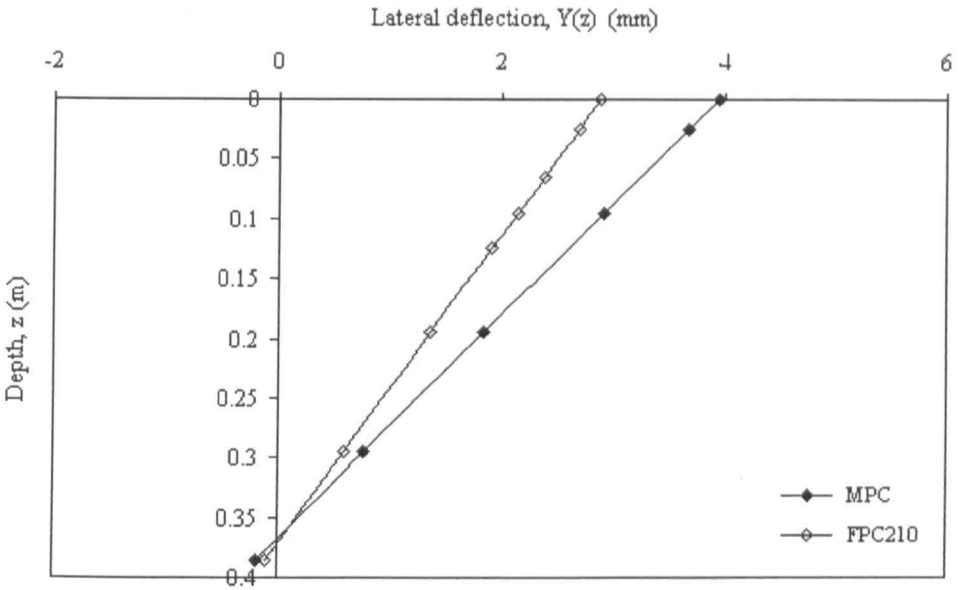

(a)

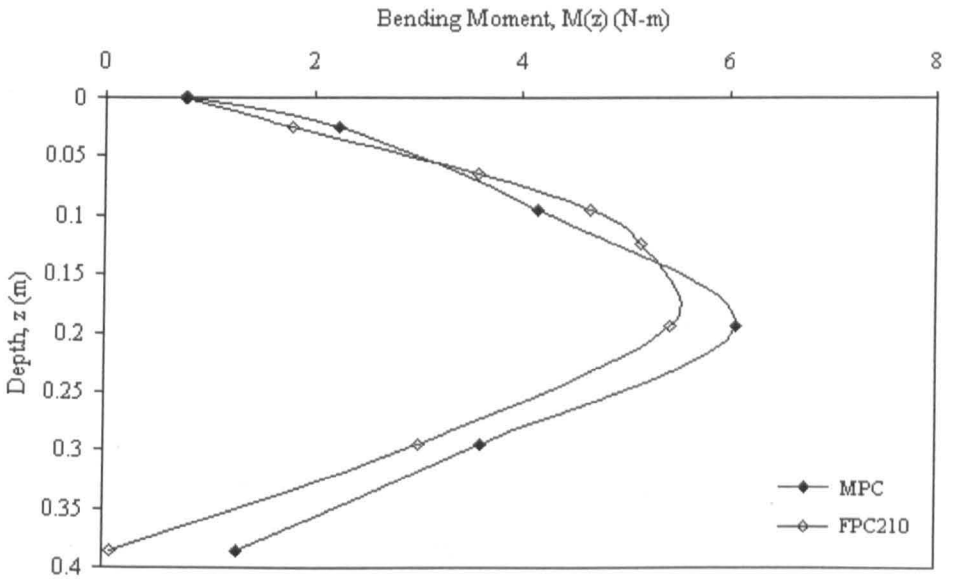

(b)

Fig. 6.12 Comparison of MPC and FPC210 under cyclic loading (a) pile deflection, (b) bending moment

The variation of shear force with depth is shown in Fig. 6.12(c). Both the pile head shear forces of MPC (31 N) and of FPC210 (38 N), obtained from regression analyses, were not too close to the measured value of 25 N. The compaction of the soil by repeated loading and the difficulty in modelling nonlinear soil behaviour could be two reasons for the over estimation of the pile head shear force.

Fig. 6.12(d) shows the variation of soil resistance along the pile. Soil resistance at the lower level of the finned and mono piles are very close; whereas, soil resistance observed at the upper section of FPC210 is greater than that for the monopile. In other words, the force acting at the pile head is resisted mainly by the upper soil around the pile. Pile tip soil resistance is the key factor to stop pile rotation. The soil resistance at the pile tip is expected to be reduced by using a finned pile due to the reduction in lateral displacement of the pile head.

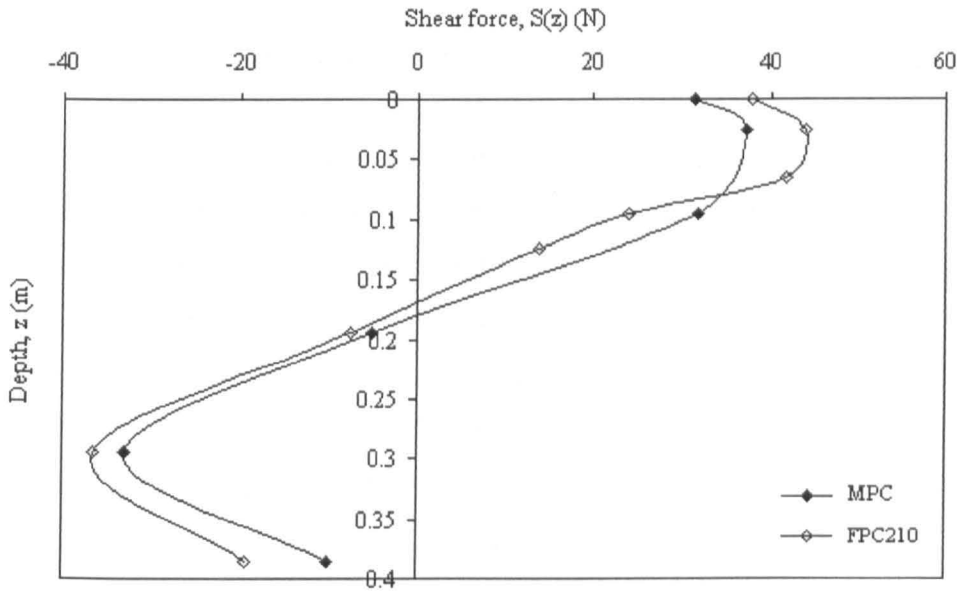

(c)

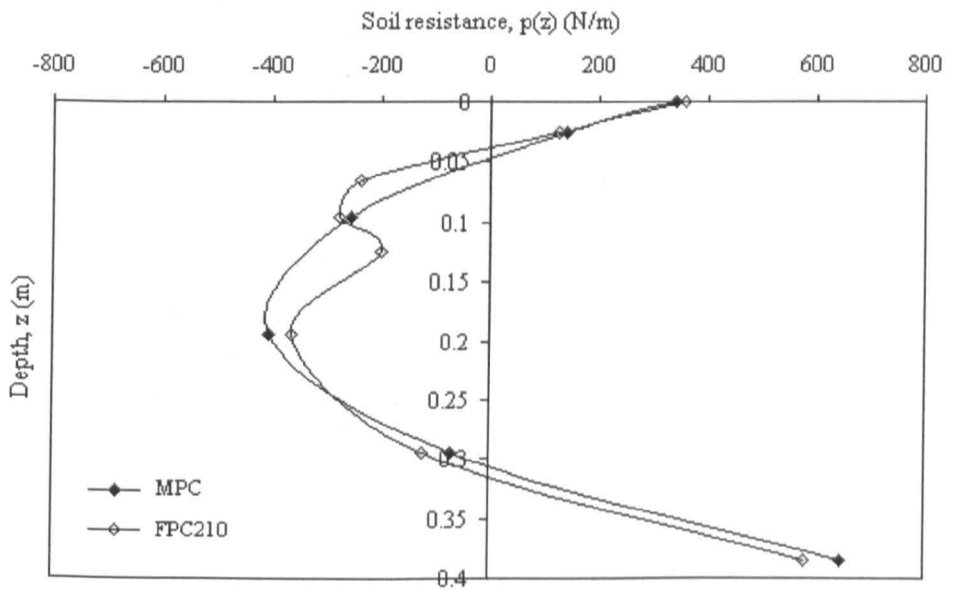

(d)

Fig. 6.12 Comparison of MPC and FPC210 under cyclic loading (c) shear force, (d) soil resistance

6.3.5. Lateral capacity of combined cyclic loading

The increase in lateral resistance by using fins under combined loading at different vertical load levels can be evaluated by the reduction of total lateral displacement according to Equation 6.3.

$$\text{Reduction},R_2\ (\%)=\frac{Y_{[MPC]Q0}-Y}{Y_{[MPC]Q0}} \tag{6.3}$$

where $Y_{[MPS]Q0}$ = lateral displacement of MPC without vertical load (Q is vertical load)

Y = lateral displacement of MPC and FPC210 subjected to different vertical loads

The displacements in Equation (6.3) at 10000th cycle are used to show the variation of reduction in displacement, R_2, with the ratio of current vertical load to ultimate vertical load (Q/Q_u) in Fig. 6.13(a) where Q_u is ultimate vertical load with no applied lateral load. The reduction of lateral displacement increases with an increase in the ratio of current vertical load to ultimate vertical load. The difference in the reduction of lateral displacement between MPC and FPC210 varies from 25% to 40% as the vertical load ratio (Q/Q_u) increases from 0 to 0.3.

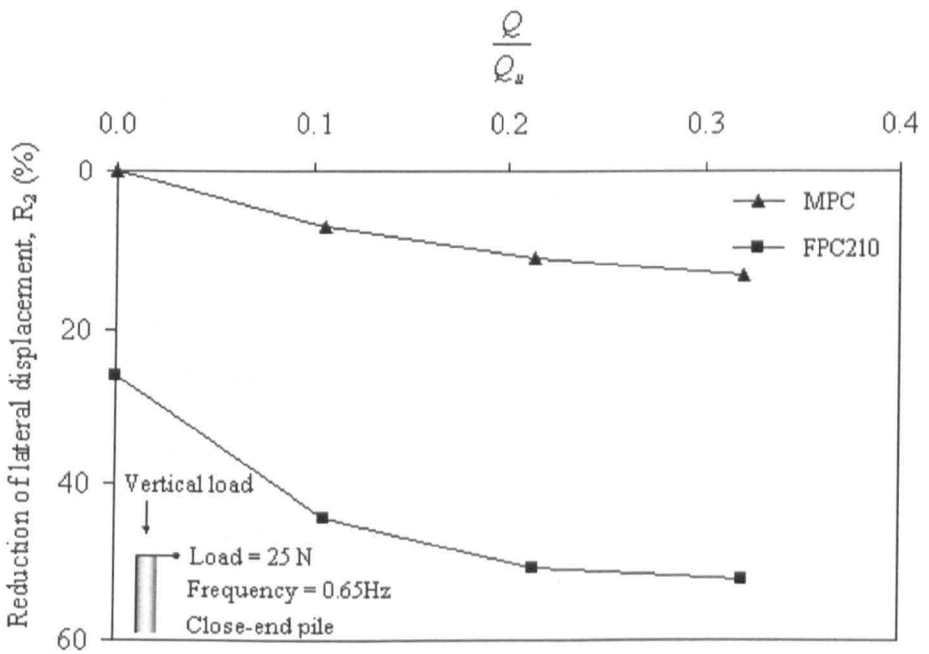

Fig. 6.13 (a) Reduction of lateral displacement versus ratio of current vertical load to ultimate vertical load

The influence of lateral load on the lateral resistance of piles under combined loading can be estimated using Equation (6.4).

$$\text{Reduction}, R_3\ (\%) = \frac{Y_{[MPC]P35} - Y}{Y_{[MPC]P35}} \tag{6.4}$$

where $Y_{[MPC]P35}$ = lateral displacement of MPC subjected to a lateral load of 35 N which is 22% of the ultimate lateral load

Y = lateral displacement of MPC and FPC210 subjected to different lateral loads

Similarly, the displacements in Equation (6.4) at 10000th cycle give the variation of reduction in lateral displacement, R_3, with the ratio of current cyclic lateral load to ultimate lateral load (P/P_u) in Fig. 6.13(b) where P_u is ultimate lateral load with no applied vertical load. The smaller the ratio of current lateral load to ultimate lateral load, the larger the reduction of lateral displacement. The difference in the reduction of lateral displacement between MPC and FPC210 varies from 15% to 40% as the lateral load ratio (P/P_u) increases from 0.1 to 0.22.

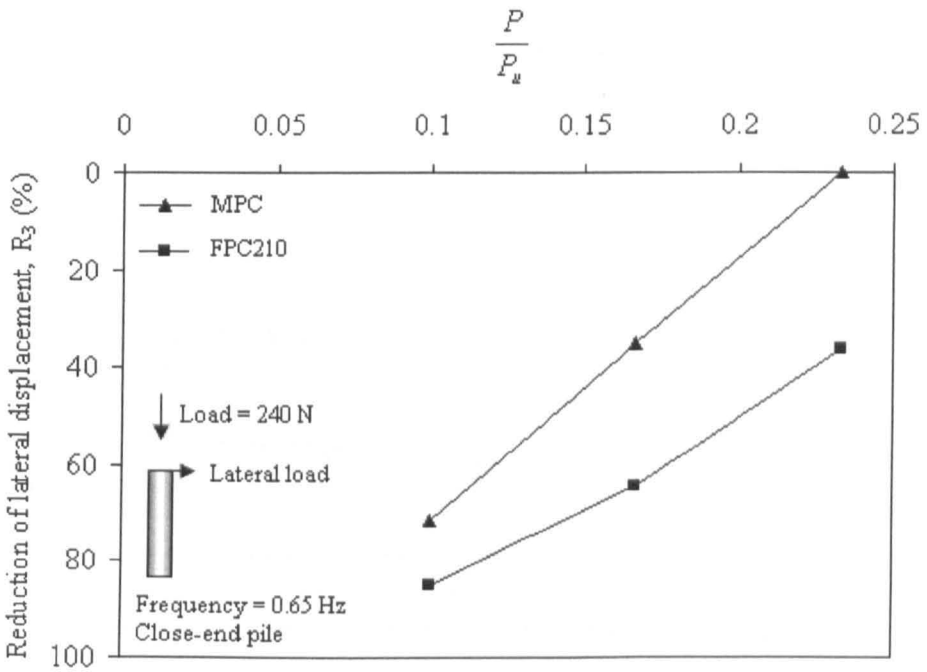

Fig. 6.13 (b) Reduction of lateral displacement versus ratio of current lateral load to ultimate lateral load

The influence of frequency on the reduction of lateral displacement at cycle 10000 can be estimated by using Equation (6.5).

$$\text{Reduction},R_4\ (\%)=\frac{Y_{[MPC]F0.94}-Y}{Y_{[MPC]F0.94}} \tag{6.5}$$

where $Y_{[MPC]F0.94}$ = lateral displacement of MPC subjected to a cyclic lateral load with a frequency of 0.94 Hz

Y = lateral displacement of MPC and FPC210 subjected to a cyclic lateral load with various frequencies

The reduction of lateral displacement (Equation 6.5) versus frequency is shown in Fig. 6.13(c). The reduction of lateral displacement increases with a decrease in frequency. The difference in the reduction of lateral displacement between MPC and FPC210 varies from 4% to 23% as the frequency increases from 0.45 Hz to 0.94Hz. The conclusion is that the performance of finned piles compared that of monopiles proportionally better at higher frequencies.

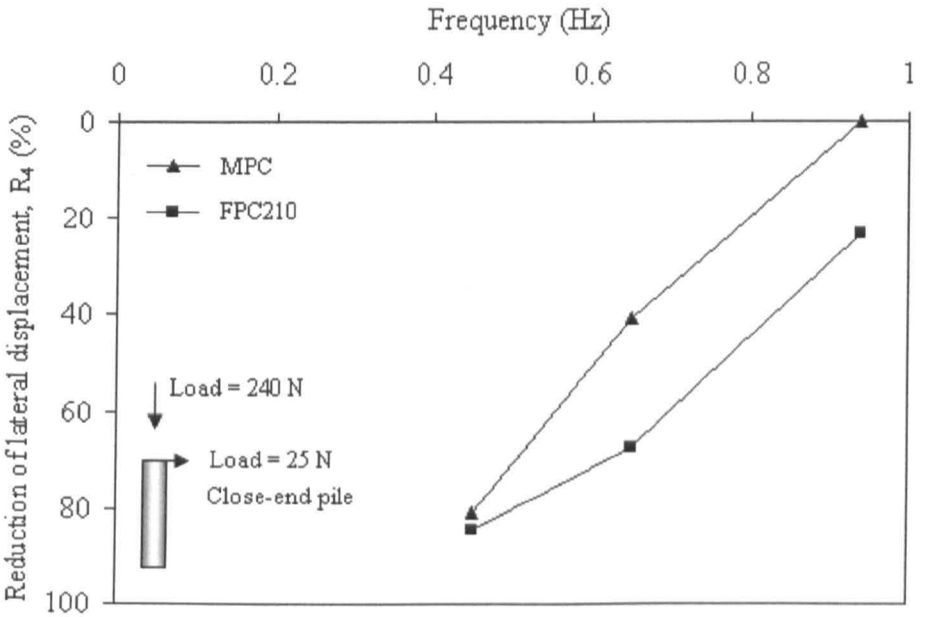

Fig. 6.13 (c) Reduction of lateral displacement versus frequency

6.4. Summary

A series of cyclic loading tests of finned piles were carried using the cyclic loading system described in Section 4.7. Finned piles with different fin lengths were tested under different loading conditions including the change in load magnitude, load frequency and the sequence of loading (Section 6.2); tests involved both open-end and closed-end piles. The reduction of lateral displacement using finned piles is presented in Section 6.3 showing that the lateral resistance increased with an increase in fin length.

Strain gauge tests were carried out to compare behaviour of a finned pile with that of a monopile (Section 6.2.4), and the efficiency of fins is presented in Section 6.3.4. The influence of fins under combined cyclic loading was investigated through a series of cyclic loading tests (Section 6.2.5), and the reduction of displacement was used to represent the efficiency of fins.

Results of cyclic loading tests are used to assess the influence of loading conditions to the efficiency of fins (Section 7.1.3 and 7.1.4), and future research is suggested. An overview of fin efficiency of cyclic loading is presented in Section 7.4.3.

7 Interpretation of the effect of fins on pile performance

7.1. Features of laterally loaded piles

7.1.1 Introduction

A series of small scale tests of finned piles subjected to static, cyclic and combined loadings was carried out to study fin efficiency. In static lateral loading tests, load and displacement curves (P-Y curves) of the pile head were used to determine the efficiency of the fins by observing the increase in load for a given displacement. In cyclic loading tests, the variation of displacement with the number of cycles was used to determine the efficiency of the fins.

Numerous relationships between fin efficiency and fin dimensions were proposed based on results from these small scale tests accompanied by some numerical analyses. Fin efficiency, however, may vary depending on conditions such as the ratio of pile to soil stiffness, load direction and fin position. Most of these factors have been briefly introduced but this chapter considers them in greater detail.

This chapter is divided into three sections to cover static, cyclic and combined loadings. In static loading, comparison of numerical analyses and laboratory tests is presented; the pile head P-Y curve is simulated using a modified method; the influence of load direction on effective area and pile stiffness is presented; the effect of fin position on lateral resistance is discussed. In cyclic loading, discussion focuses on the change in fin efficiency caused by factors such as frequency of loading, loading magnitude and loading direction. In combined loading, an additional factor, vertical load, is included to extend the outcomes from the static and cyclic loading conditions.

7.1.2 Static loading

P-Y curve

Test results

Pile head lateral load and displacement (P-Y) curves can be generated from static loading tests of laterally loaded piles. Both serviceability and ultimate lateral loads of the test piles can be determined from the P-Y curves. The serviceability load,

P_S, is defined as the lateral load when the lateral displacement reaches 10 % of the outer pile diameter (Section 2.3.1); the ultimate load, P_u, is taken as the load corresponding to the point where the curve tends towards a straight line as described in Section 6.3.2. In order to assess P-Y curves using different approaches, a small-scale monopile was used as the benchmark (dimensions shown in Table. 3.1). The P-Y curves from static loading tests are presented in Fig. 4.10. Based on the curve of MPS02, the ultimate lateral load, P_u, is 155 N and the serviceability load, P_S, is 110 N.

Assessment of prediction

There is no empirical equation proposed to predict pile head P-Y curve, and the common empirical equations (Table 7.1) are only used to predict or simulate soil resistance and displacement (p-y) curves. Variations of soil resistance and displacement (p-y) with depth are calculated using the finite element (FEM) or the finite different (FDM) analyses; through the numerical modelling, the pile head P-Y curve can be generated. In this research, the p-y curve methods proposed in Table 7.1 were not used in the numerical modelling because these methods are not supported in the computer programs, LPILE and LUSAS. The behaviour of soil was simulated

Table 7.1 Empirical equations for P-Y curves

Name	Empirical equation	Definition	
Kondner (1963)	$p = \frac{y}{(a+by)}$	p is soil resistance; y is lateral displacement; parameters of a and b are derived from regressive analysis (b = $1/P_u$, when Y → ∞)	Fit p-y curve by regression analysis
Matlock (1970)	$\frac{p}{p_u} = 0.5(\frac{y}{y_c})^{\frac{1}{3}}$	P is soil resistance; y is lateral displacement; p_u is ultimate soil resistance; y_c is lateral displacement when p is 0.5 p_u	Predict p-y curve based on known p_u and y_c
Murchison and O'Neill method (1984)	$p = \eta A p_u \tanh\left[\left(\frac{k_h z}{A\eta p_u}\right)y\right]$	p is soil resistance; y is lateral displacement; P_u is ultimate soil resistance; η is pile shape factor (= 1.0 for a circular pile); A is 3 – 0.8 (z/D) ≥ 0.9 for static loading; k_h is coefficient of soil subgrade reaction modulus which is a function of internal friction angle, ϕ (obtained from Fig. 2.21)	Predict p-y curve based on known p_u, k_h, A and η

using the Reese method (1974) in LPILE and advanced Mohr-Coulomb yield criteria in LUSAS which have been described in Section 3.2 and 3.3. Although the methods did not predict the P-Y curve through integrating soil resistance with depths, the shapes of the equations may be used to fit the pile head P-Y curved using regression analyses.

Modified methods

In order to improve the simulation of test P-Y curve, three approaches were used:

- The P-Y data were used to fit the modified hyperbolic equation from the Kondner (1963) method. Parameters 'a' and 'b' in the equation were obtained from the regression analysis to fit the test results.
- The P-Y curve was developed using a modified form of the equation from Matlock (1970). P_u and Y_c in the equation were obtained from the regression analysis.
- A modified curve was obtained from the regression analysis to achieve the best simulation of the test P-Y curve

P-Y curves obtained from these three simulations are presented in Fig. 7.1 showing that the test P-Y curve can be expressed only by the modified hyperbolic equation. The ultimate lateral load of 155 N and the serviceability load of 110 N of the test can be simulated by modified equations. The modified Matlock equation slightly overestimated the load, while the Kondner equation underestimated the load in the initial 2 mm.

The parameters a and b were obtained from the simulation of test results by modified Kondner method, and the relationship between P and Y is expressed as:

$$P = \frac{Y}{0.0217 + 0.038Y} \tag{7.1}$$

where a is 0.0217 mm/N and b is 0.038 /N.

In the cubic parabola equation developed by modified Matlock factors of Y_c and P_u were reassigned as variables. The new equation is presented as:

$$\frac{P}{71.35} = 0.5\left(\frac{Y}{0.1087}\right)^{\frac{1}{3}} \tag{7.2}$$

where Y_c is 0.1087 and P_u is 71.35 at the pile head. The value 'P_u' of 71.35 N is located at the displacement of 1.7 mm in the test P-Y curve where the maximum

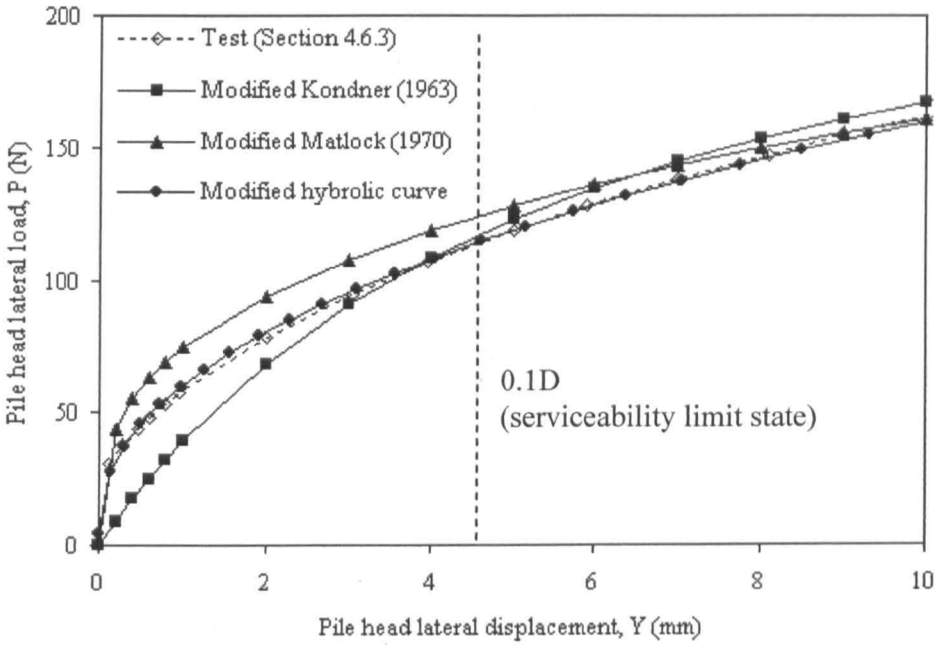

Fig. 7.1 Modified P-Y curves based on regression analysis of test results

curvature occurs, and the value 'Y_c' of 0.1087 mm is close to the point where the nonlinearity starts. The factors of P_u and Y_c in the equation should be redefined as:

- P_u is the load at the point of the P-Y curve with maximum curvature
- Y_c is the displacement at the point where the linear behaviour ends

Further curve simulation was carried out, and the curve which best matches the measured results was generated from regression analysis using a statistical programme Sigmaplot. The modified curve is shown as follows:

$$P = P_0 + a(Y)^b = 4.55 + 55.81(Y)^{0.444} \tag{7.3}$$

Compared to other equations, this equation contains the initial resistance P_0 and the power function, b, in displacement, Y, which ensures that the modified curve fits the entire measured results particularly in the high initial soil response and the low resistance developed in the larger displacement region.

Future research

Future studies of P-Y curve may focus on two targets: to improve the quality of P-Y curve simulation, and to define the parameters in the equation which should be meaningful in soil mechanics. Good qualitative simulation of the P-Y curve can be achieved by using a suitable regression formula and by adopting the correct pile soil

parameters in the calculation. The equation should include meaningful parameters such as the initial load, the ultimate lateral load, the serviceability load and the serviceability displacement or other significant factors.

Load direction

Test results

The change in the direction of a lateral load on a pile may cause changes in the lateral resistance because of changes to the mobilised pile stiffness EI and the effective area of resistance. The shape of a finned pile has the advantage of geometrical symmetry because the four fins have the same width and thickness and fins are welded onto the pile at 90° to each other. Fig. 5.3 demonstrates that the EI values of a finned pile remain the same when the service pile was subjected to a lateral load coming from different directions. Results from numerical modelling by LUSAS (Fig. 3.27) show that P-Y curves of FPS210 subjected to 0° and 45° lateral loadings to the fins are very close. Curves obtained from small scale tests indicate slightly higher resistance for 45° compared to 0° (Fig. 5.2).

Interpretation of effective area and soil resistance

In order to estimate the influence of load direction on the effective area of soil resistance, Fig. 7.2 represents the variation of fin effective area and ultimate soil resistance per unit length with two different load directions: 0° and 45° facing the fins. Smith (1987) proposed that the distribution of lateral soil resistance on a monopile is composed of normal soil resistance and shear drag as shown in Fig. 7.2(a). Based on the Smith model, the effective area and the distribution of soil resistance for a finned pile subjected to a lateral load from different directions is presented in Fig. 7.2(b) and (c). The soil around the finned pile (shown as the area enclosed by dashed line in Fig. 7.2(c)) may work as a block with the pile. According to the schematic diagrams and their equations of soil resistance in Fig. 7.2, the effective area to resist normal earth soil pressure of a finned pile subjected to a load at 0° to the fins is larger than that of a finned pile subjected to a load at 45° to the fins; the effective area to resist shear drag of a finned pile subjected to a load at 45° to the fins is larger than that of a finned pile subjected to a load at 0° to the fins. The differences of ultimate soil resistance between these models are presented in Table 7.2 showing that the influence of the load direction on the lateral resistance of a finned pile depends on the values of the

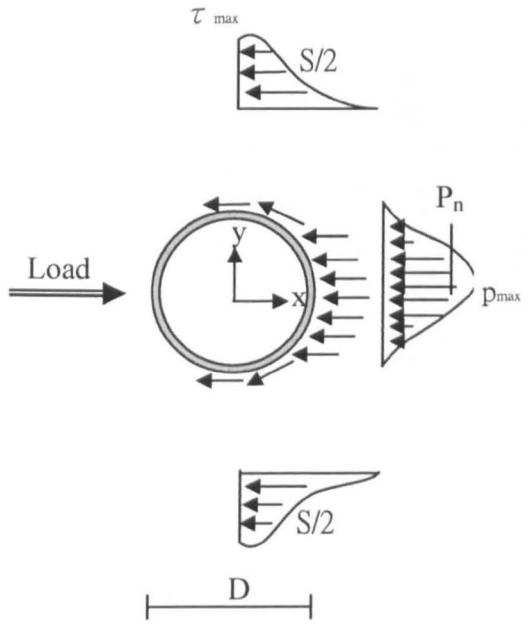

The ultimate lateral soil resistance p_u can be expressed as (Smith 1987)

$p_u = P_n + S$
$= \eta p_{max} D + \xi \tau_{max} D$

where
P_n = net ultimate frontal normal soil resistance (force/length)
S = net ultimate lateral shear drag (force/length)
η= shape factor (0.8 for circular; 1.0 for square)
ξ= shape factor for shear (1.0 for circular; 2.0 for square)
D = pile diameter

For a monopile
$p_u = P_n + S$
$= 0.8\, p_{max} D + 1.0 \tau_{max} D$

(a)

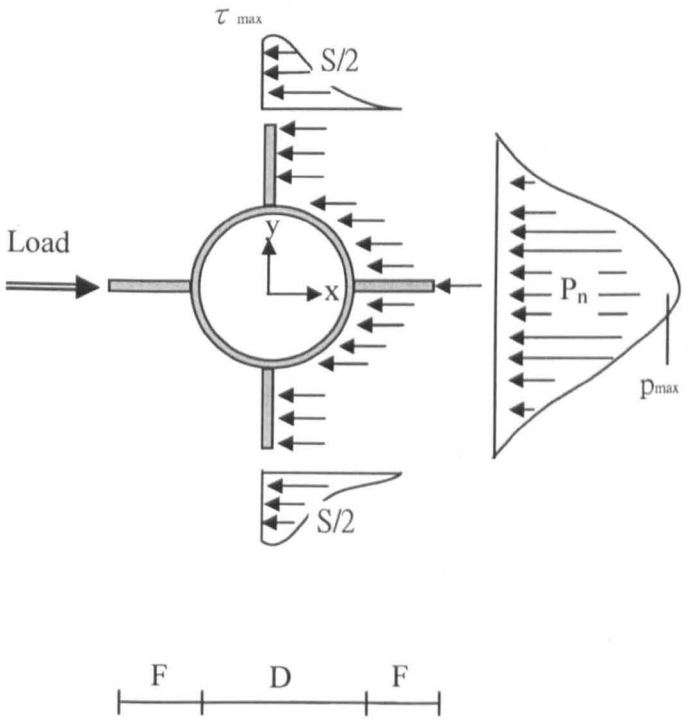

The ultimate lateral soil resistance p_u can be expressed as

$p_u = P_n + S$
$= \eta p_{max} (D+2F) +$
$\xi \tau_{max} (D+F)$
where
P_n = net ultimate frontal normal soil resistance (force/length)
S = net ultimate lateral shear drag (force/length)
η= shape factor (0.8 for circular; 1.0 for square)
ξ= shape factor for shear (1.0 for circular; 2.0 for square)
D = pile diameter
F = fin width

A finned pile subjected to load at 0°
$p_u = P_n + S$
$= 0.8 p_{max} D + 2.0 p_{max} F +$
$1.0 \tau_{max} D + 2.0 \tau_{max} F$

(b)

Fig. 7.2 Distribution of front earth pressure and side shear around the pile (a) monopile (after Smith, 1987); (b) a finned pile subjected to load at 0°

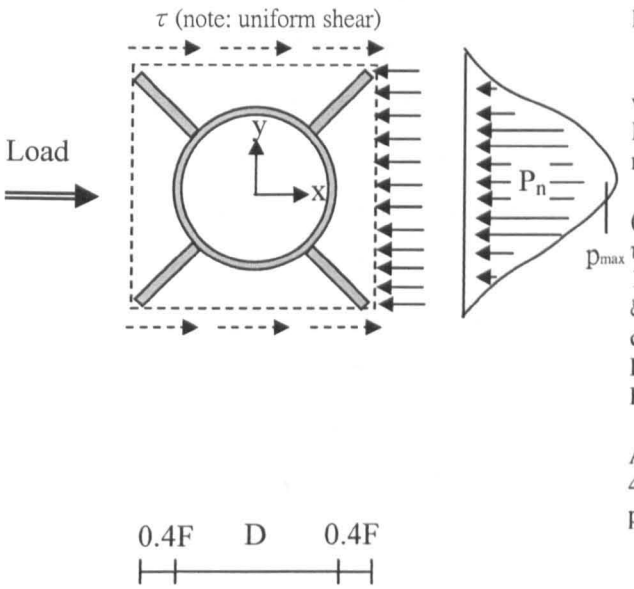

The ultimate lateral soil resistance p_u can be expressed as

$p_u = P_n + S$
$= \eta p_{max} (D+2(0.6)F) + \xi \tau_{max} (D+2(0.6)F)$

where
P_n = net ultimate frontal normal soil resistance (force/length)
S = net ultimate lateral shear drag (force/length)
η= shape factor (0.8 for circular; 1.0 for square)
ξ= shape factor for shear (1.0 for circular; 2.0 for square)
D = pile diameter
F = fin width

A finned pile subjected to load at 45°

$p_u = P_n + S$
$= 0.8p_{max}D + 1.2p_{max}F + 1.0\tau_{max}D + 2.4\tau_{max}F$

(c)

Fig. 7.2 Distribution of front earth pressure and side shear around the pile (c) a finned pile subjected to load at 45°

Table 7.2 Comparison of the ultimate soil resistances in the fin section

Model piles	Equations for the ultimate lateral resistance	
	General	Modified for assigned pile
MPS	$0.8\ p_{max}\ D + 1.0\tau_{max}\ D$	$(0.8\ p_{max} + 1.0\tau_{max})D$
FPS210 (load at 0°)	$0.8p_{max}D + 2.0p_{max}F$ $+1.0\tau_{max}D + 2.0\tau_{max}F$	$(1.8p_{max} + 2.0\tau_{max})D$
FPS210 (load at 45°)	$0.8p_{max}D + 1.2p_{max}F$ $+1.0\tau_{max}D + 2.4\tau_{max}F$	$(1.5p_{max} + 2.4\tau_{max})D$
Note: set F= 0.5D in the case of FPS210; assume p_{max} and τ_{max} are constant in the analysis		

maximum ultimate normal soil resistance, p_{max}, and the maximum shear resistance, τ_{max}. If the value of τ_{max} is between 0.1 p_{max} and 0.2 p_{max} in the analysis, the ultimate lateral load for FPS210 subjected to a load at 45° is in the range of 0.96 and 1.03 of that of FPS210 subjected to a load at 0°; this result is very close to that observed from model tests (Section 5.2.2). Note, however that 4% is insignificant compared to the assumptions made in the analysis. Therefore, in practical terms, the direction of the fins with respect to the load is insignificant.

The strain wedge model proposed by Ashor et al. (2002) was used to predict the soil response down the pile; the soil in front of the pile was presented as many passive wedges in layers as shown in Fig. 2.20. Soil resistance distribution in the fin section could be presented by the passive strain wedge. Fig. 7.3 shows the soil strain wedges established from different pile conditions. Strain wedges of the finned pile FPS210 are larger than that of the monopile MPS because of the fins. For a finned pile subjected to a load at 45° facing the fins, the wedge dimension varies according to the assumption of the reaction surface on the finned pile (Fig. 7.3(c) and (d)). The wedge shape is determined by the internal friction angles between pile and soil. The ultimate lateral resistance of FPS210 subjected to a load at 45° is between 0.9 and 1.1 that of FPS210 subjected to a load at 0°. This difference, though larger than that based on Smith's (1987) approach, is in practical terms not significant.

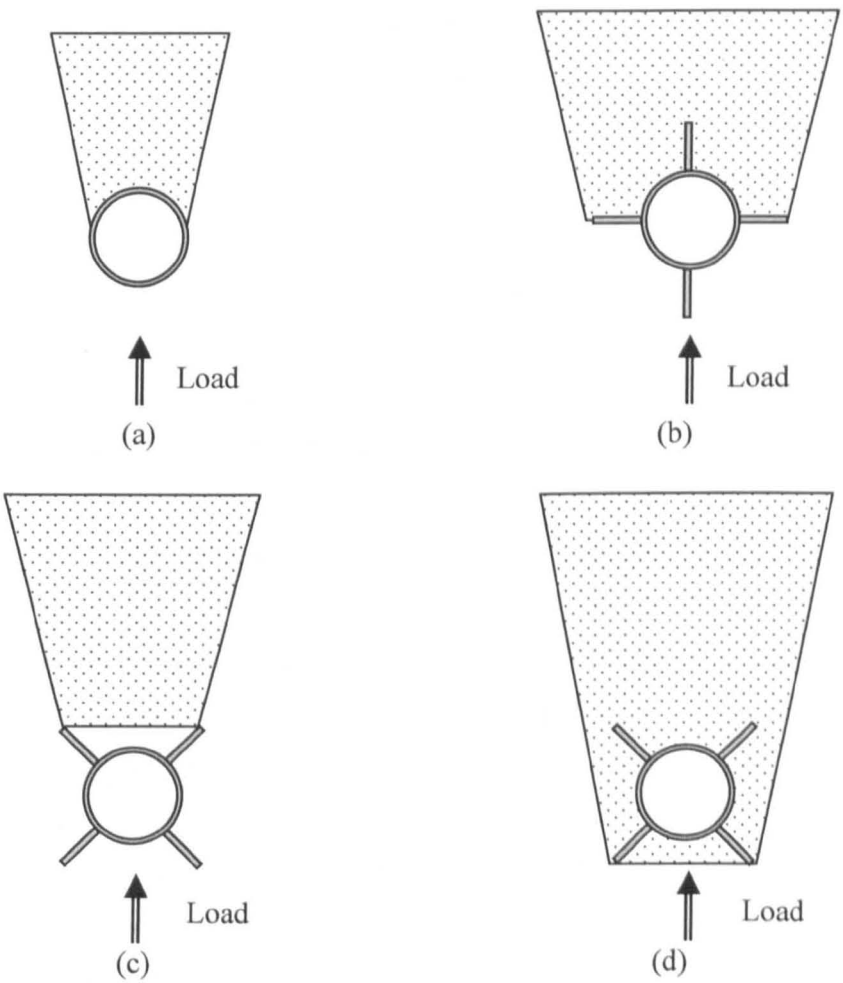

Fig. 7.3 Schematic diagrams of soil resistance region under lateral loading (a) a monopile, (b) a finned pile subjected to load at 0°; (c) a finned pile subjected to load at 45°(a conservative case) and (d) a finned pile subjected to load at 45°(a maximum response case)

The cross section of a finned pile should be maintained as shown in Fig. 3.1; the four fins should have the same dimensions. The main increase in EI comes from the front and the trail fins, and the side fins provide additional effective area to resist the load. Any changes in dimensions could lead to the loss of EI or the reduction of effective area in a critical load direction.

Future research

In future studies, the distribution of soil resistance for a finned pile should be investigated; the normal soil resistance in front of the pile and the shear drag should be assessed. It would also be important to study reasonable soil resistance factors η and ξ used for predicting soil pressure around the fins. A new soil reaction model should be able to predict the ultimate lateral resistance of a finned pile subjected to a lateral load from different directions. In addition, the pile soil interaction of finned pile with variable pile to soil stiffness should be assessed.

Fin position

The ideal fin location is on the top half of the pile as shown by numerical analyses (Fig. 3.28) and model tests (Fig. 5.5) since the soil resistance of piles with fins attached to the top and to the middle are higher than that of a pile with fins at the bottom. According to the distribution of stresses along the pile in Fig. 3.33, higher direct and shear stresses are concentrated at the upper part of the pile. The use of fins at the bottom of the pile may not provide lateral resistance particularly for long (flexible) piles because the lateral resistance is mainly provided by the section above the critical length.

The installation costs increase with an increase in the embedded depth. In order to reduce the costs of installation, the fins should be welded to the pile head. However, the scour around the pile at the sea bed level can affect the efficiency of lateral resistance of the fins. The maximum depth of scour (= 1.3D) under critical wave and sea bed conditions (DNV, 2004) means that the fins should be placed at a depth of 1.3 times the diameter of the pile underneath the sea bed to avoid the scour. This depth can be reduced if the wave condition is not very crucial or if sea bed protection is applied.

In future research, the influence of scour on the effective fin position may be investigated. The maximum depth of scour for a finned pile could be deeper than that for a monopile; the fin width should be included in the equation to determine the depth of scour.

7.1.3 Cyclic loading

Introduction

The increase in lateral resistance by using finned piles subjected to a static horizontal load is presented in Fig. 6.9. The static load was gradually increased by increasing the displacement at a very low rate of 1 mm/min to represent the static loading behaviour. An increase in fin length results in an increase in lateral resistance.

In order to investigate the influence of cyclic loading on the lateral resistance of a pile, a series of cyclic loading tests were completed (Section 6.2). Tests were carried out with up to 10,000 cycles to represent 10 years of environmental loading on a typical offshore structure with a lifetime of twenty years. This assumption is based on the number of cycles of loads developed during a hurricane (Bea et. al. in 1999) and on the principle of extreme value analysis (Holmes, 2001). The frequency of 0.65 Hz was used as the common frequency because the frequencies of environmental loads are between 0 and 1 Hz; the use of a low frequency of 0.65 Hz is able to represent cyclic loading without dynamic effects. A load magnitude of 25 N (about 16 % of the ultimate lateral load) was used as the standard load magnitude because the pile head lateral displacement of the test monopile could reach the serviceability limit state after 10000 cycles.

Frequency

Test results and interpretation

The increase in the lateral resistance of finned piles subjected to static loading was evaluated from the reduction in lateral displacement. An increase in loading frequency causes an increase in the lateral resistance of a monopile as shown in Fig. 4.16(a). Similarly, an increase in displacement with frequency also occurs in finned piles with different fin lengths (Fig. 6.3). Based on the results in Section 6.3.2, the reduction, R_I, of lateral displacement of finned piles subjected to one-way cyclic loading with different frequencies is presented in Fig. 7.4(a). The reduction in displacement increases with an increase in fin length, and the reduction at the lower

frequency (0.45Hz) is more significant than that at the higher frequency (0.65Hz). The difference in the reduction ratio, R_I, between low and high frequencies is 27% when the fin length is half of the pile length.

In current design codes for offshore pile foundations like API (1993) and DNV (2004), the influence of loading frequency is not included; the change of frequency, however, affects the lateral displacement very significantly (Fig. 6.7(c)). In the design of finned piles based on static and general cyclic equations, the fin efficiency should not be overestimated especially under high frequency conditions. A reasonable reduction factor of 0.3 for high frequency is suggested (Fig. 7.4(a)).

Future research

In future research, a low frequency of less than 0.1 Hz should be assessed in order to simulate wave impaction. Combined frequency, a frequency with over one period, may be used to replace single frequency, and combined frequency could be used to investigate finned piles subjected to load impaction at different times. High frequency may be assessed for the study of seismic loading or the potential of liquefaction.

Load magnitude

Test results and interpretation

The influence of the magnitude of the load on the increase in lateral displacement is presented in Fig. 4.16(b), showing a proportional increase in lateral displacement as the load increases. In Fig. 6.3(a) and (d), the lateral displacements of finned piles with different fin lengths increase as the load magnitude increases from 25N to 50N which represent 0.16 and 0.32 of the ultimate lateral load, P_u (155N) of a monopile, respectively.

Based on the results in Section 6.3.2, the reduction, R_I, of lateral displacement of finned piles subjected to one-way cyclic loading with different loads is presented in Fig. 7.4(b). The reduction in displacement increases with an increase in fin length. The reduction at high load magnitude ($0.32P_u$) is more significant than that at low load magnitude ($0.16P_u$); the difference of reduction of lateral displacement R_I increases from 4% to 10% when fin length increases from 25% to 50% of the pile length.

Although an increase in load magnitude causes an increase in the lateral displacements of the monopile and finned pile, an increase in fin length results in a

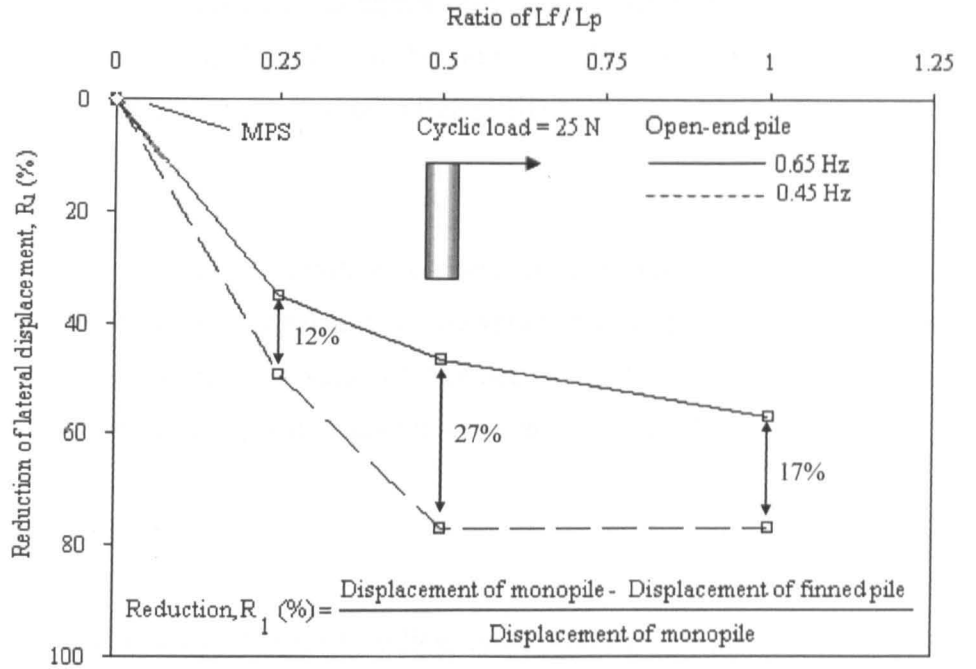

(a)

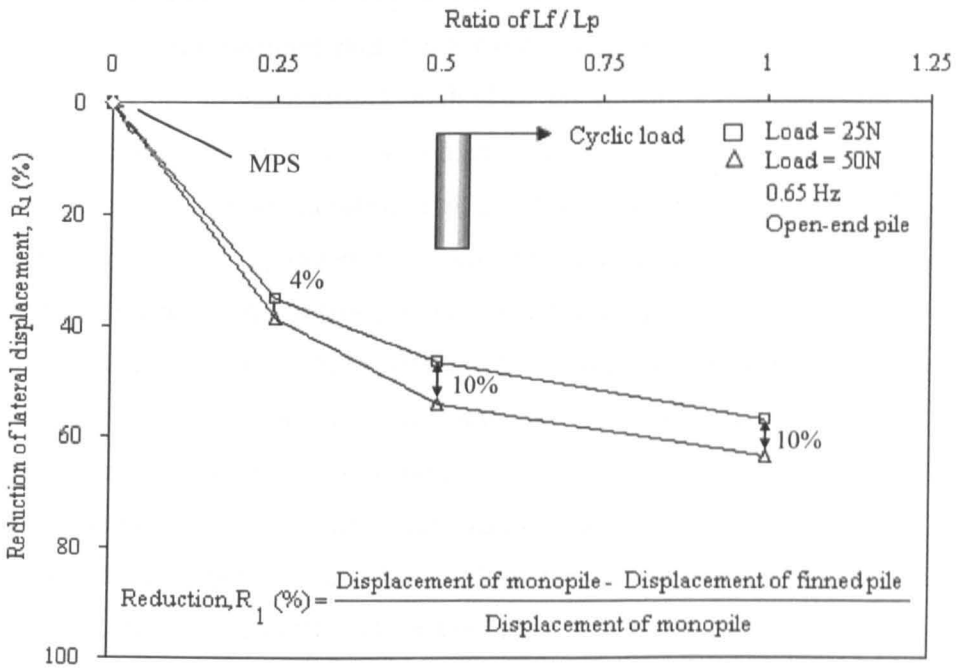

(b)

Fig. 7.4 Variation of the reduction of lateral displacement with the ratio of fin length to pile length with (a) different frequencies (b) different load magnitudes

higher reduction in lateral displacement especially at high load magnitude. Load magnitudes of cyclic loading were only less than one third of the ultimate lateral load.

If finned piles are subjected to higher cyclic loads, the corresponding reduction of lateral displacement, R_l, should be much higher than that of a monopile, demonstrating the advantage of using finned piles.

Future research

In future studies, the critical load magnitude should be assessed. The critical load is defined as the load value when the variation of displacement with cycles does not converge to a constant value of displacement. The relationship between load magnitude and frequency with regard to serviceability load should be studied.

Loading condition

Test results

Based on the direction of loading, cyclic loading on a pile can be classified as one-way, two-way balanced and two-way out of balanced. One-way cyclic loading tests are used to simulate a pile subjected to a significant cyclic load from a constant direction, with small environmental loads from other directions being ignored. One-way cyclic loading is a simplified method to investigate the relationship between lateral displacement and the impact of loading in cycles. Two-way balanced cyclic loading tests are used to simulate a pile subject to environmental loads which repeatedly act in opposing directions. Two-way out of balanced loading is a realistic method to simulate a pile subjected to combined loads including wave, current, tide and wind which could come from different directions with various magnitudes. The frequencies of loads in out of balanced loading are assumed to be the same as those in balanced loading. In two-way loading, the variation of both vertical and lateral displacements with the number of cycles was investigated.

Results in Sections 6.2.2 and 6.2.3 show that piles subjected to different kinds of loadings respond differently both in the lateral and vertical directions. Open-end piles under two-way balanced loading show insignificant lateral displacement but very large vertical displacement (Fig. 6.4(a)); the vertical displacement was reduced by installing a cap at the base of the piles (Fig. 6.4(c)). Piles under two-way out of balanced loading demonstrate less vertical displacement compared to those under balanced loading (Fig. 6.4 (a) and (b)). The lateral displacement of piles under out of balanced loading is larger than that under balanced loading (Fig. 6.4 (c) and (d)).

Finned piles reduce the vertical and lateral displacements compared to those for a monopile.

Interpretation

Fin efficiency is represented by the reduction in displacement, R_I. Under two-way balanced loading, the reduction R_I in vertical displacement for open-end piles is higher than that for close-end piles, and the difference in the reduction ratio increases with an increase in fin length (Fig. 7.5(a)). Under the same condition, the reduction, R_I, in lateral displacement for open-end piles is smaller than that for close-end piles, and the difference of R_I has the largest value when the fin length is half of the pile length (Fig. 7.5(b)). Under two-way out of balanced loading, the reduction R_I in vertical displacement for open-end piles is significantly larger than that for close-end piles; the difference of R_I rises up to 80% when the fin length is half of the pile length (Fig. 7.6(a)). Under the same loading condition, the reduction of lateral displacement for close-end piles is slightly larger than that for open-end piles (Fig. 7.6(b)).

Through this comparison of the reduction R_I in displacement by using different finned piles, four outcomes are evident as follows:

- Fins reduce the vertical and horizontal displacements for static, cyclic balanced and out of balanced loads.
- The majority of the reduction occurs with fins in the top half of the pile.
- Increasing the frequency of loading reduces the lateral resistance of piles.
- Lateral and vertical displacements for solid or close ended piles are less than those for open ended piles.

Future research

Tests for loading conditions provided typical examples to assess piles subjected to different ways of loading. It must be noted that lateral loads could come from different directions instead of being from one direction. In future studies, two-way cyclic loads 90° to each other could be applied to the pile head, and two-dimensional cyclic loading model could be established.

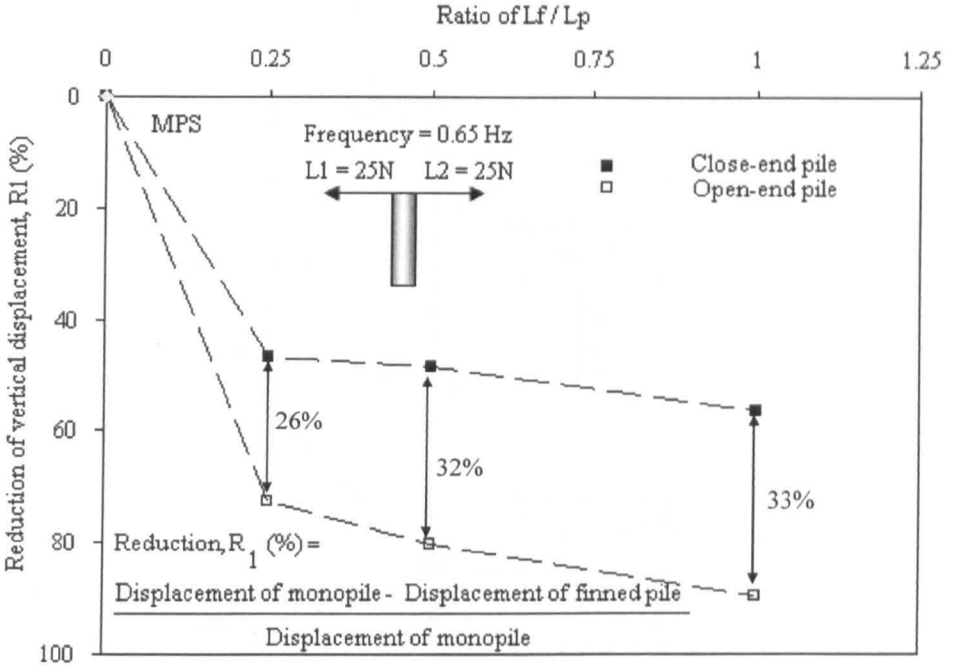

(a)

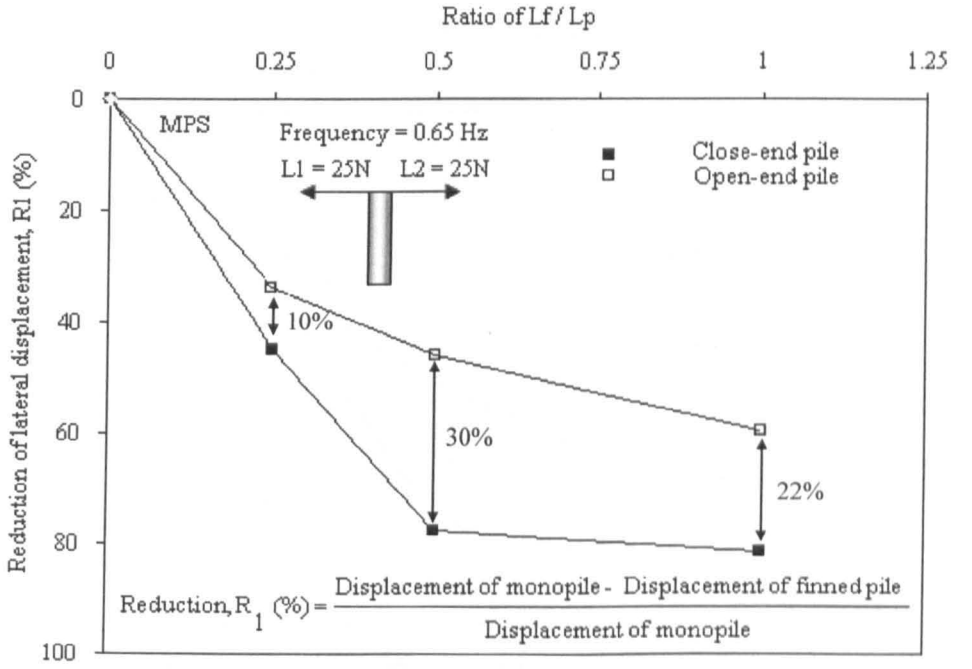

(b)

Fig. 7.5 Variation of the reduction of displacement with the ratio of fin length to pile length for piles subjected to two-way balanced cyclic loading; (a) vertical displacement, and (b) lateral displacement

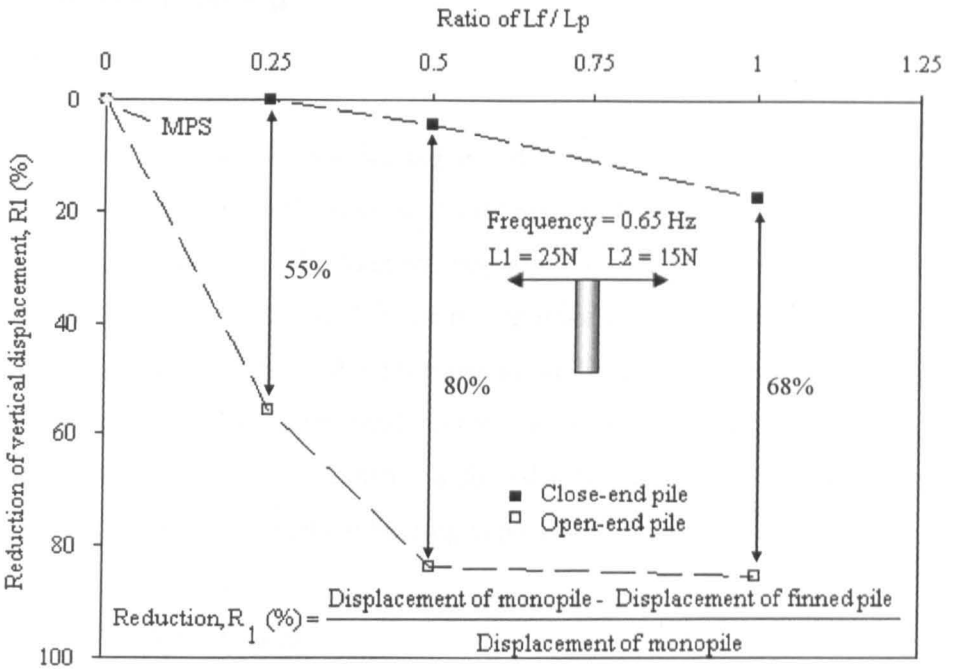

(a)

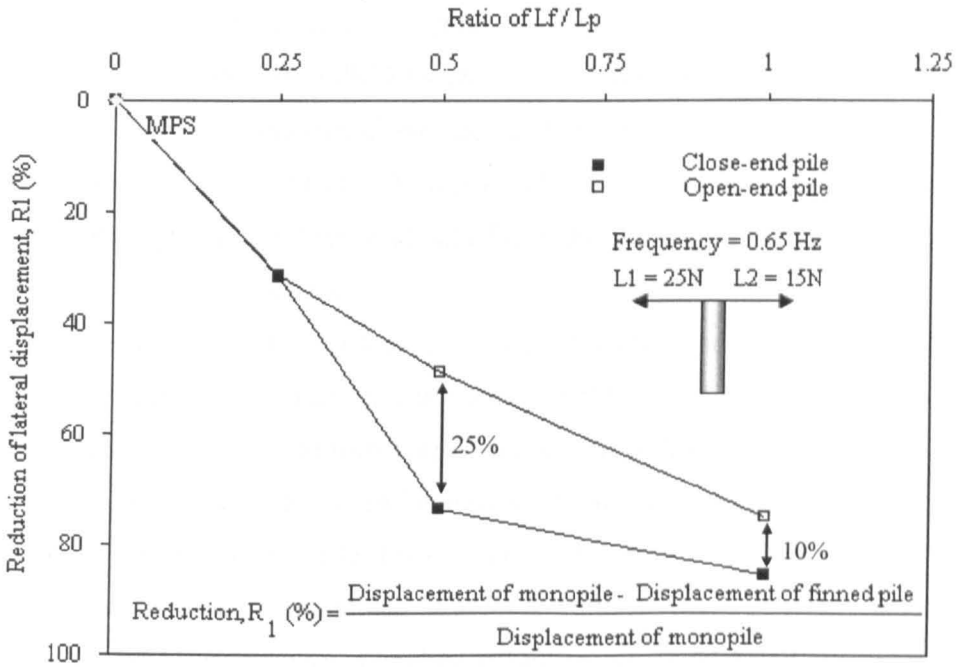

(b)

Fig. 7.6 Variation of the reduction of lateral displacement with the ratio of fin length to pile length for piles subjected to two-way out of balanced cyclic loading; (a) vertical displacement, and (b) lateral displacement

7.1.4 Combined loading

Static loading

Test results

Piles under combined loading behave differently to those under lateral loading only. Results presented in Section 5.2.5 and Section 6.2.5 show the lateral capacity of piles under static and cyclic loading, respectively. In static loading, the ultimate lateral loads of piles were about 20% of the ultimate vertical loads, and the variation of ultimate lateral load with the increase in vertical load is shown in Fig. 5.9. Normalised envelopes of combined loading in Fig. 5.14 represent a significant increase in lateral resistance by using a finned pile when the vertical loading was below 75% of the ultimate vertical bearing capacity.

Assessment of failure envelope

Fig. 7.7 compares the failure envelope taken from Equation 2.18(a) proposed by Meyerhof and Purkayatha (1985) with the envelope from the tests in Section 5.2.5. According to the Meyerhof method, the relationship between normalised vertical and lateral loads can be presented as a circular equation with a constant radius. Failure envelopes of the finned pile FPS210 were always larger than those of the monopile MPS. However, the Meyerhof method underestimated the increase in lateral resistance in both MPS and FPS210, in particular the vertical resistance ratio (Q/Q_u) was 0.8 where Q is the vertical load, and Q_u is the ultimate vertical load measured when there is no lateral loading.

In the design of laterally loaded piles of offshore wind foundations subjected to combined loading, the failure envelope should not be based on Equation 2.18 alone which is conservative. In the tests carried out by Meyerhof and Purkayatha (1985), the service pile was subjected to an inclined load with different inclined angles until failure was reached. In the model tests of this study, vertical load was applied to the pile before the increase in lateral load in order to simulate offshore wind foundations. In offshore wind farms, gravity is applied before environmental and operative loads; in the operation of wind farms, the vertical load does not increase dramatically but the lateral load may increase due to severe environmental conditions. In the Meyerhof method, the increase in lateral resistance causes a reduction in vertical resistance which ignores the fact that the pile end bearing capacity can provide significant vertical resistance. In the model tests, a tip installed at the pile base was used to

simulate close end pile which could significantly improve bearing capacity especially for short rigid piles.

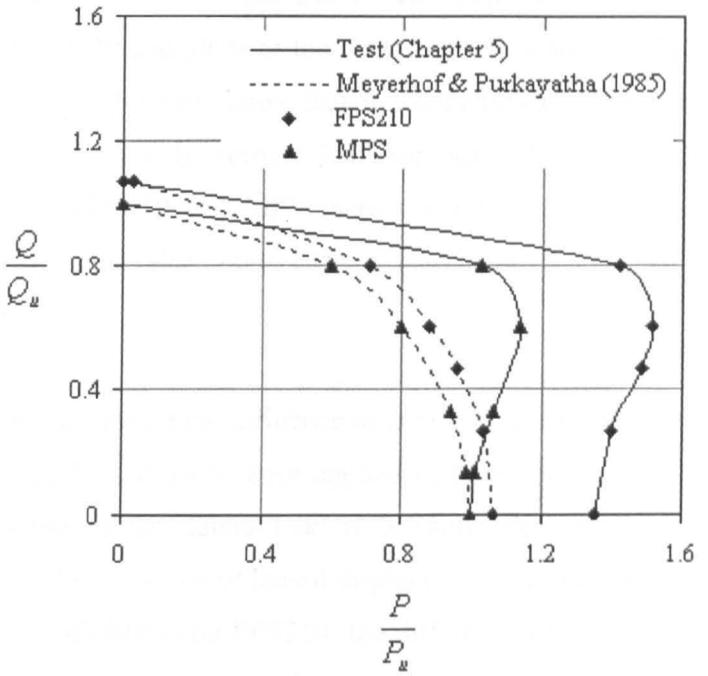

Fig. 7.7 Comparison of failure envelopes of a monopile and of a finned pile from the Meyerhof method and test results

Future research

Combined loading is used to model finned piles subjected to loading when wind farms are in operation. In further studies, the influence of the ratio of pile tip bearing capacity to shaft resistance along the pile on the failure envelope should be assessed. Unlike a long pile with high shaft resistance, a monopile is treated as a rigid pile with its bearing capacity provided mainly by pile tip resistance. In the future, failure envelopes should be established from different ratios of pile tip to pile shaft capacities.

Cyclic loading

Piles subjected to combined cyclic loading may behave differently to those under combined static loading. The increase in lateral resistance for combined cyclic loading can be evaluated by the reduction of lateral displacement of the pile head.

The fin efficiency to lateral resistance could be affected by vertical and lateral loads, and frequency as described in Section 6.3.5.

Vertical load

Vertical loads of 80, 160 and 240 N were applied in an attempt to simulate piles subjected to 10, 20 and 30 % of the ultimate vertical load of the monopile (750 N), respectively. Fig. 6.13(a) shows that the reduction of lateral displacement R_2 increases with an increase in vertical load for both MPS and FPS210. The R_2 difference between FPS210 and MPS increases with an increase in vertical load which implies that finned piles improve lateral resistance.

Lateral load

In order to investigate the influence of lateral load on combined cyclic loading, lateral loads of 15, 25 and 35 N were applied to represent piles subjected to 10%, 16% and 22% of the ultimate lateral load of the monopile (155N), respectively. Fig. 6.13(b) shows that the reduction of lateral displacement R_3 decreases with an increase in lateral load for both MPS and FPS210; the difference of R_3 between FPS210 and MPS under high lateral load is higher than that under low lateral load; resulting in an increase in fin efficiency under high lateral load.

Frequency

Three low frequencies of 0.45, 0.65 and 0.94 Hz were applied to study the influence of speed. Fig. 6.13(c) shows that the reduction of lateral displacement R_4 decreases with an increase in frequency. Although lateral displacement increases due to an increase in frequency, the larger difference of R_3 between FPS and MPS at high frequency compared to that at low frequency demonstrates that fin efficiency is higher at high speed of combined cyclic loading.

Future research

Combined cyclic loading tests provided an initial simulation to possible loading on offshore pile foundations. In order to achieve realistic modelling of operated piles, future studies should include the influence of two-way loading and the ratio of pile end bearing to pile shaft resistance.

7.2. Pile soil behaviour of finned piles

7.2.1 Introduction

Pile head load and displacement curves (P-Y curves) were used to show the increase in lateral resistance by using finned piles. The distribution of deformation, bending moment and stress when a finned pile is used to replace a monopile cannot be determined from P-Y curves. In order to improve lateral resistance efficiently by using finned piles, it is important to understand the complete behaviour of finned piles under both static and cyclic loadings.

The increase in lateral resistance is accompanied by:

- The movement of the pile rotation point, and the variations of pile displacement with depths particularly in the movement of side fins (Fig. 3.6 and 3.32).
- An increase of bending moment above the fin base, and the reduction of the maximum bending moment (Fig .3.11 and 5.13(b)).
- The distribution of shear and direct stresses of the finned pile with depths especially on the fins; the reduction of shear force by using the fins (Fig. 3.12, 3.33 and 5.13(c)).
- An increase in resistance in the fin section and the reduction of maximum soil resistance at the pile base (Fig. 3.13 and 5.13(d)).

A finite difference (FDM) analysis using the LPILE program was carried out. Results showed the variation of pile behaviour along the pile, and it verified that finned piles have better lateral resistance compared to that of monopiles. LPILE is a two dimensional analysis in which a pile is modelled as a bar with different section stiffnesses.

A finite element (FEM) analysis using the LUSAS program was conducted. The influence of fins on lateral resistance was estimated by pile head P-Y curves and three-dimensional deformation and stress charts. The effect of the fins was demonstrated showing the movement of soil around the pile and the distribution of stresses on the fins. The interface between the soil and the pile as well as the soil model needs to be improved in order to simulate the real interaction between the pile and soil.

Strain gauges were used to measure strain along a test pile. Pile and soil behaviour was estimated by transforming the measured strains to moments, shear

forces, soil resistances and displacements along the pile through polynomial equations. The effect of the fins on behaviour of finned piles can be observed.

7.2.2 Lateral displacement

Lateral displacements along the monopile, MPS and the finned pile, FPS210 were estimated by LPILE and small-scale testing. According to the variation of displacement with depth as shown in Fig. 3.6, Fig. 4.24(d) and Fig. 5.7(d), the displacement of piles has the following features:

- Both mono and finned piles rotate laterally with the point of rotation at a depth of about two-thirds of the pile length. The pile deformation was very small compared to its significant rotation. No apparent discontinuity of pile movement was observed at the base of the fins.
- The point of rotation moved down the pile as the lateral displacement of the pile head increased.
- The point of rotation for the finned pile was higher than that for the monopile; an observation made in the small scale tests.

The use of 3D LUSAS allowed a qualitative image to be generated to show the deformation of the fins (Fig. 3.2). The fins performed as cantilevers deforming due to the pressure created by soil resistance. The deformation increased as the thickness of the fins was reduced.

Pile stiffness is another important factor which directly affects the deformation of finned piles. FEM analysis was carried out to simulate the deformation of a rigid and of a flexible finned pile FPS210. The dimensions of the model rigid pile were based on the parameters shown in Table 3.1 (a) and (b). The dimensions of the flexible pile were the same as those of the rigid pile, but its thickness was reduced to only 1/1000 of that of the rigid pile. Fig. 7.8 shows the variation of deformation with depth at a pile head displacement of 20 mm. For the rigid pile, displacement was developed as a result of pile rotation. The pile did not deform. For the flexible pile, displacement was developed as a result of the pile bending. Significant pile deformation occurred at the pile head, and side fins had very large deformation. No movement was observed at the pile base.

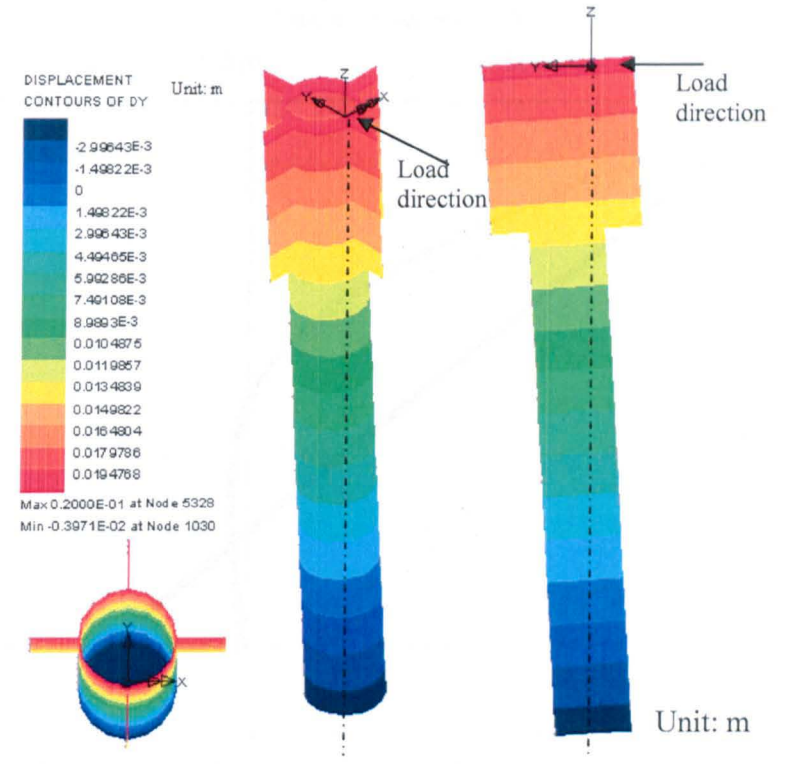

(a)

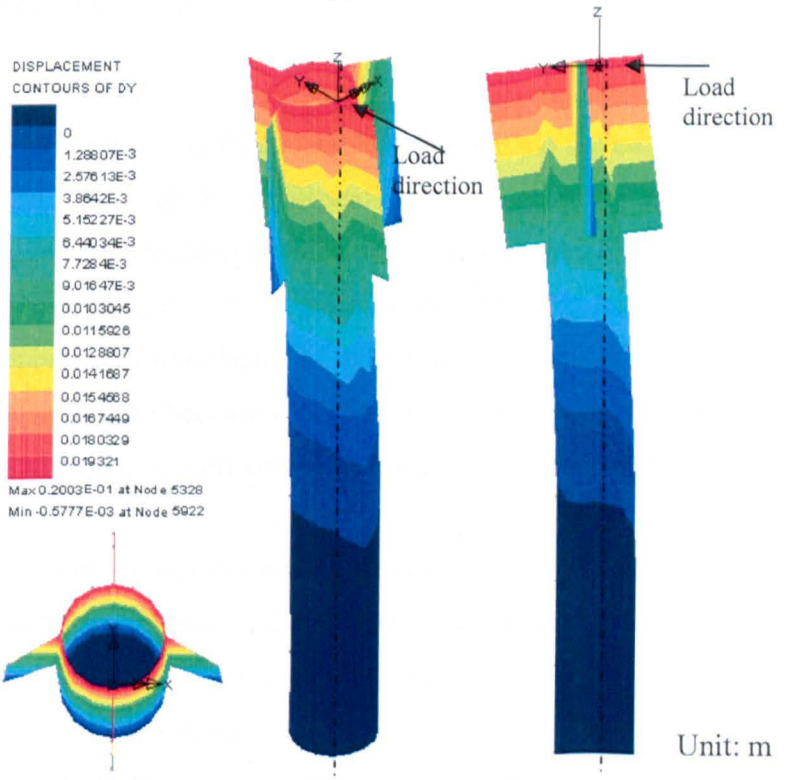

(b)

Fig. 7.8 Deformation in the direction of loading of finned piles when pile head lateral displacement is 20 mm. (a) rigid pile; (b) flexible pile (by LUSAS)

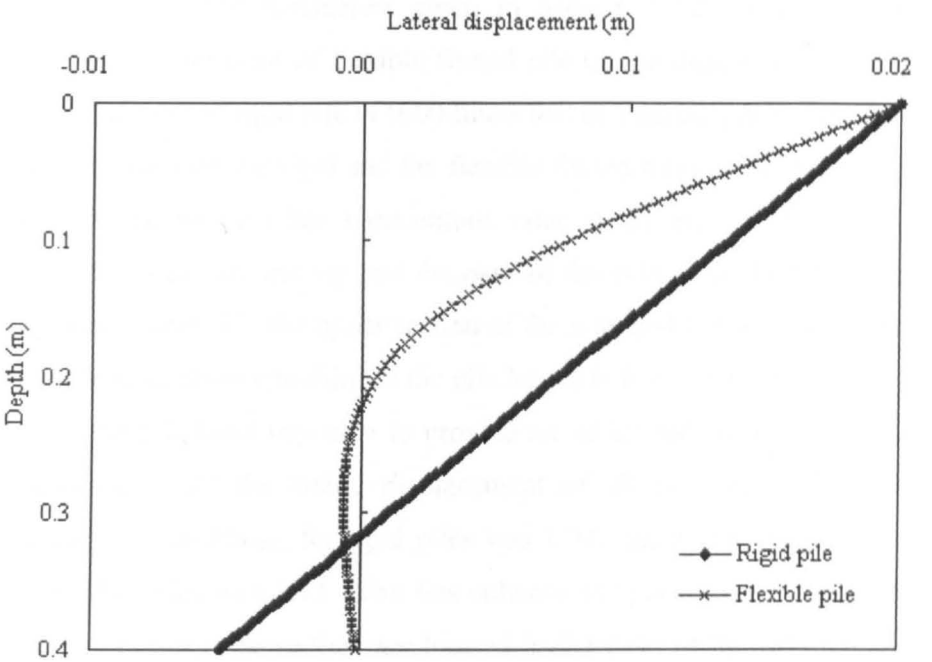

(c)

Fig. 7.8 Lateral deformation of finned piles when pile head lateral displacement is 20 mm. (c) comparison by LPILE

7.2.3 Bending moment

Bending moments along the monopile, MPS and the finned pile, FPS210 were calculated using LPILE and the small-scale tests. According to the relationship between bending moment and depth which has been presented in Fig. 3.7, Fig. 4.24(a) and Fig. 5.7(a), the bending moment of piles has the following features:

- No apparent discontinuity of pile bending moment was shown in the modelled results because a continuous equation was used. An increase in moment in the section above the fin base was presented in the measured results.
- The position of maximum bending moment moved down when the lateral displacement (or load) of the pile head increased.
- The position of maximum bending moment for a finned pile was higher than that for a monopile.

At the same lateral load magnitude or lateral displacement, the maximum bending moment of the finned pile was less than that of the monopile because fins provided more resistance which reduced the maximum bending moment on the pile.

Computer modelling by LPILE was carried out for a rigid pile and a flexible pile using the pile soil parameters given in Section 7.2.2. Fig. 7.9 shows the maximum bending moment of flexible finned pile is one-third that of the rigid pile (note: wall thickness of rigid pile is 1000 times that of flexible pile). The distribution of bending moment on the rigid and the flexible finned piles are very different. For the rigid pile, the moment has a maximum value at the middle of the pile, and it gradually reduces toward the top and the base of the pile. For the flexible pile, the moment is concentrated in the upper section of the pile, and the position of maximum bending moment is about one-third of the pile length below the ground level. The use of fins near the pile head was able to provide an additional stiffness EI to increase lateral resistance. At the lateral displacement of 20 mm, the ratio of bending moments $M_{(FPS210)}$ to $M_{(MPS)}$ for rigid piles was 1.04; under the same condition, the ratio for flexible piles was 1.13. The fins enhance the performance of flexible piles more than rigid piles because they are located in the zone of the maximum bending moment.

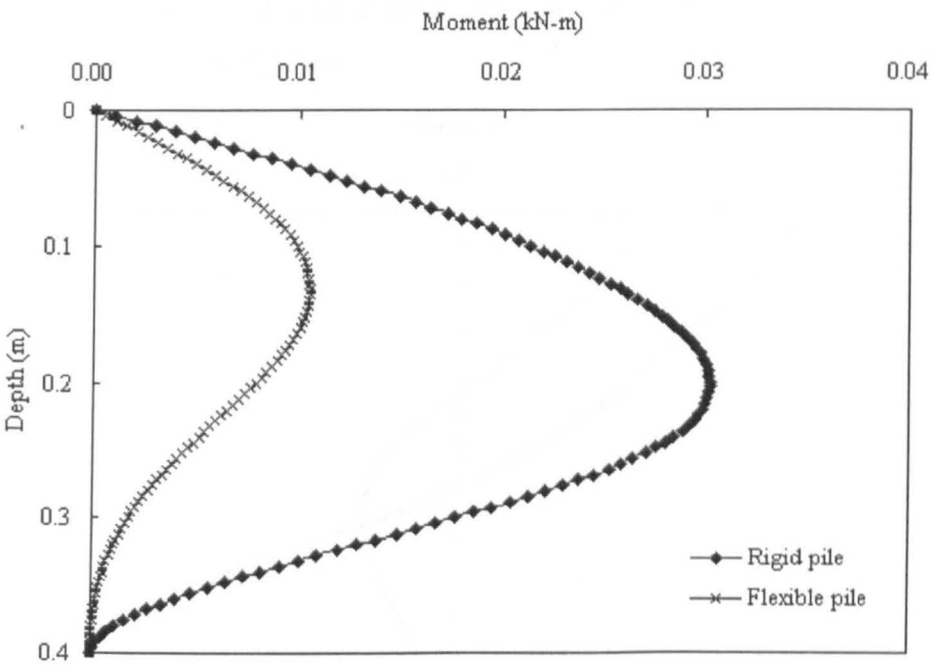

Fig. 7.9 Bending moment of finned piles when the pile head lateral displacement is 20 mm (by LPILE)

7.2.4 Shear force and stress

The distributions of shear force along finned and mono piles have been calculated by numerical methods and from strain gauge tests. An increase in shear force in the section above the fin base has been shown in Fig. 3.8(b) and Fig. 5.7(b). The discontinuity of shear force at the base of the fin is shown. The maximum shear force was reduced by using fins. The stresses on the finned pile are presented in Fig. 3.33 showing the significant direct stress at the middle section of the pile and the high shear stress close to side fins.

In order to predict the features of the shear force on flexible and rigid piles, the variation of shear force along the piles is presented in Fig. 7.10. Shear force on a flexible pile is less than that on a rigid pile at the same lateral displacement of 20 mm.

Bending and twisting of side fins should be considered especially for flexible piles due to low fin stiffness. The change of strain was used to investigate the stress distribution on the side fins because high shear strain (over 2%) reflects low stress. The variation of strain in y-z plane along the finned pile in Fig. 7.11 shows that the side fins have significant strain at the connections of the fins to the pile. The influence area and the value of strain on the side fins of the flexible pile are much higher than those of the rigid pile.

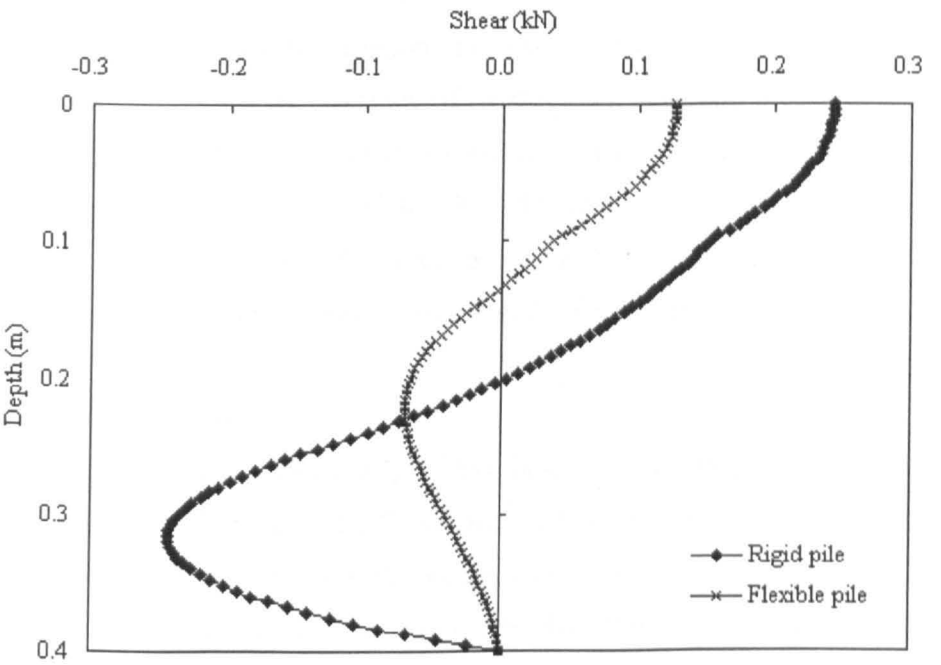

Fig. 7.10 Shear force of finned piles when the pile head lateral displacement is 20 mm (by LPILE)

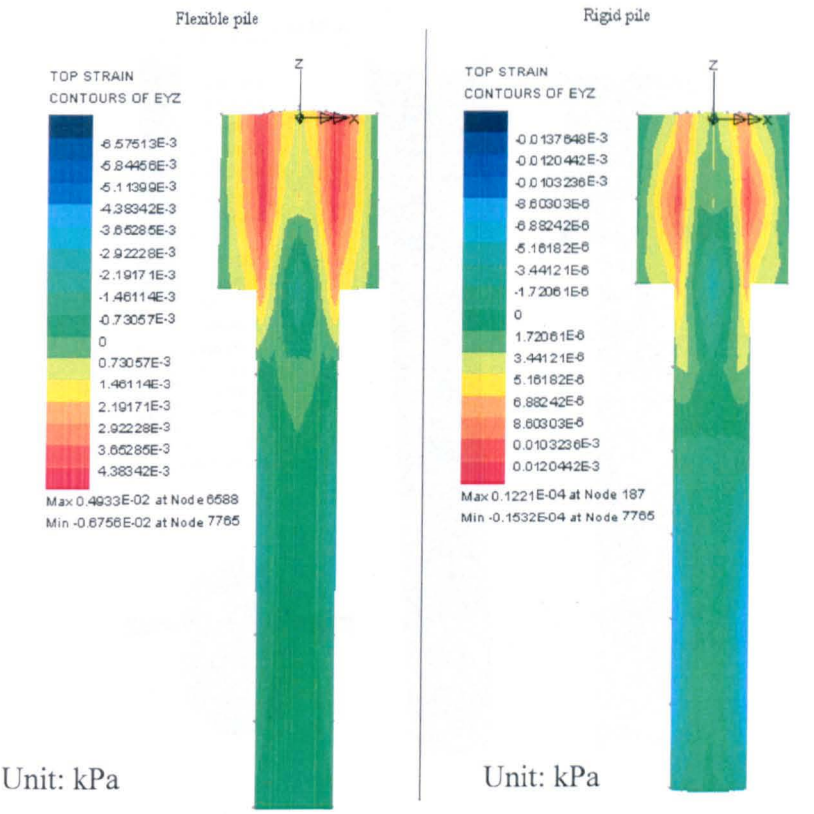

Fig. 7.11 Strain distribution in the local yz plane of finned piles when the pile head lateral displacement is 20 mm (by LUSAS)

Fig. 7.12 shows the variation of moment, Mxy, in local x-y plane along finned piles. Mxy represents the tendency of twist for pile wall and fins. For the rigid pile shown in Fig. 7.12(a), the side fins were twisted at the outer lower corner; for the flexible pile shown in Fig. 7.12(b), the side fins were twisted mainly at the outer middle section. The twist at the outer corner can be treated as a local material failure; whereas, the twist at the middle corner should be considered as a global fin failure.

7.2.5 Soil response

Soil resistance along a pile has been presented in Fig. 3.9 showing an additional soil resistance in the fin section and the discontinuity of soil resistance at the fin base. The maximum soil resistance on a pile is reduced by using fins since they provide extra resistance in the fin section (Fig. 3.13). Model tests showed similar results, but the maximum soil resistance was not reduced significantly by using a finned pile (Fig. 5.13(d)).

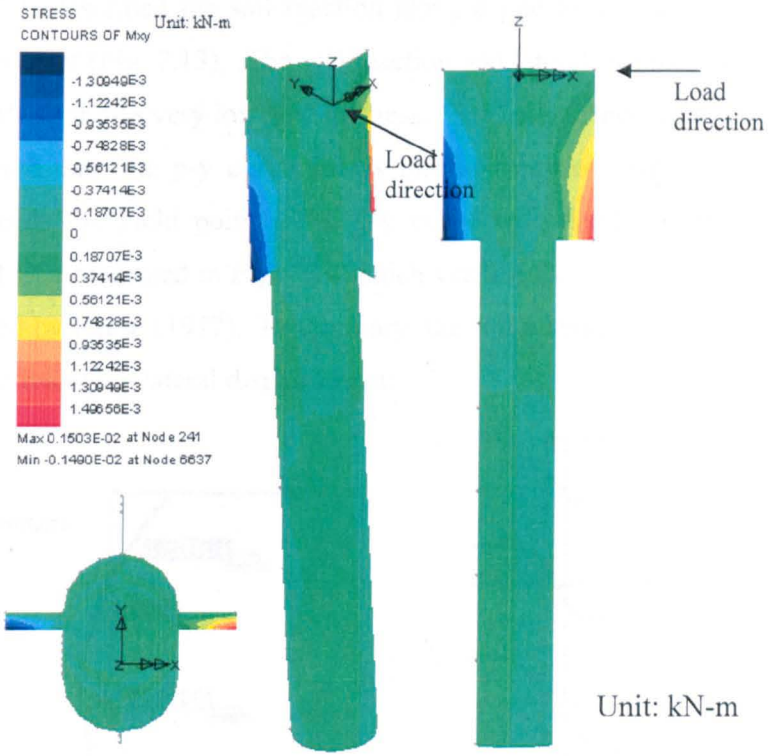

(a)

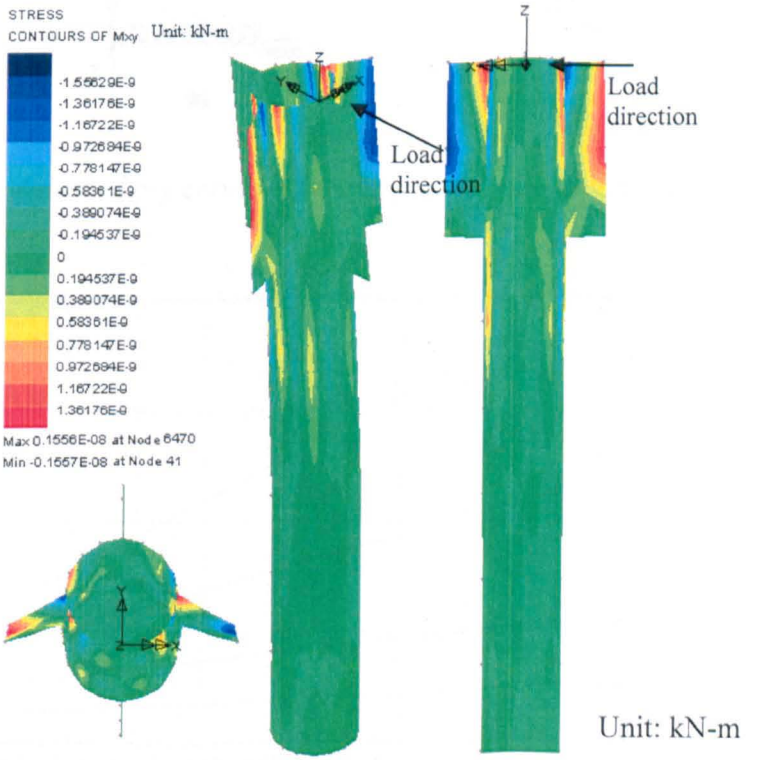

(b)

Fig. 7.12 Local twisting Mxy for finned piles (a) rigid (b) flexible

Reese (1977) described the soil reaction along a pile as a function of depth and lateral displacement (Fig. 7.13). The soil reaction and lateral displacement curve (p-y curve) at depth Z_1 shows very low soil stiffness. The soil stiffness increases with an increase in depth, and the p-y curve shows plastic behaviour when the lateral displacement exceeds the yield point. The p-y curve with depth for small scale modelling by LPILE is presented in Fig. 7.14 which verifies the relationship between p and y as proposed by Reese (1977). In summary, the soil response in a pile section depends on the depth and the lateral displacement.

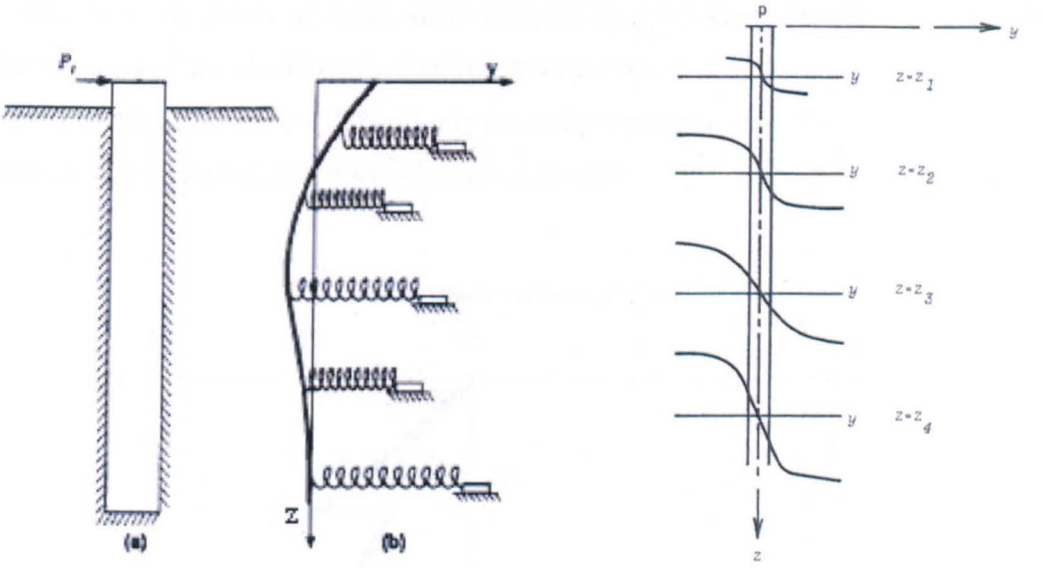

Fig. 7.13 Representation of p-y curves of laterally loaded pile (Source: Reese, 1977)

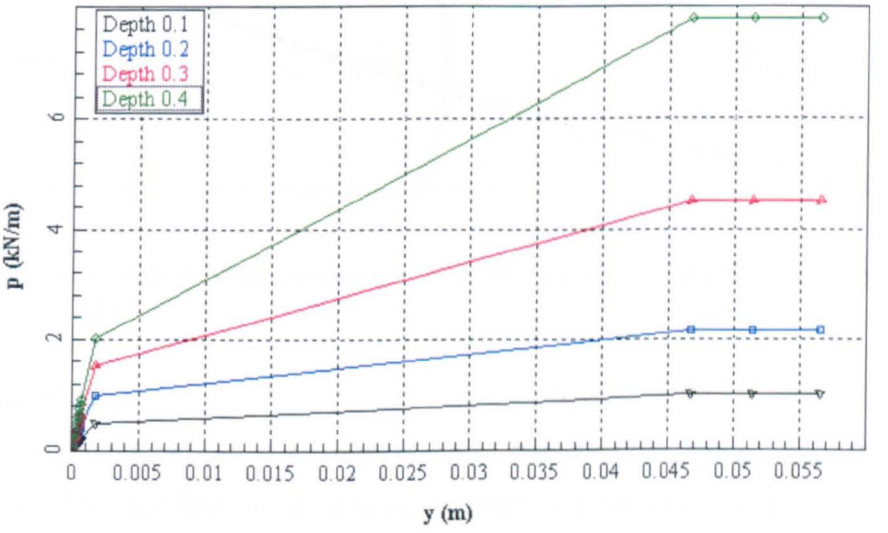

Fig. 7.14 Variation of p-y curve with depth for small scale modelling by LPILE

Soil reactions including movement and strain derived from 3D FEM analysis are shown in Fig. 3.31(c) and 3.33, respectively. The influence zone of soil response has been described in Section 3.3.5. The variation of soil resistance along the rigid and the flexible finned piles presented in Fig. 7.15 shows that the distribution of soil resistance is affected by pile stiffness. In the upper section, the p-y curves of rigid and flexible piles are the same. In the lower section, the soil resistance of the rigid pile is significantly larger than that of the flexible pile. At the pile base, the soil resistance of the rigid pile is very high because the pile rotates. According to the plastic strain diagrams of small scale analysis by LUSAS shown in Fig. 7.16, the plastic strain of the flexible pile concentrates near the ground level at the front of the pile. The plastic strain of the rigid pile not only concentrates near the ground level at the rear of the pile but also distributes along the pile.

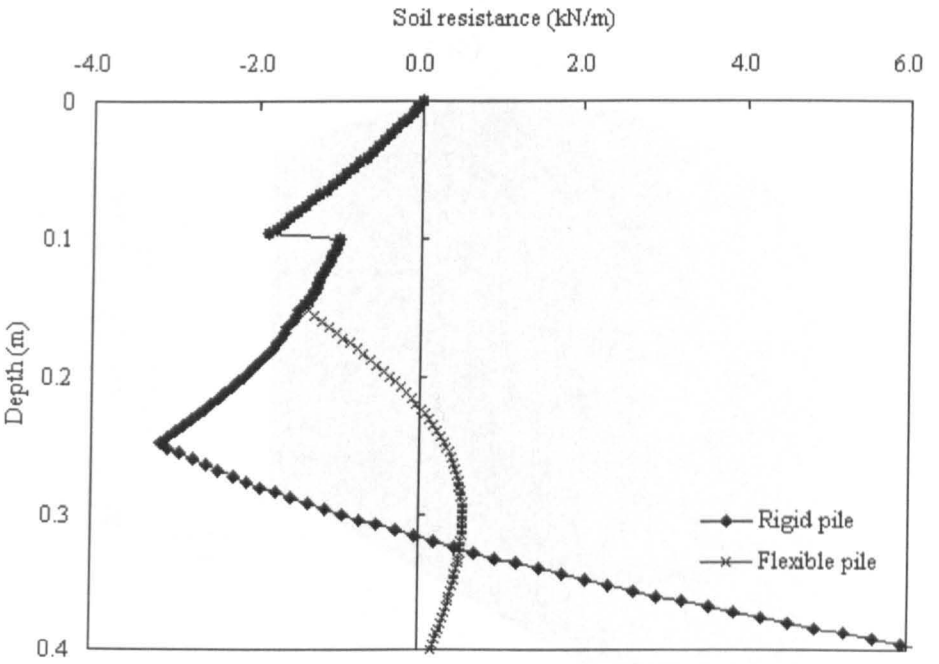

Fig. 7.15 The variation of soil resistance with depth for rigid and flexible FPS210 piles (by LPILE)

7.2.6 Summary

The behaviour of both rigid (short) and flexible (long) piles has been presented. The distribution of bending moment and stress along finned piles was studied. Fin performance to resist soil pressure is demonstrated in the diagrams of

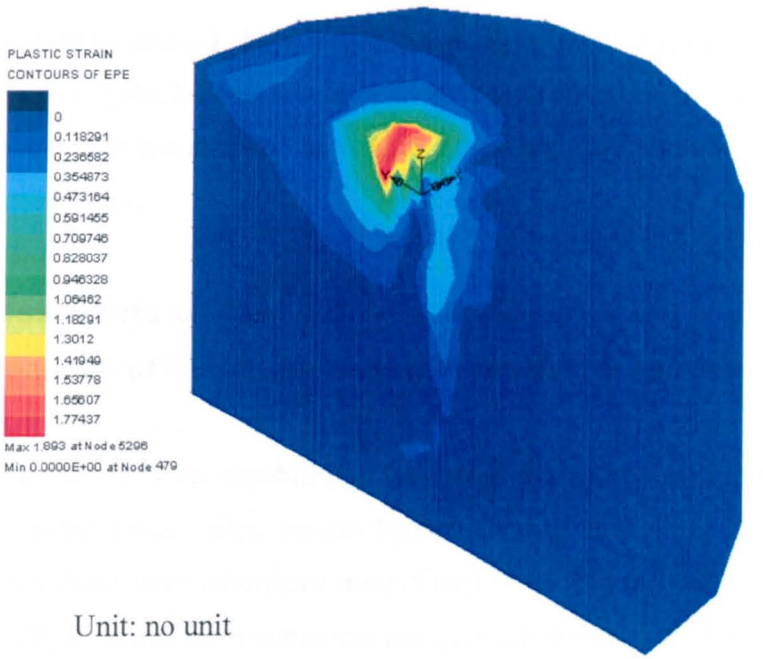

Unit: no unit

(a)

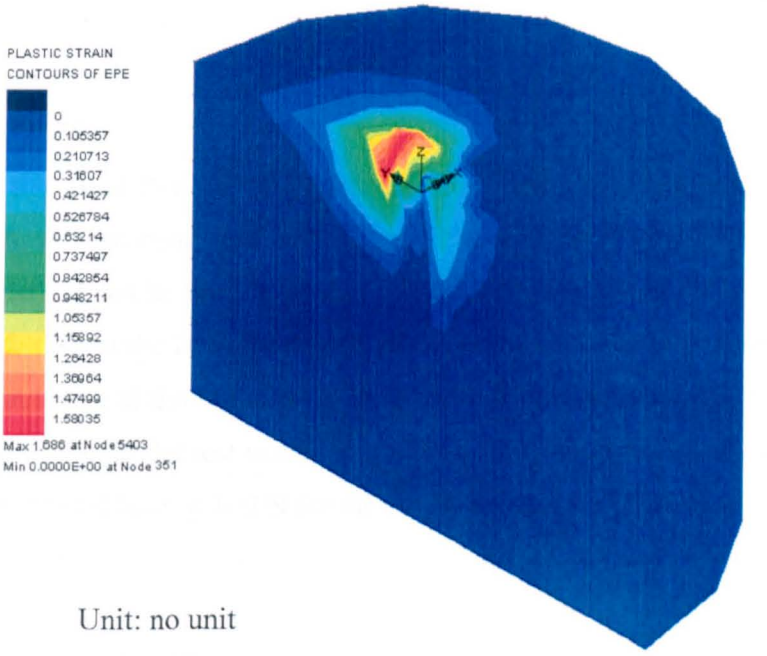

Unit: no unit

(b)

Fig. 7.16 Variation of plastic strain along finned piles (a) rigid pile (b) flexible pile (by LUSAS)

bending moment, strain and stress. This study has proved that fins improve lateral resistance by increasing the effective area and the pile stiffness in the fin section.

In future studies, quantitative analyses could be assessed. The behaviour of finned pile should be studied along with the changes in lateral displacement. Pile soil interactions under cyclic loading and combined static loading are important subjects for understanding. Both numerical analysis and the strain gauge method could be applied in future work.

7.3. Assessments of research methods

7.3.1 Comparison of laboratory tests with numerical analyses

Introduction

In order to verify the capability of numerical analyses to predict the behaviour of laterally loaded finned piles, results from numerical modelling (Chapter 3) are compared with those from laboratory tests (Chapter 5). Pile head P-Y curves of the monopile, MPS, obtained from numerical analyses and model tests are assessed. The behaviour of the monopile from difference approaches is verified at the serviceability limit state.

Comparison

P-Y curve of MPS

The pile head P-Y curves generating from numerical analyses using LUSAS and LPILE have been compared with that of the model test (Fig. 7.17(a)) showing the numerical method can be used to predict pile performance though the accuracy could be improved. When the laterally loaded pile is at the serviceability limit state with a lateral displacement at the top of the pile of 10% of pile diameter, the predicted load generated from the model test is similar to those from numerical analyses. Thus the serviceability lateral load of 100 N for the model test can be predicted from numerical analysis.

Behaviour of monopile MPS

Variations of displacement with depth of the monopile, MPS, are presented in Fig. 7.17(b) showing LUSAS is better at predicting the displacement of the lateral loaded pile than LPILE. Although FE analyses using 3D LUSAS is able to predict the displacement with depth, difficulties exist to transfer the data including bending

moment, shear force and soil resistance from 3D diagram into 2D diagram due to the limitation of the software. Bending moments generated from LPILE and the strain

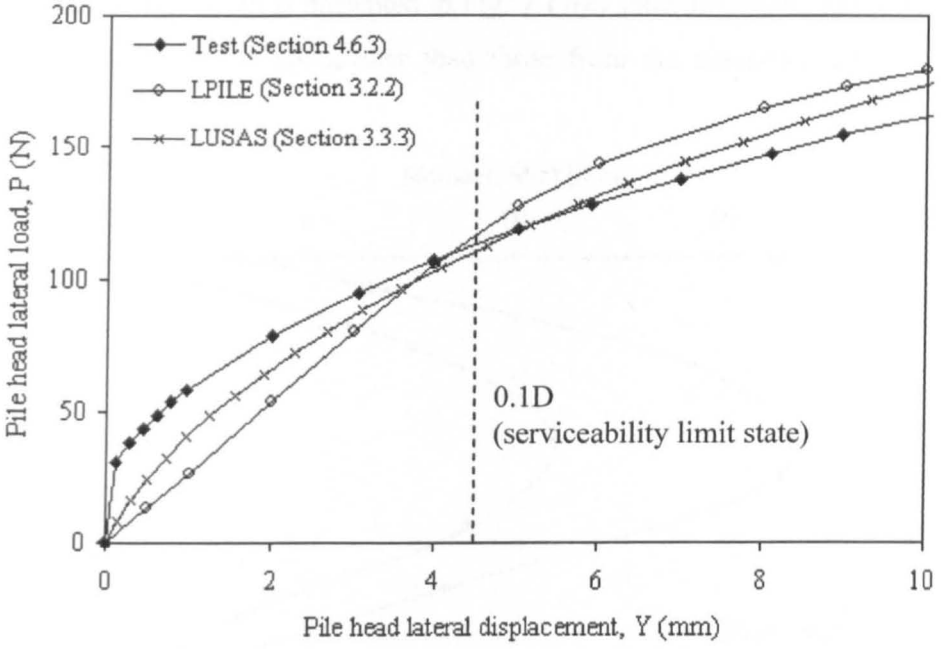

Fig. 7.17(a) P-Y curves obtained from different methods

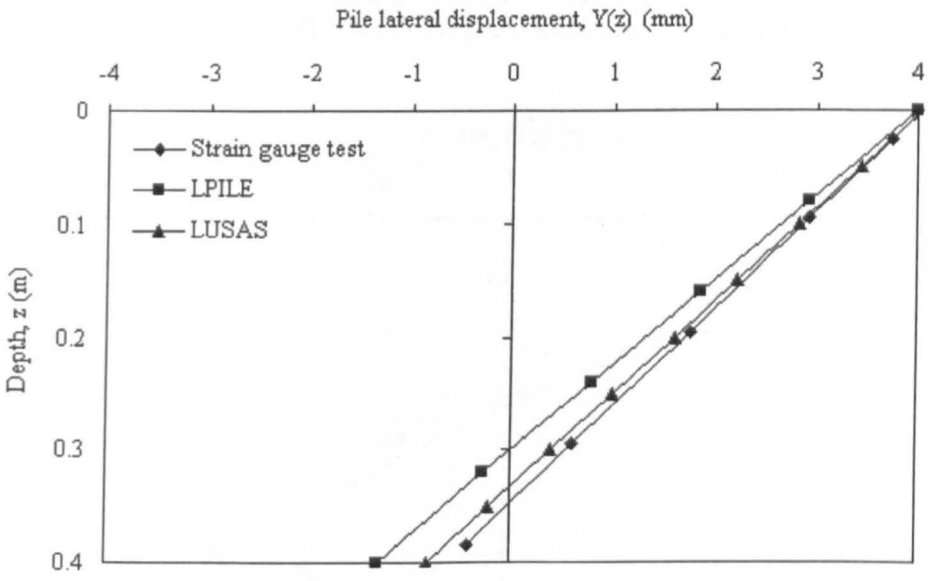

Fig. 7.17(b) Variations of lateral displacement with depth of the laterally loaded monopile obtained from different methods

gauge method are presented in Fig. 7.17(c) showing the results from LPILE are only 60% of those from strain gauge method but they are similar in shape. Fig. 7.17(d)

shows the variations of shear force with depth, and results from LPILE are the same 30% smaller than those from strain gauge method. However, the strain gauge method overestimates the pile head lateral load (135N compared to 106 N). Distribution of soil resistance with depth is presented in Fig. 7.17(e) showing results generated from the strain gauge method are greater than those from the computer analyses using LPILE.

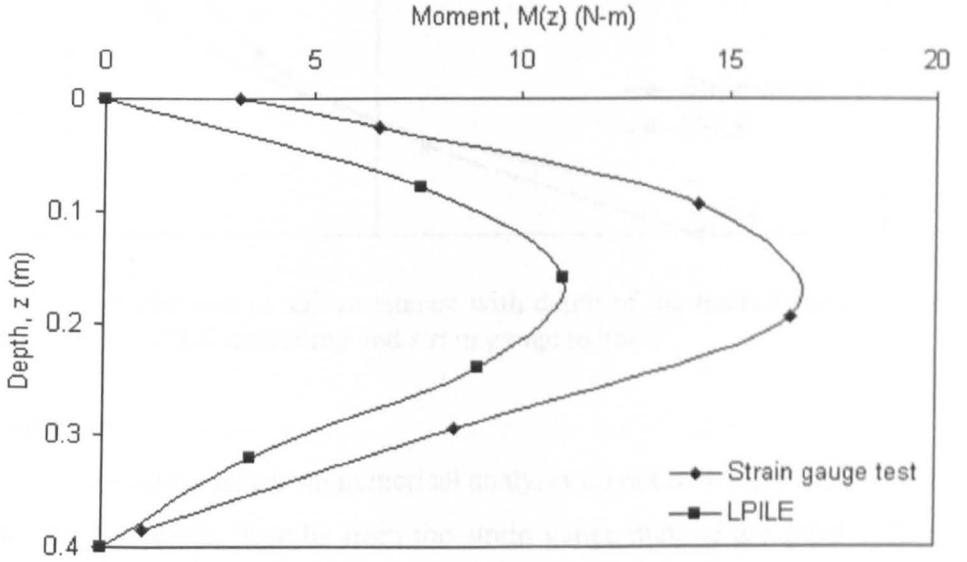

Fig. 7.17(c) Variations of bending moment with depth of the laterally loaded monopile generated from LPILE modelling and strain gauge method

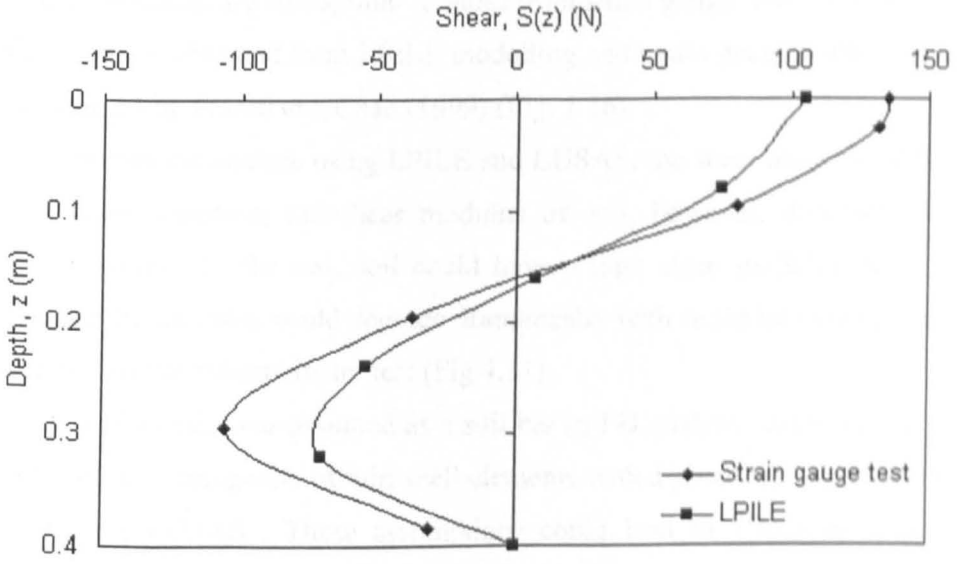

Fig. 7.17(d) Variations of shear force with depth of the laterally loaded monopile obtained from LPILE modelling and strain gauge method

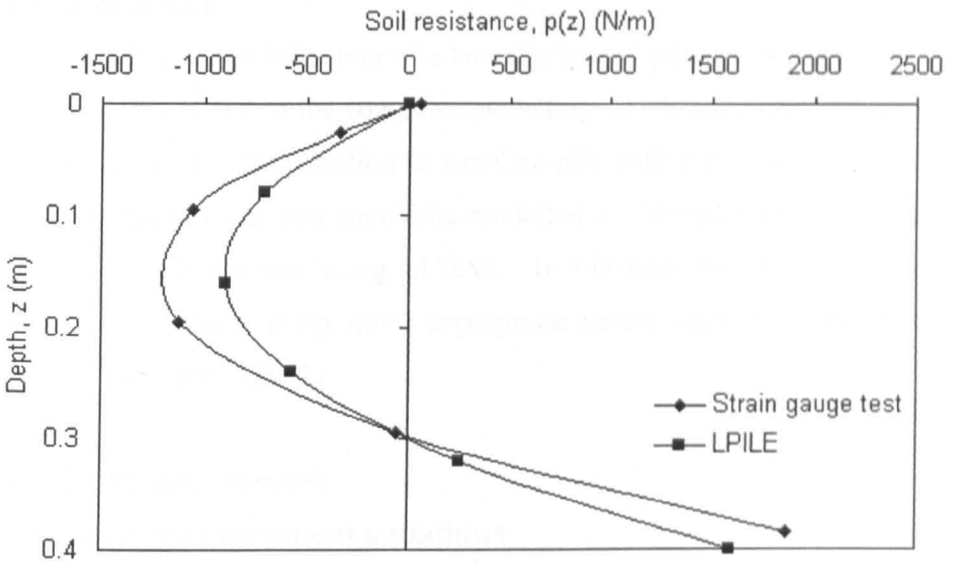

Fig. 7.17(e) Variations of soil resistance with depth of the laterally loaded monopile obtained from LPILE modelling and strain gauge method

Discussion

Results generated from numerical analyses do not match those generated from strain gauge methods. Results from the strain gauge method are greater than those from computer modelling which means an underestimate of lateral resistance in computer modelling. Although the behaviour of the laterally loaded pile can not be predicted accurately through numerical modelling, the shapes of these curves from numerical modelling are still similar to those from strain gauge tests. The distribution of soil resistance obtained from LPILE modelling and strain gauge method is similar to that assumed by Prasad and Chad (1999) (Fig. 2.16).

In numerical analyse using LPILE and LUSAS, the shear modulus of soil was assumed to be constant; the shear modulus of soil, however, decreases with an increase in strain. In the test, soil could have a high shear modulus in the initial loading, and the modulus could degrade dramatically with strain increasing according to the results in the pressuremeter test (Fig 4.21).

A hollow pile was assumed as a soil bar in FD analyses using LPILE, and it was assumed as a composite of thin shell elements with a given wall thickness in FM analyses using LUSAS. These assumptions could lead to a loss in accuracy of simulating the model pile.

Future research

Predicting the behaviour of a laterally loaded pile can be improved by using a shear modulus of soil in the computer modelling which decreases with an increase in pressure or strain. The function to simulate pile with different shapes using LPILE should be applied; the pile should be modelled by 3D solid elements instead of 2D thin shell in FE analysis using LUSAS. In FD analysis, the pile soil interaction should be simulated using more appropriate model such as strain wedge model proposed by Ashour (2002).

7.3.2 Empirical methods

Performance of empirical equations

Empirical methods were used to estimate the ultimate lateral load of piles. According to the calculated results in Table 3.2, only the method proposed by Meyerhof (1981) is able to predict the measured result of 155 N. Empirical methods proposed by Brinch Hansen (1961), Brom (1964a) and Petrasovits and Award (1972) overestimated the ultimate lateral load due to the use of excessive passive earth pressure. Methods presented by Prasad and Chari (1999) and API (1993) and DNV (2004) underestimated the ultimate lateral load since the passive earth pressure used was too small. The assumption of a reasonable earth pressure decides the accuracy of the prediction of ultimate lateral load for rigid pile foundations.

Modified coefficient of soil resistance

In order to simulate the measured lateral resistance of 155 N, the passive earth pressure coefficient, K_P, in the current empirical methods should be modified. In order to simplify the analysis, the passive earth pressure coefficient and the unit weight of soil were assumed to be constant in all layers. Broms (1964a) suggested that the soil lateral resistance acting in front of the pile increases proportionally with depth (Fig. 2.17); the earth pressure factor was suggested to be $3K_P$. In the modified equation based on the Broms method, the earth pressure factor $3K_P$ was replaced by the modified passive earth pressure, K_m, of 2.64 to fit the measured ultimate lateral earth pressure.

Petrasovits and Award (1972) suggested that pile rotation should be considered in the calculation of lateral soil resistance; the positive and the negative soil resistance are distributed above and below the rotation point of the pile,

respectively, as shown in Fig. 2.17. In order to simulate the measured ultimate lateral load, the earth pressure coefficient of (3.7 $K_P - K_a$) in the Petrasovits and Award method (1972) should be replaced by the modified earth pressure coefficient, K_m, of 10.77.

Both front and shear soil resistance were considered in the Prasad and Chari method (1999). The soil pressure distribution along the rigid monopile was established based on the equilibrium equations of moment and force. In order to simulate the test result, the effective internal friction angle, ϕ ', was 36.8° instead of the measured value of 35.2°.

Based on these back analyses, it is evident that the coefficient of earth pressure in the Broms method (1964) should not be overestimated by a factor of 3. The ultimate lateral load can be predicted from earth pressure factors without multiplying by the factor of 3. In the Prasad and Chari method (1999), 2° should be added to the internal friction angle used in the equation to match the result. In Petrasovits and Award method (1972), the earth pressure coefficient of (3.7 $K_P - K_a$) should be replaced by using 3 K_P according to back analyses. This shape factor, 3, has been suggested by Fleming (1992) and Patra and Pise (2001) in Broms (1964) and Meyerhof methods (1981), respectively.

Future research

Pile flexural stiffness, E_pI_p, is an important factor for lateral resistance which has been discussed in Section 7.2. But it was not used in the calculation of ultimate lateral load by empirical methods. Only soil stiffness and unit weight were used to calculate passive pressure in these methods. The value of soil stiffness was estimated from the angle of internal friction of soil, and this value was unable to reflect the real soil response in operation. The empirical methods are based on a linear elastic, perfectly plastic model whereas soil is nonlinear in behaviour. The real soil stiffness is a function of depth and lateral displacement; the precise calculation of lateral resistance of piles should be based on the change in soil stiffness at any stage of the loading.

In future studies involving the calculation of ultimate lateral load, the equation should include the shape factor and the non linear soil stiffness. The soil stiffness should be a function of soil depth, and soil resistance.

7.3.3 Numerical methods

Performance

The finite different (FDM) and the finite element (FEM) analyses by 2D LPILE and 3D LUSAS have been used to simulate pile soil behaviour of finned piles. Fin efficiency was evaluated fromP-Y curves taken from finned piles with different fin dimensions (Fig. 3.4 and Fig. 3.25). The reactions of the laterally loaded finned pile including displacement, bending moment, shear force as well as soil reaction along the pile have been presented in Section 3.2.3. Three-dimensional diagrams like pile soil movement and pile stress distribution were used to represent pile soil interaction especially in the area around the fins (Section 3.3.5).

Subjects for improvement

The simulated P-Y curves obtained by numerical analysis are still not very close to measured curves. In order to improve the quality of computer modelling, there are some difficulties that need to be overcome:

- The modified Mohr-Coulomb model in both FDM and FEM analyses was unable to predict the soil response accurately, and an advanced elasto-plastic soil model should be applied in the modelling.
- Pile and fins were simulated by thick shell elements instead of solid elements because the pile wall was small compared to the width and the length of the element. An advanced solid mesh which is able to accept a higher ratio of thickness to length should be developed.
- The interface between pile and soil is an important factor especially for small scale modelling due to the low effective stress inside the soil. An interface with very strong stiffness easily causes the calculation to fail to convergence due to stiffness matrix difficulty; whereas, an interface with low stiffness is easy to be compressed as a result of underestimating soil movement. An interface with low friction can lead to the easy passage of pile through the soil meshes.
- In this study, all modelling were based on piles subjected to static loading. Computer programs should have reliable functions to model piles under cyclic loading.

7.3.4 1G model tests

Test performance

To predict the increase in lateral resistance created by the use of finned piles, 1 G model tests were carried out. The static loading system provided a constant low-speed increasing load at the pile head. P-Y curves for various piles were developed to verify the increase in load at the same displacement. Pile head load and displacement curves of a monopile are presented in Fig. 4.11 showing that the three curves are not generated on the same line. Such a result could be due to slight inconsistence in sand preparation.

The cyclic loading system generated various cyclic load conditions at the pile head, and curves of displacement with the number of cycles were developed for different finned piles. The increase in lateral resistance was based on the reduction of lateral displacement. For piles under two-way balanced cyclic loading, the lateral displacement at the pile head was different for the two directions because the cyclic loading system was controlled by load (Fig. 4.16(b)). The initial increase in load could result in a significant increase in displacement causing the pile to move slightly toward one direction.

Dimensions of the soil chamber should be large enough to ease the boundary effect of the chamber wall to the pile soil response. The ideal distance between the pile and the wall is determined by the stress increase on the wall caused by the shear force along the pile; the distance should be long enough to offer the stress increase of the soil at the boundary reduced to less than 10% of that close to the pile. The ratio of the distance between the pile and the chamber wall to the pile diameter varied 11 to 15 depending on the position to place the pile (Fig. 4.7(a) and (b)). The increase in stress is proportional to the increase in strain, and the boundary could be defined based on the change of stain. Fig. 7.18 shows the ratio of pile rotation to the length of boundary. The maximum displacements of the pile head under static and cyclic loading tests were designed as 20 and 10 mm, respectively. In static loading, the pile was placed in the position as shown in Fig. 7.18(a) in order to eliminate the boundary ratio at the pile head. The pile tip boundary ratio increased due to shorting the boundary length, but the ratio is still less than that of pile head. In cyclic loading, the pile was placed in the centre of the tank (Fig. 7.18(b)) because the rotation was in both directions under two-way cyclic loading. All boundary ratios shown in Fig. 7.18

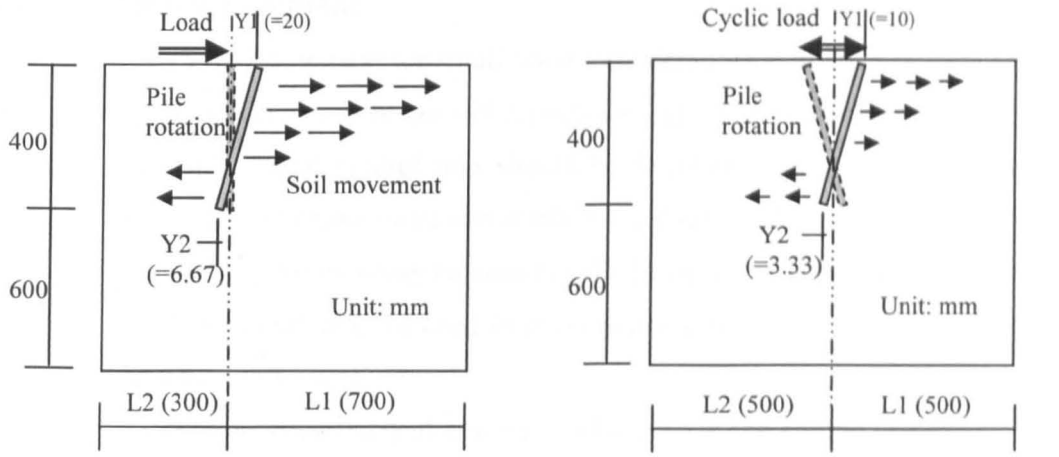

Ratio of front boundary=(Y1/L1)=20/700=2.8(%) Ratio of front boundary=(Y1/L1)=10/500=2 (%)
Ratio of back boundary=(Y2/L2)=6.7/300=2.2(%) Ratio of back boundary=(Y2/L2)=3.3/500=0.6(%)

(a) (b)

Fig. 7.18 Diagrams of boundary for pile rotation under (a) static loading and (b) cyclic loading

are less than 3% which can satisfy the limit boundary ratio of 5 % suggested by Sweeney et al. (1990).

Instead of loading devices, a simple pressuremeter and the strain gauge method were used to measure soil properties and pile soil behaviour, respectively. Although soil stiffness at different depths could be measured by the simple pressuremeter (Fig. 4.5), the ratio of shear modulus to effective lateral pressure was not very consistent (Fig. 4. 21). It was hard to control small changes in pressure by the manual increase and release of pressure.

Although strain gauge methods allowed the understanding of pile soil behaviours of piles subjected to different types of loading, some errors in measurement and simulation still occurred. Errors in measurement could be due to the fact that the reading was taken from the entire length of the gauge whereas the prediction was taken from the centre of the gauge thus resulting in differences in strain reading. The polynomial equation used to link the strain with the pile soil behaviour assumes the soil resistance to be a continuous linear spring. False readings of soil resistance occurred at the pile nonlinear section (the fin tip) and the soil resistance nonlinear section (the ground surface).

Aspects for improvement

Although the equipment for small scale tests demonstrated good performance in presenting fin efficiency, there are still aspects for improvement such as:

- A displacement control unit should be developed for the cyclic loading device to determine more accurately the influence of displacement on load particularly for two-way balanced cyclic loading. In addition, a pneumatic loading system may be used in cyclic loading tests to provide a very low speed (over 10 sec).
- A strain or stress control unit should be used in the simple pressuremeter to produce better pressure strain curves.
- Reliable and high resolution strain gauge measurements should be developed to obtain better strain results. More gauges should be installed to simulate the strain along the pile particularly at the fin base section.
- In order to verify that finned piles can be used in all soil conditions, tests should be conducted in other types of soil with different soil properties. The resistance of piles in saturated soils especially under cyclic loading should be examined.
- The ratio of pile stiffness to soil resistance is an important factor for lateral pile resistance. Piles with different wall thicknesses should be tested.

7.4. An overview of fin efficiency

7.4.1 Introduction

The increase of lateral resistance by using fins was found from:

- Static loading: to measure the increase in lateral load of the pile head.
- Cyclic loading: to measure the reduction in lateral displacement of the pile head.

In addition to these methods, the increase in lateral resistance was also evaluated by an increase in stiffness $\Delta P/\Delta Y$. For piles under combined loading, the influence of fin efficiency included vertical loading. Based on the normalised relationships of lateral resistance and fin dimension, a diagram showing the variation of normalised lateral resistance with an increase in material weight was established in Fig. 5.12.

An overview of fin efficiency to lateral resistance is based on the results of static loading derived from numerical calculations and small scale testing. The

influence of cyclic effect on fin efficiency is based on the test results. The effect of vertical load on fin efficiency is based on the results of combined loading.

7.4.2 Static loading

The variation of fin efficiency with lateral resistance has been presented in Fig. 3.2, Fig. 3.5 and Fig. 5.11 according to results from empirical methods, numerical analyses and 1G model tests, respectively. Fin efficiency was significantly underestimated by empirical methods compared to that obtained from model tests.

Fin efficiency could be predicted from the modified soil resistance as suggested in Section 7.3.2. The new fin efficiency was based on the modified API and DNV method because it has been widely used in the design of offshore pile foundations; it was also based on the modified Petrasovits and Award method. The pile was rotated and equilibrium equations of moment and shear force were applied in the calculation. The variation of fin efficiency with lateral resistance is presented in Table 7.3. Compared to the test results, fin efficiency from the modified equation is overestimated when the fin width is large and underestimated when the fin width is small. However, the prediction of the fin efficiency for FPS210 is good.

Table 7.3 Modified methods to predict fin efficiency

No.	Modified Petrasovits and Award method		Modified API and DNV method		Modified Smith (1987)		Test results (Chapter 5)	
	Pu (N)	$\frac{P_{u(FPS)}}{P_{u(MPS)}}$	Pu (N)	$\frac{P_{u(FPS)}}{P_{u(MPS)}}$	Pu (N)	$\frac{P_{u(FPS)}}{P_{u(MPS)}}$	Pu (N)	$\frac{P_{u(FPS)}}{P_{u(MPS)}}$
MPS	156.5	1.00	156.4	1.00	155.50	1.00	155	1
FPS105	160.3	1.02	164.1	1.05	161.72	1.04	162	1.05
FPS110	174.1	1.11	173.0	1.11	171.82	1.10	175	1.13
FPS120	215.5	1.38	248.6	1.59	191.26	1.23	192	1.24
FPS205	165.1	1.05	172.3	1.10	167.94	1.08	172	1.11
FPS210	189.6	1.21	193.1	1.23	188.15	1.21	189	1.22
FPS220	260.4	1.66	319.0	2.04	227.80	1.46	236	1.52
FPS405	173.1	1.11	138.9	0.89	181.15	1.16	175	1.13
FPS410	219.8	1.40	237.3	1.52	220.81	1.42	195	1.26
FPS420	349.0	2.23	479.0	3.06	300.11	1.93	264	1.7

Note: Pu = ultimate lateral load of finned piles
$Pu_{(MPS)}$ = ultimate lateral load of the monopile

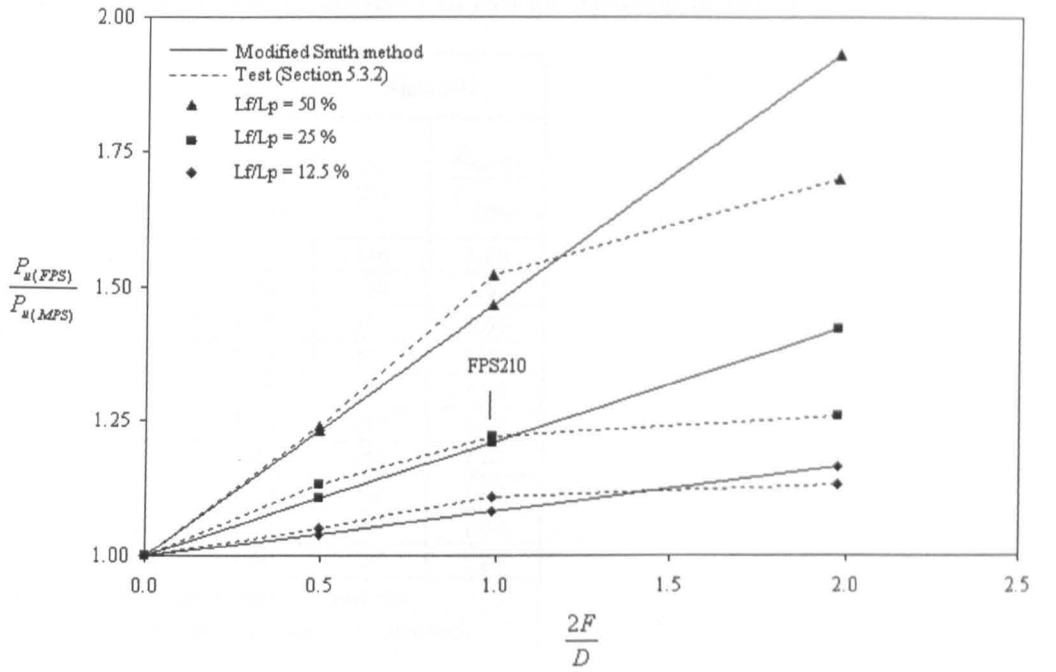

Fig. 7.19 The effect of fin dimensions on the ultimate capacity of rigid finned pile using the modified Smith method proposed in Fig. 7.3(b).

The prediction of fin efficiency was based on equations in Fig. 7.3 (b), both side shear and front soil resistance in the fin section were considered. The ratio of maximum soil resistance to maximum shear resistance was assumed to be constant, and it was assumed that only positive soil resistance occurred on the pile. The variation of fin efficiency with lateral resistance is presented in Fig 7.19 showing that the predicted results are close to test results (Fig. 3.5) when the fin width is less than half of the pile diameter. The modified equation overestimated the soil resistance and the effective area to resist soil pressure in finned pile with large fin width.

It should be borne in mind that the previous relationship of fin dimension and lateral resistance was developed from rigid finned pile behaviour involving a series of model tests and numerical analyses. In order to estimate the fin efficiency of flexible finned piles, the wall thickness of model pile was reduced to 1/1000 the original thickness which is similar to the method in Section 7.3. Table 7.4 shows the variation of fin efficiency with the pile dimensions of flexible piles. Compared to the results of rigid piles, the results of flexible piles (Fig. 7.20) show that there was not much increase in lateral resistance when the pile fin width was over half of the pile diameter. When the fin width was less than half of the pile diameter, the fin efficiencies for rigid and flexible piles were similar.

Table 7.4 Comparison of efficiency of fins for rigid and flexible piles predicted by LPILE method

No.	Flexible pile		Rigid pile	
	Pu (N)	$\frac{P_{u(FPS)}}{P_{u(MPS)}}$	Pu (N)	$\frac{P_{u(FPS)}}{P_{u(MPS)}}$
MPS	38.3	1	246	1.00
FPS105	39.8	1.04	250	1.02
FPS110	41.8	1.09	262	1.07
FPS120	47.5	1.24	302	1.23
FPS205	40.2	1.05	253	1.03
FPS210	43.5	1.14	278	1.13
FPS220	55.5	1.45	356	1.45
FPS405	40.4	1.05	262	1.07
FPS410	44.8	1.17	305	1.24
FPS420	57.3	1.49	405	1.86

Note: Pu = ultimate lateral load of finned piles
$Pu_{(MPS)}$ = ultimate lateral load of the monopile

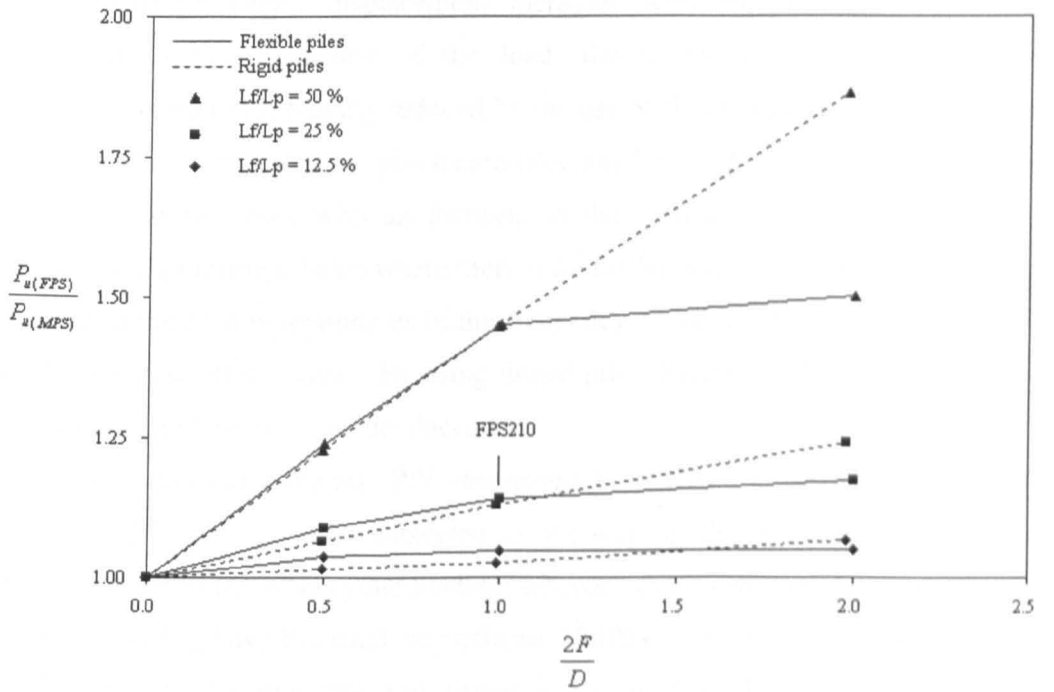

Fig. 7.20 The effect of fin dimensions on the ultimate capacity of the flexible and rigid piles predicted by LPILE method

The weight of material is one of the important features in the evaluation of the efficiency of finned piles; the increase in weight effects the manufacture, transportation and installation. According to the relationship between ultimate lateral

load and the selfweight of piles presented in Fig. 5.12, the mean curve shows an increase in lateral capacity corresponding to an increase in weight by using finned piles. The increase in capacity can be improved by selecting finned piles with optimum fin dimensions. In order to obtain the best relationship of capacity and weight which is presented in the upper bound, the fin width should be equal to half of the pile diameter. This equation may be modified when pile or soil condition changes.

7.4.3 Cyclic loading

According to the static loading tests, finned piles with a fin width of half of the pile diameter demonstrate the best lateral capacity, and this set of finned piles was used in cyclic loading. Reduction of lateral displacements, R_1, was used to measure an increase in lateral resistance by using finned piles under cyclic loading (Section 6.3.2). Results of reductions under different loading conditions are shown in Fig. 6.10. Generally, the reduction ratio, R_1, increases with an increase in fin length.

Although lateral displacement increases with an increase in either the magnitude or the frequency of the load, the tendency of increase of lateral displacement was significantly reduced by the use of finned piles especially when the fin length was over half of the pile length (Section 7.1.3). The lateral displacement of the pile head increases with an increase in the number of cycles and reaches a maximum displacement value where there is no further significant increase. Either an increase in the load magnitude or in the frequency of loading could cause the pile to reach the serviceability state. By using finned piles, lateral stability can be improved due to the reduction of lateral displacement.

The pile/soil stiffness, P/Y, measured in cycles was used to evaluate fin efficiency (Fig. 6.11). Piles subjected to one-way loading reach more stiffly than piles subjected to two-way cyclic loading; whereas, those subjected to two-way out of balanced loading have the smallest stiffness. Stiffness increases with an increase in fin length. Under one-way and two-way balanced loadings, the stiffness P/Y gradually increases with cycles; under two-way out of balanced loading, the stiffness P/Y does not increase significantly before the 10^{th} cycle and after the $1{,}000^{th}$ cycle. Pile and soil conditions under out of balanced cyclic loading do not achieve stability easily.

7.4.4 Combined loading

The fin efficiency of piles subjected to combined static loading is presented in Fig. 5.14. The normalised failure envelope of the finned pile FPS210 is larger than that of the monopile MPS particularly in the lateral direction. When the vertical load ratio, Q/Q_u, is less than 0.75, the lateral resistance of FPS varies from 1.35 to 1.55 times of that of MPS depending on the different vertical loads. In other words, the fin efficiency obtained from static loading tests shown in Section 7.4.2 is relatively conservative compared to that obtained with vertical load on the pile (when vertical load ratio is less than 0.75).

Under cyclic loading, fin efficiency can be evaluated from the reduction of lateral displacement. Fig. 6.13 shows the variation of the reduction of displacement for piles subjected to different types of combined cyclic loading. Generally, the ratios of reduction of lateral resistance increase with an increase in vertical load and with a decrease in frequency and in lateral load magnitude. However, the differences of reduction in lateral displacement between MPS and FPS210 increase with load magnitude and frequency. In other words, the fin efficiency of piles subjected to combined loads is higher than that of piles subjected to lateral load alone. Lateral resistance increases because soil is compacted through repeated loading but also becomes denser through the application of vertical load.

7.4.5 Summary

The increase in lateral resistance by using finned piles can be evaluated by using different methods based on different loading conditions. The relationship between lateral resistance and fin dimensions has been developed from the results of numerical analyses and 1G small scale tests. This relationship represents the optimum geometry ratio of fin to pile. In practice, the geometry features of finned pile can be transformed into the relationship between the use of material and lateral resistance which directly reflects the cost of construction. From previous studies, the best fin width is half of the pile diameter and the best fin length is half of the pile length.

Some factors which may affect fin efficiency are highlighted as follows:

- The influence of pile stiffness on lateral resistance has been verified, and the resistance of flexible pile is not as large as that of rigid pile when the fin width is more than half of the fin length.

- Fin efficiency (finned pile to monopile) is more apparent when the frequency or the magnitude of load level increases.
- Piles subjected to combined load demonstrate more resistance than those subjected to lateral load alone when the vertical load does not exceed a critical value.

The above factors all provide positive comments to improve lateral resistance. For finned pile design, Fig. 7.19, 7.20 and 5.12 provide a conservative method to evaluate fin efficiency to lateral resistance.

8 Conclusion

8.1. Offshore wind foundations

Offshore wind energy has been rapidly developed because of its infinite resources, low energy costs and reduced environmental constraints compared to other kinds of renewable energies. The UK government has a target that 10% of energy must come from renewable resources by 2010 (DTI, 2003). In the UK, two offshore wind farms have been operating, and there are still twelve proposed offshore wind projects being considered.

The selection of suitable offshore wind farms is based on essential features including seabed condition, wind speed, water depth, current speed, wave height and the distance from the coastline. An ideal wind farm should have good wind quality and suitable seabed conditions. Wind farms should be avoided at sites with strong currents and high waves which may increase lateral loading. Water depths offshore in the UK are between 10 and 20 m, and the sediments are mostly cohesionless siliceous soils. Monopile foundations are more advantageous than gravity, tripod and floating foundations; these merits include ease of manufacture, simple installation, and no sea bed preparation.

Onshore piled foundations are usually used to transmit large vertical loads from the superstructure through weaker subsoil into the underlying bearing strata. Horizontal loads acting on pile foundations are often ignored as they are much smaller than the vertical loads. Foundations for offshore structures, however, withstand significant environmental loads from waves, currents and wind giving rise to lateral loads that could be up to one third of the vertical loads (Soker et al., 2000). In order to improve the lateral resistance of monopile foundations, some innovative piles have been proposed like tapered and tripod piles. Although lateral resistance can be increased by using these innovative piles, their costs of manufacture and installation inhibit their use.

In order to increase the lateral capacity and reduce the use of material, finned piles have been proposed; the increase in pile flexural stiffness EI at the upper part of the pile can increase the lateral capacity; and the pile diameter or length can be reduced by using finned piles. The cross shape of fins has two main features to

increase lateral resistance: the flexural stiffness of the pile is increased by using the front and the trail fins; the area to resist soil reaction is increased by using a pair of side fins.

8.2. Study of finned piles

In order to evaluate the efficiency of the fins, three different methods, empirical, numerical and experimental, have been used. Empirical methods for laterally loaded rigid piles have been developed by a number of authors. Lateral capacity of the model finned pile could not be predicted correctly by using the empirical methods because of the simple assumptions of the distribution of soil pressure along the pile and the pile to soil stiffness. Compared to the results of 1G model tests, the fin efficiency was under estimated by using empirical methods. Fins on the pile were only presented as an increase in the pile diameter at the section above the fin base; the contribution of fin stiffness was not included. Empirical equations were also used to predict the pile head load displacement (P-Y) curves. Although the P-Y curves failed to be estimated from these empirical equations, a modified hyperbolic equation was able to fit the measured P-Y curve.

2D Numerical analyses were carried out using a finite difference program LPILE to predict the load displacement (P-Y) curves of the pile heads. Based on the P-Y curves, the increase in fin efficiency was verified. The fin efficiency obtained from LPILE was slightly less than that obtained from the results of 1G model tests. It was possible, however, to present bending moment, pile deflection, shear force and soil resistance along the pile. The increase in the pile soil response using finned piles was easily observed.

In order to overcome the limitation of two dimensional modelling, numerical analyses were carried out using the 3D finite element program LUSAS. Pile head P-Y curves of finned piles were presented, and fin efficiency obtained from FEM was found to be close to that from experimental methods. The increase in lateral resistance by using finned piles was presented in the three-dimensional charts describing pile-soil movement, strain distribution as well as stresses along the pile. In particular, the movement of the fins and the stress distribution on the fin and the soil movement around the fin were revealed.

1G static loading tests were carried out to investigate the fin efficiency. Normalised relationships between lateral resistance and fin dimensions were presented using the P-Y curves. The following conclusions were reached:

- Lateral resistance increases with the increases in length and width of the fins.
- A finned pile has the optimum fin efficiency when a fin width equals the radius of the monopile and the fin length equals half the pile length. This was based on a correlation relationship between lateral resistance and the use of material.
- Fins placed near the pile head provide more resistance than those near the pile tip.
- The load direction at 45° facing to the fins generates greater resistance than that at 0° through for design purposes the difference is insignificant.
- According to the repeated unload-reload tests, the lateral resistance increases with an increase in number of cycles, but the resistance decreases with an increase in load magnitude. Resistance of the finned piles is always higher than that of the monopile.

A series of cyclic loading tests with various loading conditions has been completed to evaluate fin efficiency. From an assessment of the relationship between the displacements, load, direction of load, number of cycles and length of fins the following conclusions can be drawn:

- Lateral displacement increases as either the frequency or magnitude of load increases.
- One-way cyclic loading causes large lateral displacements whereas two-way cyclic loading causes large vertical displacements.
- Closing the end of a pile can significantly reduce the vertical displacement of the pile yet have little effect on the lateral movement.
- Fins reduce lateral displacements of pile foundations under different kinds of lateral cyclic loading. Reductions vary from 30% up to 90% depending on the fin dimensions. The fin length should be between 25% and 50% of the pile length in order to provide the most effective lateral resistance.
- The most severe loading condition is two-way unbalanced loading because it creates large lateral movements associated with one-way loading and large settlements associated with two-way loading.

- Charts of the reduction in displacement as a function of fin length ratio under different loading conditions provide a practical design reference which can be used in offshore wind foundation design.
- Charts of the P/Y ratio show lateral pile-soil resistance with number of cycles. The lateral resistance under one-way cyclic loading creates the greatest soil stiffness; whereas the stiffness for unbalanced two-way loading is much lower hence should be taken as the worst possible case.
- Fins apparently help to increase lateral resistance, based on the observed variation of normalised stiffness with cycle number.

Model tests of piles subjected to combined loading with various loading conditions have been completed to evaluate fin efficiency. Both static and cyclic loading tests were carried out to verify the increase in lateral resistance and the reduction of lateral displacement, respectively. From an assessment of the relationship between the lateral displacement, vertical load, lateral load, number of cycles and frequency, the following conclusions can be given:

- Under combined static loading, lateral resistance increases with an increase in vertical load when the vertical load is within 75% of the ultimate vertical load.
- Compared to the increase in lateral resistance, vertical resistance does not increase significantly by the use of fins.
- Under combined cyclic loading, lateral displacement increases as either the frequency or magnitude of load increases.
- Fins help to reduce lateral displacements of pile foundations for different kinds of combined cyclic loading.
- The difference of reduction in lateral resistance between monopile and finned pile increases as either the frequency or magnitude of load increases.

Numerical methods were also used to verify piles with specific conditions including a reduced length of finned pile, a reduction in the diameter of a monopile and the change in the ratio of pile to soil stiffness. The following conclusions were:

- The length of a finned pile FPS210 can be reduced by 12.5% depending on the original length of MPS without significant influence on lateral resistance.

- The diameter of a finned pile can be reduced by 25% depending on the original diameter of MPS without a significant reduction in lateral resistance. The use of material for FPS is only 60% that of MPS.
- Rigid piles (with thick walls) have greater resistance than flexible piles (with thin wall).
- Fin efficiency of flexible piles is less than that of a rigid pile especially when the fin width exceeds half of pile diameter.

8.3. Outcomes of research

In order to explore the pile soil response of finned piles and to verify fin efficiency, both numerical and experimental methods were used. Results provide a direction to investigate the behaviour of finned piles. Relevant charts and modified equations provide practical design references which can be used in offshore wind foundation design. The innovative equipment for model tests and numerical modelling can be used in the future study of pile foundations. These important outcomes are summarised as follows:

Lateral capacity of finned pile

- The ultimate lateral loads of finned piles have been determined through the P-Y curves of 1G model tests (Table 5.1). In order to simulate the ultimate lateral load, the empirical equations and 3D finite element (FEM) analysis need to be modified (Section 7.3).
- Pile head lateral load and displacement (P-Y) curves of finned piles with different fin dimensions were established through a series of 1G model tests (Fig. 5.1) and numerical modelling (Fig.3.25). Lateral resistance increases with an increase in fin length and fin width.
- The influence of fin position and load direction was assessed through both 1G model static loading tests (Fig. 5.2 and 5.5) and the finite element analysis using LUSAS (Fig. 3.27 and 3.28). The fins should be placed near the pile head to have more lateral resistance than that at the pile tip. Lateral resistance of a finned pile is not significantly affected by the load direction.
- A series of cyclic loading tests has been carried to investigate the lateral resistance of finned piles (Section 6.2). Variations of both vertical and

lateral displacements with number of cycles were presented under cyclic loading. The displacement of the pile head can be significant reduced by using the fins.

- Lateral displacement of test piles increases with an increase in load magnitude and frequency (Fig. 6.3). One-way cyclic loading causes large lateral displacements whereas two-way cyclic loading causes large vertical displacements (Fig. 6.4). Vertical displacement can be reduced by placing a cap at the pile tip. Lateral displacement can be significant reduced by using the fins.
- Behaviour of a finned pile under combined static and cyclic loadings has been assessed through model tests. Lateral resistance increases with an increase in vertical load when the vertical load is within 75% of the ultimate vertical load (Fig. 5.9). Under cyclic loading, the lateral displacement increases with an increase in magnitude of lateral load and frequency; but the displacement decreases with an increase in vertical load (Fig. 6.7).
- The pile soil response along a finned pile under both static and cyclic loadings was assessed through a series of strain gauge tests (Section 5.2.4 and 6.2.4). Reductions of lateral displacement along the pile, and the bending moment distribution were presented. The increase in soil resistance in the fin section was observed. The finned pile behaviour under static loading was also predicted through numerical modelling by LPILE and LUSAS (Section 3.2.3 and 3.3.5).
- The stress distribution on the fins and the soil reaction around the fins were assessed using 3D LUSAS (Section 3.3.5). Interpretation of pile soil interaction between rigid and flexible piles is presented in Section 7.2.

Fin efficiency

- The empirical equations were modified to fit the ultimate lateral load observed from the model test of a monopile (Section 7.3.2). Ultimate lateral loads of finned piles can be predicted using the modified equation when the fin width is less than half of pile diameter (Fig. 7.19).
- A normalised relationship between lateral resistance and fin dimension has been established to represent efficiency of fins under static loading (Fig. 5.11). It is suggested that the fin length should be half of the pile length

and the fin width should be half of the pile diameter to provide the optimum resistance.

- The normalised relationship between lateral resistance and weight of finned piles was established (Fig. 5.12). In order to achieve the optimum resistance (on the top line of Fig, 5.12), the fin width should be half of the pile diameter.
- The increase in lateral resistance of finned piles subjected to cyclic loading was estimated from the reduction of displacement (Section 6.3.2). Although the lateral displacement increases with an increase in load magnitude and frequency, the displacement can be significantly reduced by using finned piles (Fig. 7.5 and 7.6)
- Normalised failure envelopes were established using static combined loading tests (Fig. 5.14). The failure envelope can be extended up to 50% by using a finned pile.

8.4. Future research

Research presented in this thesis is a milestone in the study of finned piles. In order to improve the reliability and the efficiency in the use of finned piles, further studies should focus on the following subjects:

- Advanced pile and soil models should be applied in numerical analyses, and a reliable computer program for the analysis of laterally loaded finned piles should be developed.
- Model tests of finned piles should be carried out in different pile soil conditions, e.g. by using flexible piles, in clay and in saturated conditions.
- A series of large scale tests of finned piles should be carried out in order to assess the effects of scale.
- Practical empirical methods and design guidelines for the design of offshore finned pile foundations should be developed.

9 References

Abou-matar, H. and Gole, G.G. (1997) "STP dynamic analysis and measurements," *Journal of Geotechnical and Geoenvironmental Engineering*, ASCE, V.123, pp.921-928.

American Petroleum Institute (API) (1993) *Recommended Practice for Planning, Designing and Constructing Fixed Offshore Platforms-Load and Resistance Factor Design*, First edition, USA.

American Society for Testing and Materials (ASTM) (1992) *Annual book of ASTM standards*, Vol. 04.08

Ashour, M., Norris, G. and Pilling, P. (2002) "Strain wedge model capability of analyzing behaviour of laterally loaded isolated piles, drilled shafts, and pile groups," *Journal of Bridge Engineering*, ASCE, Vol. 7, pp. 245-254.

Bea, R.G., Jin, Z., Valle, C., and Ramos, R. (1999) "Evaluation of reliability of platform pile foundations," *Journal of Geotechnical and Geoenvironmental Engineering*, ASCE, Vol. 125, pp. 696-704

Belkhir S, Mezazigh S and Levacher D (1999) "Non-linear behavior of lateral-loaded pile taking into account the shear stress at the sand," *Geotechnical Testing Journal*, ASTM, Vol 22, pp.308-316.

Bhusan, K. (1982) "Discussion: New Design Correlations for Piles in Sands." *Journal of the Geotechnical Engineering* Division, ASCE, Vol. 108, pp. 1508-1510.

Blaney, G. W. and O'Neill, M. W. (1989) "Dynamic lateral response of pile group in clay," *Geotechnical Testing Journal*, ASTM, Vol. 12, pp. 22-29.

Briaud, J. and Shields, D. H. (1980) "A special pressure meter and pressure meter test for pavement evaluation and design," *Geotechnical Testing Journal*, ASTM. Vol. 2, pp. 143-151.

Brinch Hansen, J. (1961) "The ultimate resistance of rigid piles against transversal forces," *Geoteknisk Institut. Bull.* No.12, Copenhagen.

British Geology Survey (BGS) (1992) *The geology of the English Channel*, Nature Environment Research Council, London.

British Geology Survey (BGS) (1993) *The geology of the Malin-Hebrides sea area*, Nature Environment Research Council, London.

British Standard Institution (1986) *BS8004: Code of practice for Foundations*, London.

British Standard Institution (1990) *BS1377-9: Methods of test for Soils for civil engineering purposes – Part 9: in-situ tests*, London.

Broms, B. B. (1964a) "Lateral Resistance of Piles in Cohesive Soils," *Journal of Soil Mechanic and Foundation Design*, ASCE, Vol. 90, SM2, pp. 27-63.

Broms, B. B. (1964b) "Lateral Resistance of Piles in Cohesionless Soils," *Journal of Soil Mechanic and Foundation Design*, ASCE, Vol. 90, SM3, pp. 123-156.

Brown, D. A., Scott, A. H., and Zhang, S. (1994) "Determination of P-Y curves using inclinometer data," *Geotechnical Testing Journal*, ASTM, Vol. 17, pp. 150-158.

Byrne, B.W. and Houlsby, G.T. (2003) "Foundations for Offshore Wind Turbines", Philosophical Transactions of the Royal Society of London, Series A, Vol. 361, pp 2909-2930.

Byrne, B.W. and Houlsby, G.T. (2004) "Experimental investigations of the response of suction caissons to transient combined loading", *Journal of Geotechnical and Geoenvironmental Engineering*, ASCE, Vol. 130, pp. 240-253.

Chan, S. and Hanna, T.H. (1980) "Repeated loading on single piles in sand," *Journal of Geotechnical Engineering Division*, ASCE, pp. 171-188.

Clarke, B. G. (1981) "In situ testing of clays using the Cambridge self-boring pressuremeter," PhD thesis, Cambridge University.

Comodromos, E. M., Anagnostopoulos, C. T. and Georgiadis, M. K. (2003) "Numerical assessment of axial pile group response based on load test," *Computers and Geotechnics*, ELSEVIER, Vol. 30, pp. 505-515.

Das, B. M. (1995) *Principle of Foundation Engineering*, Third edition, PWS Publishing Company, Boston, USA.

Department of Trade and Industry (DTI) (2003) "Our energy future – creating a low carbon economy," *Energy White Paper*, The Stationary Office, London.

Det Norske Veritas (DNV) (2004) *Design of offshore wind turbine structures*, Norway.

Dunnavant, T. W. and O'Neill, M. W. (1989) "Experimental p-y model for submerged stiff clay," *Journal of Geotechnical Engineering*, ASCE, Vol. 115, 95-114.

El Naggar, M. H. and Novak, M. (1996) "Nonlinear analysis for dynamic lateral pile response," *Soil dynamics and earthquake engineering*, ELSEVIER, Vol. 15, 233-244.

EI Naggar, M. H. and Wei, J. Q. (1999) "Response of tapered piles subjected to lateral loading", *Canada Geotechnical Journal*, NRC, Vol.36, pp. 52-71.

EI Naggar, M. H. and Wei, J. Q. (2000) "Cyclic response of axially loaded tapered piles", *Geotechnical Testing Journal*, ASTM, Vol.23, pp. 100-115.

El Naggar, M. H. and Bentley, K. J. (2000) "Dynamic analysis for laterally loaded piles and dynamic p-y curves," *Canadian Geotechnical Journal*, NRC, Vol. 37, pp.1166-1183.

European Committee for Standardization (2004) *Eurocode 7: Geotechnical Design - Part 1: General rules*. CEN, Brussel.

Fleming, W. G. K., Weltman, A. J., Randolph, M. F., and Elson, W. K. (1992). Piling engineering. Surrey University Press, London.

Gere J. M., Timoshenko, S. P. (1990) *Mechanics of Materials*, third edition, ITP, USA.

GWI (1997) *Strain gauge instruction manual*, Graham and White Instruments Ltd.

Hameed, R. A., Gunaratne, M., Putcha, S., Kuo, C., and Johnson, S. (2000) "Lateral load behaviour of jetted piles," *Geotechnical Testing Journal*, ASTM, Vol. 23, pp. 358-368.

Hetenyi, M. (1946) *Beams on elastic foundations*, University of Michigan Press, Michigan.

Hirany, A. and Kulhawy, F. H. (1989) "Interpretation of Load Tests and Drilled Shafts--Part 3: Lateral and Moment," *Foundation engineering*, ASCE, 1160-1172.

Holmes, J. D., 2001. Wind loading of structures, Spon Press, London

Irvine J.H., Allan P.G., Clarke B.G., Peng, J. (2003) "Improving the lateral stability of monopile foundations," *International Conference on Foundations*, BGA, UK, pp. 371-380.

Ismael, N. F. (1991) "Behaviour of laterally loaded bored piles in cemented sands." *Journal of Geotechnical Engineering*, ASCE, Vol. 116, pp.1678-1699.

Jamiolkowski, M., Ladd, C.C., Germaine, J. T. and Lancellotta, R. (1985) "New developments in field and laboratory testing of soils," *Proceedings, 11th international conference on soil mechanics and foundation engineering*, Vol. 1, pp. 57-153.

Janes, M. C., Bermingham, P. D., and Horvath, R. C. (1991) "An innovative dynamic test method for piles," *Proceedings of second international conference on recent advances in geotechnical earthquake engineering and soil dynamics*, St. Louis, pp. 252-256.

Klar, A. and Frydman, S. (2002) "Three-dimensional analysis of lateral pile response using two-dimensional explict numerical scheme," *Journal of Geotechnical and Geoenvironmental Engineering*, ASCE, Vol. 128, pp775-784.

Kondner, R. L. (1963). "Hyperbolic stress-strain response: cohesive soil." *Journal of Soil Mechanic and Foundation Division*, ASCE, Vol.89. I lS- 143.

Kramer, K. L. (1992) "Use of air bag system for instrumentation of lateral load tests on previously pipe piles," *Geotechnical Testing Journal*, ASTM, Vol. 15, pp. 399-403.

Kulhawy, F. H. and Mayne, P. W. (1990) *Manual on estimating soil properties for foundation design*, Electric power research institute, California.

Lee, P. Y. and Gilbert, L. W. (1980) "The Behavior of Steel Rocket Shaped Pile," *Symposium on Deep Foundation*, ASCE. 244-266.

Lin, S. and Liao, J. (1999) "Permanent strains of piles in sand due to cyclic lateral loads," *Journal of Geotechnical and Geoenvironmental Engineering*, ASCE, Vol. 125, pp. 798-802.

Little, R. L. and Briaud, J. (1988) "Full scale cyclic lateral load tests on six single piles in sand," *Miscellaneous paper GL-88-27*, Geotechnical Div., Texas A&M University, USA.

Long, J. H. and Vanneste G. (1994) "Effect of cyclic lateral loads on piles in sand," *Journal of Geotechnical Engineering*, ASCE, Vol. 120, pp -225-244.

LUSAS (1996) *LUSAS manual* for FEM computer program, FEA Ltd.

Mahmoud, M., and Burley, E. (1994) "Lateral load capacity of single piles in sand," *Geotechnical Engineering*, ICE, Vol. 107, pp.155-162.

Marchetti, S. (1980) "In situ test by flat dilatometer," *Journal of Geotechnical Engineering Division*, ASCE, Vol. 106, pp. 299-321.

Marchetti, S., Monaco, P., Totani, G. and Calabrese, M. (2001) *The flat dilatometer (DMT) for soil investigation*, ISSMGE, Indonesia

Marcuson, W. F. and Bieganousky, W. A. (1977) "SPT and relative density in coarse sands," *Journal of Geotechnical Engineering Division*, ASCE, Vol. 103, pp. 1295-1309.

Martin, G. R. and Chen, C. (2005) "Response of piles due to lateral slope movement," *Computers and Structures*, ELSEVIER, Vol. 83, pp.588-598.

Matlock, H., and Reese, L. C. (1960) "Generalized solution for laterally loaded piles," *Journal of Soil Mechanic and Foundation*, Div, ASCE, V86, pp. 1220-1246.

Matlock, H. (1970) "Correction for design of laterally loaded piles in soft clay," *2nd annu. offshore technology conference*, pp. 577-588.

Mayne, P. W. and Kemper, J. B. (1988). "Profiling OCR in stiff clays by CPT and SPT," *Geotechnical Testing Journal*, ASTM, Vol. 11, pp. 139-147.

McVay, M. C., Shang, T., and Casper, R. (1996) "Centrifuge testing of fixed-head laterally loaded battered and plumb pile groups in sand," *Geotechnical Testing Journal*, ASTM, Vol. 19, pp. 41-50.

Meimon, Y., Baguilin, F. and Jezequel, J. (1986) "Pile ground behaviour under long time lateral monotonic and cyclic loading," *Proceeding, third international conference, Numerical methods in offshore piling*, Nantes, pp. 285-302.

Meyerhof, G. G. and Ranjan, G. (1972) "The Bearing Capacity of Rigid Piles under Inclined Loads in Sand: I. Vertical Piles," Canadian Geotechnical Journal, Vol. 9, pp430-445.

Meyerhof, G. G. and Hanna, A. M. (1978) "Ultimate Bearing Capacity of Foundations on Layered Soil Under Inclined Load." *Canadian Geotechnical Journal*, NRC, Vol. 15, No.4, pp. 565-572.

Meyerhof, G. G., Mathur, S. K. and Valsangkar, A. J. (1981) "Lateral resistance and deflection of rigid wall and piles in layered soils." *Canadian Geotechnical Journal*, NRC, Vol. 18, pp 159-170.

Meyerhof, G. G. and Purkayatha, R. D. (1985) "Ultimate pile capacity in layered soil under eccentric nad inclined loads," *Canadian Geotechnical Journal*, NRC, Vol. 22, pp. 399-402.

Meyerhof, G. G., Ststry, V. V. R. N. (1987) "full-displacement pressuremeter method for rigid piles under lateral loads and moments," *Canadian Geotechnical Journal*, NRC, Vol 24, pp 471-478.

Mokwa R. L. and Duncan, J. M. (2003) "Rotational restraint of pile caps during lateral loading," *Journal of Geotechnical and Geoenvironmental Engineering*, ASCE, Vol. 129, pp. 829-837.

Muqtadir, A. and Desai, C.S. (1986) "Three-dimensional analysis of a pileogroup foundation," *International Journal of Numerical Analysis Methods in Geomechanics*, Vol. 10, pp.41-58.

Murchison , J. M.and O'Neill, M. W. (1984) "Evaluation of P-y relationships in cohesionless soils," *Analysis and design of pile foundations*, Proceeding, Geotechnical Engineering Division, ASCE, USA, pp. 174-192.

Ng C. W. W. and Zhang, L. M. (2001) "Three-dimensional analysis of performance of laterally loaded sleeved piles in sloping ground," *Journal of Geotechnical and Geoenvironmental Engineering*, ASCE, Vol. 127, pp.499-509.

Ng C. W. W. and Zhang, L. M., and Nip, D. C. N. (2001) "Response of laterally loaded large-daimeter bored pile groups," *Journal of Geotechnical and Geoenvironmental Engineering*, ASCE, Vol. 127, pp.658-669.

OWE (2001) Concerted Action on Offshore Wind Energy in Europe- Offshore technology, Final report. Delft, Netherlands.
Http://www.offshorewindenergy.org/index.php

Ozsu, E. (2005) Behaviour of laterally loaded tripod foundations, Undergraduate final year project report. University of Newcastle upon Tyne.

Pan, J.L., Goh, A.T.C., Wong, K. S. and Teh, C. I. (2000) "Model Tests on Single Piles in Soft Clay," *Journal of Canadian Geotechnical*, NRG, Vol.37, pp. 890-897.

Parry, R. H. G. (1977) "Estimating Bearing Capacity in Sand from SPT Values," *Journal of the Geotechnical Engineering Division*, American Society of Civil Engineers, Vol. 103, No. 9, pp. 1014-1019.

Patra, N.R. and Pise, P.J. (2001) "Ultimate lateral resistance of pile groups in sand," *Journal of Geotechnical and Geoenvironmental Engineering*, ASCE vol. 127, No.6, pp481-487.

Peng, J., Rouainia, M., Clarke, B., Allan, P., and Irvine, J. (2004) "Lateral resistance of finned piles established from model tests," *Proceeding of the International Conference on Geotechnical Engineering – Beirut*, CFMS, Lebanon, pp. 565-571.

Petrasovits, G. and Award, A. (1972) "Ultimate lateral resistance of a rigid pile in cohesionless soil," *Proceeding of 5th European Conference*, SMEF, Madrid.

Poulos, H. G. and Davis E. H. (1980) *Pile Foundation Analysis and Design*, Wiley, New York.

Poulos, H.G. (1982) "Single pile response to cyclic lateral load," *Journal of Geotechnical Engineering Division*, ASCE, pp. 355-375.

Powergen Renewables (2002) UK Offshore Wind, London http:/www.powergenrenewables.com/harnessingoffshorewindpower.htm

Prakash, S. and Sharma, H.D. (1989) *Pile foundations in engineering practice*, A Wiley-Interscience Publication, USA, pp 322-405.

Prasad, V.S.N.Y and Chari, T.R. (1999) "Lateral capacity of model rigid piles in cohesionless soil", *Soils and Foundation*, Tokyo, vol. 39, pp21-29

Pressley, J.S. and Poulos, H.G. (1986) "Finite element analysis of mechanisms of pile group behaviour," *Inst. Jnl. For Num. and Anal. Methods In Geomechanics*, Vol 10, pp. 213-221.

Purkayastha, R. D., and Basack, S. (1999) "Response of model piles under cyclic loadings," *International Conference on Offshore and Nearshore Geotechnical Engineering*, pp. 227-232.

Ramakrishna, V.G.S.T., and Rao, S.N. (1999) "Critical cyclic load levels for laterally loaded piles in soft clays," *International Conference on Offshore and Nearshore Geotechnical Engineering*, GEOshore, pp. 301-307.

Rao, S. N., Ramakrishna, V.G.S.T., and Rao, M. B. (1998) "Influence of rigidity on laterally loaded pile groups in marine clay," *Journal of Geotechnical and Geoenvironmental Engineering*, ASCE, Vol. 124, pp 542-549.

Rao, K. M., Prasad, K. N., and Pullaiah, M. (1999) " Influence of shape of pile on lateral response of pile foundations," *Internation Conference on Offshore and Nearshore Geotechnical Engineering*, GEOshore, pp. 283-288.

RDP (2002) *Capacitive load cell type mcl*, manual, RDP Electronics Ltd. UK.

Reese, L.C., Cox, W. R., and Koop, F. D. (1974) "Analysis of laterally loaded piles in sand," *Proceedings of the VI annual offshore technology conference*, Huston, Texas, pp.672-690.

Reese, L. C. (1977) "Laterally loaded piles: program documentation," Journal of Geotechnical Engineering, Division, ASCE, V 103, pp. 287-305.

Reese, L. C. (1985) *LPILE1 (computer program)*, Ensoft, Inc., USA.

Reeves, A. (2003) *Wind Energy for Electric Power*, Renewable Energy Policy Project, USA.

Robertson, P. K., Campanella, R. G., Brown, P. T., Grof, I. and Hughes, J. M. O. H. (1985) "Design of axially and laterally loaded piles using in situ tests: A case history," *Canadian Geotechnical Journal*, Vol. 22, pp. 518-527.

Robinsky, E.I., Sagar, W.L., and Morrison, C. F. (1964) "Effect of shape and volume on the capacity of model piles in sand," *Canadian Geotechnical Journal*, Vol. 1, pp. 189-204.

Rollins, K. M., Peterson, K. T., and Weaver, T. J. (1998) "Lateral load behaviour of full-scale pile group in clay," *Journal of Geotechnical and Geoenvironmental Engineering*, ASCE, Vol. 124, pp. 468-478.

Rollins, K. M., Lane, J. D., and Gerber, T. M. (2005) "Measured and computed lateral response of a pile group in sand," *Journal of Geotechnical and Geoenvironmental Engineering*, ASCE, Vol. 131, pp. 103-114.

Sastry, V .V. R. N., and Meyerhof, G. G. (1986) "Behaviour of rigid piles in layered soils under eccentric and inclined loads," *Can. Geotech. J.*, NRC. Vol. 23, pp. 451-457.

Sastry, V .V. R. N., and Meyerhof, G. G. (1994) "Behaviour of flexible piles in latered sands under eccentric and inclined loads," *Can. Geotech. J.*, NRC. Vol. 31, pp. 513-520.

SeaScape Energy (2001) http://www.seascape-energy.co.uk/

Seed, H. B., Wong, R. T., Idrss, I. M., Tokimatsu, K. (1986) "Moduli and damping factors for dynamic analysis of cohesinless soils," *Journal of Geotechnical Engineering*, ASCE, Vol. 112, pp. 1016-1032.

Smith, T. D. (1987) "Pile horizontal modulus values," *Journal of Geotechnical Engineering*, Vol. 113, 1040-1044.

Soker, H., Rehfeldt, K., Santjer, F., Strack, M. and Schreiber, M. (2000) *Offshore Wind Energy in the North Sea.* Deutsches Windenergie-Institut (DEWI), Wihelmshaven.

Sweeney, B. P. and Clough. G. W. (1990) "Design of a large calibration chamber," Geotechnical Testing Journal, ASTM, Vol. 13, pp 36-44.

Tomlinson M. J. (2001) *Foundation Design and Construction*, Seventh edition, Personal Education Ltd., UK.

Tong, K. C. (1998) "Technical and economic aspects of a floating offshore wind farm." *Journal of Wind Engineering and Industrial Aerodynamics*, 74-76, 399-410.

Trochanis, A. M., Bielak, J. and Christiano, P. (1991) "Three-dimensional nonlinear study of piles," *Journal of Geotechnical Engineering*, ASCE, Vol. 117, pp.429-447.

University College London and CLRC Rutherford Appleton Laboratory (2001) *Multiple Unit Floating Offshore Wind farms (MUFOWs)*. London.

Vesic, A. S. (1977) *Design of Pile Foundation, National Cooperative Highway Research Program Synthesis of Practice No. 42*, Transportation Research Board, Washington, D. C., USA.

Wei, J. and EI Nagger, M. H. (1998) "Response of tapered piles subjected to lateral loading", *Canada Geotechnical Journal*, NRC, Vol.35, pp. 641-654.

Wolff, T. F. (1989) "Pile capacity prediction using parameter functions," *Proceedings, European Symposium on Penetration Testing*, Vol. 2.2, pp. 367-375.

Wroth, C. P., and Wood, D. M. (1976) "The correlation of some basic properties of soils, and its implication in the assessment of poor quality data." *Res. Rep. CUED/C-soils TR31*, University of Cambridge.

Zaaijer, M. B. (2002) "Tripod support structure - Pre-design and natural frequency assessment for the 6 MW" Dutch Offshore Wind Energy Converter project http://www.ecn.nl/docs/dowec/10063_002.pdf

Zhang, L., Silva, F. and Grismala, R. (2005) "Ultimate lateral resistance to piles in cohesionless soils," *Journal of Geotechnical and Geoenvironmental Engineering*, ASCE, Vol. 131, 78-83.